UCGE Reports
Number 20177

Department of Geomatics Engineering

Techniques to Improve Ground-Based Wireless Location Performance Using a Cellular Telephone Network

(URL: http://www.geomatics.ucalgary.ca/links/GradTheses.html)

by

Changlin Ma

June 2003

THE UNIVERSITY OF CALGARY

Techniques to Improve Ground-Based Wireless Location Performance Using a Cellular Telephone Network

by

Changlin Ma

A THESIS

SUBMITTED TO THE FACULTY OF GRADUATE STUDIES

IN PARTIAL FULFILMENT OF THE REQUIREMENTS FOR THE

DEGREE OF DOCTOR OF PHILOSOPHY

DEPARTMENT OF GEOMATICS ENGINEERING

CALGARY, ALBERTA

JUNE, 2003

© Changlin Ma 2003

ABSTRACT

The primary objective of this thesis is to seek a ground-based location scheme suitable for mobile positioning in cellular phone networks. To this end, several techniques are proposed to handle issues that may occur in a cellular network and which may deteriorate wireless location performance. These issues include the lack of signal availability due to co-channel interference, the inefficiency in mobile location calculations, and the significant Non-Line-of-Sight (NLOS) errors resulting from multipath propagation. With the IS-95 CDMA pilot signal as an example, signal availability - or hearability - is thoroughly analyzed. The analysis shows that hearability is poor for location purposes. To improve signal hearability, two methods that are known to be effective - the enhanced signal processing method and the idle period down link (IPDL) method - are fully discussed. Another promising solution in poor signal hearability environments is the combination of cellular network-based methods with other positioning methods. As an example, the integration of GPS and a cellular network is proposed. Better location performance can be obtained by epoch-by-epoch Least Squares (LS)-based integration schemes or by Kalman filter-based integration schemes. The position of a mobile handset is normally obtained by solving non-linear equations. However, it represents a high computational burden and may suffer from a convergence problem. To resolve these issues, an enhanced two-step LS solution is proposed for hybrid time difference of arrival (TDOA)/angle of arrival (AOA) wireless location schemes. This method can provide

performance which is almost equivalent to that of Taylor-series-based solutions while imposing a low computational burden. Because NLOS errors within time of arrival (TOA), TDOA, and AOA measurements are very large compared to receiver noise, NLOS errors should be mitigated before the measurements are used in the position calculation. Two NLOS error mitigation methods are proposed. One is a distribution function-based method which depends on system redundancy and a high clear intersection density. The other is a channel estimation-based method which mitigates NLOS errors by using only the earliest signal from among all multipath replicas. The effectiveness of all of the proposed methods has been proved by simulation tests, verifying that these methods can be successfully applied in an actual wireless location system design.

ACKNOWLEDGEMENTS

I would like to express my sincere appreciation to my supervisors, Dr. Gérard Lachapelle and Dr. Richard Klukas, for their continuous guidance and support during my PhD program. I will always remember their sincere spirit of cooperation, their positive attitude, and understanding.

I would like to acknowledge the following graduate students for the breadth and depth of their support and kindness: Junjie Liu, Yan Lu, ChaoChao Wang, Glenn MacGougan, Mark Petovello, Oleg Mezentsev, and Aaron Morton.

I would also like to thank the professors, students, and staff of the Department of Geomatics Engineering who have made my time fruitful and enjoyable.

My deepest thanks go to my dear wife, Lei Dong, who supported me tremendously throughout my study, and to my son, Xingyu, for bringing so much joy into my life. I am also indebted to my parents and parents-in-law for their untiring support.

TABLE OF CONTENTS

ABSTRACT ..... **iii**
ACKNOWLEDGEMENTS ..... **v**
TABLE OF CONTENTS ..... **vi**
LIST OF TABLES ..... **x**
LIST OF FIGURES ..... **xii**
LIST OF SYMBOLS ..... **xx**
LIST OF ABBREVIATIONS ..... **xxiii**

CHAPTER 1
INTRODUCTION **1**
1.1 Motivations for Wireless Location 1
1.2 Technical Challenges in Wireless Location 2
1.2.1 The Accuracy Problem 3
1.2.2 The Hearability Problem 3
1.2.3 The Non-Line-of-Sight (NLOS) Propagation Problem 4
1.3 Scope of Research 5
1.4 Thesis Outline 9

CHAPTER 2
AN OVERVIEW OF WIRELESS NETWORK AND WIRELESS LOCATION TECHNIQUES **11**
2.1 Introduction 11
2.2 Wireless Communications Systems 11
2.2.1 Cellular Network Architecture 13
2.2.2 Cellular Coordinate System 14
2.3 Effects of Signal Propagation through Wireless Channels 17
2.4 Wireless Location Techniques 20

2.4.1 Cellular Network-Related Techniques....20
2.4.2 Satellite-Based Positioning Techniques....25
2.4.3 Performance Comparison of Location Techniques....31
2.5 Dilution of Precision....33

CHAPTER 3
HEARABILITY ANALYSIS....40
3.1 Introduction....40
3.2 IS-95 CDMA Forward Link (Pilot Channel) Hearability Analysis....41
3.2.1 IS-95 Forward Link Signals....41
3.2.2 IS-95 CDMA Pilot Channel Signal....42
3.2.3 SIR Model of Pilot Signals....44
3.3 Hearability Improvement....56
3.3.1 Enhanced Signal Receiving Technique....56
3.3.2 IPDL Technique to Improve Forward Link Hearability....73
3.4 Conclusions....80

CHAPTER 4
AN ENHANCED TWO-STEP LEAST SQUARED APPROACH FOR TDOA/AOA WIRELESS LOCATION....82
4.1 Introduction....82
4.2 Hybrid TDOA/AOA Wireless Location Scheme....84
4.3 Solutions to the Hybrid TDOA/AOA Scheme....85
4.3.1 Taylor-series Linearization Method....86
4.3.2 Original Two-Step LS Method....88
4.3.3 Enhanced Two-Step LS Method....93
4.4 Simulation Results....99
4.4.1 Algorithms Studied....99
4.4.2 Performance Comparison at One Point....100
4.4.3 Performance Comparison with Respect to Different MS-BS Separations....103
4.4.4 Performance Comparison When NLOS Errors Exist....108

4.4.5 Computational Burden Comparison 114
4.5 Conclusions 116

CHAPTER 5
A NON-LINE-OF-SIGHT ERROR MITIGATION METHOD FOR TOA MEASUREMENTS 117
5.1 Introduction 117
5.2 The Error Issue 118
5.3 NLOS Error Mitigation Algorithm 121
5.3.1 Hyperbola Intersection Calculation 123
5.3.2 Construction of Distribution Function 124
5.3.3 MS Location Estimation 127
5.3.4 NLOS Identification 127
5.3.5 NLOS Error Correction 134
5.3.6 NLOS Error Detection Ability 135
5.4 Simulation Results 137
5.4.1 Successful NLOS Error Detection Probability with Respect to the Number of BSs Used 138
5.4.2 MS Location Accuracy 140
5.4.3 NLOS Error Mitigation Capability with Respect to Measurement Noise 146
5.5 Conclusions 154

CHAPTER 6
NLOS ERROR MITIGATION FOR AOA MEASUREMENT 155
6.1 Introduction 155
6.2 TOA-AOA Distribution in a Multipath Channel 156
6.2.1 TOA Spread (Delay Spread) 157
6.2.2 Angle of Arrival (AOA) Spread 158
6.3 GBSB Model 159
6.4 Vector Channel Estimation 167
6.5 TOAs and AOAs Estimation via 2D UESPRIT Super-Resolution Method 177

6.6 Simulation Results 179
6.6.1 Performance of 2-D Unitary-ESPRIT Algorithm 179
6.6.2 TOA-AOA Estimation Accuracy for a Single BS 183
6.6.3 Estimation accuracy of MS location 187
6.7 Conclusions 192

CHAPTER 7
INTEGRATION OF GPS AND NETWORK-BASED WIRELESS LOCATION METHODS 194
7.1 Introduction 194
7.2 Property Comparison between GPS Signals and Cellular Network Signals 195
7.3 Epoch-by-Epoch Integration of GPS and Cellular Network-Based Methods 199
7.4 Kinematic Tracking of MSs Based on Kalman Filter Techniques 210
7.4.1 Position Domain Kalman Filtering Technique 211
7.4.2 Measurement Domain Kalman Filtering Technique 215
7.5 NLOS Error Mitigation in GPS and Cellular Network Integration 223
7.6 Conclusions 232

CHAPTER 8
CONCLUSIONS AND FUTURE WORK 234
8.1 Conclusions 234
8.2 Future Work 241

REFERENCES 244

LIST OF TABLES

Table 2.1: Comparison among Wireless Location Techniques 33

Table 3.1: Parameters Used in Hearability Analysis 50

Table 3.2: CCIR Model Parameters 51

Table 3.3: Hearability Improvement due to Enhanced Signal Reception ($P_F = 5\%$) 70

Table 3.4: Receiver Hearability with PR-IPDL ($P_F = 5\%$) 75

Table 3.5: Receiver Hearability with TA-IPDL ($P_F = 5\%$) 80

Table 4.1: Algorithms for Comparison 100

Table 4.2: Positioning Error with the Cumulative Probability of 50% (4TDOAs 2AOAs STD_{TDOA} = 100 m) 103

Table 4.3 Typical NLOS Error Parameter Values for Different Environments 109

Table 5.1: Minimum Detectable NLOS Error 132

Table 5.2: Ratios of Clear Intersections to Total Intersections in TDOA Wireless Location 137

Table 5.3: Receiver Noise for Six Scenarios 147

Table 7.1: Positioning Error of Epoch-by-Epoch LS Combination [m] 209

Table 7.2: Positioning Error of Position Domain KF Based Combination [m] 215

Table 7.3: Positioning Error of Measurement Domain KF Based Combination [m] 222

Table 7.4: Horizontal Positioning Error Comparison 223

Table 7.5: Performance Degradation Due to NLOS Errors and Receiver Noise 224

Table 7.6: Performance Improvement Due to NLOS Error Mitigation 228

Table 7.7: Performance of GPS Assisted NLOS Error Mitigation 232

LIST OF FIGURES

Figure 1.1: Proposed Wireless Location Scheme 5

Figure 2.1: 2G Network Architecture 13

Figure 2.2: Hexagonal Shape Associated with Circular Coverage Area 15

Figure 2.3: Non-orthogonal Cellular Coordinate System 15

Figure 2.4: Ring Cellular Coordinate System 16

Figure 2.5: A Typical Wireless Propagation Environment 18

Figure 2.6: Effect of Large Scale Fading and Small Scale Fading 19

Figure 2.7: CELL-ID Wireless Location Method 22

Figure 2.8: AOA Wireless Location Method 23

Figure 2.9: TOA Wireless Location 24

Figure 2.10: TDOA Wireless Location 25

Figure 2.11: GPS 26

Figure 2.12: AGPS 30

Figure 2.13: Performance Comparison between Location Methods 32

Figure 2.14: 7-Cell Sub-System Used in DOP Analysis 35

Figure 2.15: HDOP and VDOP with 4 BSs Involved 35

Figure 2.16: HDOP and VDOP with 5 BSs Involved 36

Figure 2.17: HDOP and VDOP with 6 BSs Involved 36

Figure 2.18: HDOP and VDOP with 7 BSs Involved 36

Figure 2.19: HDOP and VDOP with 5 BSs and 1 GPS Satellite Involved 37

Figure 2.20: HDOP and VDOP with 5 BSs and 2 GPS Satellite Involved 38

Figure 2.21: Variation of HDOP and VDOP with 5 BSs and 1 GPS Satellite Involved with Respect to GPS Satellite Position 38

Figure 2.22: Variation of HDOP and VDOP with 5 BSs and 2 GPS Satellite Involved with Respect to GPS Satellite Position 38

Figure 3.1: Generation of Pilot Channel Signals 43

Figure 3.2: Other-Cell Interference at MS (r,θ) 46

Figure 3.3: Geometry of Other-Cell Interference 47

Figure 3.4: Comparison of Same-Cell Interference and Other-Cell Interference 48

Figure 3.5: Hearability of a Normal Cellular Network 49

Figure 3.6: Hearability in a Log-Normal Propagation Channel Cell size: 3000 m 4^{th} order propagation model log-normal standard deviation $\sigma = 8$ dB 55

Figure 3.7: Two Cases in the Hearability Analysis 55

Figure 3.8: Diagram of IS-95 Signal Acquisition 57

Figure 3.9: pdfs of Central Chi-Squared Distribution 61

Figure 3.10: pdfs of Non-Central Chi-Squared Distribution 62

Figure 3.11: Pilot Signal Detection 63

Figure 3.12: Upper Bound on Detection Probability versus False Alarm Probability in the Case of $E_c/\mathcal{N}_0 = -15$ dB 64

Figure 3.13: Relationship Between Integration Length and Receiver Sensitivity (P_F fixed) 66

Figure 3.14: Relationship Between Integration Length and Receiver Sensitivity (P_D fixed) 66

Figure 3.15: Relationship between Non-Centrality Parameter and Integration Length with Respect to Frequency Error 69
Figure 3.16: Hearability of Receiver Rx1 (Integration Length = 112 Chips)..... 71
Figure 3.17: Hearability of Receiver Rx2 (Integration Length = 650 Chips)..... 72
Figure 3.18: Hearability of Receiver Rx3 (Integration Length = 1500 Chips)..... 72
Figure 3.19: PR-IPDL Idle Period Pattern (Shaded Block Represents the Idle Period)... 74
Figure 3.20: Difference between Non-IPDL Methods and PR-IPDL Methods..... 75
Figure 3.21: Hearability of Receiver RX1 with PR-IPDL..... 76
Figure 3.22: Hearability of Receiver Rx2 with PR-IPDL..... 77
Figure 3.23: Hearability of Receiver Rx3 with PR-IPDL..... 77
Figure 3.24: TA-IPDL Idle Period Pattern 78
Figure 3.25: Difference between PR-IPDL Method and TA-IPDL Method 79
Figure 4.1: Relationship Among x , y and r_1 94
Figure 4.2: Cone Approximation 96
Figure 4.3: Original and Desired Approximation 98
Figure 4.4: Approximation Error 98
Figure 4.5: Algorithm Performance Comparison at a Single Point (4 TDOAs, 2 AOAs, STD_{TDOA} =100 m, STD_{AOA} =1 degree)..... 100
Figure 4.6: Influence of AOA Measurement Accuracy on Location Accuracy 4 TDOAs, 2 AOAs, STD_{TDOA} =100 m, STD_{AOA} =5 degrees 102
Figure 4.7: Influence of AOA Measurement Accuracy on Location Accuracy 4 TDOAs, 2 AOAs, STD_{TDOA}=100 m, STD_{AOA} =0.3 degree..... 102
Figure 4.8: HDOP with Respect to MS-Serving BS Separation..... 104

Figure 4.9: Positioning Accuracy Comparison in the Case of Different AOA Measurement Accuracies and the same TDOA Measurement Accuracy (σ_{TDOA} = 35 m) 106

Figure 4.10: Positioning Accuracy Comparison in the Case of Different AOA Measurement Accuracies and the same TDOA Measurement Accuracy (σ_{TDOA} = 100 m) 107

Figure 4.11: Positioning Accuracy with NLOS Errors Exist (σ_{TDOA} = 35 m) 111

Figure 4.12: Positioning Accuracy with NLOS Errors Exist (σ_{TDOA} = 100 m) 112

Figure 4.13: Histogram of Exponential NLOS Errors in an Urban Environment 113

Figure 4.14: Samples of Exponential NLOS Errors in an Urban Environment..... 113

Figure 4.15: Processing Time Comparison between Taylor-Series Method and Two-Step LS Method (Initial Error: 450 metres) 114

Figure 4.16: Processing Time Comparison between Taylor-Series Method and Two-Step LS Method (Initial Error: 0 metres) 115

Figure 5.1: NLOS Error 118

Figure 5.2: Hyperbola Intersection 121

Figure 5.3: Intersections Offset by NLOS Errors 122

Figure 5.4: Steps in NLOS Mitigation Algorithm 123

Figure 5.5: Selection of ε for Distribution Function Construction 126

Figure 5.6: The Distribution of γ_c^i for NLOS-Free BS and NLOS-Corrupted BS 131

Figure 5.7: Determination of Minimum Detectable NLOS Error..... 131

Figure 5.8: NLOS Error Correction 134

Figure 5.9: Successful NLOS Error Detection Probability with Two NLOS Errors (250 m, 450 m), (350 m, 550 m) , and (450 m, 750 m) 139
Figure 5.10: Successful NLOS Error Detection Probability with Three NLOS Errors (250 m, 350 m, 450 m), (350 m, 450 m, 550 m) and (450 m, 550 m, 750 m) 140
Figure 5.11: MS Position Estimation Accuracy with One NLOS Error of 200 m 141
Figure 5.12: MS Position Estimation Accuracy with One NLOS Error of 300 m 142
Figure 5.13: MS Position Estimation Accuracy with One NLOS Error of 400 m 142
Figure 5.14: Positioning Accuracy with Two NLOS Errors (of 250 m, 450 m) 143
Figure 5.15: Positioning Accuracy with Two NLOS Errors (of 350 m, 550 m) 144
Figure 5.16 Positioning Accuracy with Two NLOS Errors (of 450 m, 750 m) 144
Figure 5.17: Positioning Accuracy with Three NLOS Errors (250 m, 350 m, 450 m)... 145
Figure 5.18: Positioning Accuracy with Three NLOS Errors (350 m, 450 m, 550 m)... 145
Figure 5.19: Positioning Accuracy with Three NLOS Errors (450 m, 550 m, 700 m)... 146
Figure 5.20: Probability of Successful NLOS Error Detection (Both missing detection and false detection not allowed) 148
Figure 5.21: Probability of Successful NLOS Error Detection (Missing detection not allowed; False detection allowed)..... 149
Figure 5.22: Estimated NLOS Errors for Each BS 150
Figure 5.23: Positioning Accuracies of Three Positioning Methods 151
Figure 5.24: Positioning Accuracy with σ_{TOA}=100 m 152
Figure 5.25: Positioning Accuracy with σ_{TOA}=35 m 153
Figure 5.26: Positioning Accuracy with σ_{TOA}=10 m 153
Figure 6.1: Macrocell Power-Delay Profiles (Vanderveen, 1997) 158

Figure 6.2: GBSB Macrocell Model 160
Figure 6.3: Scatterer Region of a GBSB Macrocell Model 161
Figure 6.4: Joint TOA/AOA Distribution of GBSB Macrocell Model 162
Figure 6.5: AOA Distribution with All multipaths Signals Considered 163
Figure 6.6: AOA Distribution with Only Early Multipath Signals Considered 164
Figure 6.7: GBSB Microcell Model 164
Figure 6.8: Joint TOA/AOA Distribution in a Microcell (GBSB Microcell Model) 166
Figure 6.9: Marginal AOA Distribution for GBSB Microcell Model 167
Figure 6.10: Vector Channel Estimation 168
Figure 6.11: Uniform Linear Array 169
Figure 6.12: Raised Cosine Pulse Function 171
Figure 6.13: Dual Direction Shift Invariance Structure of a URA (Chareyre, 2002) 178
Figure 6.14: Mean AOA Estimation Errors vs. SIR and Sensor Number 181
Figure 6.15: Mean TOA Estimation Errors vs. SIR and Sensor Number 181
Figure 6.16: RMS of AOA Estimation Errors vs. SIR and Sensor Number 182
Figure 6.17: RMS of TOA Estimation Errors vs. SIR and Sensor Number 182
Figure 6.18: The Probability of Successful Estimation 184
Figure 6.19: The Mean of TOA Estimation Errors 185
Figure 6.20: The RMS of TOA Estimation Errors 185
Figure 6.21: Mean of AOA Estimation Errors 186
Figure 6.22: RMS of AOA Estimation Errors 186
Figure 6.23: The Cellular System Used in Simulation 188

Figure 6.24 Mean and RMS of Location Errors for Scenario 1 (4 TOAs plus 1 AOA without LOS component)..... 189
Figure 6.25: Mean and RMS of Location Errors for Scenario 2 (4 TOAs plus 1 AOA with LOS component)..... 189
Figure 6.26: Mean and RMS of Location Errors for the Scenario 3 (7 TOAs plus 3 AOAs without LOS component)..... 191
Figure 6.27: Mean and RMS of Location Errors for Scenario 4 (7 TOA plus 3 AOA with LOS component)..... 191
Figure 7.1: Hearability of a Normal Cellular Receiver..... 196
Figure 7.2: GPS Signal Fading Distribution in Open Sky Area 198
Figure 7.3: GPS Signal Fading Distribution in Urban Canyon Area..... 198
Figure 7.4: GPS Signal Fading Distribution inside a Garage 199
Figure 7.5: ECEF System, WGS84, and Local Level Frame 200
Figure 7.6: System Layout for Simulation..... 204
Figure 7.7: Benchmark Trajectory and Observed GPS DOPs for Epoch-by-Epoch Combination..... 206
Figure 7.8: Trajectory and DOPs of Two TDOAs-Only Solution..... 206
Figure 7.9: Trajectory and DOPs of Three TDOAs-Only Solution..... 207
Figure 7.10: Trajectory and DOPs of One TDOA Plus Two GPS Satellites Solution... 207
Figure 7.11: Trajectory and DOPs of Two TDOAs Plus Two GPS Satellites Solution. 208
Figure 7.12: Trajectory and DOPs of Three TDOAs Plus Two GPS Satellites Solution208
Figure 7.13: Architecture of GPS and Cellular Network Combination..... 210

Figure 7.14: Benchmark Trajectory for Position Domain Kalman Filter-Based Combination 214
Figure 7.15: Trajectories of Position Domain KF Based TDOA only Solution 214
Figure 7.16: Trajectories of Position Domain KF Based TDOAs and GPS Combination 215
Figure 7.17: System Dynamic Model Used in the Measurement Domain Kalman Filter 216
Figure 7.18: Estimated Trajectories by TOA only Measurement Domain Kalman Filter 220
Figure 7.19: Estimated Trajectories by TOA/ GPS Measurement Domain Kalman Filter 221
Figure 7.20: Performance Degradation Due to NLOS Errors and Receiver Noise 225
Figure 7.21: Performance Improvement Due to NLOS Error Mitigation 229
Figure 7.22: Performance of GPS-Assisted NLOS Error Mitigation 232

LIST OF SYMBOLS

β_i	AOA of MS with respect to BS_i; fading of a multipath replica
$\boldsymbol{\theta}$	Vector of AOAs of multipath signals
λ	Non-centrality parameter
μ	Path loss power
ρ_i	GPS pseudorange
ς_p	Fraction of transmit power allocated to the pilot signal
σ_m^2	Variance of measurements
σ_p^2	Variance of location estimate
$\boldsymbol{\Gamma}$	DFT matrix
$\mathbf{a}(\theta_i)$	Steering vector of an antenna array
$g(t)$	Waveform shaping function
$\mathbf{h}(t)$	Discrete vector channel impulse response
k	Boltzman's constant
r_i	TOA or distance between MS and BS_i
r_{ij}	TDOA or distance difference between MS-BS_i and MS-BS_j
(u,v)	Coordinates in a non-orthogonal cell coordinate system
$\mathbf{x}$	MS position
$\hat{\mathbf{x}}$	Estimate of MS position

$\mathbf{A}$	Design matrix
$\mathbf{A}(\boldsymbol{\theta})$	Array manifold matrix
$C_I(t)$	I-channel PN sequence
$C_Q(t)$	Q-channel PN sequence
E	Eastern coordinate in local level frame
E_C	Chip energy
F	Noise Figure
$\mathbf{F}$	Time array manifold matrix
$\mathbf{G}$	Design matrix
G_C	Base station antenna gain
G_m	Mobile antenna gain
L	Path loss
N	Northern coordinate in local level frame
N_0	Thermal noise power density
P_C	Total transmit power of a BS
P_I	Interference power
$P_{I,SC}$	Same-cell interference
$P_{O,SC}$	Other-cell interference
P_P	Pilot signal power
$\mathbf{Q}$	Variance-covariance matrix of measurements
R_c	Cell size

P_D	Detection probability
P_F	False alarm probability
U	Up coordinate in local level frame
$\mathbf{X}_i$	Position of BS_i

Conventions

a) Matrices are uppercase and bold

b) Vectors are lowercase and bold

c) The following operators are defined

$\dot{\mathbf{x}}$	Derivative with respect to time
$\mathbf{A}^T$	Matrix transpose
$\mathbf{A}^H$	Matrix conjugate transpose
$\mathbf{A}^{-1}$	Matrix inverse
$f(\ )$	Function of
$\hat{\mathbf{x}}$	Estimation of or adjusted value

LIST OF ABBREVIATIONS

AGPS	Assisted GPS
AMPS	Advanced Mobile Phone System
AOA	Angle of Arrival
BS	Base Station
BSC	Base Station Controller
BST	Base Station Transceiver
CDMA	Code Division Multiple Access
DF	Distribution Function
DFT	Discrete Fourier Transformation
DLL	Delay Locked Loop
DOP	Dilution of Positioning
E-911	Enhanced-911
EDOP	Eastern DOP
ESPRIT	Estimation of Signal Parameters via Rotational Invariance Techniques
FCC	Federal Communication Commission
FDMA	Frequency Division Multiple Access
FM	Frequency Modulation
GBSB	Geometric Based Single Bounced
GPS	Global Positioning System
GSM	Groupe Speciale Mobile or Global Systems for Mobile Communication

HDOP	Horizontal DOP
INS	Inertial Navigation System
IPDL	Idle Period Downlink
IS-95	Interim Standard 95
KF	Kalman Filter
LOS	Line-of-sight
LS	Least Squared
MS	Mobile Station
MSC	Mobile Switching Centre
NDOP	North DOP
NLOS	Non-line-of-sight
P code	Precise Code
PL	Pass Loss
PLL	Phase Locked Loop
PN code	Pseudorandom Noise code
PR-IPDL	Pseudorandom IPDL
PSTN	Public Switched Telephone Network
PUF	Power Up Function
RMS	Root Mean Squared
SIR	Signal Interference Ratio
TACS	Total Access Communications System
TA-IPDL	Time Aligned IPDL
TDMA	Time Division Multiple Access

TDOA	Time Difference of Arrival
TOA	Time of Arrival
TTFF	Time to First Fix
ULA	Uniform Linear Arrays
UMTS	Universal Mobile Telephone Service
URA	Uniform Rectangular Arrays
WGS84	World Geodetic System 1984

CHAPTER 1

INTRODUCTION

1.1 Motivations for Wireless Location

The basic problem of wireless location is that of estimating the geographic position of cellular phones. It has received considerable attention over the past few years. The impetus for this research stems mainly from a series of regulations passed in 1996 by the United States Federal Communications Commission (FCC). The intent of these regulations is to encourage cellular service providers to improve the quality of Enhanced 911(E-911) service for cellular phone users. The mandate was deemed necessary due to the rising number of emergency calls made from cellular phones. A recent study shows that wireless 911 calls account for 43 percent of all 911 calls received and that this percentage is increasing rapidly (Porcino, 2001). The accuracy requirement of the E-911 mandate was initially set to within 125 metres for 67% of users and within 300 metres for 95% of users. However, these numbers were subsequently reduced to within 50 metres and 150 metres, respectively, for handset-based solutions; 100 metres and 300 metres, respectively, for network-based solutions (FCC, 2001). Besides FCC E-911, there are other benefits that motivate wireless location, such as roadside assistance, fleet management, and intelligent transportation systems (Caffery and Stüber, 1994). Wireless

location can also be used for cellular network performance improvement (Paton et al, 1991); for example, it can be used in mobile management and for handover assistance.

Generally, ground-based wireless location methods utilize signals of a cellular network itself. The raw measurements can be signal strength, signal transmission time, or signal transmission direction. The position of a mobile station (MS) can be determined by multilateral or multi-angular principles. Ground-based wireless location methods can be further divided into network-based methods and MS-based methods in terms of the functionalities of the MS and the cellular network involved in. More detailed discussion can be found in Chapter 2.

Unfortunately, wireless location was not a consideration in the original cellular phone system design. Due to the complexity of mobile channels, there exist many challenges in realizing a wireless location scheme meeting the performance requirements proposed in the FCC E-911 mandate. Among the most significant of these challenges are hearability, multipath/NLOS propagation, and interference problems (Caffery, 2000). In this thesis, several methods are proposed to handle these issues to mitigate wireless location errors.

1.2 Technical Challenges in Wireless Location

At first glance, the accuracy requirement appears to be relatively loose, since the most stringent accuracy requirement is 50 metres at a probability of 67%. However, several error sources stemming from the complicated system of radio channels make this a

difficult level to reach. The following are challenges that need to be considered when designing a wireless location system.

1.2.1 Accuracy Problem

Two types of accuracies are often studied. One is measurement accuracy and the other is location estimate accuracy. These two classes of accuracy are related by the following formula

$$\sigma_p = DOP \cdot \sigma_m \tag{1.1}$$

where σ_p is the standard deviation of location estimate; σ_m is the standard deviation of measurements; and DOP is the dilution of precision (DOP). This formula indicates that in order to get a better location estimate one needs to not only improve measurement accuracy but also receive signals from multiple base stations (BSs) with good geometry to minimize DOP .

1.2.2 Hearability Problem

Hearability is defined in this thesis as the ability of a mobile station (MS) to receive signals from multiple BSs, and it is evaluated by the number of BSs that a MS can detect or hear. The higher the value, the better is the hearability (Bartlett, 2002). Significantly, there exists an operational conflict between wireless location and wireless communications. Whereas wireless location requires that the MS hear as many BSs as possible to improve location accuracy, wireless communications tries to minimize the power of all signals to mitigate interference and to increase system capacity. As a

consequence, it is difficult for an MS to detect enough BSs for location purposes in current cellular phone networks. The lack of available BSs limits the location service coverage area and impedes the implementation of location systems.

1.2.3 The Non-Line-of-Sight (NLOS) Propagation Problem

Most location systems require Line-of-Sight (LOS) communication links. However, such direct links do not always exist in reality because of the intrinsic complexity of mobile channels. Quite often, an MS can only hear multipath signals from a BS, resulting in the introduction of Non-Line-of-Sight (NLOS) errors. NLOS errors are normally much larger than receiver noise and can degrade the location estimate substantially. Several papers have addressed this issue. In Woo et al (2000), NLOS errors are identified by calculating the standard deviation of a series of range measurements and comparing that with a certain threshold. A time-history based hypothesis test is proposed in Wylie and Holtzman (1996) to identify and remove NLOS errors. In Borrás et al (1998), a theoretical decision framework for NLOS identification is formulated where NLOS errors are modeled as non-zero mean Gaussian random variables. For an unknown NLOS error distribution, a residual weighting algorithm is proposed in Chen (1999b) for a time of arrival location system to identify BSs which suffer from NLOS propagation, based on the weighted residuals for all possible BS combinations.

1.3 Scope of Research

This thesis is a study of ground-based wireless location system design. It discusses, and then attempts to solve, some critical problems that may appear in real world wireless location system implementation. Finally, it proposes feasible wireless location schemes. The study in the thesis is in fact a high level concept study since all algorithms proposed herein are based on raw measurements that are independent of the signals and techniques used. As a result, the algorithms are somewhat universal and can be applied to GSM, CDMA, and UMTS systems. It is worth noting that the pilot signal based on the IS-95 CDMA system is taken as an example in the hearability analysis, but the method that is developed in this thesis to conduct the analysis can be applied to other systems.

The diagram of a proposed wireless location scheme containing the major work of this thesis is shown in Figure 1.1.

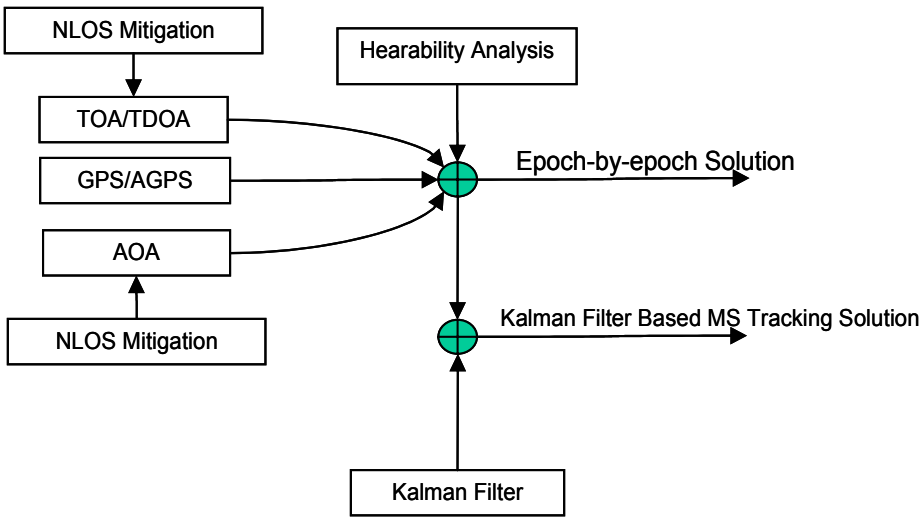

Figure 1.1: Proposed Wireless Location Scheme

Hybrid solutions are usually preferred since they are able to make use of more information to achieve superior performance. In the thesis, such a hybrid algorithm- time difference of arrival/angle of arrival (TDOA/AOA) solution is discussed in detail. Both a strictly theoretical study and simulation tests have been done to analyze algorithm performance. As expected, the results demonstrate an obvious performance improvement compared to TDOA-only solutions.

In a TDOA wireless location system, the position of an MS is obtained by solving a hyperbolic system as that in the LORAN-C navigation system (Enge et al, 1990). This is by no means a trivial problem. In reality, a Taylor-series linearization method and two-step least squares (LS) method (Chan and Ho, 1994) can be applied. However, both of these techniques have their drawbacks. The former imposes a heavy computational burden and divergence issues while the latter provides inferior location accuracy. To improve performance on these fronts, a so-called enhanced two-step LS method is proposed. Simulation tests show that it has almost the same level of accuracy as that of a Taylor-series linearization method while maintaining the computational advantage of the original two-step LS method.

As mentioned above, NLOS propagation errors are a significant concern in wireless location because they are much larger than receiver noise and are difficult to eliminate due to their time variant property. If not properly handled, they can result in poor MS position estimation. This thesis proposes two methods to remove or mitigate NLOS errors. The first is called the Distribution Function-based method. It mitigates NLOS

errors in TOA/TDOA measurements by studying the spatial distribution of all the possible MS locations that are actually the intersections of hyperbolas derived from TDOA measurements. The second is a channel estimation-based method. It mitigates NLOS errors of both TOA measurements and AOA measurements by only using the earliest signals since, the earlier the arriving signal, the smaller the NLOS error. To extract the earliest signals, a two dimensional array signal processing technique, 2-D Unitary-ESPRIT (Haardt and Nossek, 1995), is utilized. It can estimate both TOAs and AOAs accurately while imposing a low computational burden.

Hearability is another important consideration in wireless location. Cellular Network-based schemes require that at least three BSs be heard by the MS to be located. However, hearability is poor for normal cellular systems due to the near-far effect and multiple access interference. Two methods are fully discussed in the thesis to improve hearability. One is an enhanced signal processing method which tries to improve hearability by extending the integration time of incoming signals. The second method is the idle period down link (IPDL) method (Ericsson, 1999) where the near-far effect is mitigated by stopping the transmission at the serving BS to let MSs hear signals from other BSs.

MS tracking is usually realised by Kalman Filter (KF) techniques. Compared to the normal LS method, a KF-based method can make use of past data to improve location performance. Kalman filtering is also an ideal technique to integrate data from different sensors. In the thesis, KF is used to integrate GPS data and cellular network data since both systems suffer from hearability or signal availability issues and the combination of

them provides more information for location estimation. Test results show that the integration can improve location accuracy and availability.

Original Work

The summary of the original work in this thesis is as follows:

- Proposes the enhanced two-step LS algorithm and applies it to the hybrid TDOA/AOA wireless location scheme. This algorithm can decrease computational burden while maintaining positioning accuracy.
- Proposes a Distribution Function-based NLOS error mitigation algorithm for TOA/TDOA measurements.
- Proposes a channel estimation-based NLOS error mitigation algorithm for AOA measurements.
- Proposes two schemes to integrate GPS with cellular network measurements to improve wireless location performance. They are an epoch-by-epoch integration scheme and a Kalman filter-based MS tracking scheme.
- Signal availability/hearability is also fully discussed herein. Hearability improvement due to the enhanced signal processing technique and IPDL techniques is demonstrated by both theoretical analysis and simulation results although these two methods are originally proposed by other researchers.

1.4 Thesis Outline

After a brief introduction in this chapter, an overview of the background knowledge related to ground-based wireless location is presented in Chapter 2. The background information includes the basic principles of a cellular system, commonly used wireless location algorithms, and a general description of the mobile signal channel architecture. In Chapter 3, the hearability analysis is addressed and the performance of the enhanced signal processing technique and the IPDL technique is fully discussed.

Chapter 4 proposes an enhanced two-step LS TDOA wireless location algorithm. This method can achieve similar accuracy to that of a Taylor-series linearization method while maintaining the computational advantage of the original two-step LS method.

To mitigate NLOS errors, two efficient methods are proposed in Chapters 5 and 6. The distribution function method discussed in Chapter 5 identifies and removes NLOS errors by studying the spatial distribution of hyperbola intersections that are actually coincident with possible MS locations. The channel estimation-based method discussed in Chapter 6 mitigates NLOS errors in both TOA and AOA measurements by only using early arriving signals.

MS tracking is discussed in Chapter 7 where an extended KF is introduced to integrate GPS and cellular network measurements. Compared to cellular network only solutions, the method presented herein improves both location determination accuracy and solution

availability. Chapter 8 contains the final conclusions and some recommendations for future work.

CHAPTER 2

AN OVERVIEW OF WIRELESS NETWORK AND WIRELESS LOCATION TECHNIQUES

2.1 Introduction

Ground-based wireless location techniques need to measure signals emitted from either base stations or mobile stations. To develop high performance wireless location schemes, it is, thus, important to know how a cellular system works; how signals are propagated in wireless channels; and how various wireless location schemes work. Thus, three major areas are covered in this chapter:

- Wireless communications systems
- Wireless channels
- Overview of wireless location techniques

2.2 Wireless Communications Systems

In recent times, wireless communications have had profound effects on our day-to-day lives. In less than 10 years, cellular telephones have attracted more than several hundred million subscribers in the United States, Europe, and Asia (Caffery, 2000). This dramatic

development is just the start of the forthcoming revolution in telecommunication services. In the near future, telecommunication devices will be associated with homes, offices, and vehicles. To meet the unprecedented demand for a new mode of communications, a significant number of wireless communication techniques have emerged sine the 1970's (Kuruppillai et al, 1997).

The first-generation cellular systems which appeared in the 1980's were analog systems, such as the AMPS (Advanced Mobile Telephone System) in Northern America and TACS (Total Access Communications System) in Europe. AMPS and TACS use a frequency modulation (FM) technique for radio transmission. Cellular traffic is multiplexed onto an FDMA (frequency division multiple access) system at a data rate of 8 to 10 kbps.

The second-generation (2G) systems used digital multiple access technologies such as TDMA (time division multiple access) and CDMA (code division multiple access). 2G systems, such as GSM in Europe and IS-95 CDMA in North America, appeared in the 1990's and operate using a data rate of 14.4 kbps.

Currently, third-generation systems are being developed to try to solve several challenging technical issues, such as the provision of seamless services across both wired and wireless networks and universal mobility. Examples of third-generation systems include UMTS in Europe and CDMA2000 in North America. Both of these systems use wide band CDMA techniques to increase the data rate up to 2 Mbps. Such a high data

rate makes these two systems suitable for high-volume data transactions including multimedia communications.

2.2.1 Cellular Network Architecture

A 2G cellular network is composed out of the following entities (Walters and Kritzinger 2000) as shown in Figure 2.1:

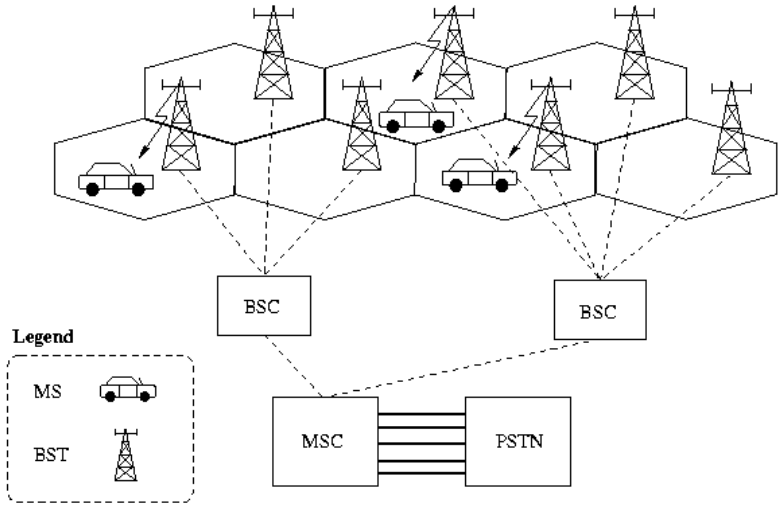

Figure 2.1: 2G Network Architecture

- Mobile station (MS) - Device used to communicate over the cellular network.
- Base station transceiver (BST) - Transmitter/receiver used to transmit/receive signals over the radio interface of the network.
- Base station controller (BSC) - Controls communications between a group of BSTs and a single MSC.
- Mobile switching centre (MSC) - The heart of the network, it sets up and maintains calls made over the network.

- Public switched telephone network (PSTN) - The land-based section of the network.

Figure 2.1 illustrates how the entities are related to one another within the network. BSTs and their controlling BSC are often collectively referred to as the base station (BS) subsystem. A geographic region is divided into cells. Each cell has a BST which transmits data via a radio link to MSs within the cell. A group of BSTs are connected to a BSC. A group of BSCs, in turn, are connected to a mobile switching center (MSC) via either microwave links or telephone lines. The MSC connects to the public switched telephone network (PSTN), which switches calls to other mobile stations or to land-based telephones.

2.2.2 Cellular Coordinate System

In this section, the Cellular Coordinate System (Lee and Miller, 1998) is discussed as an important fundamental concept in understanding cellular systems and in conducting simulations to verify proposed algorithms. Conceptually, an omni-directional base station transmitter has a circular coverage area. As illustrated in Figure 2.2, a large geographical area can be divided into overlapping circular areas. If the circles completely cover the area (i.e. there are no "holes" in coverage) and are all of the same size, they support the concept of hexagonal "cells," each defined as the location affiliated with the nearest base station. Note that the "size" of a hexagonal cell can be given as R_c, the radius of the coverage area, or as $R = R_c \cos 30^o = \left(\sqrt{3}/2\right)R_c = 0.866R_c$.

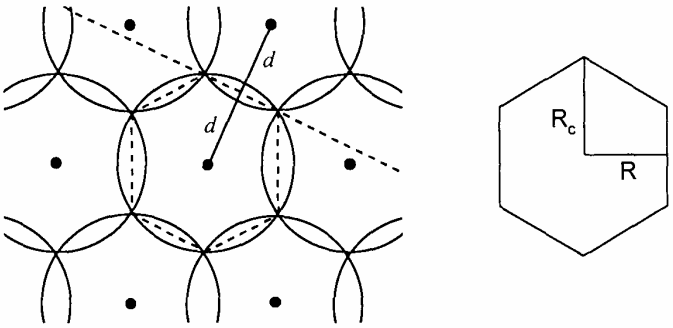

Figure 2.2: Hexagonal Shape Associated with Circular Coverage Area

Figure 2.3 shows a detail of a hexagonal cell layout in a non-orthogonal coordinate system. Using the cell position coordinates (u,v) in this system, the cell centres are located at the positions defined by the coordinate pair,

$$(u,v)=\left(R_c\sqrt{3}i, R_c\sqrt{3}j\right), \tag{2.1}$$

where i and j are integers. In terms of the (u,v) coordinate system, an arbitrary position in a rectangular (x,y) coordinate system with the same origin is

$$x=u\cos 30^{\circ}=\frac{1}{2}u\sqrt{3}\,,\ \ y=u\sin 30^{\circ}+v=\frac{1}{2}u+v \tag{2.2}$$

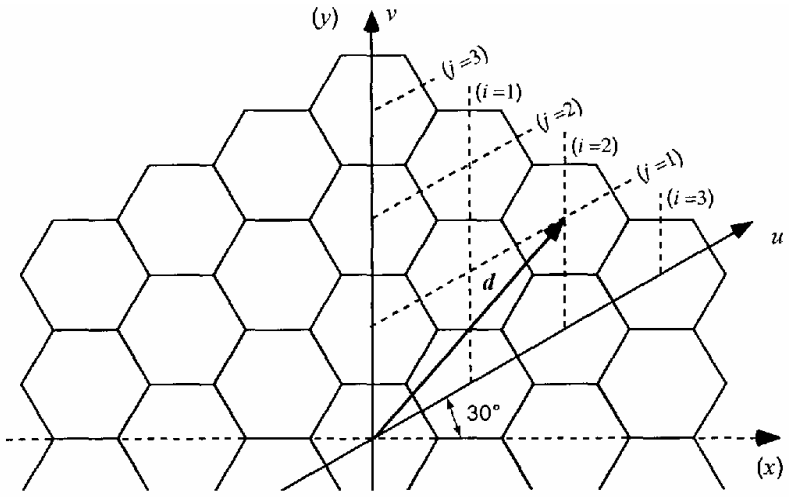

Figure 2.3: Non-orthogonal Cellular Coordinate System

Therefore, the square of the distance between the centres of cell a, whose centre is located at (u_a, v_a), and cell b, whose centre is located at (u_b, v_b), can be computed as

$$\begin{aligned} d_{ab}^2 &= (x_a - x_b)^2 + (y_a - y_b)^2 = \frac{3}{4}(u_a - u_b)^2 + \left(\frac{1}{2}u_a + v_a - \frac{1}{2}u_b - v_b\right)^2 \\ &= (u_a - u_b)^2 + (v_a - v_b)^2 + (u_a - u_b)(v_a - v_b) \\ &= (2R)^2\left[(i_a - i_b)^2 + (j_a - j_b)^2 + (i_a - i_b)(j_a - j_b)\right] \\ &= (3R_C)^2\left[(i_a - i_b)^2 + (j_a - j_b)^2 + (i_a - i_b)(j_a - j_b)\right] \end{aligned} \tag{2.3}$$

In particular, the distance of a cell's centre from the origin of this coordinate system is

$$d = 2R\sqrt{i^2 + j^2 + i \cdot j} = 3R_c\sqrt{i^2 + j^2 + i \cdot j} \tag{2.4}$$

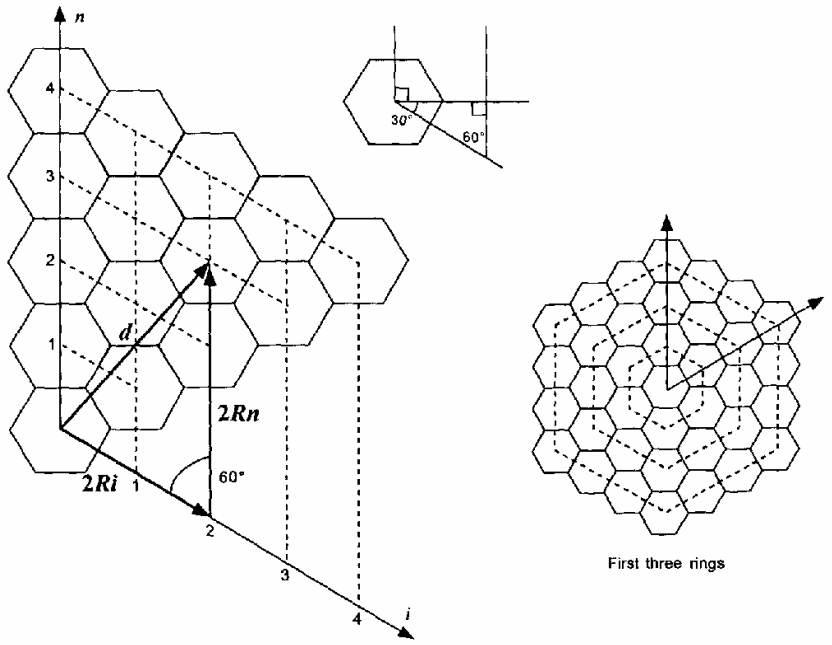

Figure 2.4: Ring Cellular Coordinate System

Another cellular geometry emphasizes the rotational symmetry of the hexagonal grid system by using the notion of a hexagonal "ring" of cells around a center cell, as shown in Figure 2.4. The diagram consists of the centre cell and one of the six 60° sectors around the origin. The coordinates of a cell in the sector are (n, i), where n is the "ring"

number and $i = 1,2,\cdots,n$ indexes the cells in the sector that are in ring n. The squared distance of the nth ring is

$$\begin{aligned} d^2(n,i) &= (2Rn)^2 + (2Ri)^2 - 2(2Rn)(2Ri)\cos 60^\circ \\ &= 4R^2\left(n^2 + i^2 - ni\right) \end{aligned} \tag{2.5}$$

which gives the distance formula

$$d(n,i) = 2R\sqrt{n^2 + i^2 - ni} = R_c\sqrt{3}\sqrt{n^2 + i^2 - ni} \tag{2.6}$$

2.3 Effects of Signal Propagation through Wireless Channels

Wireless channels pose a great challenge for reliable high-speed communications. When a radio signal is transmitted through a wireless channel, the wave propagates through a physical medium and interacts with physical objects and structures, such as buildings, hills, trees, moving vehicles, etc. (Rappaport, 1996). The propagation of radio waves through such an environment is a complicated process that involves diffraction, refraction, and multiple reflections. Also, the speed of the mobile impacts how rapidly the received signal level varies as the mobile moves in space. Modeling all these phenomena effectively has been one of the most challenging tasks related to wireless system design.

A typical wireless communication scenario in an urban area usually involves an elevated fixed base-station antenna, a mobile handset, and a line-of-sight (LOS) propagation path in addition to many reflected paths due to the presence of natural and man-made objects between the mobile and the base station. Figure 2.5 illustrates such an environment (e.g.

Sengupta, 1998). The different propagation paths (LOS as well as reflected paths) change with the movement of the mobile or the movement of objects in its surroundings.

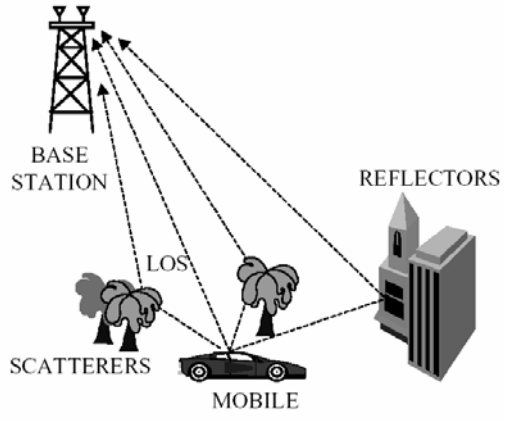

Figure 2.5: A Typical Wireless Propagation Environment

Radio propagation models usually attempt to predict the average signal strength based upon the separation between the transmitter and the receiver. In terms of signal strength variation rate, signal fading can be roughly divided into two categories. Variation in average signal strength over large distances (typically several hundreds of metres) is called large scale fading. Rapid signal strength fluctuation over short distances (typically a few wavelengths) is called small scale fading.

2.3.1 Large Scale Fading

Both theoretical analysis and experimental measurements indicate that the large scale fading is proportional to some power of the distance between the transmitter and the receiver:

$$L(d) \propto \left(\frac{d}{d_0} \right)^{\mu} \tag{2.7}$$

or in dB

$$L(d) = L(d_0) + 10\mu \log_{10}\left(\frac{d}{d_0}\right) \tag{2.8}$$

where d is the separation between the transmitter and the receiver; d_0 is a reference distance which is determined from measurements close to the transmitter; and μ is the large scale fading exponent. The fading exponent determines the rate at which the path loss increases with the separation, d; its value depends on the propagation environment.

2.3.2 Small Scale Fading

Small scale fading refers to rapid variations in signal strength over short distances or short time intervals. It results mainly from multipath propagation due to the presence of reflectors and scatterers near the transmitter and receiver. These paths may add up either constructively or destructively depending on the relative phase differences between individual paths. The amplitude of the composite signal varies over time and distance rapidly because of the short signal wavelength and thus gives rise to small scale fading.

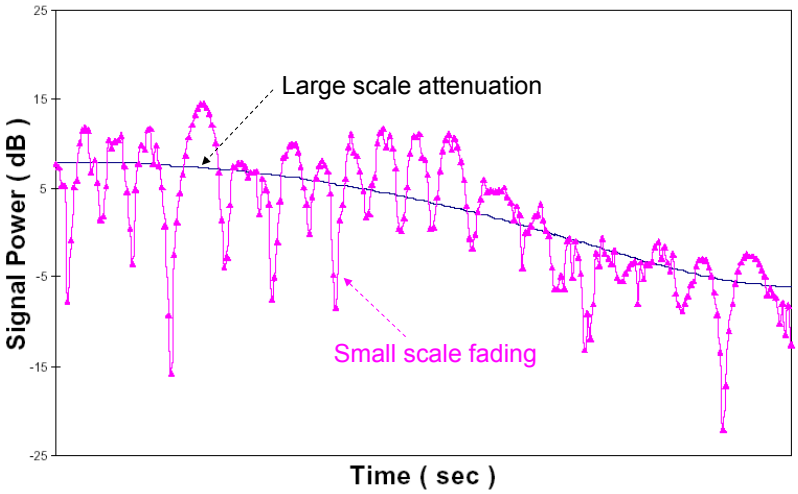

Figure 2.6: Effect of Large Scale Fading and Small Scale Fading

Figure 2.6 shows the signal strength changes with respect to propagation distance (Said, 2002 and Caffery, 2002). The low frequency component is due to large scale fading, and the high frequency component is due to small scale fading resulting from multipath propagation.

From a statistical point of view, the following three statistical distributions are normally represented in a wireless channel: log-normal, Rayleigh, and Ricean. The log-normal distribution describes the envelope of the received signal shadowed by obstructions such as hills, buildings, and trees. The Rayleigh distribution describes the envelope of the received signal resulting from multipath propagation only. The Ricean distribution describes the envelope of the received signal with multipath propagation plus a line-of-sight component. The statistical properties of a wireless channel are discussed in detail in Lee (1997).

2.4 Wireless Location Techniques

2.4.1 Cellular Network-Related Techniques

Cellular network-related wireless location methods can be subdivided into three categories according to the MS and network functionalities. These three categories are pure network-based methods, MS-assisted network-based methods, and MS-based network-assisted methods (Laitinen et al, 2001).

For a pure network-based method, the network fulfills all the positioning functionalities including location measuring and position calculations. An MS itself does not take any active part in the process. Obviously, these methods are applicable to legacy cellular phones. However, the network may require some modifications to accommodate a wide range of hardware products.

The second category, MS-assisted network-based methods, consists of methods which require at least some *active* participation from the MSs. An MS can take part in location measuring or doing some other positioning-dedicated tasks, while most of the positioning functionalities are still completed in the network. The role of an MS is solely to assist the network in positioning.

In MS-based network-assisted methods, the roles of the MSs and the cellular network are reversed in comparison to those in the second category method. An MS makes location measurements and calculates its own position. Thus, the role of the network is simply to assist MSs in location estimation. Methods of this type enable a more dense position fixing rate. In the following section, several network-related wireless location methods are briefly discussed.

2.4.1.1 CELL-ID

CELL-ID is the simplest method for locating a cellular phone and is based on cell identification. An MS can be assigned a location if the cell in which the MS is located can be identified. Since this is an inherent feature of all cellular systems, minimal

changes to existing systems are needed. A cell only has to be associated with a location, such as by association with the coordinates of the BS of this cell, as shown in Figure 2.7.

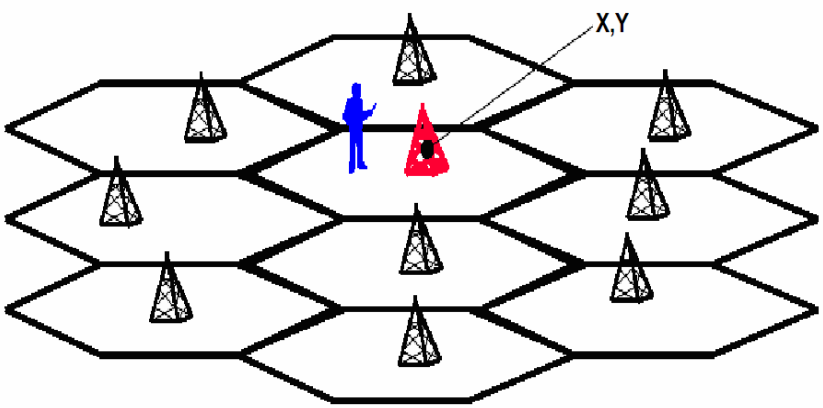

Figure 2.7: CELL-ID Wireless Location Method

This method boasts the additional advantage that no calculations are needed to obtain location information. Thus, the CELL-ID based method is fast and suitable for applications requiring high capacity. However, the drawback is that accuracy depends directly on cell radius which can be very large, especially in rural areas.

2.4.1.2 Angle of Arrival (AOA) Methods

The AOA-based location method is one of the oldest positioning methods. Its early use began during the development of radar, sonar, and antenna array techniques. By means of array signal processing techniques, the direction of an MS with respect to BSs can be measured at BSs. Thus, the MS is at the intersection of the lines derived from AOA measurements as illustrated in Figure 2.8.

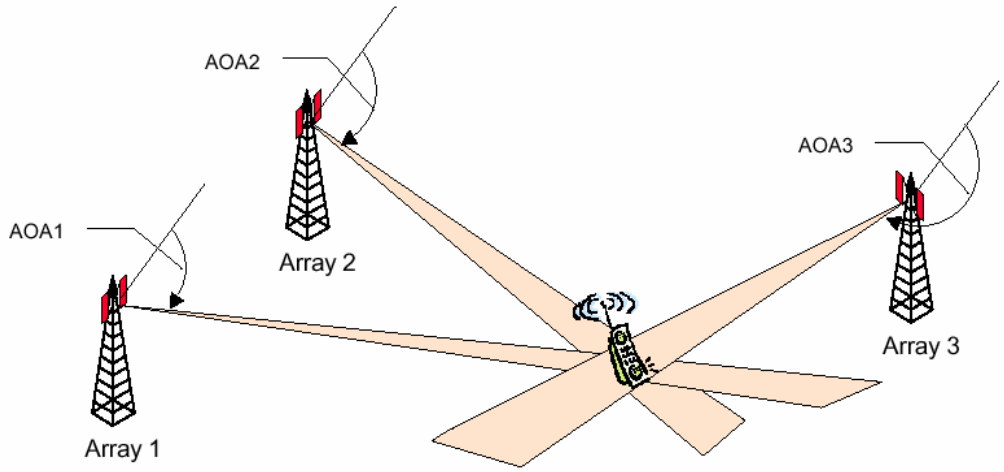

Figure 2.8: AOA Wireless Location Method

The accuracy of the AOA method is dependent on the distances between the MS to be located and the antenna arrays at BSs. The further the MS is from the antenna arrays, the larger is the positioning uncertainty. NLOS signal propagation is a significant source of inaccuracy. When NLOS components exist, AOA measurements will be distorted, thus resulting in degraded positioning accuracy.

2.4.1.3 Time of Arrival (TOA) Methods

The measurements required in this type of positioning method are the absolute signal transmission times between MS and BSs that are equivalent to MS-BS distances. The MS is located at the intersection of several circles, of which the centres are the BSs used, and the radii are the measured MS-BS distances. At least three TOA measurements are required to uniquely determine the 2-D position of an MS, as shown in Figure 2.9.

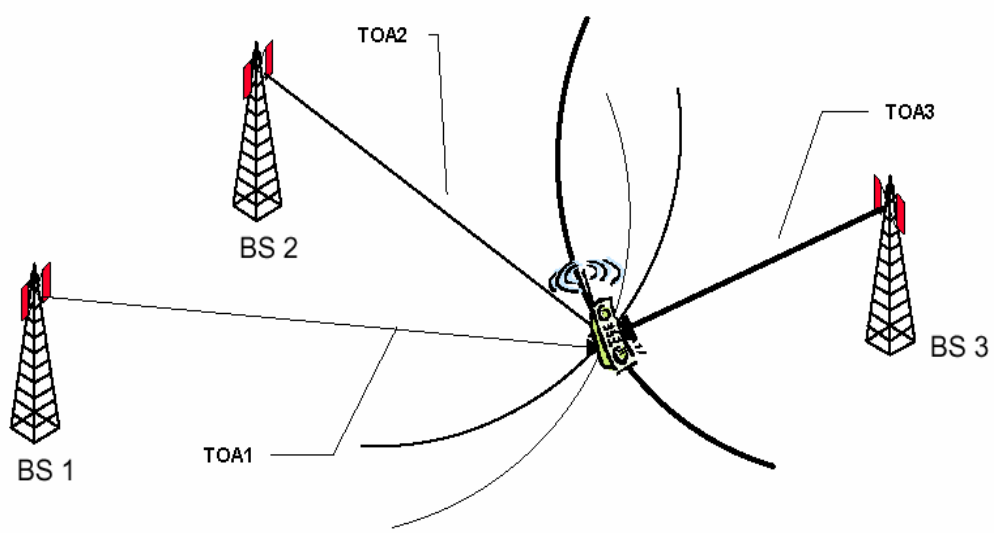

Figure 2.9: TOA Wireless Location

TOA wireless location methods require that all base stations be precisely synchronized to each other and that the MS to be located also be synchronized to the network. For this reason, TOA positioning is feasible only in fully synchronized networks; for example, in IS-95 CDMA systems (Caffery and Stüber 1998).

2.4.1.4 Time Difference of Arrival (TDOA) Methods

The measurements in this type of methods are relative signal transmission times which are equivalent to distance differences. A TDOA measurement defines a hyperbola with the two BSs as the foci. At least three hyperbolae are needed for unique MS position determination, as shown in Figure 2.10

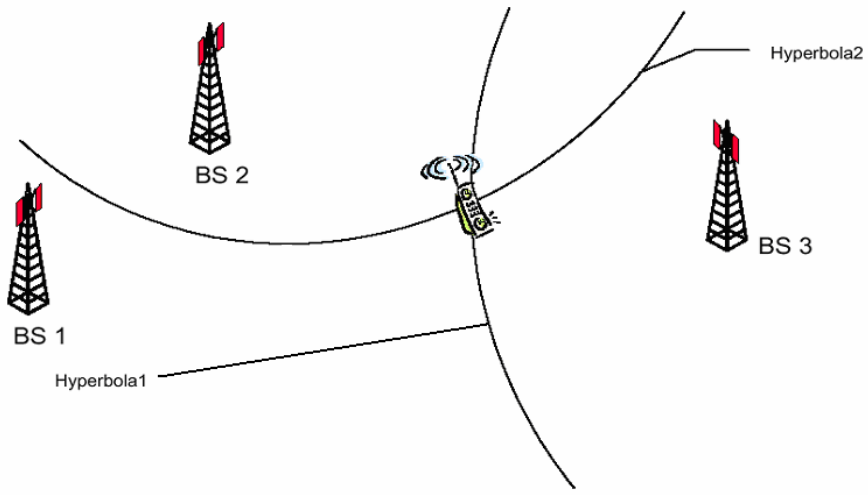

Figure 2.10: TDOA Wireless Location

A TDOA method requires that all base stations involved be synchronized. This can be done either by synchronizing all BSs physically or by bringing all BSs to a common reference time by measuring time differences between BSs. MSs do not need to be synchronized since the MS clock bias is the same with respect to all BSs and differencing any two TOA measurements will cancel out the MS clock bias.

2.4.2 Satellite-Based Positioning Techniques

2.4.2.1 GPS

The Global Positioning System (GPS) is a satellite-based positioning system that can provide 3-D position, velocity and time information to users anytime and anywhere on or near the surface of the Earth. The system currently consists of 28 satellites operated by the United States Air Force, under the control of the U.S. Department of Defence (DoD).

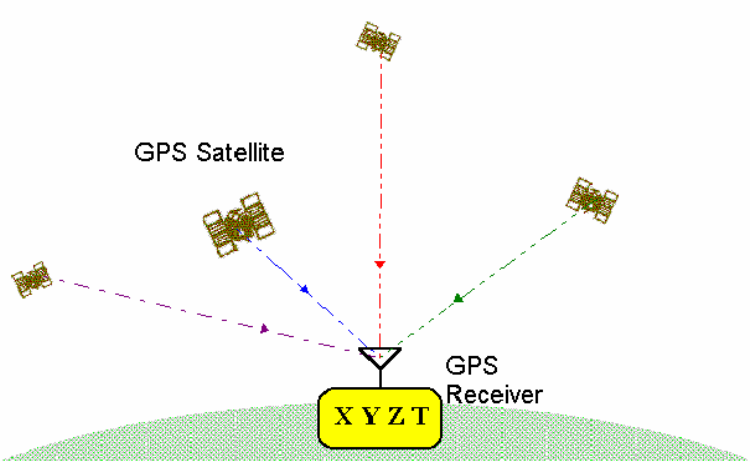

Figure 2.11: GPS

The signals transmitted by GPS satellites are the Course Acquisition (C/A) code and the Precise (P) code, both of which are modulated by navigation messages. By means of well designed phase locked loop and delay locked loop (PLL/DLL) techniques (Kaplan 1996), a GPS receiver can acquire and keep track of such GPS signals to provide very accurate pseudorange measurements. The positioning error of a stand-alone GPS receiver is at the metre level (Parkinson and Spilker, 1996). As shown in Figure 2.11 (Dana, 2000), a GPS receiver can calculate its three-dimensional location using measurements from at least four satellites.

The main advantages of GPS are its global coverage and high accuracy, especially without selective availability (SA) degradation. Another advantage of this location technique is that GPS receivers are not required to transmit anything to satellites, so there is no limit to the number of users that can use the system simultaneously.

However, there also exist several issues that affect the effectiveness of GPS, especially in dealing with emergency services: response time, time-to-first-fix (TTFF), accuracy, and service coverage in weak signal case. GPS signals are quite weak in city core areas and inside buildings. In such environments, a GPS receiver cannot track a sufficient number of satellites because of serious signal attenuation and, therefore, cannot provide location information. Besides these limitations, weak signals require a long processing time which will result in longer response time and longer TTFF. Taking all of these drawbacks into consideration, one finds that traditional GPS techniques are not suitable for wireless location applications.

2.4.2.2 High Sensitivity GPS (HS-GPS)

The GPS signal is not specifically designed for indoor use. The guaranteed signal level, on the surface of the earth, for a right hand circular polarized antenna is –130 dBm. This is a very low power with the signals buried deep in noise and the signals must be acquired through the correlation process which gives a large processing gain. The signal power becomes even lower, less than -150 to -160 dBm, in urban canyons or inside buildings due to extra attenuation. A GPS receiver with higher sensitivity is required in these situations.

In general a longer correlation time enables a receiver to extract or detect signals with lower power levels because the signal to noise ratio at the output of the correlators is in part defined by the integration interval (the time for which the correlation is carried out).

Analysis of detection performance of a single sample of correlation output is well known in detection theory.

However, the integration time is limited by the following factors:

- Time to acquisition: Signal acquisition inside a GPS receiver is a frequency-code delay two dimensional search process. The integration time is the dwell time in a search bin. Obviously, given the frequency-code delay search region, the longer the integration time, the longer the time to acquisition. Besides this, the integration time also affects bin size. A longer coherent integration time implies smaller frequency bins since the power goes to zero at a smaller frequency error. This means smaller bin sizes have to be used when the integration time is extended, which will also increase the time to acquisition for a given search region.
- Data bit transition: The data bits in the GPS signal cause the polarity of the coherent integration to change. This disallows very long coherent integration. If data bits cannot be correctly removed, the maximum integration time is 20 ms. However, the integration time can exceed this limit if the data bits can be correctly predicted and removed.

To decrease the acquisition time, two techniques have been proposed:

- Massive correlator technique: Several hundred or as many as one or two thousand correlators are used in parallel. Thus, the GPS receiver can search multiple bins at the same time to decrease acquisition time.

- Signal frequency prediction technique: The frequency search region can be dramatically narrowed down if the frequency drift can be roughly estimated. Frequency drift is due to three factors: GPS satellite movement which can be easily predicted; receiver clock drift which can be estimated via aiding information; user movement which can predicted in low dynamic situations.

To exceed the 20 ms integration limit, the data bit transition needs to be removed. Two methods are proposed:

- Stand-alone GPS receiver case: Utilize receiver position and other information to predict message bits (Syrjärinne, 2001).
- Assisted GPS: Utilize reference GPS receiver together with communication links to transmit message bits to a high sensitive GPS receiver. This is a promising method in wireless location and will be discussed in the following section.

2.4.2.3 Assisted GPS (AGPS)

Any GPS positioning operation needs to fulfill four principal functions (Baumann et al, 2001):

- determining the code phases (pseudoranges) to the various GPS satellites
- demodulating the satellite navigation message
- determining the time of arrival for measured pseudoranges based on the navigation message

- computing the user's positions via the measured pseudoranges, timing and navigation message data.

Most commercial GPS receivers perform all of these operations independently and allow satellite navigation messages to be extracted from GPS signals after they have been acquired and tracked. With respect to the E-911 requirements, two factors are problematic: collecting information is time-consuming - typically taking between thirty seconds and several minutes - and a high received signal level is required.

Assisted GPS is simply a variation of the conventional GPS system. It works by increasing GPS receiver sensitivity and decreasing the time to first fix (TTFF). In an assisted GPS system, the above functions are distributed among a GPS reference receiver, a location server and a GPS-enabled MS. An example of this system (Porcino, 2001) is shown in Figure 2.12:

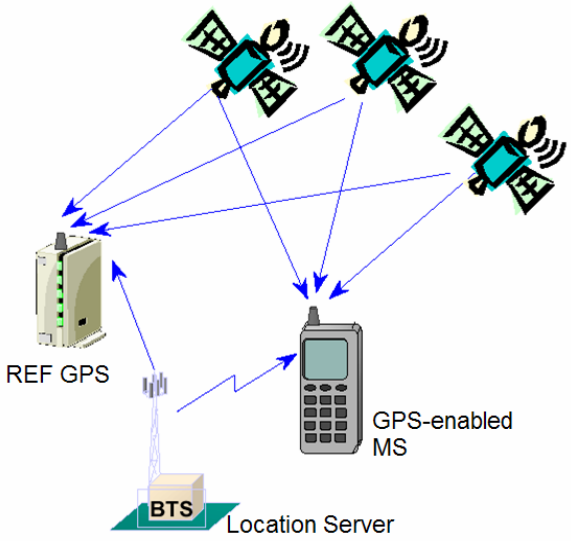

Figure 2.12: AGPS

A reference GPS receiver gathers navigation message and differential GPS (DGPS) correction data for all visible satellites. The location server receives and stores data from the reference GPS receiver and provides aiding data to GPS-enabled MSs. The final MS location can be calculated onboard the MS itself or in the location server. The aiding data consist of a list of satellites in view from the MSs and their relative Doppler offsets. With aiding information, a MS can acquire and track GPS signals much faster than in the unaided case. It can also track far weaker GPS signals because longer integration beyond one message bit can be conducted to obtain a higher processing gain (Chansarkar and Garin, 2002).

Compared to standard GPS schemes, an Assisted-GPS system provides smaller response times, reduced power consumption, higher accuracy, higher sensitivity, and higher location availability in serious fading environments such as urban areas and inside buildings.

2.4.3 Performance Comparison of Location Techniques

Performance comparisons between several wireless location algorithms are presented in this section. The results shown in Figure 2.13 are based on a combination of theoretical analysis and empirical data (Syrjärinne, 2002). The methods under comparison include GPS, AGPS, CELL-ID, TOA and TDOA as described above.

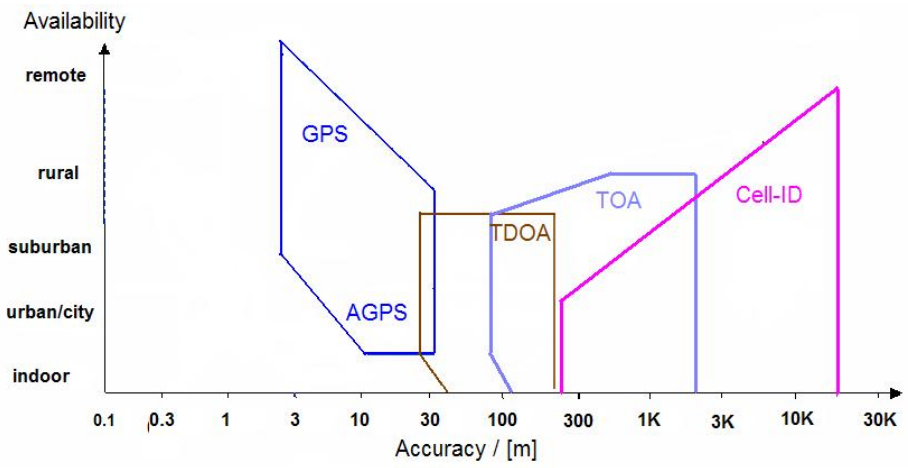

Figure 2.13: Performance Comparison between Location Methods

In the figure, the horizontal axis represents location accuracy and the vertical axis represents location availability. As shown, the CELL-ID method provides very good positioning availability but very poor location accuracy because it depends only on the cell identification technique. The TOA and TDOA methods are moderate in both location accuracy and location availability. The GPS method provides high accuracy from several metres to tens of metres, which is within the range of E-911 requirements. However, its location availability is not good, especially in urban areas and indoor environments due to serious signal attenuation. Such poor location availability can be improved by HSGPS/ AGPS methods since it allows tracking of weak signals with the addition of aiding information. Table 2.1, which is repeated from Syrjärinne (2001), depicts performance differences in terms of reliability, latency, and applicability. Latency is evaluated by TTFF and applicability is evaluated by such factors as power consumption, hardware and software size, network dependency, cost and standardization issues. It is clear from this table and Figure 2.13 that the TDOA and AGPS methods may be feasible for a real world

realization if the effects of environments that produce serious signal attenuation are taken into consideration.

Table 2.1: Comparison among Wireless Location Techniques

Position Techniques		Reliability	Latency	Applicability
GPS	Stand-alone	high	<35 s	High
	AGPS	medium	1-10 s	Medium
Cellular Network	AOA	medium	~10 s	Low
	TOA/TDOA	medium	<10 s	Low

2.5 Dilution of Precision

DOP is an indication of the geometry between the MS to be located and the BSs used in location estimation. It significantly affects the final positioning accuracy. After linearization, a location system can be expressed by

$$\mathbf{l} = \mathbf{A}\mathbf{x} \tag{2.9}$$

where $\mathbf{l}$ are the raw measurements, $\mathbf{x}$ is the MS position to be estimated, and $\mathbf{A}$ is the design matrix. Applying the LS method, $\mathbf{x}$ can be solved as

$$\mathbf{x} = \left(\mathbf{A}^{\mathrm{T}}\mathbf{Q}\mathbf{A}\right)^{-1}\mathbf{A}^{\mathrm{T}}\mathbf{Q}\cdot\mathbf{l} \tag{2.10}$$

where $\mathbf{Q}$ is the variance-covariance matrix of the measurements.

If all of the measurements are assumed to be of the same accuracy and are independent, $\mathbf{Q}$ is a diagonal matrix is of the following form $\mathbf{Q} = \sigma_{\mathrm{l}}^2 \cdot \mathbf{I}$. In this case, the variance-covariance matrix of the MS position is

$$\mathbf{P} = \mathrm{E}\left(\mathbf{x} \cdot \mathbf{x}^T\right) = \left(\mathbf{A}^T\mathbf{A}\right)^{-1} \cdot \sigma_1^2 . \tag{2.11}$$

Obviously, $\left(\mathbf{A}^T\mathbf{A}\right)^{-1}$ is the matrix of multipliers of raw measurement variance which in turn gives position variance. It is thus named the DOP matrix. It contains east DOP (EDOP), north DOP (NDOP), vertical DOP (VDOP), and some covariance terms, and has the following format if suitably arranged

$$\left(\mathbf{A}^T\mathbf{A}\right)^{-1} = \begin{bmatrix} EDOP^2 & & \text{covariance terms} \\ & NDOP^2 & \\ \text{covariance terms} & & VDOP^2 \end{bmatrix} \tag{2.12}$$

Given equation (2.11), smaller DOP values, which indicate better geometry, are desired. Normally, position DOP (PDOP), horizontal DOP (HDOP), and vertical DOP (VDOP) are preferred in positioning accuracy analysis. They are related by the following equations.

$$HDOP = \sqrt{NDOP^2 + EDOP^2} \tag{2.13}$$

$$PDOP = \sqrt{NDOP^2 + EDOP^2 + VDOP^2} = \sqrt{HDOP^2 + VDOP^2} \tag{2.14}$$

The DOP matrix is only dependent on MS-BSs directions. If the direction of the MS to BS_i is evaluated by azimuth angle (Az_i) and elevation angle (E_i) with the MS at the origin, the design matrix can be expressed as

$$\mathbf{A} = \begin{bmatrix} \cos(E_1)*\sin(Az_1) & \cos(E_1)*\cos(Az_1) & \sin(E_1) \\ \cos(E_2)*\sin(Az_2) & \cos(E_2)*\cos(Az_2) & \sin(E_2) \\ \vdots & \vdots & \vdots \\ \cos(E_M)*\sin(Az_M) & \cos(E_M)*\cos(Az_M) & \sin(E_M) \end{bmatrix} \tag{2.15}$$

where M is the number of BSs involved in location estimation.

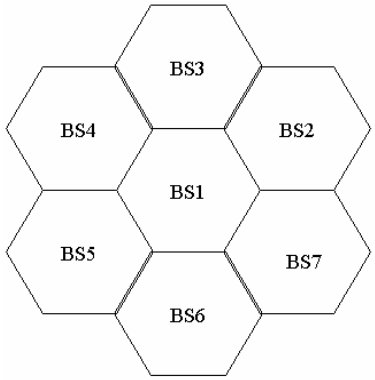

Figure 2.14: 7-Cell Sub-System Used in DOP Analysis

In the following, a 7-cell network, shown in Figure 2.14, is taken as an example to study the variation of the HDOP and VDOP with respect to the number and positions of BSs involved. For simplicity, the MS is assumed to be in the central cell and BSs are selected as a function of their distance to the MS. For example, if 5 BSs are used, the 5 BSs nearest to the MS are selected. All of the 7 cells are of the same size with a cell radius of 3 km and all of the BS antennas are of the same height, i.e. 30 metres.

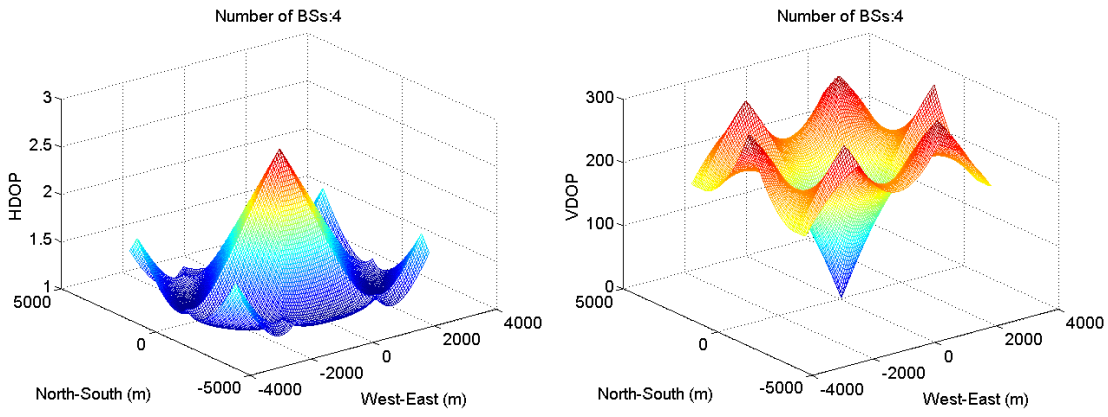

Figure 2.15: HDOP and VDOP with 4 BSs Involved

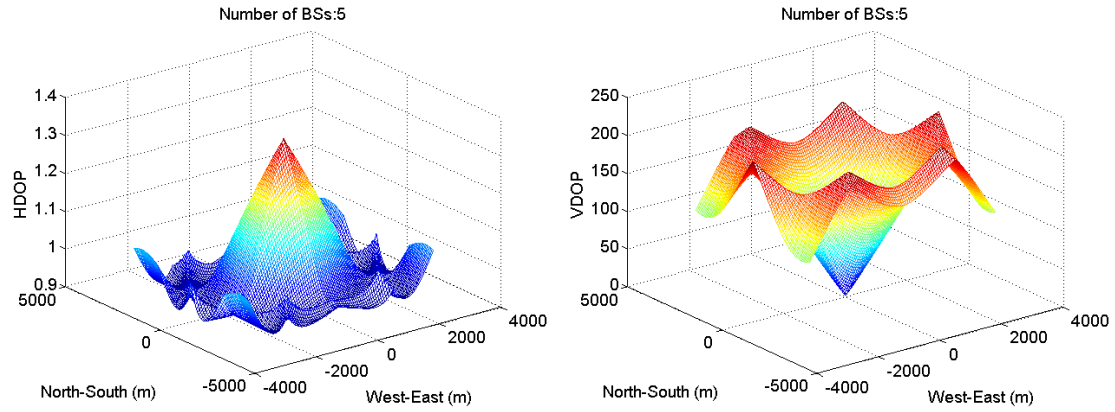

Figure 2.16: HDOP and VDOP with 5 BSs Involved

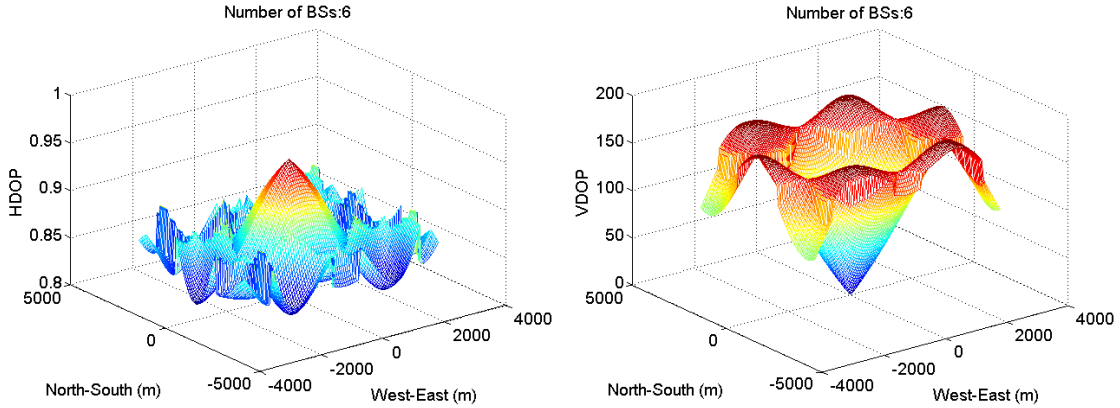

Figure 2.17: HDOP and VDOP with 6 BSs Involved

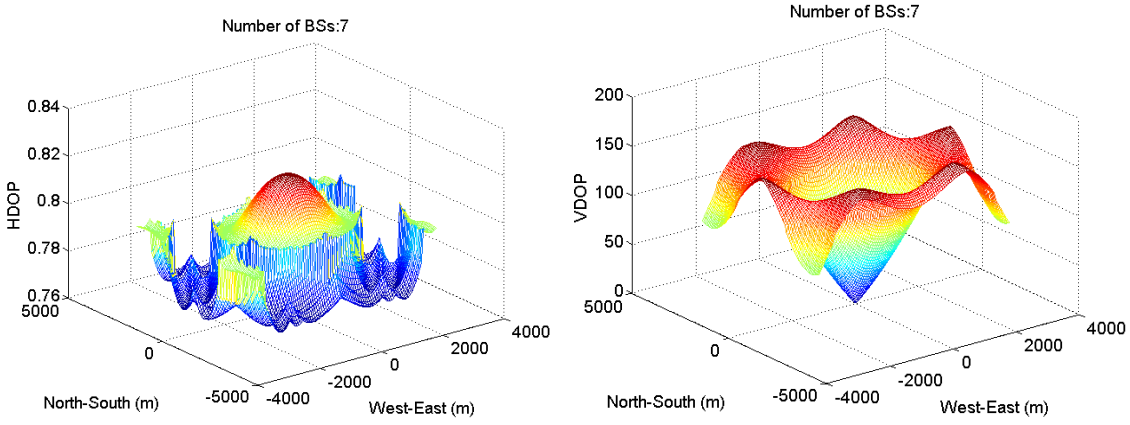

Figure 2.18: HDOP and VDOP with 7 BSs Involved

Figures 2.15 to 2.18 demonstrate HDOPs and VDOPs as a function of MS location when 4, 5, 6, and 7 BSs are used. Obviously, the greater the number of BSs involved, the better the HDOPs. But, the VDOPs in all of these scenarios are extremely bad. This is because BSs are normally very low in height difference (tens of metres) compared to the MS-BS separations (several kilometres) and thus the elevation angle is very small giving a poor VDOP.

If GPS is also available, GPS satellites can be used as extra BSs to improve DOPs. Figures 2.19 and 2.20 demonstrate the HDOPs and VDOPs when 5 BSs and 1 or 2 GPS satellites are available. It is evident that with the help of GPS satellites, VDOP can be significantly reduced from about 200 to 1.3 when GPS satellites are in favourable locations.

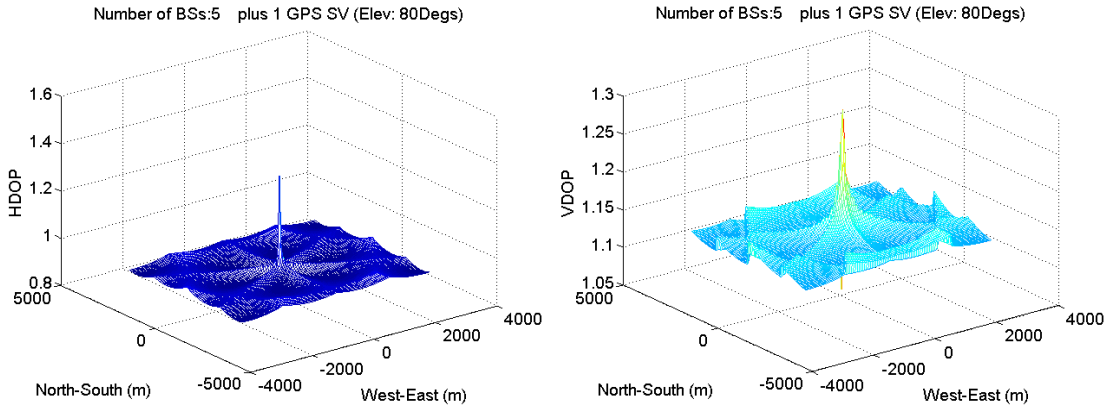

Figure 2.19: HDOP and VDOP with 5 BSs and 1 GPS Satellite Involved

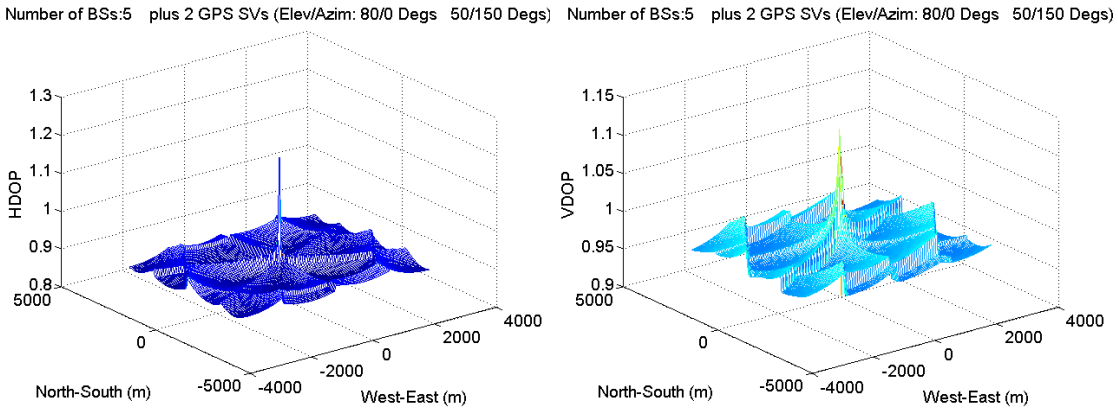

Figure 2.20: HDOP and VDOP with 5 BSs and 2 GPS Satellite Involved

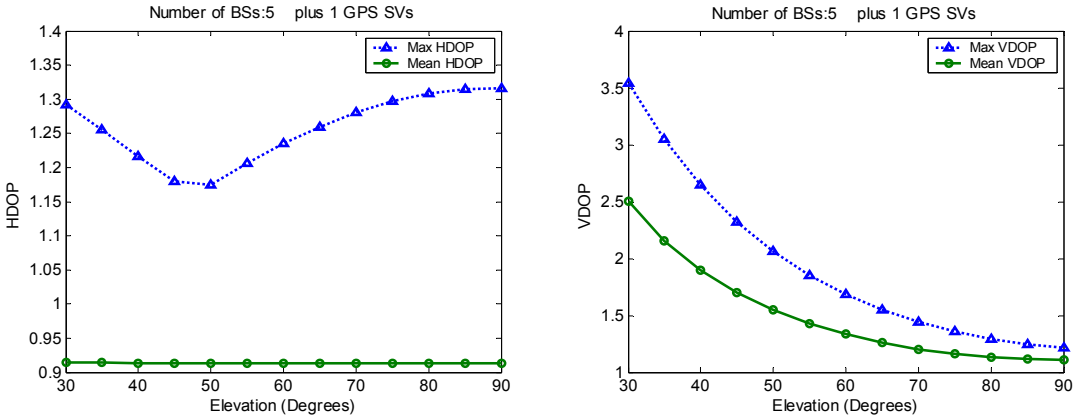

Figure 2.21: Variation of HDOP and VDOP with 5 BSs and 1 GPS Satellite Involved with Respect to GPS Satellite Position

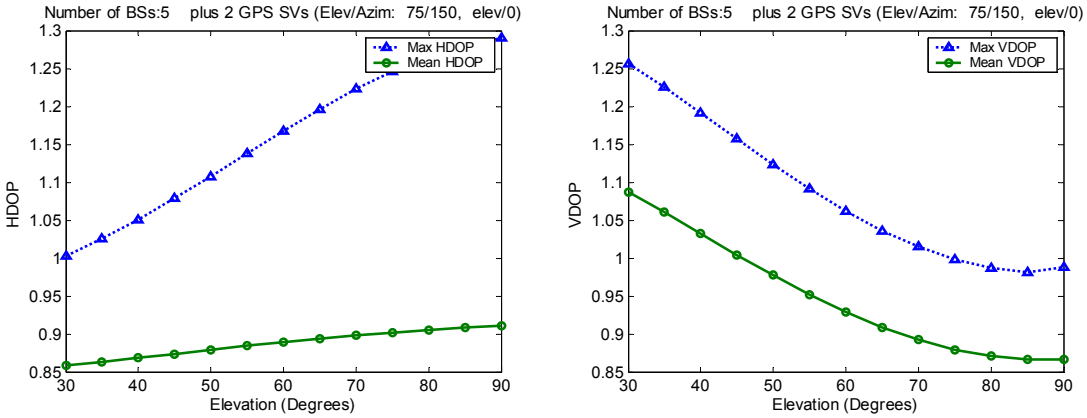

Figure 2.22: Variation of HDOP and VDOP with 5 BSs and 2 GPS Satellite Involved with Respect to GPS Satellite Position

Figures 2.21 and 2.22 show the variation of HDOP and VDOP with respect to GPS satellite position. The positions of GPS satellites do not change the HDOP very much since the ground-based BSs have already provided a reasonably good geometry, especially when the number of BSs used is more than 5. VDOP changes significantly with the change of satellite positions. Generally, the higher the satellites, the smaller the VDOP. For example, when 5 BSs and 1 GPS are involved, the VDOP decreases from about 3.5 when the GPS satellite is low to about 1.2 when the GPS satellite is high.

CHAPTER 3

HEARABILITY ANALYSIS

3.1 Introduction

To locate a cellular phone using network-based methods such as TOA and TDOA, the cellular phone needs to be able to communicate with at least three geometrically dispersed BSs. Unfortunately, this computational condition may not be satisfied due to the "near-far" effect occurring in some radio channels such as CDMA channels. Hearability is further deteriorated by a "Power Control" scheme which attempts to adjust signal power to the minimum required level to maximize system capacity.

Several methods have been proposed to improve hearability. The strategies include: expanding signal integration time (Bartlett, 2002); the Power Up Function method (PUF) (Landa et al, 2000); and Idle Period Down Link method (IPDL) (Ericsson, 1999). Taking the IS-95 CDMA pilot signal as an example, this chapter evaluates the improvement in hearability due to each of the above-mentioned methods. The discussion is conducted in a step by step manner, as follows. First, the pilot signals used for wireless location are discussed. Then the nature and degree of Same-cell interference, Other-cell interference, and Signal to Interference Ratio (SIR) of the desired signal at receivers are discussed in

detail since it is the SIR that determines whether or not a signal can be reliably received. Finally, to what extent these methods can improve the hearability is evaluated by theoretical analysis and simulation experiments.

3.2 IS-95 CDMA Forward Link (Pilot Channel) Hearability Analysis

3.2.1 IS-95 Forward Link Signals

There are 64 physical channels in the forward link of an IS-95 CDMA cellular system; these are distinguished by the 64 orthogonal Walsh functions, $\{W_i : i = 0,1,2,\cdots,63\}$ which serve as digital carriers. These physical channels form four types of logical channels of which the functionalities can be summarized as follows (Chen, 1999a).

- Pilot Channel: The channel is identified by Walsh function zero, W_0 . It continuously broadcasts a known signal to provide the MSs a robust time, frequency, and phase reference for demodulation in other channels.
- Synchronization Channel: The channel is identified by Walsh function, W_{32} , and is also a continuously broadcasting channel. It provides MSs with BS timing information, cell site identification number, and other information for synchronization.
- Paging Channel: There can be up to seven paging channels, with carriers from W_1 to W_7. A paging channel contains paging messages and conveys other control messages from the BSs to the MSs.

- Traffic Channel: There are at least 55 traffic channels. They carry user information. They also carry control messages using “blank and burst” or “dim and burst” techniques.

The pilot channel signal is preferred for wireless location purposes because it provides some advantages over other signals from the location estimation point of view:

- The pilot channel possesses dominant transmission power. Approximately 15-20% of the maximum transmission power of a BS is dedicated to the pilot channel to ensure the visibility of the pilot signal over the coverage area. This also makes pilot signals more easily acquired from neighbouring cells as well.
- The pilot signal is a known continuous broadcasting signal. It enables an MS to keep locked on the pilot Pseudo Noise (PN) code.
- All BSs transmit the same PN sequence but with different offsets. This makes it easier in the search process of a receiver to acquire TDOA measurements.

3.2.2 IS-95 CDMA Pilot Channel Signal

The process of generating a pilot signal is shown in Figure 3.1. Walsh function zero with a chip rate of 1.2288 Mcps (mega chips per second) is first modulated by the pilot baseband “data”. Then, this intermediate signal is separated into an I-component and a Q-component to further modulate the I-channel PN sequence and the Q-channel PN sequence. Wave shaping, amplification, and RF carrier modulation are finally conducted to generate the actual signal transmitted to MSs.

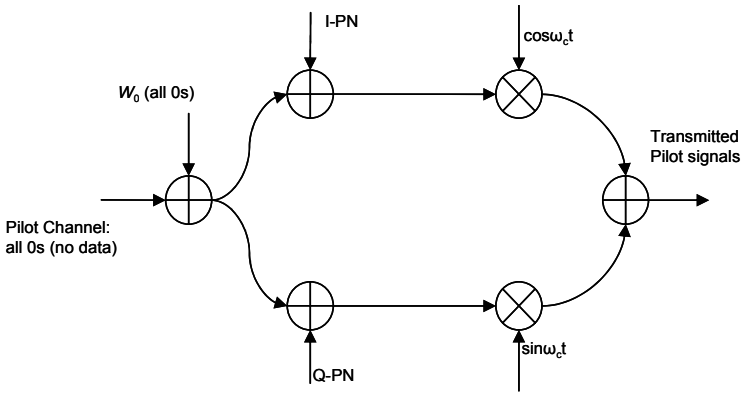

Figure 3.1: Generation of Pilot Channel Signals

The Walsh code is one type of orthogonal code. It is used in IS-95 CDMA systems to separate different physical channels. One can refer to Lee and Miller (1998) for detailed information about the Walsh code. Both the I-channel PN sequence and the Q-channel PN sequence are maximal length sequences generated by 15-stage shift registers and lengthened by the insertion of one chip per period in a specific location in the sequences. Thus, the sequence length is $2^{15}-1+1=32768$ chips. Each base station is distinguished by a different phase offset in both the I-channel and the Q-channel PN sequences. The offset is a multiple of 64 PN chips, which yields 512 possible 64-chip offsets. At a rate of 1.2288 Mcps, the I-sequence and Q-sequence repeat every 26.66 ms, or 75 times every 2 seconds. The characteristic polynomials of the I-sequence and Q-sequence are

$$f_I(x)=1+x^2+x^6+x^7+x^8+x^{10}+x^{15}, \tag{3.1}$$

$$f_Q(x)=1+x^3+x^4+x^5+x^9+x^{10}+x^{11}+x^{12}+x^{15} \tag{3.2}$$

which can be generated using the modular shift register generator. It must be emphasized that the signal modulating PN sequences are actually at a constant value of 0 since both the pilot data bits and the Walsh function 0 bits are all zeros. This means that,

theoretically, coherent signal integration can be done for a longer time because there is no data bit change. The demodulation of a pilot signal is the reverse process of signal generation, and is fully discussed in Section 3.3.1.

3.2.3 SIR Model of Pilot Signals

In IS-95 CDMA systems, a pilot signal can be reliably received only when its SIR is larger than a threshold (Chen, 1999a). The SIR of a pilot signal can be expressed as

$$SIR = \frac{P_P}{P_I + P_N} \tag{3.3}$$

where P_P is the power of the received pilot signal; P_I is the cellular network interference; and P_N is the MS receiver thermal noise. According to signal propagation theory, the received signal power is related to the transmitted power, the transmitter/receiver antenna pattern, and path loss. Thus, the received pilot signal power can be further expressed as

$$P_P = \varsigma_P \cdot P_C \cdot G_C \cdot G_m \cdot L \tag{3.4}$$

where

ς_P = fraction of the transmit power allocated to the pilot channel

P_C = total transmit power of the BS being studied

G_C = BS antenna gain, including cable loss

G_m = mobile antenna gain, including cable loss

L = propagation loss

The cellular network interference, P_I , contains two components, namely Same-Cell interference, $P_{I,SC}$, and Other-Cell interference $P_{I,OC}$ (Lee and Miller, 1998),

$$P_I = P_{I,SC} + P_{I,OC} . \tag{3.5}$$

Same-Cell interference results from the multipath reception of the serving BS if different forward link channels are assumed to be perfectly orthogonal. Suppose that $P_{0,f}$ is the total received power at the MS due to the serving BS and that $P_{0,k}$ is the received power for the signal of path k . We have the following equation if there are K multipath replicas:

$$P_{0,f} = \sum_{k=1}^{K} P_{0,k} = \sum_{k=1}^{K} \beta_k P_{0,f} = P_{0,f} \sum_{k=1}^{K} \beta_k , \tag{3.6}$$

where β_k is the fraction of the received power of path k with respect to total received power $P_{0,f}$. Obviously,

$$\sum_{k=1}^{K} \beta_k = 1 . \tag{3.7}$$

A common assumption about Same-Cell interference is that it is of the same power as that of the direct signal (Lee and Miller, 1998). This assumption means that $\sum_{k=2}^{K} \beta_k = 1/2$ and the power of Same-Cell interference is

$$P_{I,SC} = P_{0,direct} = P_C \cdot G_C \cdot G_m \cdot L . \tag{3.8}$$

Signals received from the base stations of other CDMA cells act as Other-Cell interference to an MS, as shown in Figure 3.2. Thus, the average interference power can be calculated via a propagation loss model,

$$P_{I,OC} = \sum_i P_{I,i} = \sum_i P_C \cdot L(r_i) = P_C \sum_i L(r_i), \tag{3.9}$$

where all BSs are assumed to have the same transmission power, P_C . $L(r_i)$ is the corresponding propagation loss which is a function of MS position, BS position, and an appropriate propagation model.

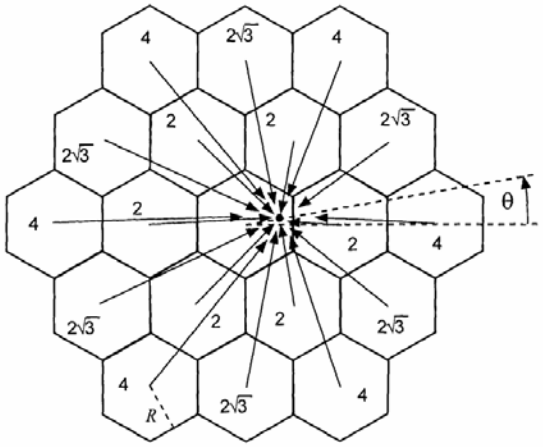

Figure 3.2: Other-Cell Interference at MS (r, θ)

From Figure 3.3, the distance from the MS to the *i*th interfering base station is

$$r_i(r, d_i, \theta_i) = \sqrt{r^2 + d_i^2 - 2rd_i \cos(\theta_i)}\,. \tag{3.10}$$

Assuming a μth order power propagation model, $L(r_i) = \varepsilon \times r_i^{-\mu}$ where ε is a constant coefficient, the total Other-Cell interference after considering all surrounding BSs can be easily found as

$$P_{I,OC} = \varepsilon \cdot P_C \cdot \sum_i \left(r_i(r, d_i, \theta_i)\right)^{-\mu}\,. \tag{3.11}$$

Recalling that Same-Cell interference actually can also be expressed as

$$P_{I,SC} = \varepsilon \cdot P_C \cdot r^{-\mu},$$

the ratio of Other-Cell interference power to Same-Cell interference power at the MS becomes

$$\frac{P_{I,OC}}{P_{I,SC}} = \sum_i \frac{r^{\mu}}{\left[r_i\left(r, d_i, \theta_i\right)\right]^{\mu}} . \tag{3.12}$$

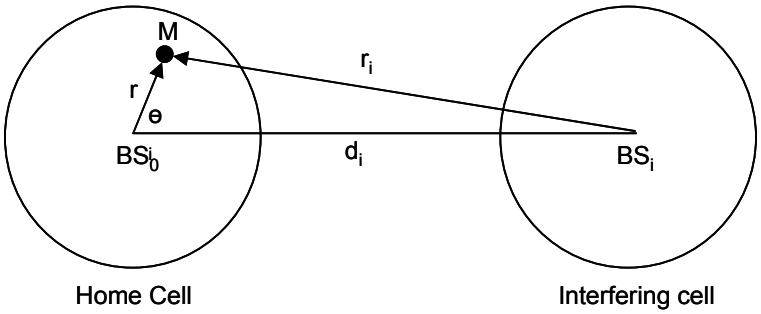

Figure 3.3: Geometry of Other-Cell Interference

This equation shows the relationship between Same-Cell interference and Other-Cell interference. The ratio is a function of propagation channel and BS-MS distances. As illustrated in Figure 3.4, Same-Cell interference (shaded in red) is normally strongest because the serving BS is closest to the MS especially when the MS is in the central area of the serving cell. The Other-Cell interference resulting from the inner-most ring cells (shaded in orange) is weaker compared to that of the serving cell. The Other-Cell interference resulting from the second or the third ring cells (shaded in pink) is much weaker because of the longer distances between these BSs and the MS inside the serving cell. We know from this phenomenon that the hearability is affected mainly by the nearest BSs such as the serving BS. As a result, hearability can be improved if these major interference sources can be eliminated.

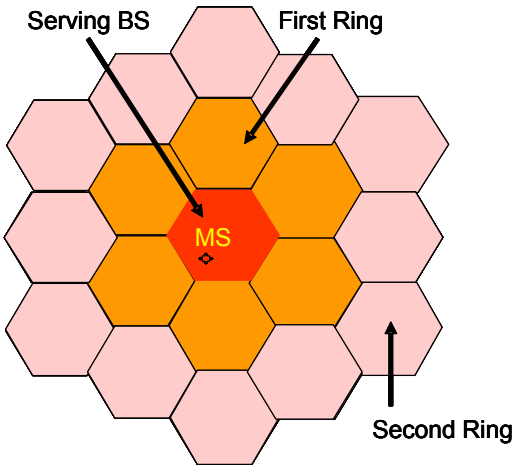

Figure 3.4: Comparison of Same-Cell Interference and Other-Cell Interference

Finally, receiver thermal noise needs to be evaluated to determine the SIR of pilot signals. The power of the thermal noise can usually be calculated either from the noise temperature or from the noise figure (Lee and Miller, 1998). For the IS-95 CDMA system, the thermal noise power density at a MS antenna can be expressed as

$$\begin{aligned} N_o &= kT_0F \\ &= \left(1.38\cdot 10^{-23}\, J/^o K\right)\left(293^o K\right)F \\ &= 4.043F\cdot 10^{-21}\, W/Hz \end{aligned} \tag{3.13}$$

Expressed in terms of dB and including the noise figure,

$$N_0(dB) = -203.9\, dBW/Hz + NF(dB) \tag{3.14}$$

where k is Boltzman's constant, T_0 is the reference noise temperature in Kelvin, F is the noise factor, and NF represents the noise figure. For a MS receiver, the noise figure is normally around 5 to 8 dB, thus the noise density is about $N_0(dB) = -199\ dBW/Hz = -169\, dBm/Hz$.

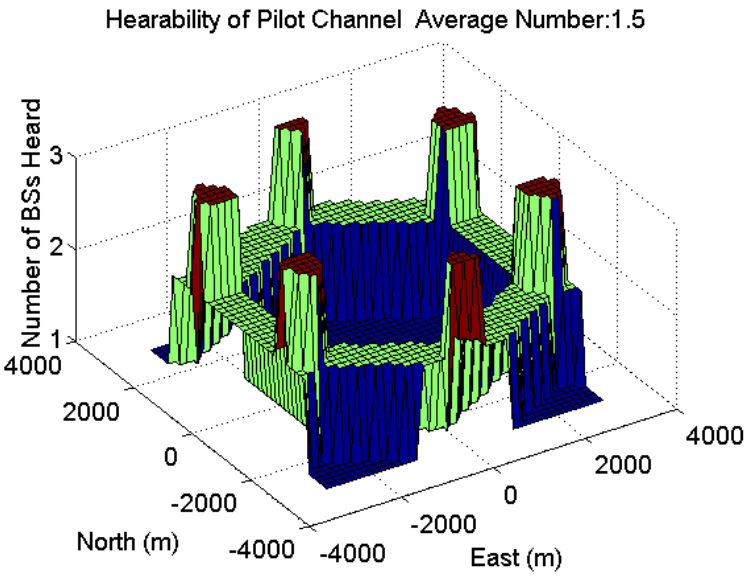

Figure 3.5: Hearability of a Normal Cellular Network

Figure 3.5 demonstrates the hearability of pilot signals; the parameters used in the calculation are summarized in Table 3.1. The two horizontal axes in the figure represent the Eastern and Northern coordinates with the serving BS at the origin. The vertical axis represents the number of BSs that can be heard from an MS located within the cell being studied. It is apparent that the number of BSs that can be heard is 1 when the MS is in the area near the centre of the cell; 2 when the MS is at the edge area of the cell; and 3 when the MS is at the tri-cell boundary where the MS has the chance to be "close" to three BSs. The average number of BSs heard over all places inside the serving cell is only about 1.5 and significantly less than 3. The poor hearability that characterizes the original cellular network diminishes its usefulness for location purposes.

Table 3.1: Parameters Used in Hearability Analysis

Cellular phone network	37 Cell layout
Cell size	Radius: 2 km
Propagation model	CCIR model with antenna height of 20 m
Detection threshold	-15 dB
BS transmit power	16 W
Pilot signal fraction	0.2
BS antenna gain	0 dB
MS antenna gain	0 dB
Noise Figure	8 dB

The propagation model used in the simulation is the CCIR model (Lee and Miller, 1998). It is normally used for typical 850 MHz cellular systems, with the mobile height assumed to be 2 m. The median pass loss is

$$L(dB) = \alpha + \beta \log_{10} d_{km} - B \tag{3.15}$$

where α and β describes a "power law" propagation loss; d_{km} is the distance between the MS and the BS; and B is a correction factor. Table 3.2 depicts the empirical parameter values of the model where h_1 is the transmitter antenna height. B depends on the construction density of the built-up environment. It can be chosen as 0 dB when about 15% of an area is covered by buildings or –2.5 dB when 20% of the area is covered by buildings.

Table 3.2: CCIR Model Parameters

h_1	α	β
10 m	131.09	38.35
20 m	126.93	36.38
30 m	124.50	35.22

The number of BSs that can be heard at a particular location is actually a random variable since mobile signal propagation suffers from channel fading; the path loss is of log-normal distribution which is of the following form:

$$L(dB) = L_{med}(dB) + \sigma_c(dB) \times \mathrm{N}(0,1) \tag{3.16}$$

where $\mathrm{N}(0,1)$ denotes a zero-mean Gaussian random variable with unit variance; σ_c, normally between 8 dB and 10 dB, is the log-normal fading variance; and $L_{med}(dB)$ is the median path loss discussed above which can be described by equation (3.15) or by several other propagation models (Lee, 1997). Written into ratio format, the above equation becomes

$$L = \frac{A}{d^{\mu}} 10^{\frac{\xi}{10}} \tag{3.17}$$

where d is the distance between the MS and a BS; μ is the pass loss exponent order; A is a coefficient describing transmitted signal power and $\xi \sim \mathrm{N}(0, \sigma_c^2)$ is a Gaussian random variable describing the log-normal fading. In the following, L in equation (3.17) is used to analyze the stochastic property of the hearability.

If receiver thermal noise is neglected and a derivation similar to that appearing in Chen (1999) is followed, then the SIR for BS_i can be expressed as

$$SIR_i = \frac{\varsigma_P}{1+\sum_{k\neq i}^{K} \frac{P_{Ck} L(d_k, \mu, \xi_k)}{P_{Ci} L(d_i, \mu, \xi_i)}}. \tag{3.18}$$

It can easily be seen that

$$\sum_{k\neq i}^{K} \frac{P_{Ck} L(d_k, \mu, \xi_k)}{P_{Ci} L(d_i, \mu, \xi_i)} = \sum_{k\neq i}^{K} \frac{P_{Ck}}{P_{Ci}} \left(\frac{d_i}{d_k}\right)^{\mu} 10^{\frac{\xi_k - \xi_i}{10}} \tag{3.19}$$

is a sum of scaled log-normal random variables. Applying the results in Yeh and Schwart (1984) to the above equation, the sum of these log-normal random variables can be closely approximated by another log-normal random variable as

$$\sum_{k\neq i}^{K} \frac{P_{Ck}}{P_{Ci}} \left(\frac{d_i}{d_k}\right)^{\mu} 10^{\frac{\xi_k - \xi_i}{10}} \approx 10^{\frac{z_i}{10}} \tag{3.20}$$

where z_i is a Gaussian random variable with the mean and the variance expressed as

$$m_{z_i} = 10\log_{10}\left(\frac{m^2}{\sqrt{v}}\right)$$

$$\sigma_{z_i}^2 = \lambda 10\log_{10}\left(\frac{v}{m^2}\right)$$

where

$$m = \mathrm{E}\left(10^{\frac{z_i}{10}}\right) = e^{\lambda^2\sigma_c^2} \sum_{k\neq i}^{K} C_{ik}$$

$$v = \mathrm{E}\left(\left(10^{\frac{z_i}{10}}\right)^2\right) = e^{4\lambda^2\sigma_c^2} \sum_{k\neq i}^{K} C_{ik}^2 + e^{3\lambda^2\sigma_c^2} \sum_{k\neq i}^{K} \sum_{j\neq i,k}^{K} C_{ik} C_{ij}$$

$$\lambda = \frac{\ln 10}{10} \approx 0.23$$

$$C_{ik} = \frac{P_{Ck}}{P_{Ci}}\left(\frac{d_i}{d_k}\right)^{\mu}.$$

σ_c^2 is the variance of the Gaussian random variable; and ξ_i characterizes the log-normal fading and is assumed to be the same for all BSs. Thus, the final SIR is also a random variable with the following expression:

$$SIR_i = \frac{\varsigma_P}{1+10^{\frac{z_i}{10}}}. \tag{3.21}$$

Whether or not the pilot signal of a BS can be heard is, in fact, a random event. Denoting this event with a random variable, A_i, one has the following event description

$$A_i = \begin{cases} 1 & \text{when SIR}_i \geq \text{detection threshold T} \\ 0 & \text{otherwise} \end{cases}$$

Thus, the number of BSs being heard is the summation of all of these random variables,

$$H = \sum_i^K A_i \tag{3.22}$$

with its mean and variance derived as follows, if all events related to these BS's are assumed to be independent,

$$m_H = \sum_{i=}^K m_{A_i} \tag{3.23}$$

$$\sigma_H^2 = \sum_{i=1}^K \sigma_{A_i}^2. \tag{3.24}$$

In order to determine m_{A_i} and $\sigma_{A_i}^2$, it is first noted that A_i is a two-value variable

$$A_i = \begin{cases} 1 & \textit{with probability} \quad p_i \\ 0 & \textit{with probability} \quad 1-p_i \end{cases}.$$

Thus

$$m_{A_i} = p_i$$

$$\sigma_{A_i}^2 = \mathrm{E}\left(A_i^2\right) - \mathrm{E}\left(A_i\right)^2 = p_i - p_i^2 = p_i\left(1 - p_i\right)$$

where p_i is the probability that the pilot signal of BS_i can be heard, and can be determined by the following formula:

$$\begin{aligned} p_i &= prob\left(SIR_i \geq \text{detection threshold } T\right) \\ &= prob\left(\frac{\varsigma_P}{1 + 10^{\frac{z_i}{10}}} \geq T\right) \\ &= prob\left(z_i \leq 10\log_{10}\left(\frac{\varsigma_P}{T} - 1\right)\right) \\ &= 1 - Q\left(\frac{10\log_{10}\left(\frac{\varsigma_P}{T} - 1\right) - m_{z_i}}{\sigma_{z_i}}\right) \end{aligned} \tag{3.25}$$

Here, $Q(\cdot)$ is the complementary Cumulative Distribution Function (CDF) of the standard normal distribution, $Q(s) = \frac{1}{\sqrt{2\pi}}\int_s^\infty e^{-t^2/2}dt$.

Figure 3.6 shows the mean and the standard deviation of the number of BSs that can be heard. The horizontal axis represents the distance between the MS and its serving BS; the solid curve and the error bars are the mean and the standard deviation, respectively, of the number of BSs heard. Figure 3.6(a) is the random property when an MS moves along a line directly connecting its serving BS and an adjacent BS as shown by line O-A in Figure 3.7. Figure 3.6(b) is the random property when an MS moves on a line which passes its serving BS and has the same distance to two adjacent BSs as shown by line O-B in Figure 3.7. In both cases, we can see that an MS can hear only its serving BS when it

is near its serving BS. Only at the edge of the cell can an MS hear 2 or 3 BSs. However, this is still not sufficient for location purposes and, in order to improve the chief deficiency, hearability, special techniques need to be applied.

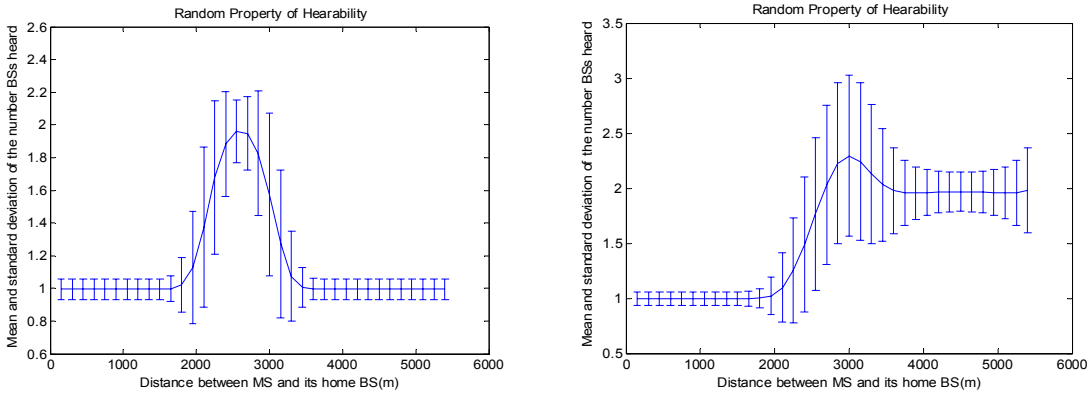

(a) O-A direction (b) O-B direction

Figure 3.6: Hearability in a Log-Normal Propagation Channel
Cell size: 3000 m 4th order propagation model log-normal standard deviation $\sigma = 8$ dB

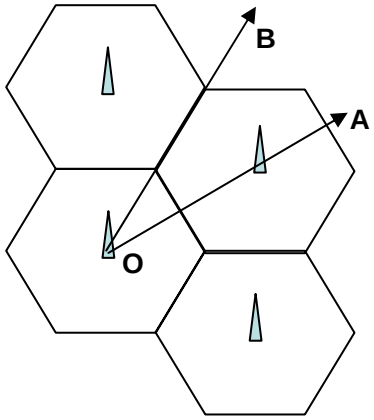

Figure 3.7: Two Cases in the Hearability Analysis

3.3 Hearability Improvement

Several methods have been proposed to increase hearability while maintaining communication performance. An attempt to resolve this problem is presented in IS-95B where a feature called the Power Up Function (PUF) enables a MS to sporadically increase its transmission power in order to enhance its visibility to other BSs. A detailed study of this method through the use of simulations can be found in Landa et al (2000). Another method proposed is the so-called enhanced signal receiving method (Chen, 1999a and Bartlett, 2002). Enhanced signal receiving makes use of the signal structure of pilot signals by increasing the signal integration time to increase receiver sensitivity. The hearability is improved since the required minimum SIR for pilot signal reception becomes smaller. The third method is the well-known Idle Period Downlink (IPDL) method (Ludden and Lopes, 2000), proposed for application in the UMTS system. The near-far effect is mitigated by interrupting the signal transmission at the serving BS to let the MS inside the cell to measure pilot signals of other cells. In this section, how the hearability is improved by the latter two methods is fully discussed. The results of this discussion provide context and guidance to all of the simulations presented in the following chapters.

3.3.1 Enhanced Signal Receiving Technique

In this section, an IS-95 pilot signal is taken as an example to depict the hearability improvement that is achieved by extending the signal integration time. Figure 3.8 (Lee and Miller, 1998) shows how a pilot signal is acquired and detected inside an IS-95

CDMA receiver. The received pilot signal is first down-converted to base band, and then the in-phase PN code and the quadrature phase PN code are removed from the I and Q components. After being integrated for a certain length of time, the I and Q components form the final signal that is used for signal detection and acquisition. Pilot signal acquisition is a two-dimensional searching process; one dimension is carrier searching, the other being PN code searching. The detection threshold - otherwise known as receiver sensitivity - is related to the signal integration time.

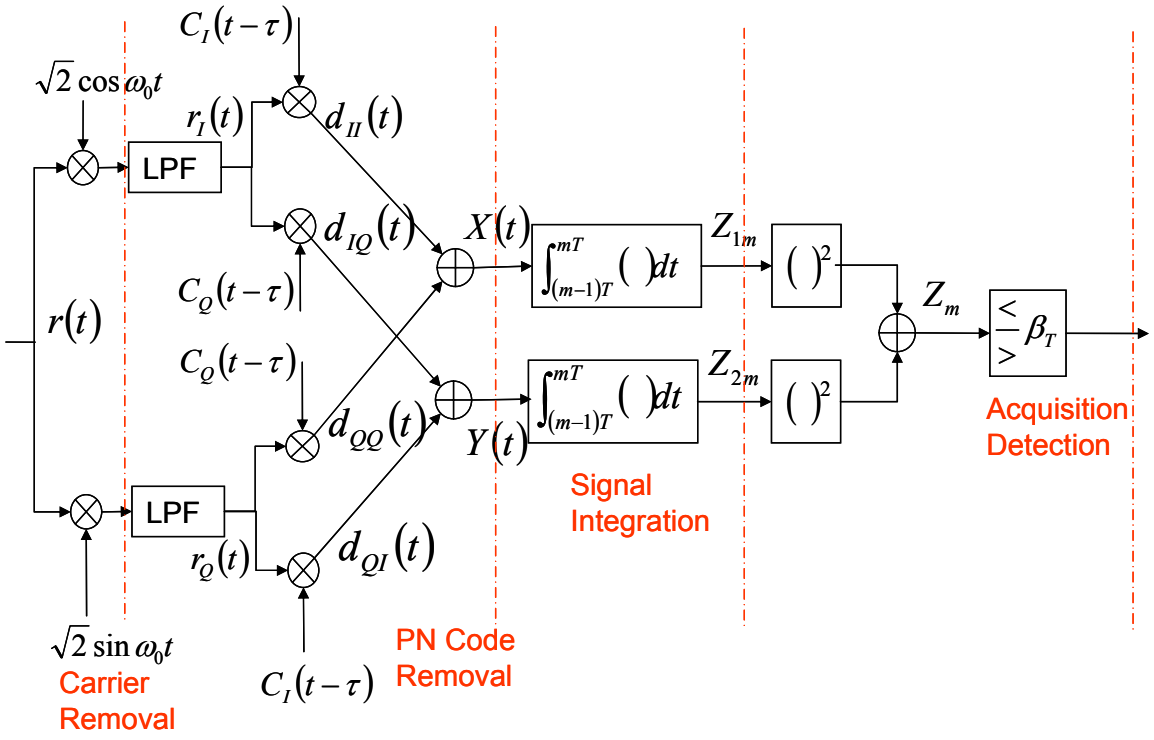

Figure 3.8: Diagram of IS-95 Signal Acquisition

As shown by Lee and Miller (1998), the received pilot signal is

$$r(t)=\sqrt{\frac{2E_c}{T_c}}\left[C_I(t)\cos(\omega_0 t+\phi_\omega)+C_Q(t)\sin(\omega_0 t+\phi_\omega)\right]+n(t) \tag{3.26}$$

where E_c is the chip energy of the received pilot signal; T_c is chip length; and $C_I(t)$ and $C_Q(t)$ are the I-channel and Q-channel PN sequences, respectively, which assume ± 1 values. The noise represents both receiver noise and noise coming from other signals acting as interference and is assumed to be narrow band additive white Gaussian noise around the carrier frequency.

$$n(t) = \sqrt{2}n_c(t)\cos\omega_0 t - \sqrt{2}n_s(t)\sin\omega_0 t \tag{3.27}$$

with

$$\overline{n^2(t)} = \overline{n_c^2(t)} = \overline{n_s^2(t)} = \sigma^2 = \frac{1}{2}\mathcal{N}_0 \tag{3.28}$$

where σ^2 is the noise power and $\mathcal{N}_0/2$ is the two-sided noise power spectral density. After being processed through the down converter and low pass filter, the I and Q components of the pilot signal are of the following form

$$r_I(t) = \sqrt{\frac{E_c}{T_c}}C_I(t)\cos\phi_\omega + \sqrt{\frac{E_c}{T_c}}C_Q(t)\sin\phi_\omega + n_I(t) \tag{3.29}$$

and

$$r_Q(t) = \sqrt{\frac{E_c}{T_c}}C_Q(t)\cos\phi_\omega + \sqrt{\frac{E_c}{T_c}}C_I(t)\sin\phi_\omega + n_Q(t) \tag{3.30}$$

where ϕ_ω is the phase difference between the incoming carrier and the locally generated carrier; and $n_I(t)$ and $n_Q(t)$ are in-phase noise and quadrature phase noise, respectively, with a power spectral density of $\mathcal{N}_0/2$. Removing the I-channel PN code and Q-channel PN code, and combining the PN free signals results in completion of the second phase shown in Figure 3.8. At this point, two intermediate signals are obtained, $X(t)$ and $Y(t)$, to be used in the subsequent signal integration phase

$$X(t) = r_I(t)C_I(t-\tau) + r_Q(t)C_Q(t-\tau)$$
$$= \sqrt{\frac{E_c}{T_c}}\left[C_I(t)C_I(t-\tau) + C_Q(t)C_Q(t-\tau)\right]\cos\phi_\omega + n_X(t) \tag{3.31}$$

$$Y(t) = r_I(t)C_Q(t-\tau) + r_Q(t)C_I(t-\tau)$$
$$= \sqrt{\frac{E_c}{T_c}}\left[C_I(t)C_I(t-\tau) + C_Q(t)C_Q(t-\tau)\right]\sin\phi_\omega + n_Y(t) \tag{3.32}$$

Integrating $X(t)$ and $Y(t)$ for a time interval, $T = N \cdot T_c$, produces two additional intermediate signals

$$Z_{1m} = \int_{(m-1)T}^{mT} X(t)dt$$
$$= \sqrt{\frac{E_c}{T_c}}\cos\phi_\omega \int_{(m-1)T}^{mT}\left[C_I(t)C_I(t-\tau) + C_Q(t)C_Q(t-\tau)\right]dt + \int_{(m-1)T}^{mT} n_X(t)dt \tag{3.33}$$
$$= 2T\sqrt{\frac{E_c}{T_c}}\cos\phi_\omega R(\tau) + N_1$$

and

$$Z_{2m} = \int_{(m-1)T}^{mT} Y(t)dt$$
$$= \sqrt{\frac{E_c}{T_c}}\sin\phi_\omega \int_{(m-1)T}^{mT}\left[C_I(t)C_I(t-\tau) + C_Q(t)C_Q(t-\tau)\right]dt + \int_{(m-1)T}^{mT} n_Y(t)dt \tag{3.34}$$
$$= 2T\sqrt{\frac{E_c}{T_c}}\sin\phi_\omega R(\tau) + N_2$$

In the above integration, it is assumed that ϕ_ω is unchanged and that the autocorrelation functions of $C_I(t)$ and $C_Q(t)$ are the same

$$\frac{1}{T}\int_0^T C_I(t)C_I(t-\tau)dt = \frac{1}{T}\int_0^T C_Q(t)C_Q(t-\tau)dt = R(\tau) \tag{3.35}$$

N_1 and N_2 represent the noise components in Z_{1m} and Z_{2m}. They contain receiver noise, along with some co-channel and cross-quadrature interference. Normally, they are of the following distributions:

$$N_1 \sim \mathrm{G}\left(0, \mathcal{N}_0^{'}\right) \quad \text{and} \quad N_2 \sim \mathrm{G}\left(0, \mathcal{N}_0^{'}\right) \tag{3.36}$$

where $\mathcal{N}_0^{'}$ is the effective noise spectral density that is due to both receiver noise and interference. The final decision variable is given by

$$Z_m = Z_{1m}^2 + Z_{2m}^2 \tag{3.37}$$

Pilot signal acquisition is a two dimension searching process, one dimension is in frequency and the other is in code. When the current searching bin does not coincide with the received pilot signal, Z_m is a central Chi-squared random variable with two degrees of freedom since both Z_{1m} and Z_{2m} contain only noise in this case. As shown in Figure 3.9, the probability density function (pdf) is

$$p_{Z_m}(\alpha) = \begin{cases} \dfrac{1}{2\mathcal{N}_0^{'}T} e^{-\frac{\alpha}{2\mathcal{N}_0^{'}T}}, & \alpha \geq 0 \\ 0, & \textit{otherwise} \end{cases} \tag{3.38}$$

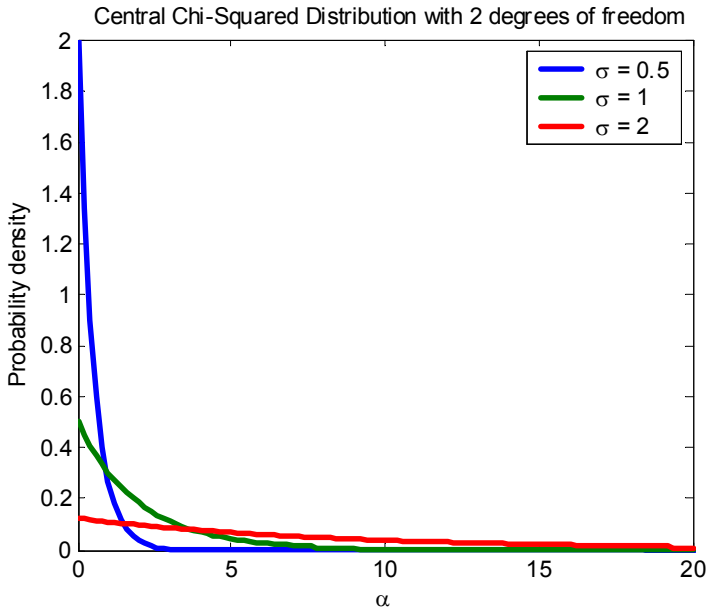

Figure 3.9: pdfs of Central Chi-Squared Distribution

When the current searching bin coincides with the received pilot signal, Z_m is a non-central Chi-squared random variable with two degrees of freedom since Z_{1m} and Z_{2m} contain both signals and noise in this case. The non-centrality parameter is

$$\lambda = 4N \cdot R^2(\tau) \cdot \frac{E_c}{\mathcal{N}_0^{'}} \tag{3.39}$$

and the pdf is

$$p_{Z_m}(\alpha) = \begin{cases} \frac{1}{2\sigma^2} e^{-\frac{1}{2}\left(\lambda + \frac{\alpha}{\sigma^2}\right)} I_0\left(\sqrt{\frac{\lambda\alpha}{\sigma^2}}\right) & \alpha \geq 0 \\ 0, & \text{otherwise} \end{cases} \tag{3.40}$$

where $\sigma^2 = \mathcal{N}_0^{'} T \approx \mathcal{N}_0 T$ and $I_0()$ is the modified Bessel function of the first kind. Such pdfs are plotted in Figure 3.10.

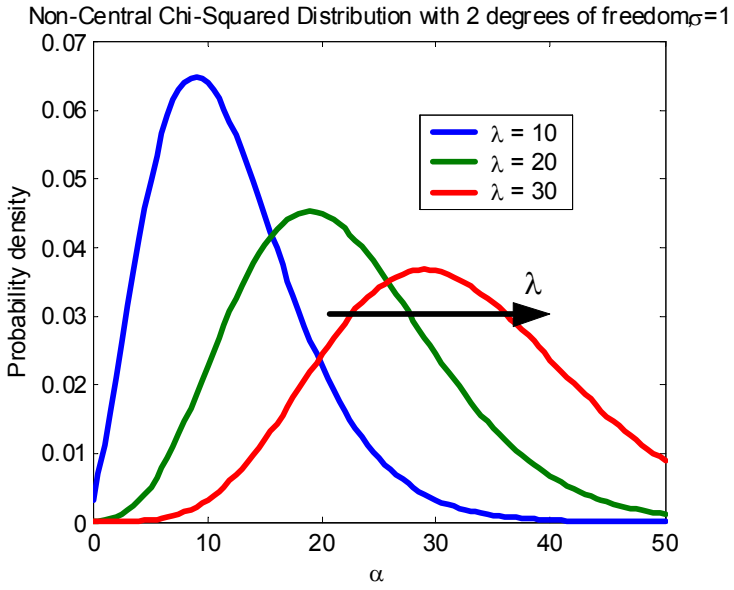

Figure 3.10: pdfs of Non-Central Chi-Squared Distribution

In this figure, the pdf of a non-central Chi-squared distribution shifts to the right when λ increases. Actually, λ is proportional to the ratio of signal power to noise power. The larger the λ, the further the shift to the right, and the easier the detection of pilot signals. Thus, to increase receiver sensitivity a larger λ is preferred.

Signal detection is actually a hypothesis test problem: H_0 denotes that the received pilot signal does not reside in the current searching bin, whereas H_1 denotes that the received pilot signal resides in the current searching bin. A signal is thought to be detected if H_1 is accepted. The probability density functions conditioned on H_0 and H_1 are

$$p_{Z_m}(\alpha|H_0) = \frac{1}{2\mathcal{N}_0' T} e^{-\frac{\alpha}{2\mathcal{N}_0' T}} \tag{3.41}$$

$$p_{Z_m}(\alpha|H_1) = \frac{1}{2\mathcal{N}_0 T} e^{-\frac{1}{2}\left(\lambda+\frac{\alpha}{\mathcal{N}_0 T}\right)} I_0\left(\sqrt{\frac{\lambda\alpha}{\mathcal{N}_0 T}}\right) \tag{3.42}$$

To solve this hypothesis test problem, a detection threshold, β_T, needs to be derived first from a selected false alarm probability threshold, P_F, and a selected detection probability threshold, P_D. As shown in Figure 3.11, the vertical line corresponds to β_T. If Z_m is larger than β_T, then Z_m is expected to have a non-central Chi-squared distribution. Therefore, H_1 is accepted and a pilot signal is thought to be successfully detected.

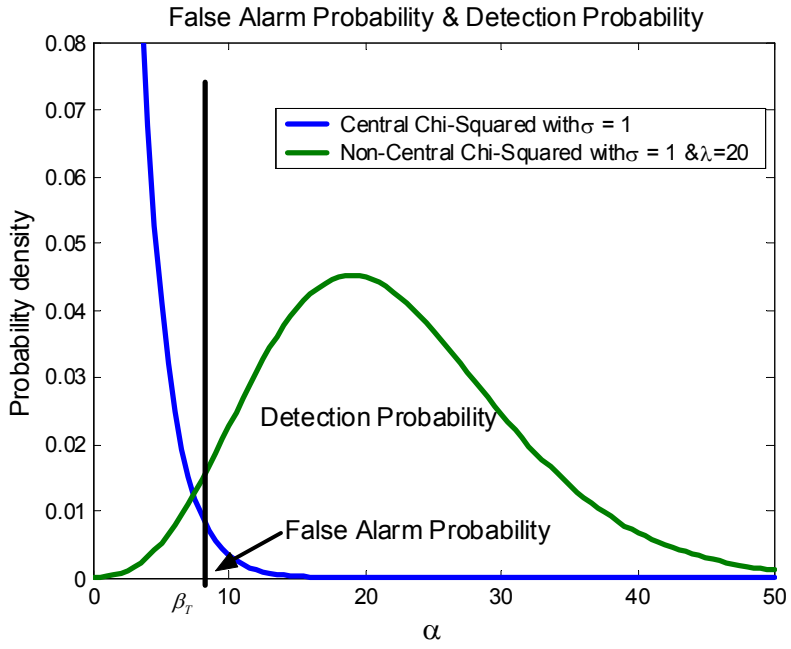

Figure 3.11: Pilot Signal Detection

After some simplification derived in Lee and Miller (1998), the relationship among P_D, P_F, signal integration time (N), and the required minimum signal SIR ($E_c/\mathcal{N}_0$) can be expressed as

$$P_D \le Q\left(\sqrt{-2\ln P_F} - 2\sqrt{\frac{NE_c}{\mathcal{N}_0}}\right) \tag{3.43}$$

where $Q(t)$ denotes Gaussian complementary cumulative probability function $Q(a)=\int_a^{\infty}\frac{1}{\sqrt{2\pi}}e^{-\frac{\lambda^2}{2}}d\lambda$.

An illustration of the above relationship is shown in Figure 3.12. The horizontal axis represents false alarm probability while the vertical axis represents detection probability. As an example, it can be found that an integration time equivalent to 112 chips is required to achieve a detection probability of 95% and a false alarm probability of 10% when $E_c/\mathcal{N}_0$ equals -15 dB. This relationship can be used to determine how long a signal needs to be integrated to decrease the required minimum $E_c/\mathcal{N}_0$ to a certain value.

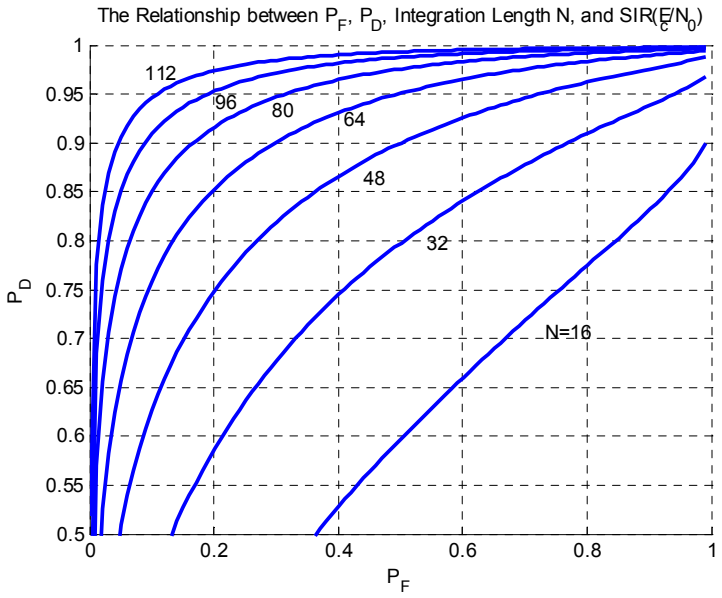

Figure 3.12: Upper Bound on Detection Probability versus False Alarm Probability in the Case of $E_c/\mathcal{N}_0=-15\,\text{dB}$

Figure 3.13 shows the change of the required minimum $E_c/\mathcal{N}_0$ with respect to the change of integration time, N. The false alarm probability threshold is kept constant at 5%. The four plots correspond to four detection probabilities: 95%, 90%, 80%, and 70%. The horizontal axis is the length of signal integration time and the vertical axis is the required minimum $E_c/\mathcal{N}_0$. Figure 3.14 also shows the change of the required minimum $E_c/\mathcal{N}_0$ with respect to the change of integration time but with the detection probability fixed at the 90% level. The four plots correspond to four false alarm detection probabilities, 5%, 10%, 15%, and 20%. The horizontal axis still represents the length of signal integration time and the vertical axis still represents the required minimum $E_c/\mathcal{N}_0$. It is obvious from both figures that the required minimum $E_c/\mathcal{N}_0$ decreases when the integration time increases. This means that receiver sensitivity is increased accordingly.

Longer signal integration is preferred for detecting and tracking very weak pilot signals and improving signal hearability for wireless location purposes. Unfortunately, there are at least two factors that prevent integration of signals for very long periods of time. First, the required minimum $E_c/\mathcal{N}_0$ is not sensitive to the integration time when the integration time is already large. From Figures 3.13 and 3.14, it can be clearly seen that the required $E_c/\mathcal{N}_0$ decreases rapidly when N is small, while quite slowly when N is already large. This means that there exists an efficient length of signal integration time. Empirically, the longest integration time should preferably fall within 1000 to 1500 chips.

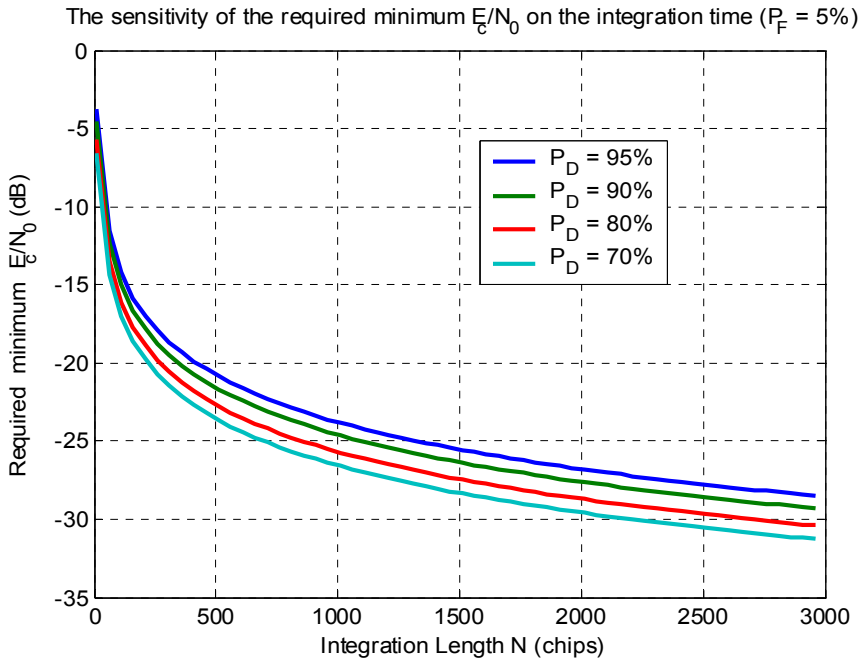

Figure 3.13: Relationship Between Integration Length and Receiver Sensitivity (P_F fixed)

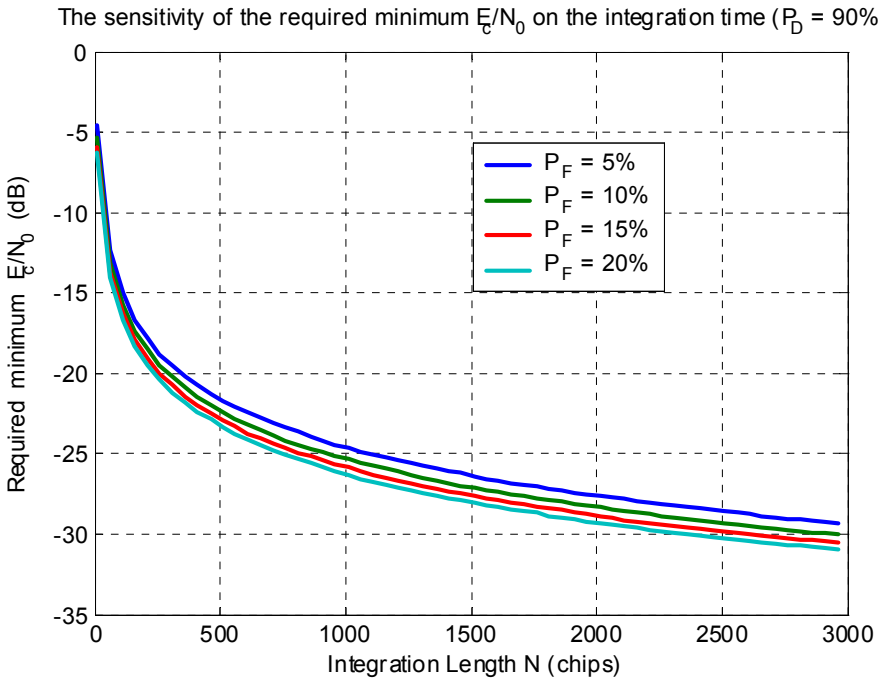

Figure 3.14: Relationship Between Integration Length and Receiver Sensitivity (P_D fixed)

The second factor preventing longer integration is phase uncertainty. As mentioned above, the phase difference, ϕ_ω , should not change during the period of signal integration. However, the following two reasons may result in a changed phase difference:

- Message bit transition
- Frequency uncertainty

For IS-95 CDMA pilot signals, the integration time is constrained only by frequency uncertainty since the message bits of pilot signals are constant. Such frequency uncertainty is caused by:

- Oscillator frequency deviation: The oscillator of an MS is steered to the pilot signal of its serving BS; but the oscillators of BSs contain frequency deviations from their theoretical values. As a result, pilot signal reception will suffer from the oscillator errors.
- Doppler Frequency Shift: The movement of an MS will introduce a shift to its carrier frequency as well. This is the Doppler frequency, $\Delta f_{Doppler} = \frac{v}{c} f_c$, where c is the speed of propagation, v is the MS speed, and f_c is the carrier frequency.

The signal part in the final detection variable becomes weaker if frequency errors exist. The non-centrality parameter, in this case, changes to

$$\begin{aligned} \lambda_f &= 4N \cdot R^2(\tau) \cdot \frac{E_c}{\mathcal{N}_0'} \cdot D(\Delta f, N) \\ &= D(\Delta f, N) \cdot \lambda \end{aligned} \tag{3.44}$$

Compared to the λ in the frequency error-free cases, λ_f is degraded by $D(\Delta f, N)$ which is of the following form (Viterbi, 1995):

$$D(\Delta f, N) = \left[\frac{\sin(\pi \Delta f N T_c)}{\pi \Delta f N T_c} \right]^2 \tag{3.45}$$

where Δf is the frequency error, N is the integration time in chips, and T_c is the chip duration.

Figure 3.15 shows that the non-centrality parameter is actually a function of integration time and frequency errors. If there is no frequency error ($\Delta f = 0$), the non-centrality parameter increases linearly with integration time. If there are frequency errors, the non-centrality parameter, however, will drop from its maximum values after a certain integration time depending on the amount of frequency errors. For $\Delta f = 400$ Hz, the non-centrality parameter reaches its maximum with an integration time of around 1000 chips. For $\Delta f = 1000$ Hz, the non-centrality parameter is maximized when the integration time is about 500 chips. As aforementioned, the non-centrality parameter is an indication of receiver sensitivity; the larger the non-centrality parameter, the higher the receiver sensitivity. Thus, a large non-centrality parameter is preferred for hearability improvement and the maximum integration time needs to be carefully selected to prevent λ from being deteriorated by frequency errors.

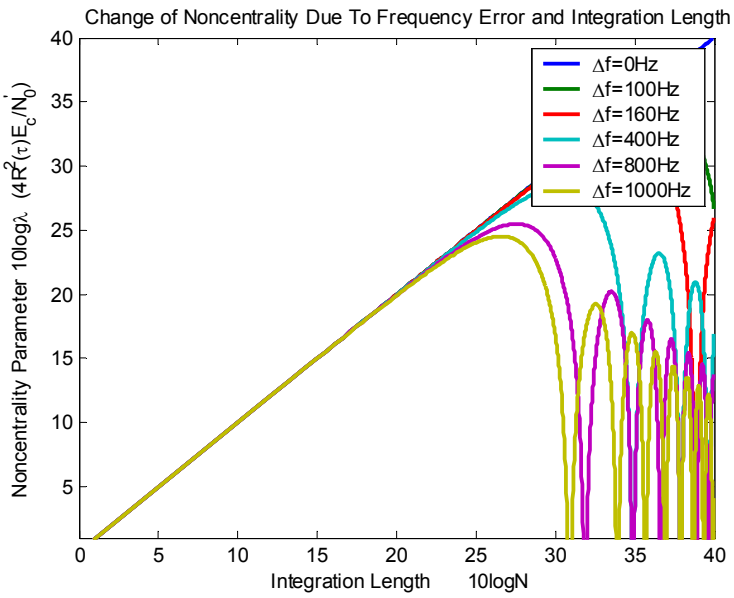

Figure 3.15: Relationship between Non-Centrality Parameter and Integration Length with Respect to Frequency Error

In the following, three types of receivers are studied to demonstrate the hearability improvement due to this enhanced signal receiving technique. The first receiver, Rx1, is a normal receiver of which the integration time is 112 chips. The second receiver, Rx2, is an enhanced signal receiving receiver of which the maximum frequency error is assumed to be 400 Hz and the integration time is 650 chips; and the third receiver, Rx3, is also an enhanced signal receiving receiver but with a maximum frequency error of 160 Hz and an integration time of 1500 chips.

The propagation model used in the simulations is a log-normal propagation model of the following form:

$$L(dB) = L_{med}(dB) + \sigma_c(dB) \times \mathrm{N}(0,1) \tag{3.46}$$

$L_{med}(dB)$ is described by the CCIR model; $\sigma_c(dB)$ is the random path-loss of which the typical value is from 8 dB to 10 dB; and $\mathrm{N}(0,1)$ is the standard Gaussian distribution.

Table 3.3 shows the simulation results when the false alarm probability, P_F, is fixed at 5% while the detection probability, P_D, is varied between 95%, 90%, and 80%. $E_c/\mathcal{N}_0$ is the required minimum SIR; $\#m$ is the smallest number of BSs heard; and $\#M$ is the largest number of BSs heard. Except for the detection threshold which depends on the length of integration time, all of the other parameters used are the same as those in Table 3.1.

Table 3.3: Hearability Improvement due to Enhanced Signal Reception ($P_F = 5\%$)

Receiver	Freq Error (Hz)	Integ. Length (chips)	$P_D = 95\%$			$P_D = 90\%$			$P_D = 80\%$		
			$\frac{E_c}{\mathcal{N}_0}$ (dB)	$\#_m$	$\#_M$	$\frac{E_c}{\mathcal{N}_0}$ (dB)	$\#_m$	$\#_M$	$\frac{E_c}{\mathcal{N}_0}$ (dB)	$\#_m$	$\#_M$
				Mean			Mean			Mean	
Rx1		112	-14.3	1	3	-15.1	1	3	-16.2	1	3
				1.40			1.52			1.69	
Rx2	400	650	-21.9	1	4	-22.7	1	4	-23.8	1	4
				2.65			2.85			3.23	
Rx3	160	1500	-25.5	1	6	-26.4	1	6	-27.4	1	8
				3.91			4.33			4.93	

From the simulation results, it can be seen that the required minimum, $E_c/\mathcal{N}_0$, decreases from approximately –15 dB to –25 dB when the enhanced receiver technique is used. Such a dramatic increase of receiver sensitivity can produce better hearability for wireless location purposes. Taking the $P_D = 90\%$ case as an example, the maximum number of

base stations heard increases from 3 to 6 and the average number of BSs increases from 1.5 to 4.3. To describe the above results more clearly, hearability plots for these three receivers are drawn in Figures 3.16 to 3.18. Here, the false alarm probability, P_F, is set at 5% and the detection probability, P_D, is chosen as 90%. The required minimum $E_c/\mathcal{N}_0$ decreases from -15 dB for receiver Rx1, to -22.7 dB for receiver Rx2, and to -26.4 dB for receiver Rx3. Consequently, the average number of BSs heard increases from 1.5, to 2.9, and to 4.3, respectively. The area with optimal hearability for location purposes also increases accordingly.

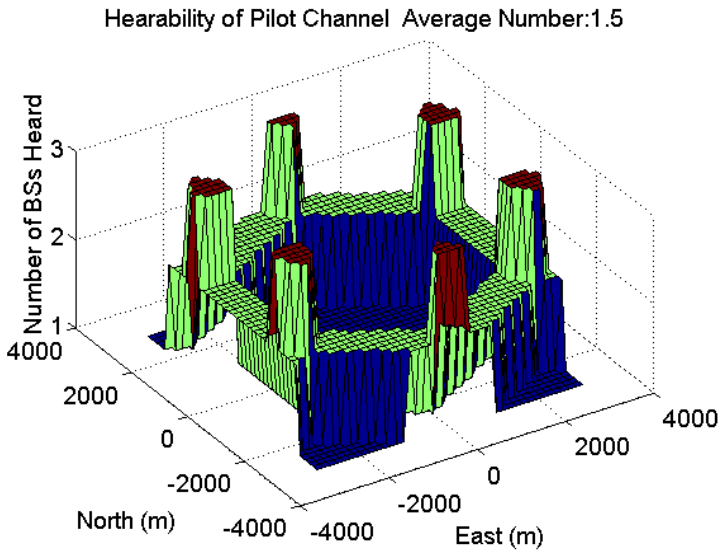

Figure 3.16: Hearability of Receiver Rx1 (Integration Length = 112 Chips)

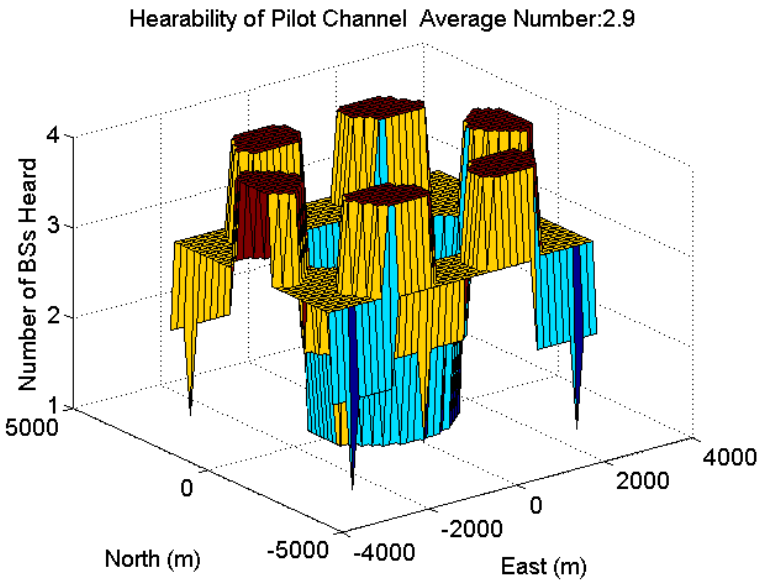

Figure 3.17: Hearability of Receiver Rx2 (Integration Length = 650 Chips)

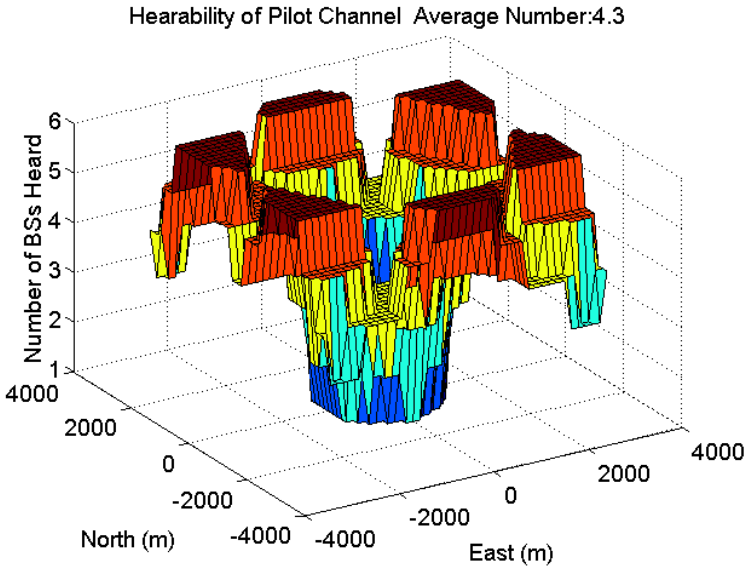

Figure 3.18: Hearability of Receiver Rx3 (Integration Length = 1500 Chips)

3.3.2 IPDL Technique to Improve Forward Link Hearability

The hearability in the region near the BSs is still very poor. This is because of serious "near-far" effects resulting from the signal transmission at the serving BS. To mitigate this effect for further hearability improvement, a BS can discontinue signal transmission for a short time to provide an opportunity for the MSs inside its cell to hear BSs of other cells. This is the so-called Idle Period Down Link (IPDL) method. There exist two IPDL schemes. One is the pseudorandom–IPDL (PR-IPDL) scheme (Ericsson, 1999); the other is the time aligned-IPDL (TA-IPDL) scheme (Motorola, 1999 and Ludden and Lopes, 2000). For the sake of performance comparison with the previous hearability analysis results, the IS-95 pilot signal is used here to study the hearability improvement produced by IPDL techniques.

3.3.2.1 PR-IPDL (Pseudorandom--IPDL)

In this scheme, the idle periods are arranged with a pseudo random pattern among BSs as shown in Figure 3.19 and made known to all MSs in advance. The frequency of idle periods is a parameter that the operator can change to trade off positioning response time against capacity loss. The idle period frequency and the length of the idle period should be as short as possible to ensure that capacity loss is minimized. Normally, the idle frequency is about 1~10 Hz, and the idle period is about 5 or 10 256 chip intervals (Ericsson, 1999).

Figure 3.19: PR-IPDL Idle Period Pattern (Shaded Block Represents the Idle Period)

Let Non-IPDL denote the methods that do not employ IPDL techniques. The difference between a Non-IPDL method and a PR-IPDL method is depicted in Figure 3.20. In the Non-IPDL case, measurements are made when all BSs are transmitting signals. However, in the PR-IPDL case, measurements are made only during the idle period of its serving cell. Therefore, the interference is mitigated due to the lack of strong Same-Cell interference and the SIR of a pilot signal of a non-serving BS at a MS becomes

$$SIR = \frac{\varsigma P_P \cdot L}{P_{I,OC} + P_N} \tag{3.47}$$

where L is path loss due to the transmission from the non-serving BS to the MS. This equation does not contain Same-Cell interference which is actually the strongest interference. The simulation results are summarized in Table 3.4. To make the performance comparison more equitable, the parameters used here are the same as those in Tables 3.1 and 3.3.

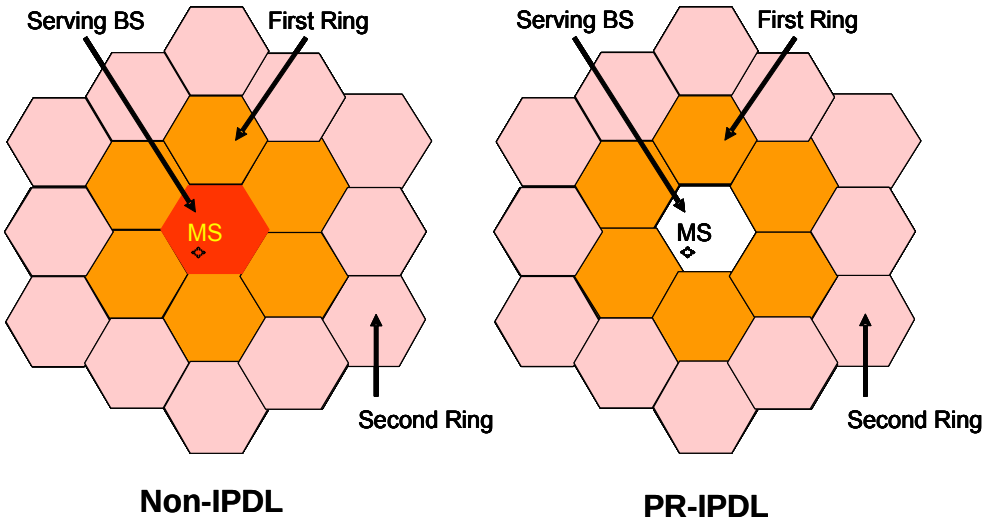

Figure 3.20: Difference between Non-IPDL Methods and PR-IPDL Methods

Table 3.4: Receiver Hearability with PR-IPDL ($P_F = 5\%$)

Receiver	Freq Error (Hz)	Integ. Length (chips)	$P_D = 95\%$			$P_D = 90\%$			$P_D = 80\%$		
			$\frac{E_c}{\mathcal{N}_0}$ (dB)	$\#_m$	$\#_M$	$\frac{E_c}{\mathcal{N}_0}$ (dB)	$\#_m$	$\#_M$	$\frac{E_c}{\mathcal{N}_0}$ (dB)	$\#_m$	$\#_M$
				Mean			Mean			Mean	
Rx1		112	-14.3	1	3	-15.1	1	3	-16.2	1	3
				2.20			2.42			2.72	
Rx2	400	650	-21.9	1	7	-22.7	1	7	-23.8	1	8
				4.90			5.31			6.16	
Rx3	160	1500	-25.5	1	8	-26.4	1	10	-27.4	1	12
				7.91			8.83			10.75	

Hearability improves significantly, as compared to the results shown in Table 3.3. Taking the $P_D = 90\%$ case as an example, although the minimum number and the maximum number of base stations heard for receiver Rx1 are still 1 and 3, respectively, the average number increases from around 1.5 to 2.4. The maximum number of BSs heard increases

dramatically from 4 to 7 for enhanced receiver Rx2 and from 6 to 10 for enhanced receiver Rx3, The average number increases from 2.9 to 5.3 for receiver Rx2 and from 4.3 to 8.8 for receiver Rx3. To further describe this, 3D herability plots for several scenarios are shown in Figures 3.21 to 3.23. These scenarios depict: a normal receiver Rx1 with $P_F = 5\%$, $P_D = 90\%$, and a required minimum $E_c/\mathcal{N}_0$ of -15.1 dB; an enhanced receiver Rx2 with $P_F = 5\%$, $P_D = 90\%$, and a required minimum $E_c/\mathcal{N}_0$ of -26.4 dB; and an enhanced receiver Rx3 with $P_F = 5\%$, $P_D = 90\%$, and a required minimum $E_c/\mathcal{N}_0$ of -25.7 dB. Compared to Figures 3.16 to 3.18, there is a marked increase in the size of the area with better hearability.

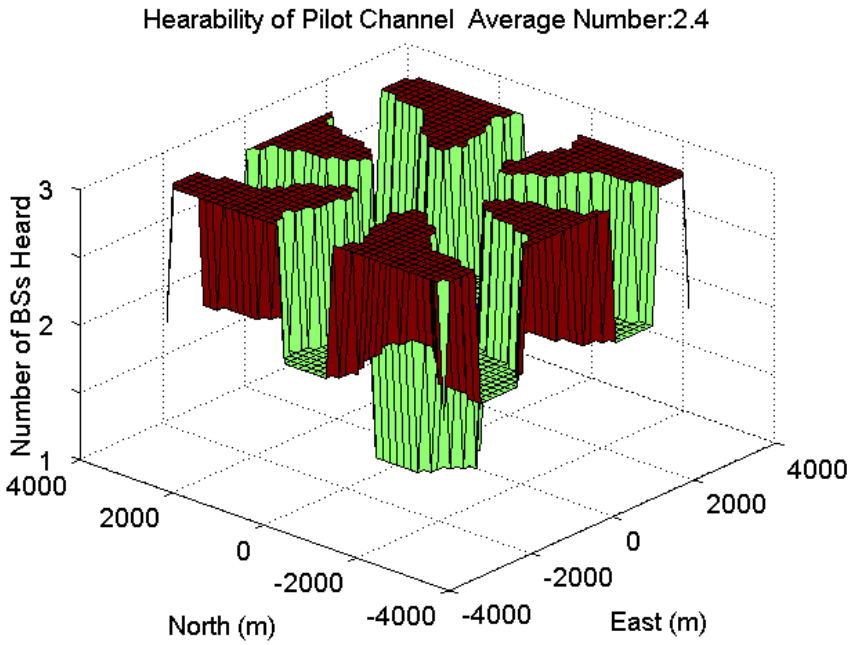

Figure 3.21: Hearability of Receiver RX1 with PR-IPDL

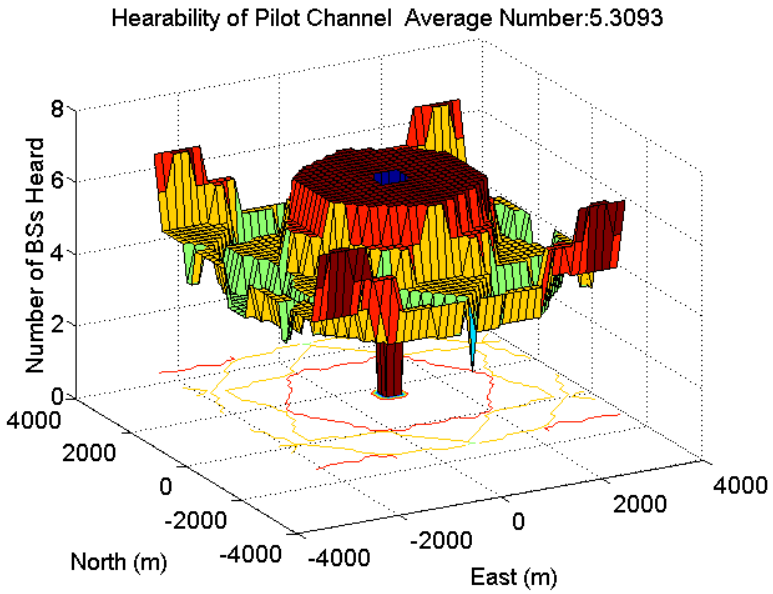

Figure 3.22: Hearability of Receiver Rx2 with PR-IPDL

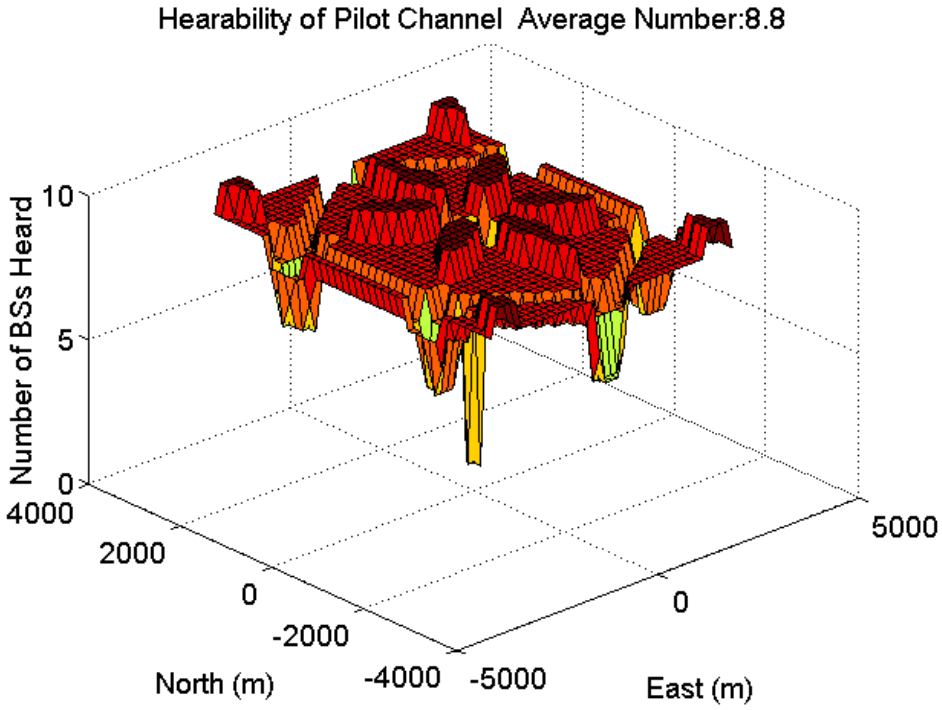

Figure 3.23: Hearability of Receiver Rx3 with PR-IPDL

In a real world implementation, a BS cannot shut off its transmit power completely during the short idle period; normally, it experiences only a –35 dB attenuation instead. Such power leakage will result in poor levels of hearability in the area very close to the serving BS. The existence of this phenomenon can be inferred from the above figures.

3.3.2.2 TA-IPDL (Time Aligned - Idle Period Down Link)

Unlike PR-IPDL, the idle periods in TA-IPDL are synchronized so that each BS goes idle at the same time in the idle frame. The idle pattern is shown in Figure 3.24. During the idle period, all BSs either transmit only pilot signals or keep silent.

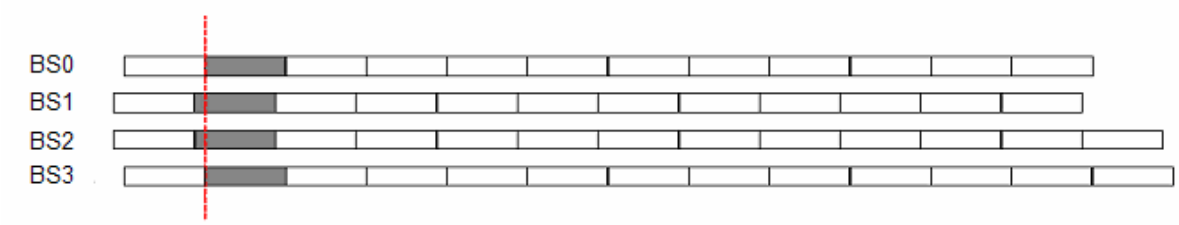

Figure 3.24: TA-IPDL Idle Period Pattern

Such synchronization of idle periods offers some advantages by providing chances to further improve hearability. First, a BS can boost the pilot transmit fraction from 0.1~0.15 to 1.0 since it does not transmit any other signals. This could potentially result in a gain of 7–13 dB in transmit power, thus increasing the pilot range by 1 to 2 octaves depending on the path loss. Secondly, interference can be further decreased since BSs transmit their pilot signal with a probability less than one, namely 0.3 (Thomas, 2001). However, the TA-IPDL method also has disadvantages. First, the time interval between two consecutive measurements has to be extended since the pilot signal of a BS is not transmitted in every idle period. Second, tight synchronization between BSs is required

although it does not impose an additional burden to the cellular network since time synchronization between BSs is necessary for TDOA wireless location. The difference between PR-IPDL and TA-IPDL is depicted in Figure 3.25. During the idle period of the serving BS, all BSs of other cells transmit signals in the PR-IPDL case while only some BSs transmit signals in the TA-IPDL case. Thus, the interference is further mitigated via TA-IPDL.

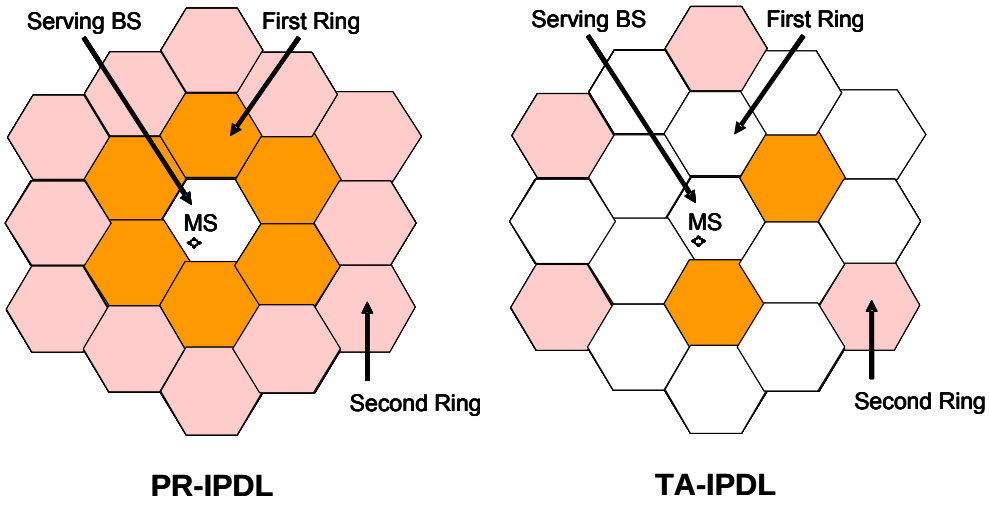

Figure 3.25: Difference between PR-IPDL Method and TA-IPDL Method

In TA-IPDL, the SIR of a pilot signal is

$$SIR = \frac{P_P \cdot L}{\sum_{\substack{i=1 \\ i \neq serving\ BS \\ i \neq BS\ to\ be\ studied}}^{M} \rho_i P_P \cdot L_i + P_N} \tag{3.48}$$

where P_P is the total transmitting power of a BS which is assumed to be equal for all BSs; L_i is the path loss; and ρ_i is the probability that BS_i transmits a pilot signal during an idle period. Compared to that of a Non-IPDL method and a PR-IPDL method, the interference here contains only a portion of Other-Cell noise.

Table 3.5 contains the simulation results from the TA-IPDL method used. The scenario parameters are the same as those in previous experiments. It can be seen that an enhanced receiver can even detect more than 20 base stations. This improvement results from the two advantages mentioned above. Actually, the BSs of the first ring are preferred since they are close to the mobile and introduce less errors to time and direction measurements. In the following chapters, a 7-cell cellular system is often used for simulation tests.

Table 3.5: Receiver Hearability with TA-IPDL ($P_F = 5\%$)

Receiver	Freq Error (Hz)	Integ. Length (chips)	$P_D = 95\%$			$P_D = 90\%$			$P_D = 80\%$		
			$\frac{E_c}{\mathcal{N}_0}$ (dB)	$\#_m$	$\#_M$	$\frac{E_c}{\mathcal{N}_0}$ (dB)	$\#_m$	$\#_M$	$\frac{E_c}{\mathcal{N}_0}$ (dB)	$\#_m$	$\#_M$
				Mean			Mean			Mean	
Rx1		112	-14.3	1	7	-15.1	1	7	-16.2	1	9
				5.85			6.58			7.68	
Rx2	400	650	-21.9	1	19	-22.7	1	19	-23.8	1	23
				15.58			16.73			20.63	
Rx3	160	1500	-25.5	1	31	-26.4	1	34	-27.4	1	37
				25.60			28.60			31	

3.4 Conclusions

In this chapter the concept of hearability has been examined. It has been shown that in a CDMA system the hearability is poor for a normal mobile due to very strong co-channel

interference and receiver noise. Such a poor level of hearability makes wireless location almost impossible.

Special techniques are needed to improve system hearability. One method is the enhanced signal receiving technique. It decreases the required minimum $E_c/\mathcal{N}_0$ by expanding the signal integration time in signal detection and acquisition. However, the integration length is limited by at least two factors, the sensitivity of the decrease of the $E_c/\mathcal{N}_0$ threshold on longer integration time and the frequency difference between incoming pilot signals and local replicas.

Another strategy is found in the IPDL method which improves hearability by mitigating Same-Cell and Other-Cell interference. Two IPDL schemes, PR-IPDL and TA-IPDL, are fully discussed. Simulation results show that both schemes are able to improve the hearability to a satisfactory level: a MS can hear at least 5 BSs at any place inside the cellular network.

CHAPTER 4

AN ENHANCED TWO-STEP LEAST SQUARED APPROACH FOR TDOA/AOA WIRELESS LOCATION

4.1 Introduction

Various wireless location schemes have been proposed (e.g. Reed and James, 1997; Lähteenmäki, 2000; and Caffery and Stüber, 1998). In this chapter, two types of schemes are explored in particular. The first one is a time-based location scheme where the TOAs (time of arrival) or TDOAs (time difference of arrival) of incoming signals are measured and used in MS location estimation. The second one is a direction-based location scheme where AOAs (angles of arrival) of incoming signals are measured and used in MS location estimation. Both schemes have their unique advantages and disadvantages. TDOA/TOA schemes require at least three BSs be heard for a two-dimensional location estimation and generally have a better accuracy than that of AOA schemes. AOA schemes, on the other hand, require only two BSs for location purposes. In practice, these two schemes are often combined, resulting in greater accuracy based on the larger amount of information that is accessible in comparison to individual implementations.

It is not trivial to solve the TDOA/AOA wireless location problem because of the nonlinear relationship between the MS location and TDOA/AOA measurements. Two methods have been proposed to solve this nonlinear problem. In Foy (1976) and Torrieri (1984), a Taylor-series is applied to linearize the problem and calculate the solution. This method is of high accuracy but suffers from a heavy computational burden and divergence issues. To overcome these drawbacks, a two-step LS solution is proposed for TDOA wireless location in Friedlander (1987), Chan and Ho (1994), and Cong and Zhuang (2002). It is a closed-form solution. An intermediate estimate of the MS location is derived in the first step which approximates the original nonlinear problem with a linear one by assuming that MS location is independent of the distance between the reference BS and the MS, although they are actually correlated. The second step attempts to achieve a better result by taking into consideration the relationship between the MS location and the distance between the reference BS and the MS.

However, the original two-step LS approach does not produce the optimal solution because the aim of the second step is to adjust the intermediate result to fit only the relationship between the MS and the reference station. It does not take into account any measurement equations although they actually constrain the final solution. As a result, the original approach exhibits inferior performance. In this chapter, an enhanced two-step LS method is proposed to take care of this deficiency. This enhanced method differs from the original approach only in the second step where it begins by approximating the relationship between the MS and the reference BS with a linear model around the intermediate result; it then transforms the original nonlinear TDOA/AOA wireless

location system into a linear one by combining the approximated MS-reference BS relationship with all the measurements used in the computation of the intermediate solution. The final result of this enhanced method is a constrained LS solution of this linear system.

As an example, this enhanced Two-Step LS approach is applied to a hybrid TDOA/AOA wireless location scheme. In addition to this, the performance differences between the TDOA-only solution and the TDOA/AOA hybrid solution are also compared to show the extent to which AOA measurements can help to increase estimation accuracy. The organization of this chapter is as follows: following this introduction, the hybrid TDOA/AOA wireless location scheme, the Taylor-Series solution, and the original two-step LS solution are discussed in succession. The enhanced two-step LS approach is then explained in detail and simulation results are presented to demonstrate the performance improvement achieved.

4.2 Hybrid TDOA/AOA Wireless Location Scheme

A TDOA wireless location system is a hyperbolic system in which the MS to be located is at the intersection of two or more hyperbolas. The TDOA scheme also constitutes a non-linear problem and tries to solve the following optimization problem to find the MS position (Chen, 1999a):

$$\hat{\mathbf{x}} = \arg\min_{\mathbf{x}} \sum_{i,j \in S, i \neq j} \left(r_{ij} - \left\| \mathbf{x} - \mathbf{X}_i \right\| - \left\| \mathbf{x} - \mathbf{X}_j \right\| \right)^2 \tag{4.1}$$

where r_{ij} is the range difference measurement of the MS to the ith and jth BSs; S is the set of all BSs; and $\mathbf{X}_i$ and $\mathbf{X}_j$ are coordinates of BS_i and BS_j, respectively.

An AOA system normally tries to solve the following problem to determine the MS location (Chen, 1999a):

$$\begin{aligned} \hat{\mathbf{x}} &= \arg\min_{\mathbf{x}} \sum_{i \in S} \mathrm{dist}(\mathbf{x}, \beta_i)^2 \\ \mathrm{dist}(\mathbf{x}, \beta_i) &= \left| -\sin\beta_i (x - x_i) + \cos\beta_i (y - y_i) \right| \end{aligned} \tag{4.2}$$

where the function $\mathrm{dist}(\mathbf{x}, \beta_i)$ is the distance between the MS position (x, y) and the direction line specified by the angle measurement β_i at BS_i.

To improve positioning accuracy, it is best to use as much of the available information as possible. One possible hybrid solution is the hybrid TDOA/AOA wireless location scheme which combines TDOA and AOA measurements together to solve the following problem:

$$\hat{\mathbf{x}} = \arg\min_{\mathbf{x}} \left(\sum_{i,j \in S, i \neq j} \left(r_{ij} - \left\| \mathbf{x} - \mathbf{X}_i \right\| - \left\| \mathbf{x} - \mathbf{X}_j \right\| \right)^2 + \sum_{i \in S'} \mathrm{dist}(\mathbf{x}, \beta_i)^2 \right) \tag{4.3}$$

4.3 Solutions to the Hybrid TDOA/AOA Scheme

The hybrid TDOA/AOA scheme is a nonlinear problem, so it is not trivial to produce a closed-form solution. The most convenient way to solve this problem may be a Gauss-Newton method together with a Taylor-Series linearization. However, this method is recursive and is, thus, computationally burdensome and may suffer from convergence

issues. Another method, the two-step LS method, can yield a closed-form solution and overcome the disadvantages of a Taylor-series method. However, it is not an optimal solution because it does not make use of as much measurement information as possible to maximize solution accuracy.

4.3.1 Taylor-series Linearization Method

The hybrid TDOA/AOA wireless location method tries to solve the following equations in a Least Squares sense:

$$\begin{cases} r_{i1} = \sqrt{(x-x_i)^2+(y-y_i)^2} - \sqrt{(x-x_1)^2+(y-y_1)^2} + n_{i1}^{TDOA} & i \in S \\ \beta_k = \arctan\left(\dfrac{y-y_k}{x-x_k}\right) + n_{\beta k}^{AOA} & k \in S' \end{cases} \tag{4.4}$$

which are equivalent to

$$\begin{cases} r_{i1} = \sqrt{(x-x_i)^2+(y-y_i)^2} - \sqrt{(x-x_1)^2+(y-y_1)^2} + n_{i1}^{TDOA} & i \in S \\ 0 = (x-x_k)\sin\beta_k + (y-y_k)\cos\beta_k + \underbrace{\sqrt{(x-x_k)^2+(y-y_k)^2}\, n_{\beta k}^{AOA}}_{\text{due to AOA measurement noise}} & k \in S' \end{cases} \tag{4.5}$$

where r_{i1} is the TDOA measurement with BS_1 as the reference BS; S is the BS set that generates TDOA measurements; S' is the BS set that generates AOA measurements; $(x_1, y_1)^T$ and $(x_i, y_i)^T$ are locations of the reference BS and other BSs generating TDOA measurements respectively; $(x_k, y_k)^T$ are the locations of the BSs generating AOA measurements; and n_{i1}^{TDOA} and $n_{\beta k}^{AOA}$ are TDOA measurement error and AOA measurement error. The above equations form a nonlinear parametric case LS problem. After linearization with a Taylor-Series expansion, the final solution can be derived as

$$\begin{bmatrix} x \\ y \end{bmatrix} = \begin{bmatrix} x_0 \\ y_0 \end{bmatrix} + \left(\mathbf{G}^T\mathbf{Q}^{-1}\mathbf{G}\right)^{-1}\mathbf{G}^T\mathbf{Q}^{-1}\left(\begin{bmatrix} r_{21} \\ \vdots \\ r_{K1} \\ 0 \\ \vdots \\ 0 \end{bmatrix} - \begin{bmatrix} r_{21}^0 \\ \vdots \\ r_{K1}^0 \\ -(x_0 - x_{k1})\sin\beta_{k1} + (y_0 - y_{k1})\cos\beta_{k1} \\ \vdots \\ -(x_0 - x_{kd})\sin\beta_{kd} + (y_0 - y_{kd})\cos\beta_{kd} \end{bmatrix}\right) \quad (4.6)$$

where

$$\mathbf{G} = \begin{bmatrix} \frac{x_0 - x_2}{r_2} - \frac{x_0 - x_1}{r_1} & \frac{y_0 - y_2}{r_2} - \frac{y_0 - y_1}{r_1} \\ \vdots & \vdots \\ \frac{x_K - x_2}{r_K} - \frac{x_0 - x_1}{r_1} & \frac{y_K - y_2}{r_K} - \frac{y_0 - y_1}{r_1} \\ -\sin\beta_{k1} & \cos\beta_{k1} \\ \vdots & \vdots \\ -\sin\beta_{kd} & \cos\beta_{kd} \end{bmatrix}$$

$$r_{i1}^0 = \sqrt{(x_0 - x_i)^2 + (y_0 - y_i)^2} - \sqrt{(x_0 - x_1)^2 + (y_0 - y_1)^2}$$

and $\mathbf{Q}$ is the variance-covariance matrix of TDOA and AOA measurements which can be derived as follows

$$\mathbf{Q} = \mathrm{E}\left(\begin{bmatrix} \mathbf{n}_{TDOA} \\ \mathbf{n}_{AOA} \end{bmatrix}\begin{bmatrix} \mathbf{n}_{TDOA} \\ \mathbf{n}_{AOA} \end{bmatrix}^T\right) = \begin{bmatrix} \mathrm{E}\left(\mathbf{n}_{TDOA}\mathbf{n}_{TDOA}^T\right) & \mathbf{0} \\ \mathbf{0} & \mathrm{E}\left(\mathbf{n}_{AOA}\mathbf{n}_{AOA}^T\right) \end{bmatrix} = \begin{bmatrix} \mathbf{Q}_{TDOA} & \mathbf{0} \\ \mathbf{0} & \mathbf{Q}_{AOA} \end{bmatrix} \quad (4.7)$$

since the TDOA measurement noise and the AOA measurement noise are zero mean noise and uncorrelated with each other. The noise in one TDOA measurement is actually the combination of the measured BS TOA noise and the reference BS noise, so the variance-covariance matrix of TDOA measurements, $\mathbf{Q}_{TDOA}$ is of the following form

$$\mathbf{Q}_{TDOA} = \mathrm{E}\left(\begin{bmatrix} n_2 - n_1 \\ \vdots \\ n_K - n_1 \end{bmatrix}\begin{bmatrix} n_2 - n_1 \\ \vdots \\ n_K - n_1 \end{bmatrix}^T\right) = \sigma_{TOA}^2\begin{bmatrix} 2 & 1 & \cdots & 1 \\ 1 & 2 & \ddots & \vdots \\ \vdots & \ddots & \ddots & 1 \\ 1 & \cdots & 1 & 2 \end{bmatrix} \quad (4.8)$$

The AOA measurement noise at different BSs is assumed to be uncorrelated but related to the separation between the MS and the BS. The variance-covariance matrix of AOA measurements, $\mathbf{Q}_{AOA}$, is of the following form

$$\mathbf{Q}_{AOA} = \begin{bmatrix} D_{\beta 1}^2 \sigma_\beta^2 & & \mathbf{0} \\ & \ddots & \\ \mathbf{0} & & D_{\beta d}^2 \sigma_\beta^2 \end{bmatrix} = \sigma_\beta^2 \begin{bmatrix} D_{\beta 1}^2 & & \mathbf{0} \\ & \ddots & \\ \mathbf{0} & & D_{\beta d}^2 \end{bmatrix} \tag{4.9}$$

where σ_β^2 is AOA observation variance in radians and is assumed identical for all BSs where AOA measurements are available, $D_{\beta k}$ is the distance between the MS to be located and the BSs where AOA measurements are available.

4.3.2 Original Two-Step LS Method

The two-step LS method, originally proposed for a TDOA location system, can provide closed-form solutions and overcome the drawbacks of the recursive LS method by transforming this non-linear problem into two constituent linear problems. This method is based on two relationships. On the one hand, $r_i = r_{i1} + r_1$. Squaring this quantity, it can be found that

$$r_i^2 = r_{i1}^2 + 2 r_1 r_{i1} + r_1^2 \tag{4.10}$$

where r_i is the distance between the MS to be located and BS_i. On the other hand, $r_i = \|\mathbf{x} - \mathbf{x}_i\|$. Squaring this expression and writing it in component form gives

$$\begin{aligned} r_i^2 &= (x_i - x)^2 + (y_i - y)^2 \\ &= x_i^2 + y_i^2 - 2(x_i x + y_i y) + x^2 + y^2. \end{aligned} \tag{4.11}$$

Letting

$$K = x^2 + y^2 \qquad \text{and} \qquad K_i = x_i^2 + y_i^2 ,$$

the above equation can be written as

$$r_i^2 = K_i - 2(x_i x + y_i y) + K \tag{4.12}$$

Equalizing equations (4.10) and (4.12) gives

$$(x_i - x_1)x + (y_i - y_1)y + r_{i1} r_1 = \frac{1}{2}\left(K_i - K_1 - r_{i1}^2\right) \tag{4.13}$$

Taking all TDOA measurements into consideration, the equations in matrix form are

$$\begin{pmatrix} x_2 - x_1 & y_2 - y_1 & r_{21} \\ \vdots & \vdots & \vdots \\ x_N - x_1 & y_N - y_1 & r_{N1} \end{pmatrix} \begin{pmatrix} x \\ y \\ r_1 \end{pmatrix} = \frac{1}{2} \begin{pmatrix} K_2 - K_1 - r_{21}^2 \\ \vdots \\ K_N - K_1 - r_{N1}^2 \end{pmatrix} \tag{4.14}$$

where all variables except r_1, x, and y are known either from measurements or system design. The system becomes a linear system if r_1, x, and y are independent. However, they are actually related by

$$r_1^2 = (x_1 - x)^2 + (y_1 - y)^2 \tag{4.15}$$

Because of this, such a system is called a *pseudo-linear* system. This property results in the original two-step LS method. In the first step, r_1, x, and y are assumed to be independent and an intermediate result is calculated by solving this pseudo-linear system. In the second step, the intermediate result is further adjusted to satisfy equation (4.15), the relationship among r_1, x, and y.

Such a two-step LS method can also be applied to a hybrid TDOA/AOA wireless location scheme. Taking both TDOA and AOA measurements into consideration, the *pseudo-linear* system becomes

$$\begin{pmatrix} x_2 - x_1 & y_2 - y_1 & r_{21} \\ \vdots & \vdots & \vdots \\ x_N - x_1 & y_N - y_1 & r_{N1} \\ \sin\beta_{k1} & -\cos\beta_{k1} & 0 \\ \vdots & \vdots & \vdots \\ \sin\beta_{kd} & -\cos\beta_{kd} & 0 \end{pmatrix} \begin{pmatrix} x \\ y \\ r_1 \end{pmatrix} = \begin{pmatrix} \left(K_2 - K_1 - r_{21}^2\right)/2 \\ \vdots \\ \left(K_N - K_1 - r_{N1}^2\right)/2 \\ x_{k1}\sin\beta_{k1} - y_{k1}\cos\beta_{k1} \\ \vdots \\ x_{kd}\sin\beta_{kd} - y_{kd}\cos\beta_{kd} \end{pmatrix} \tag{4.16}$$

Or, in matrix form,

$$\mathbf{Gz} = \mathbf{l} \tag{4.17}$$

In this way, the intermediate result, $\mathbf{z}^0 = \begin{bmatrix} x^0 & y^0 & r_1^0 \end{bmatrix}^T$, can be calculated using the normal LS method

$$\mathbf{z}^0 = \left(\mathbf{G}^T\mathbf{Q}^{-1}\mathbf{G}\right)^{-1}\mathbf{G}^T\mathbf{Q}^{-1}\mathbf{l} \tag{4.18}$$

where $\mathbf{Q}$ is the variance-covariance matrix of measurements $\mathbf{l}$. The derivation of $\mathbf{Q}$ for the two-step LS method can be explained as follows. Due to the measurement noise, (4.16) cannot exactly hold and a non-zero misclosure vector $\mathbf{w}$ thus exists

$$\mathbf{w} = \begin{pmatrix} \mathbf{w}_{TDOA} \\ \mathbf{w}_{AOA} \end{pmatrix} = \begin{pmatrix} x_2 - x_1 & y_2 - y_1 & r_{21} \\ \vdots & \vdots & \vdots \\ x_N - x_1 & y_N - y_1 & r_{N1} \\ \sin\beta_{k1} & -\cos\beta_{k1} & 0 \\ \vdots & \vdots & \vdots \\ \sin\beta_{kd} & -\cos\beta_{kd} & 0 \end{pmatrix} \begin{pmatrix} x \\ y \\ r_1 \end{pmatrix} - \begin{pmatrix} \left(K_2 - K_1 - r_{21}^2\right)/2 \\ \vdots \\ \left(K_N - K_1 - r_{N1}^2\right)/2 \\ x_{k1}\sin\beta_{k1} - y_{k1}\cos\beta_{k1} \\ \vdots \\ x_{kd}\sin\beta_{kd} - y_{kd}\cos\beta_{kd} \end{pmatrix} \tag{4.19}$$

Since the TDOA measurement noise and the AOA measurement noise are uncorrelated with each other, $\mathbf{Q}$ is a block diagonal matrix

$$\mathbf{Q} = \begin{bmatrix} \mathbf{Q}_{TDOA}^a & \mathbf{0} \\ \mathbf{0} & \mathbf{Q}_{AOA}^a \end{bmatrix} \tag{4.20}$$

Comparing (4.6) and (4.16) gives

$$\mathbf{Q}_{AOA}^{a} = \mathbf{Q}_{AOA} = \sigma_{\beta}^{2}\begin{bmatrix} D_{\beta 1}^{2} & & \mathbf{0} \\ & \ddots & \\ \mathbf{0} & & D_{\beta d}^{2} \end{bmatrix} \tag{4.21}$$

$\mathbf{Q}_{TDOA}^{a}$ can be determined by studying a TDOA related misclosure element, for example, w_i which is equal to

$$w_i = (x_i - x_1)x + (y_i - y_1)y + r_{i1}r_1 - \frac{1}{2}\left(K_i - K_1 - r_{i1}^2\right). \tag{4.22}$$

Expressing r_{i1} as $r_{i1}^0 + n_{i1}^{TDOA}$ and substituting it and $r_{i1}^0 = r_i^0 - r_1^0$ into the above equation gives

$$w_i = r_i^0 n_{i1}^{TDOA} + \frac{1}{2}\left(n_{i1}^{TDOA}\right)^2 \tag{4.23}$$

Thus, the TDOA related misclosure vector is

$$\mathbf{w}_{TDOA} = \begin{bmatrix} w_2 \\ \vdots \\ w_N \end{bmatrix} = \mathbf{B}\cdot\mathbf{n}_{TDOA} + \frac{1}{2}\mathbf{n}_{TDOA}\otimes\mathbf{n}_{TDOA} \tag{4.24}$$

where $\mathbf{B} = \mathrm{diag}\left(r_2^0, r_3^0, \cdots, r_N^0\right)$, $\mathbf{n}_{TDOA} = \begin{bmatrix} n_{21} & \cdots & n_{N1} \end{bmatrix}^T$, and $\otimes$ represents the element-by-element product. Therefore, $\mathbf{Q}_{TDOA}^{a}$ is

$$\begin{aligned} \mathbf{Q}_{TDOA}^{a} &= \mathrm{E}\left(\mathbf{w}_{TDOA}\cdot\mathbf{w}_{TDOA}^{T}\right) \\ &= \mathbf{B}\cdot\mathrm{E}\left(\mathbf{n}_{TDOA}\cdot\mathbf{n}_{TDOA}^{T}\right)\cdot\mathbf{B}^{T} + \frac{1}{2}\mathbf{B}\cdot\mathrm{E}\left(\mathbf{n}_{TDOA}\cdot\left(\mathbf{n}_{TDOA}^{T}\otimes\mathbf{n}_{TDOA}^{T}\right)\right) \\ &\quad + \frac{1}{2}\mathrm{E}\left(\mathbf{n}_{TDOA}\otimes\mathbf{n}_{TDOA}\cdot\mathbf{n}_{TDOA}^{T}\right)\cdot\mathbf{B}^{T} + \frac{1}{4}\mathrm{E}\left(\left(\mathbf{n}_{TDOA}\otimes\mathbf{n}_{TDOA}\right)\cdot\left(\mathbf{n}_{TDOA}^{T}\otimes\mathbf{n}_{TDOA}^{T}\right)\right) \end{aligned} \tag{4.25}$$

In practice, the TDOA measurement noise is usually much smaller than the separation between a MS and the BSs, i.e., $n_{i1}^{TDOA} << r_i^0$. In this case, $\mathbf{Q}_{TDOA}^{a}$ can be simplified to

$$\mathbf{Q}_{TDOA}^{a} = \mathbf{B}\cdot\mathrm{E}\left(\mathbf{n}_{TDOA}\cdot\mathbf{n}_{TDOA}^{T}\right)\cdot\mathbf{B}^{T} = \mathbf{B}\cdot\mathbf{Q}_{TDOA}\cdot\mathbf{B} \tag{4.26}$$

where $\mathbf{Q}_{TDOA}$ is the variance-covariance matrix of the original TDOA measurement noise and is of the form shown in equation (4.8).

In the second step, this intermediate result $\mathbf{z}^0$, is further adjusted to account for the relationship among r_1, x, and y by means of an artificially created linear problem which is of the following form:

$$\begin{pmatrix} 1 & 0 \\ 0 & 1 \\ 1 & 1 \end{pmatrix} \begin{pmatrix} (x - x_1)^2 \\ (y - y_1)^2 \end{pmatrix} = \begin{pmatrix} (x^0 - x_1)^2 \\ (y^0 - y_1)^2 \\ (r_1^0)^2 \end{pmatrix} \tag{4.27}$$

or

$$\mathbf{G}_a \begin{pmatrix} z_a^x \\ z_a^y \end{pmatrix} = \mathbf{l}_a . \tag{4.28}$$

Thus,

$$\begin{pmatrix} z_a^x \\ z_a^y \end{pmatrix} = \left(\mathbf{G}_a^T \mathbf{Q}_a^{-1} \mathbf{G}_a\right)^{-1} \mathbf{G}_a^T \mathbf{Q}_a^{-1} \mathbf{l}_a \tag{4.29}$$

where $\mathbf{Q}_a$ is the variance-covariance matrix of measurements, $\mathbf{l}_a$, and the detailed derivation can be found in Chan and Ho (1994). The final solution of the MS position, $(x, y)^T$, is

$$\begin{aligned} x &= \pm\sqrt{z_a^x} + x_1 \\ y &= \pm\sqrt{z_a^y} + y_1 \end{aligned} \tag{4.30}$$

Solution ambiguity exists since there are four candidate solutions and special care should be taken to select the correct one. For example, with some effort, the candidate solution

associated with the region of interest can be selected – an element of the problem that is known in advance.

4.3.3 Enhanced Two-Step LS Method

As mentioned above, the original two-step LS approach is not optimal because, in the second step, the method takes only the relationship among r_1, x, and y into account. However, in addition to this, the equations in the pseudo-linear system also need to be satisfied by the final result so as to maintain positioning accuracy. The enhanced two-step LS approach is proposed to take care of this deficiency by making use of equations (4.15) and (4.16) simultaneously. In the second step, the enhanced approach first studies equations (4.15) and (4.16) in (x, y, r_1) 3-D space to identify the non-linear component; then it approximates the non-linear component with a linear one around the intermediate result to make the whole system truly linear. In the last stage, it applies a constrained LS method to calculate the final result which is of higher accuracy than that of the original two step LS method.

Rewriting equations (4.15) and (4.16) gives:

$$\begin{bmatrix} x_2 - x_1 & y_2 - y_1 & r_{21} \\ \vdots & \vdots & \vdots \\ x_M - x_1 & y_M - y_1 & r_{M,1} \\ \sin\beta_1 & -\cos\beta_1 & 0 \\ \vdots & \vdots & \vdots \\ \sin\beta_d & -\cos\beta_d & 0 \end{bmatrix} \begin{bmatrix} x \\ y \\ r_1 \end{bmatrix} = \begin{bmatrix} \left(K_2 - K_1 - r_{21}^2\right)/2 \\ \vdots \\ \left(K_M - K_1 - r_{M1}^2\right)/2 \\ \sin\beta_1 x_{k1} - \cos\beta_1 y_{k1} \\ \vdots \\ \sin\beta_d x_{kd} - \cos\beta_d y_{kd} \end{bmatrix} \tag{4.31}$$

$$r_1^2 = (x_1 - x)^2 + (y_1 - y)^2 \tag{4.32}$$

If x , y , and r_1 are considered as three independent variables of a 3-D space, the equations in (4.31) actually represent a set of planes. They form a linear subsystem. However, equation (4.32) - the relationship among x , y and, r_1 - is nonlinear. It is actually a cone in 3-D space as shown in Figure 4.1.

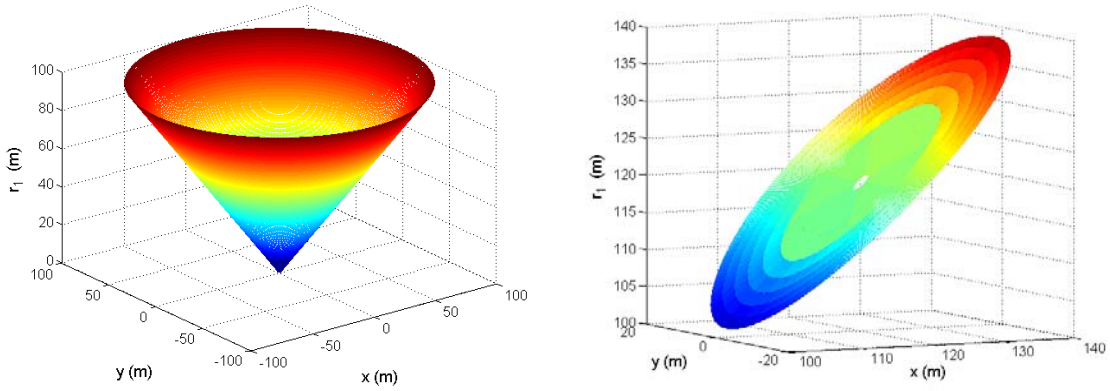

(a) Relationship between x , y and r_1 is a Cone (b) Small Region of the Cone

Figure 4.1: Relationship Among x , y and r_1

It can be found from the above plot that a small region of the cone closely approximates a plane especially when the MS is far from the reference base station. This prompts the approximation of the small region of the cone near the intermediate result with a plane

$$r_1 = ax + by + c \tag{4.33}$$

where a , b , and c are parameters to be determined. Since only equation (4.32) is nonlinear, the whole system becomes a true linear system after this approximation, and LS can then be used to determine the better final result.

The idea behind the approximation of the cone with a plane in a small area is straightforward. First, select an initial point surrounding a region of interest on the cone

based on the intermediate result; then approximate this region with a plane passing through this initial point; and, finally, adjust this plane to best fit the region of interest. Supposing the intermediate result computed in the first step is (x', y', r_1'), the linearization can be made around (x', y') where the MS is assumed to be located. For the sake of simplicity, the coordinates of the reference base station, BS_1, are assumed to be $x_1 = 0$ and $y_1 = 0$ in the following discussion. Thus, the initial point corresponding to (x', y', r_1') on the cone can be chosen as $\mathrm{P} = \left(x', y', \sqrt{(x')^2 + (y')^2} \right)$. The best plane passing through P to approximate the cone is the one that is tangent to the cone. To find it, the normal vector of the cone passing point P is needed. From the relationship among x, y and r_1, it can found that this normal vector is $\left\langle -x', -y', \sqrt{(x')^2 + (y')^2} \right\rangle$. Thus, the best plane passing through point P is:

$$-x'(x - x') - y'(y - y') + \sqrt{x'^2 + y'^2}\left(r_1 - \sqrt{x'^2 + y'^2}\right) = 0 \tag{4.34}$$

However, this plane, named the original approximation plane, is not optimal because the distance between this plane and the cone is not minimized. To get a strictly optimal result, the following problem needs to be solved

$$\mathrm{plane} = \arg\min \iint_S \mathrm{dist}^2(\mathrm{Point}_{cone}(s), \mathrm{plane})\, ds \tag{4.35}$$

where S is the region of interest. It is difficult to solve this optimization problem and, in reality, it is also not necessary since the shape of the cone is well defined and can easily be described as a reasonably adequate plane, even if it is not, strictly speaking, the optimal plane. This desired plane is chosen in the way shown in Figure 4.2

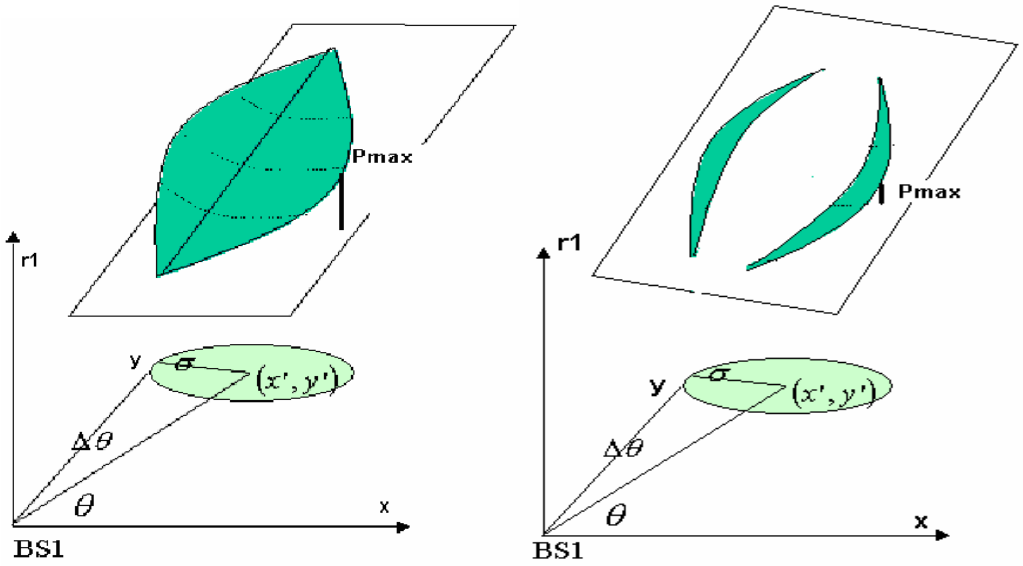

(a) Original approximation (b) Final desired approximation

Figure 4.2: Cone Approximation

In this figure, the circular area with the centre at (x', y') and the radius of σ is the region of interest. σ, determines the region's size, and is related to the accuracy of the intermediate result. Rectangles represent the planes that are optimized. The leaf-shaped region is the conical region of interest. In Figure 4.2(a), the plane is the one expressed by equation (4.34). It passes through the initial point and is tangent to the cone as well, but it is not the optimal. If only the region of interest is investigated, then the maximum distance from the cone to this plane occurs at point P_{max} of which the coordinates are:

$$\begin{aligned} x_p &= \sqrt{x'^2 + y'^2 + \sigma^2}\cos(\theta \pm \Delta\theta) \\ y_p &= \sqrt{x'^2 + y'^2 + \sigma^2}\sin(\theta \pm \Delta\theta) \\ r_{1p} &= \sqrt{x'^2 + y'^2 + \sigma^2} \end{aligned} \tag{5.36}$$

where $\theta = \tan^{-1}\left(y'/x'\right)$ and $\Delta\theta = \tan^{-1}\left(\sigma/\sqrt{x'^2+y'^2}\right)$. The maximum distance is

$$d_{\max} = \frac{\left|-x'x_p - y'y_p + \sqrt{x'^2+y'^2}r_{1p}\right|}{\sqrt{2\left(x'^2+y'^2\right)}}. \tag{4.37}$$

The desired approximation in Figure 4.2(b) is the shifted version of this original plane. The shift is conducted in such a way that the maximum distance between the cone and the desired plane is one-half of the original maximum distance. Supposing the desired plane is

$$-x'x - y'y + \sqrt{x'^2+y'^2}r_1 + D = 0, \tag{4.38}$$

the maximum distance is

$$d = \frac{\left|-x'x_p - y'y_p + \sqrt{x'^2+y'^2}r_{1p} + D\right|}{\sqrt{2\left(x'^2+y'^2\right)}} = \frac{d_{\max}}{2}. \tag{4.39}$$

Thus

$$\begin{aligned} &2\left|-x'x_p - y'y_p + \sqrt{x'^2+y'^2}r_{1p} + D\right| \\ &\quad = \left|-x'x_p - y'y_p + \sqrt{x'^2+y'^2}r_{1p}\right| \end{aligned} \tag{4.40}$$

and D can be easily determined from this equation as

$$D = \frac{1}{2}\left(x'x_p + y'y_p - \sqrt{x'^2+y'^2}r_{1p}\right). \tag{4.41}$$

Figure 4.3 illustrates the result of the original approximation and the desired approximation. Figure 4.4 illustrates the approximation accuracy in terms of the maximum distance between the cone and the desired plane. Obviously, the larger the region of interest, the larger the approximation error; and the farther the MS position is

away from the reference station, the smaller the approximation error. σ can be selected at a value from 100 m to 150 m, depending on the accuracy of the intermediate result. In this case, the maximum approximation error is normally at the level of 3 to 10 metres.

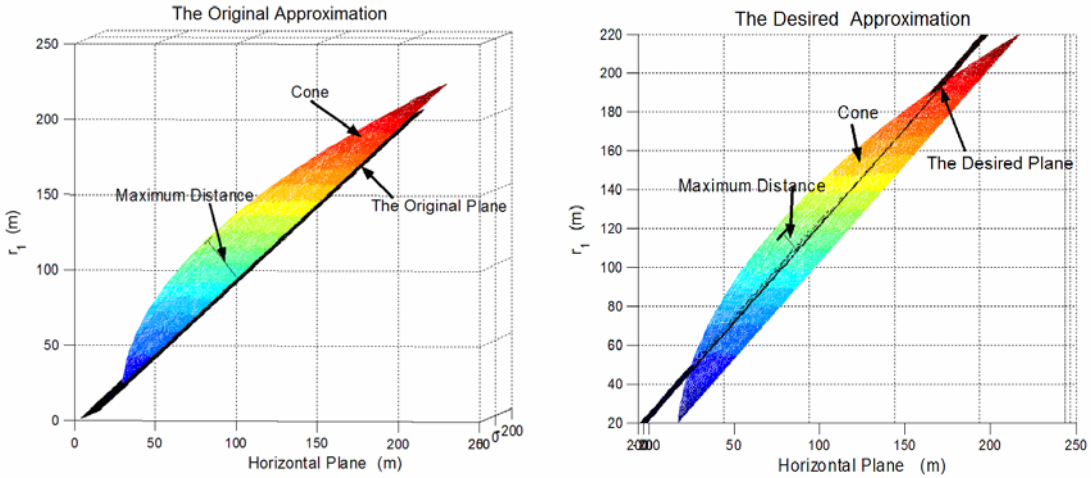

Figure 4.3: Original and Desired Approximation

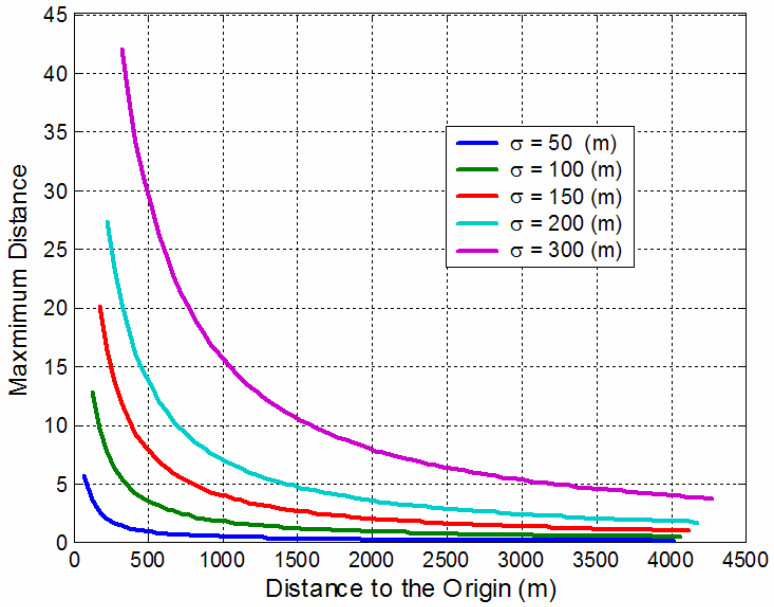

Figure 4.4: Approximation Error

After the approximation, the combination of equations (4.31) and (4.32) becomes a true linear system. MS location can be readily solved from equation (4.31) by means of a constrained LS algorithm with the constraint,

$$-x'x - y'y + \sqrt{x'^2 + y'^2}\, r_1 + D = 0 . \tag{4.42}$$

4.4 Simulation Results

This section presents simulation results to demonstrate the performance improvement of the enhanced two-step LS approach compared to the original two-step LS method and the Taylor-series method. In the simulation, a 7-cell 2-D cellular phone system layout is assumed, as shown in Figure 2.14. Furthermore, it is also assumed that the MS to be located is in the central hexagonal cell, surrounded by six adjacent hexagonal cells of the same size. The cell radius is 2 km. For simplicity, all TDOA measurement noise is assumed to be of the same standard deviation. All experiments here are Monte Carlo experiments and each scenario contains 1000 independent runs.

4.4.1 Algorithms Studied

In this section, a performance comparison among the Taylor-series method, the original two-step LS method, and the enhanced two-step method is conducted. Also investigated is the performance improvement in comparing TDOA-only methods to hybrid TDOA/AOA methods and the influence of AOA measurement accuracy on the final positioning accuracy. The following table summarizes all algorithms studied here.

Table 4.1: Algorithms for Comparison

TDOA-Only Algorithms	TDOA/AOA Algorithms
TDOA-Only Taylor Series	TDOA/AOA Taylor Series
Original TDOA-Only Two Step LS	Original TDOA/AOA Two Step LS
Enhanced TDOA-Only Two Step LS	Enhanced TDOA/AOA Two Step LS

4.4.2 Performance Comparison at One Point

Figures in this subsection demonstrate performance differences at one point. In this scenario, it is assumed that only 4 TDOA measurements and 2 AOA measurements are available and the MS is at (1000 m, 1000 m) with its serving BS at the origin. The method employed to evaluate positioning accuracy is shown in Figure 4.5 where the cumulative probability with respect to position error threshold is shown. The horizontal axis represents the position error threshold and the vertical axis represents the cumulative probability by which the positioning error is smaller than the corresponding error threshold. Obviously, the higher the cumulative probability, the better the performance.

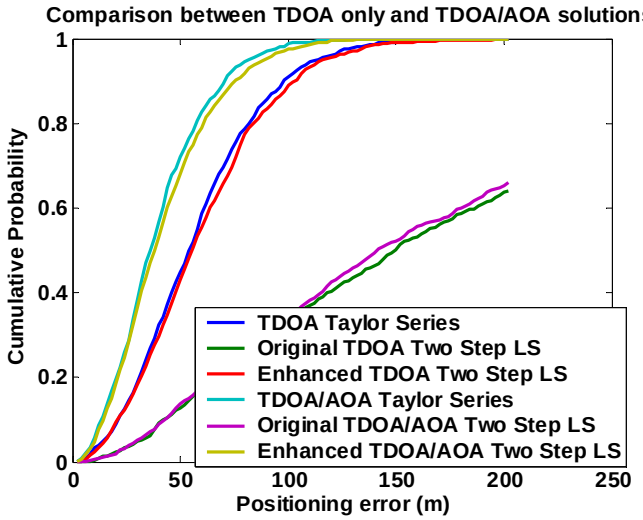

Figure 4.5: Algorithm Performance Comparison at a Single Point
(4 TDOAs, 2 AOAs, STD_{TDOA} =100 m, STD_{AOA} =1 degree)

In the scenario for Figure 4.5, the standard deviation of TDOA measurements is assumed to be 100 m; the standard deviation of AOA measurements is assumed to be 1 degree; and the cell size is 2 km in radius. It can be seen from the figure that: (1) the TDOA/AOA Taylor-series method and enhanced TDOA/AOA two-step LS method produce the best performance and the accuracy difference between these two methods is insignificant; (2) the original TDOA/AOA two step LS method and original TDOA-only two step LS method yield the worst performance; and that AOA information is not extremely helpful in accuracy improvement in this case; and (3) the TDOA-only Taylor-series method and enhanced TDOA-only two-step LS method offer moderate performance as compared to the above methods. It can concluded that the enhanced two-step LS method yields comparable performance to that of the Taylor-series method from an accuracy point of view. With the incorporation of AOA information, the positioning accuracy of both the Taylor-series method and enhanced two-step method can be improved. By comparison, the original two-step LS method provides degraded performance even if AOA information is available. This is expected since the original method does not take TDOA/AOA measurements into account when the intermediate result is modified to fit equation (4.32) in the second step.

To investigate the influence of AOA measurement accuracy on final positioning accuracy, an additional pair of experiments were conducted. In the first experiment, shown in Figure 4.6, the standard deviation of AOA measurements is 5 degrees. In this case there is almost no performance improvement when AOA information is used. This is because the accuracy of the AOA measurements is so poor that it provides no useful

information. In the second experiment, the results of which are shown in Figure 4.7, the standard deviation of the AOA measurements is 0.3 degrees and it is evident that location accuracy is significantly improved for the TDOA/AOA Taylor-series and enhanced TDOA/AOA two step LS methods.

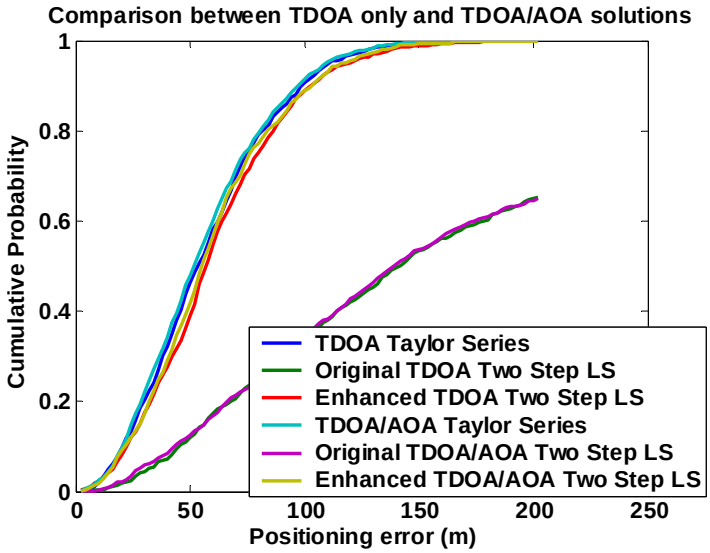

Figure 4.6: Influence of AOA Measurement Accuracy on Location Accuracy
4 TDOAs, 2 AOAs, STD_{TDOA} =100 m, STD_{AOA} =5 degrees

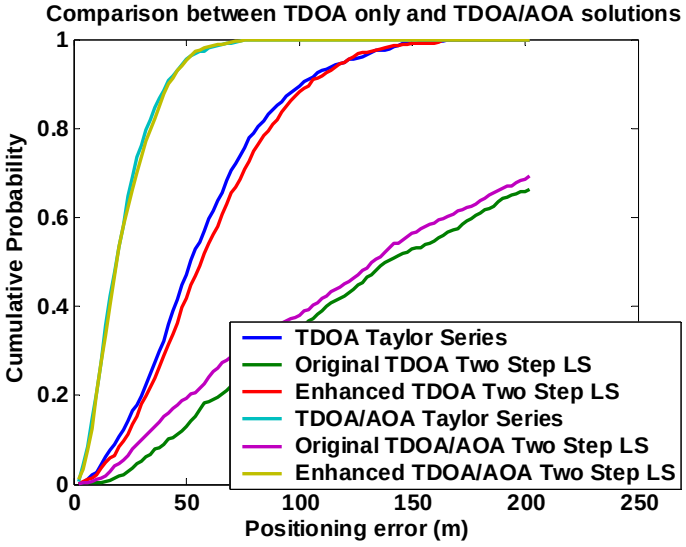

Figure 4.7: Influence of AOA Measurement Accuracy on Location Accuracy
4 TDOAs, 2 AOAs, STD_{TDOA}=100 m, STD_{AOA} =0.3 degree

Table 4.2 shows the positioning error of all the above methods when the accumulative probability is 50%. The values give an evaluation of the performance of these solutions.

Table 4.2: Positioning Error with the Cumulative Probability of 50%
(4TDOAs 2AOAs STD_{TDOA} = 100 m)

	STD_{AOA} = 0.3 degrees	STD_{AOA} = 1 degrees	STD_{AOA} = 5 degrees
TDOA-Only Taylor Series	51.8 m	54.5 m	53.6 m
Original TDOA-Only Two Step LS	133.5 m	150.6 m	142.9 m
Enhanced TDOA-Only Two Step LS	56.8 m	56.4 m	57.2 m
TDOA/AOA Taylor Series	18.6 m	29.5 m	51.9 m
Original TDOA/AOA Two Step LS	140.0 m	142.9 m	140.4 m
Enhanced TDOA/AOA Two Step LS	18.6 m	32.1 m	55.6 m

4.4.3 Performance Comparison with Respect to Different MS-BS Separations

The simulations presented in this section demonstrate the positioning accuracy of the above methods with respect to the distance between the MS to be located and its serving BS. The cellular system used here is still the 7-cell system but with a radius of 3 km. The MS is located in the central cell and all 7 BSs are assumed to be available for TOA/TDOA measurements, while only the serving BS is assumed to be available for AOA measurement.

Figure 4.8 shows the variation of HDOP with respect to different MS-serving BS separations. It can be seen that HDOP is about 0.8 and is almost constant when all of the BSs are available.

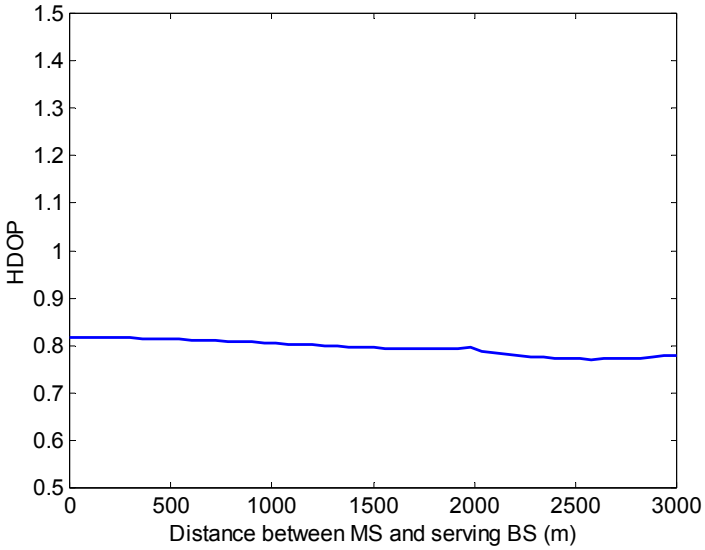

Figure 4.8: HDOP with Respect to MS-Serving BS Separation

Figures 4.9(a) to 4.9(d) are the results when the standard deviation of TDOA measurements is 35 m and the standard deviations of AOA measurements are 0.2 degrees, 1 degree, 5 degrees, and 10 degrees, respectively. The horizontal axis represents the MS-serving BS separation in metres and the vertical axis represents the RMS value of horizontal positioning errors, also plotted in metres. From these figures, the following conclusions are drawn:

- The TDOA/AOA Taylor-series method and enhanced TDOA/AOA two step LS method produce the best performance
- The TDOA-only Taylor-series method and enhanced TDOA-only two step LS method are the second-best methods
- The final positioning accuracy of the Taylor-series method and the enhanced two step LS method are almost the same. Therefore, the enhanced two step LS method

is preferred since its computational burden is light and it does not suffer from divergence issues.

- The original two step LS method is the worst. Its RMS error is 2~4 times higher than that of the Taylor-series and enhanced two step LS methods. Furthermore, the error increases at a faster rate with the increase of MS-BS separation.
- AOA information allows improvement in positioning accuracy; the higher the accuracy of AOA, the greater the improvement.
- With the increase of MS-BS separation, the uncertainty introduced by AOA measurements will also increase. As a result, the incremental improvement due to AOA information is lessened as MS-BS separation increases.

Figures 4.10(a) to 4.10(d) are the simulation results when the standard deviation of TDOA measurements is 100 m and the standard deviations of AOA measurements are 0.2 degrees, 1 degrees, 5 degrees, and 10 degrees. Compared to Figure 4.9, it can be seen that there is no marked difference except that the location accuracy decreases somewhat owing to the larger TDOA measurement errors. Similar conclusions can be drawn from Figure 4.10 as those drawn from Figure 4.9. The only difference is that AOA information can improve location performance more in the situation represented in Figure 4.10 than that in Figure 4.9. This distinction is obvious since TDOA measurements in the scenario of Figure 4.10 are noisier; by comparison, AOA measurements are able to contribute credible and useful information to the solution due to the superiority.

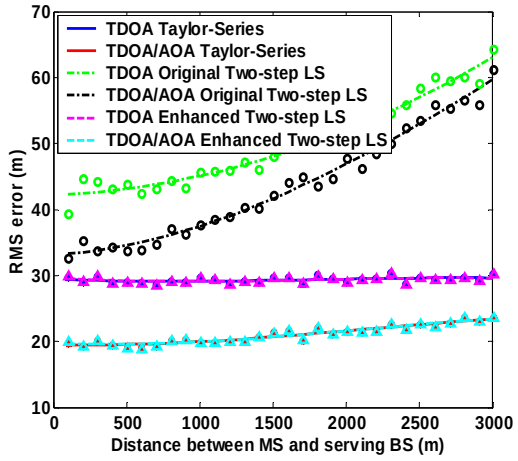

(a) σ_{AOA} = 0.2 degrees

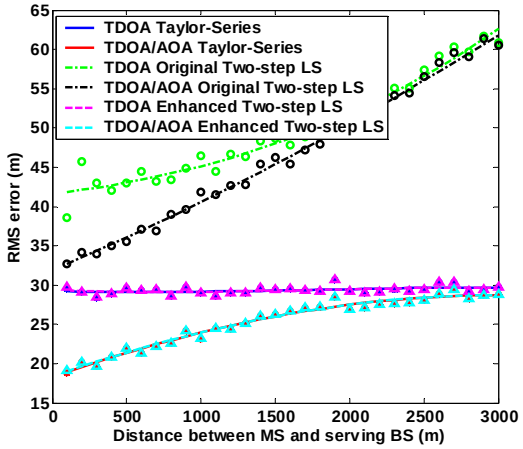

(b) σ_{AOA} = 1 degree

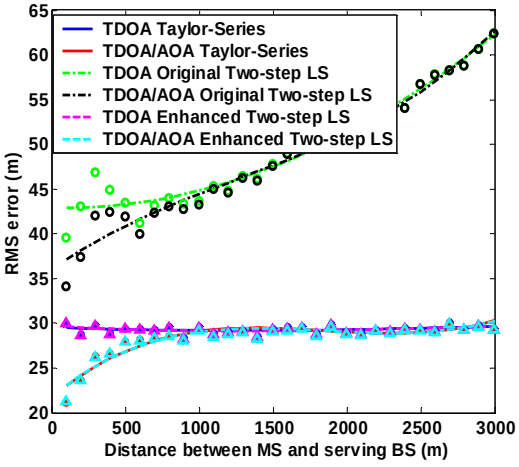

(c) σ_{AOA} = 5 degrees

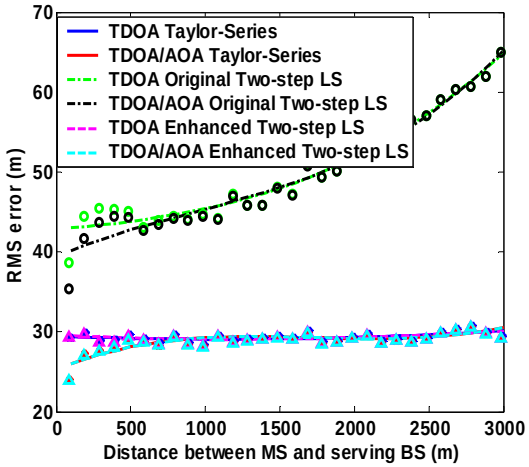

(d) σ_{AOA} = 10 degrees

Figure 4.9: Positioning Accuracy Comparison in the Case of Different AOA Measurement Accuracies and the same TDOA Measurement Accuracy (σ_{TDOA} = 35 m)

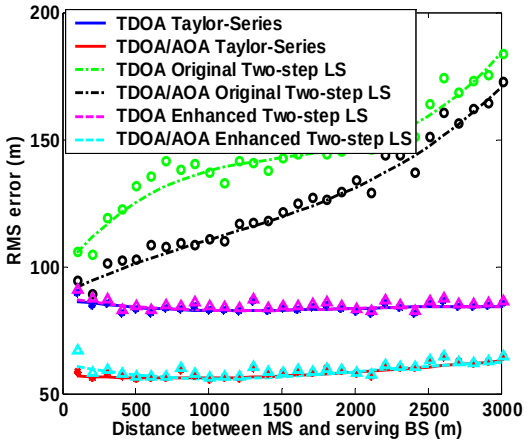

(a) σ_{AOA}=0.2 degree

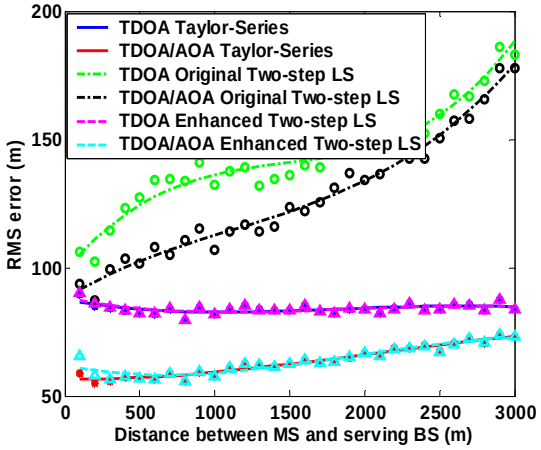

(b) σ_{AOA} = 1 degree

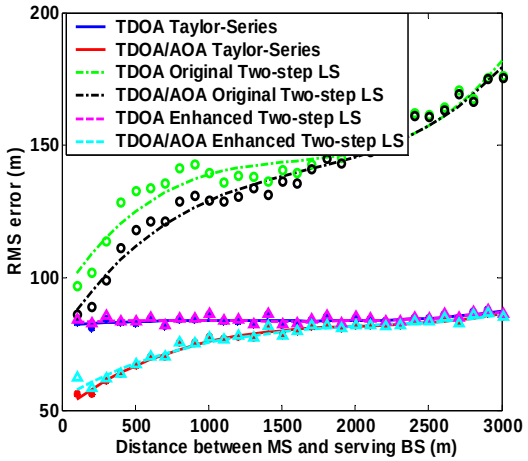

(c) σ_{AOA} = 5 degrees

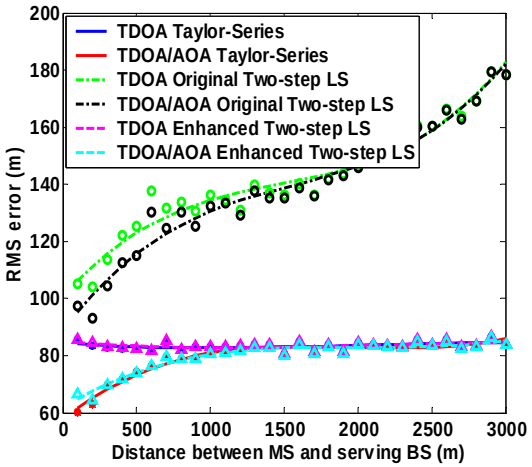

(d) σ_{AOA} = 10 degrees

Figure 4.10: Positioning Accuracy Comparison in the Case of Different AOA Measurement Accuracies and the same TDOA Measurement Accuracy (σ_{TDOA} = 100 m)

4.4.4 Performance Comparison When NLOS Errors Exist

Only measurement noise was considered in the TOA measurements in the previous section. Here, the influence of NLOS errors on the performance of all methods is studied. NLOS errors are obtained as the excessive delay multiplied by the speed of light. Their magnitude depends on the nature of the propagation environment, and is subject to change from time to time. NLOS errors are normally treated as random variables and can be derived from the delay profiles described by a probability density function of excessive propagation delay with respect to a direct path. Three frequently used delay profiles to generate random NLOS errors are presented here.

- Exponential Distribution (Yacoub,1993)

$$D(\tau)=\begin{cases}\dfrac{1}{\tau_{rms}}\exp\left(-\dfrac{\tau}{\tau_{rms}}\right) & \tau>0\\ 0 & otherwise\end{cases} \tag{4.43}$$

- Uniform Distribution:

$$D(\tau)=\begin{cases}\dfrac{1}{2\sqrt{3}\tau_{rms}} & 2\sqrt{3}\tau_{rms}>\tau>0\\ 0 & otherwise\end{cases} \tag{4.44}$$

- Delta Distribution (Lee, 1997)

$$D(\tau)=\begin{cases}\dfrac{1}{2}\left[\delta(\tau)+\delta(\tau-2\tau_{rms})\right] & \tau>0\\ 0 & otherwise\end{cases} \tag{4.45}$$

where τ_{rms} is the delay spread which depends on the physical environment. Greenstein et al (1997) suggested that τ_{rms} is log-normally distributed and could be further characterized by four environmental dependence variables.

$$\tau_{rms} = T_1 d^{\varepsilon} \xi \tag{4.46}$$

where

T_1 is the median value of τ_{rms} at $d = 1$ km

d is the distance between the transmitter and receiver in kilometres

ε is an exponent that lies between 0.5-1.0

ξ is a log-normal random variable. Specifically, $10\log\xi$ is a Gaussian random variable having zero mean and a standard deviation, σ_{ξ}, that lies between 2-6 dB.

The typical values of these parameters for bad urban, typical urban, suburban, and rural areas are listed in Table 4.3. A typical urban area represents a non-hilly urban area where multipath signals are not clustered; a bad urban area represents a hilly area where multipath signals are clustered. In the simulations that follow, τ_{rms} is chosen as 0.6 μs for a typical urban situation.

Table 4.3 Typical NLOS Error Parameter Values for Different Environments

Environment types	$T_1\,(\mu s)$	ε	σ_{ξ}
Bad Urban	1.0	0.5	4 dB
Urban	0.4	0.5	4 dB
Suburban	0.3	0.5	4 dB
Rural	0.1	0.5	4 dB

Two methods can be used to create samples of a random variable with a special distribution. They are the inversion method and the rejection method (Klukas, 1997). In

this chapter, exponential NLOS errors are simulated. So, only the inversion method is briefly described here.

Inversion method: Let $F(x)$ be the cumulative distribution function of X. A random number from distribution $F(x)$ can be generated by the following two steps: (1) Generate $u \sim \text{uniform}(0,1)$; (2) Solve $u = F(x)$ for x and return x as a generated random number. Taking the exponential NLOS error distribution (4.43) as an example, the cumulative distribution function is

$$F(\tau) = 1 - \exp\left(-\frac{\tau}{\tau_{rms}}\right) \qquad \tau > 0 \tag{4.47}$$

Solving this equation gives

$$\tau = -\tau_{rms} \ln(1-u) \tag{4.48}$$

τ is of the desired exponential distribution when u is uniformly distributed in $(0,1)$.

Figures 4.11 and 4.12 depict positioning errors of the methods being studied. The standard deviations of TDOA measurements are 35 m in Figure 4.11 and 100 m in Figure 4.12. The associated standard deviations of AOA vary between 0.2 degrees, 1 degree, 5 degrees, and 10 degrees. TOA measurements are assumed to suffer from NLOS errors with urban exponential distribution (4.43) of which the distribution and the samples are shown in Figures 4.13 and 4.14. Although the absolute positioning accuracies are different, the changes of the positioning accuracies for all of the methods in these two figures are similar to those presented in Figures 4.9 and 4.10. The inference can, therefore, be drawn that NLOS errors affect all of the methods in a similar manner. This is a reasonable conclusion since all methods studied here are merely different solutions to

essentially the same location problem. To improve positioning accuracy, such NLOS errors need to be mitigated or removed from the measurements before an MS position can be calculated. An effective NLOS mitigation algorithm is proposed in the next chapter.

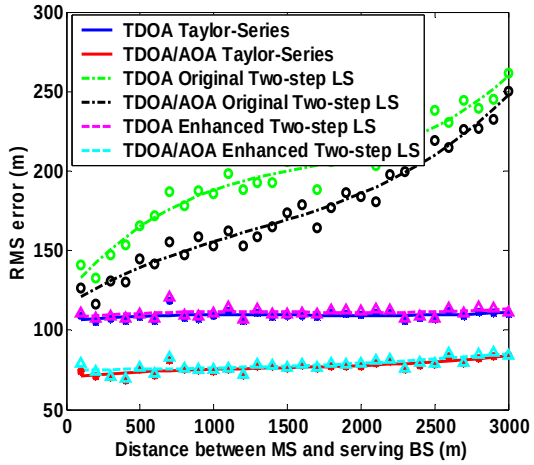

(a) σ_{AOA} = 0.2 degree

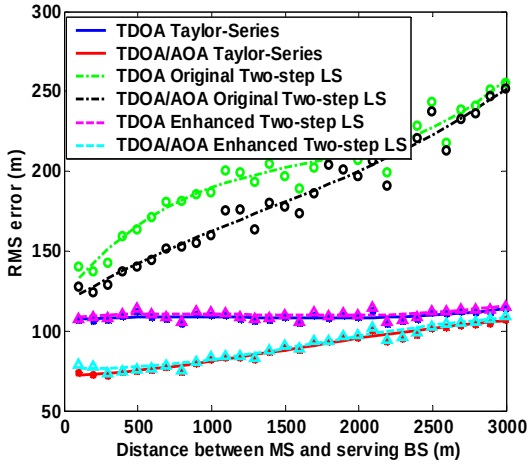

(b) σ_{AOA} = 1 degree

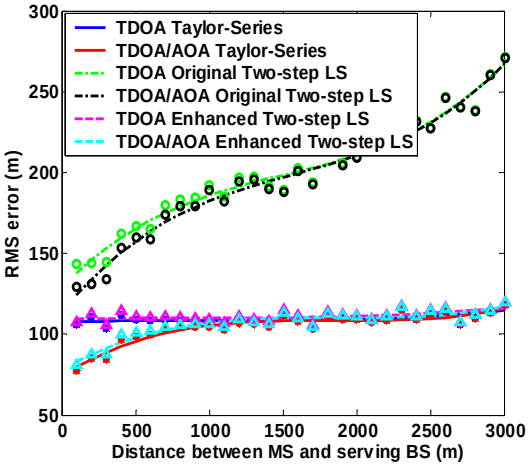

(c) σ_{AOA} = 5 degrees

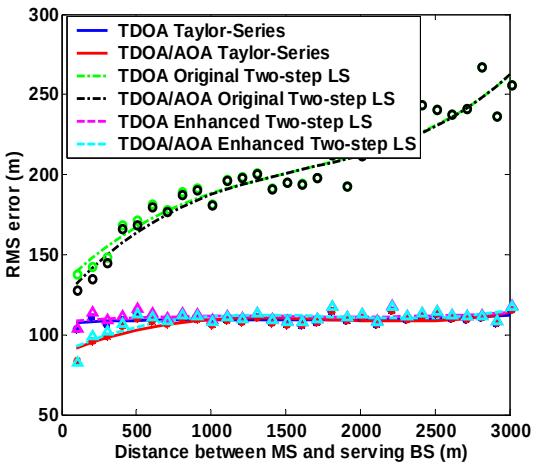

(d) σ_{AOA} = 10 degrees

Figure 4.11: Positioning Accuracy with NLOS Errors Exist (σ_{TDOA} = 35 m)

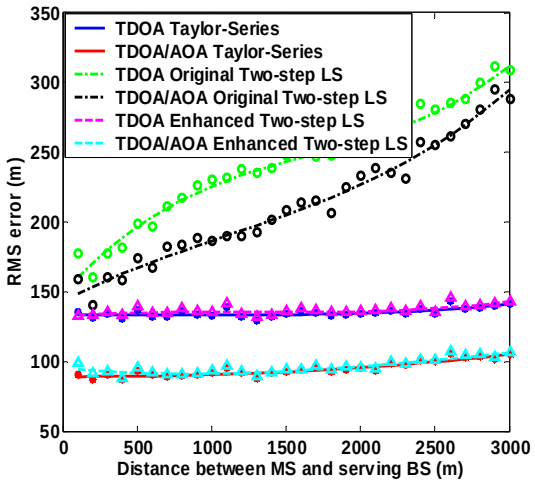

(a) σ_{AOA} = 0.2 degree

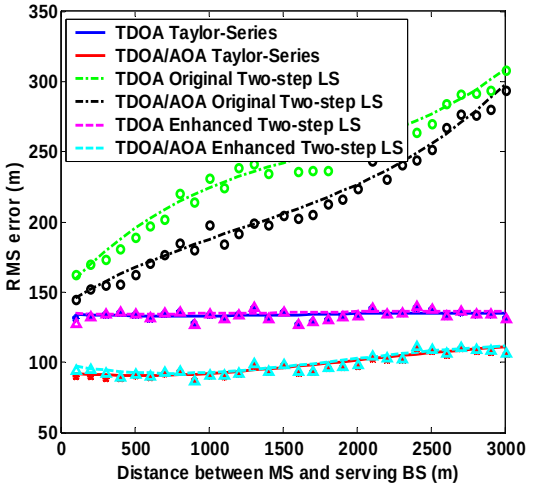

(b) σ_{AOA} = 1 degree

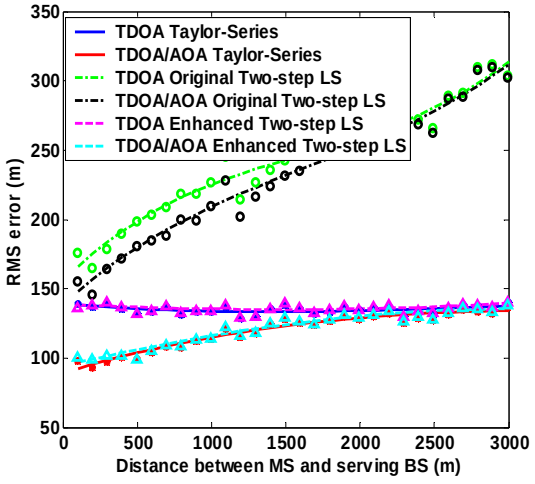

(c) σ_{AOA} = 5 degrees

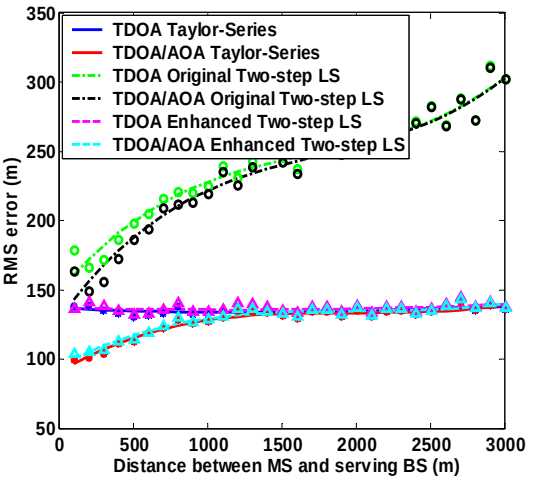

(d) σ_{AOA} = 10 degrees

Figure 4.12: Positioning Accuracy with NLOS Errors Exist (σ_{TDOA} = 100 m)

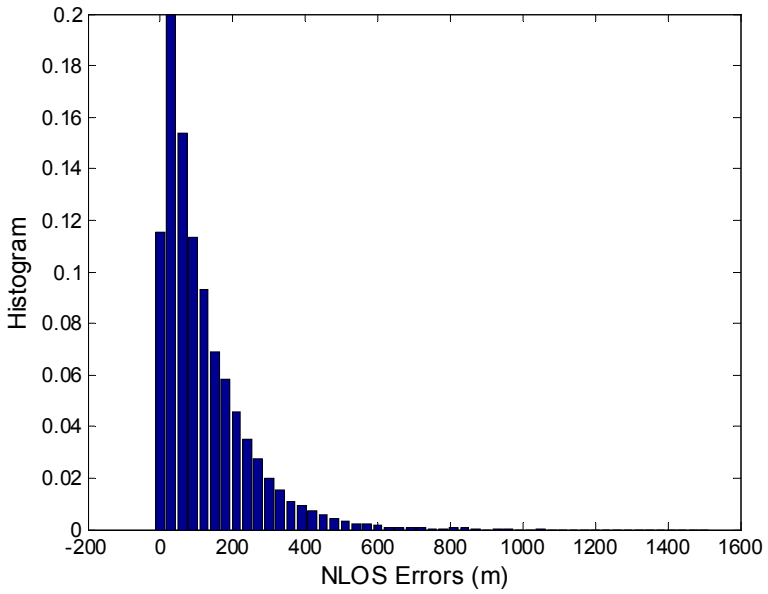

Figure 4.13: Histogram of Exponential NLOS Errors in an Urban Environment

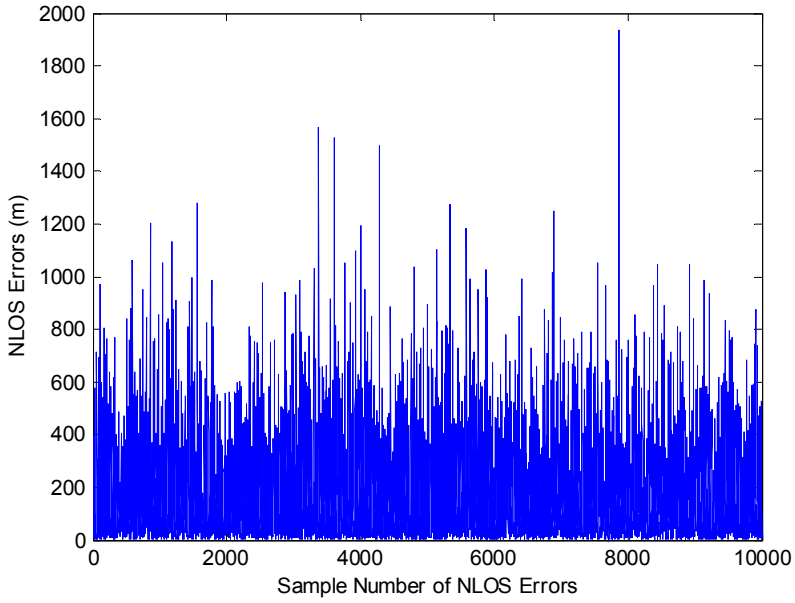

Figure 4.14: Samples of Exponential NLOS Errors in an Urban Environment

4.4.5 Computational Burden Comparison

In this section, the computational burdens of these methods are briefly compared. The methodology used is to compare the processing time for each method to complete the same task. This is an easy and reasonable method since the necessary processing time is proportional to computational burden. The computer used is a desktop computer with a Pentium 4 CPU (Speed: 2.4 GHz) and 512 Mega byte memory; and the software used is MATLAB 6.5 with the Windows XP operating system.

Figures 4.15 and 4.16 demonstrate the variation of processing time for each method with respect to MS-serving BS separations. The difference between these two figures is the initial point selected for the Taylor-series method. The initial point for Figure 4.15 is selected 450 metres away from the true MS position while the initial point for Figure 4.16 coincides with the true MS position. Each scenario in the figures contains 1000 independent runs and the Taylor–series solution stops when the difference between two sequential MS position estimates is less than 1 metre.

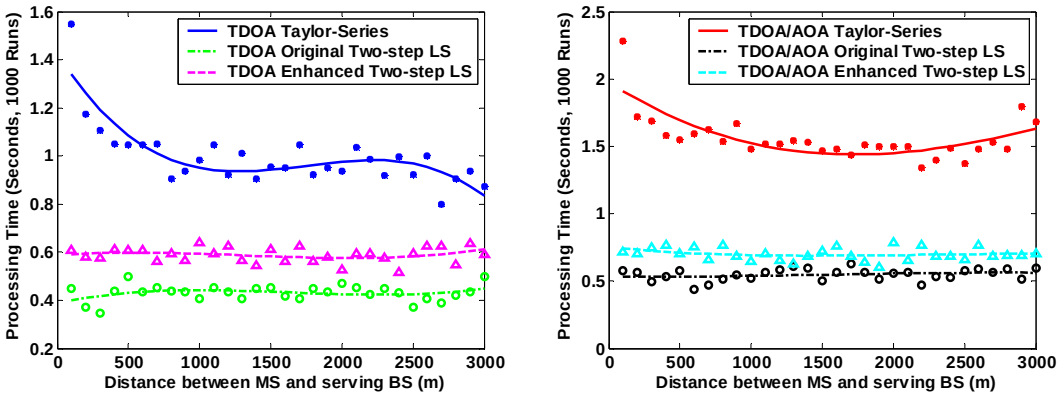

Figure 4.15: Processing Time Comparison between Taylor-Series Method and Two-Step LS Method (Initial Error: 450 metres)

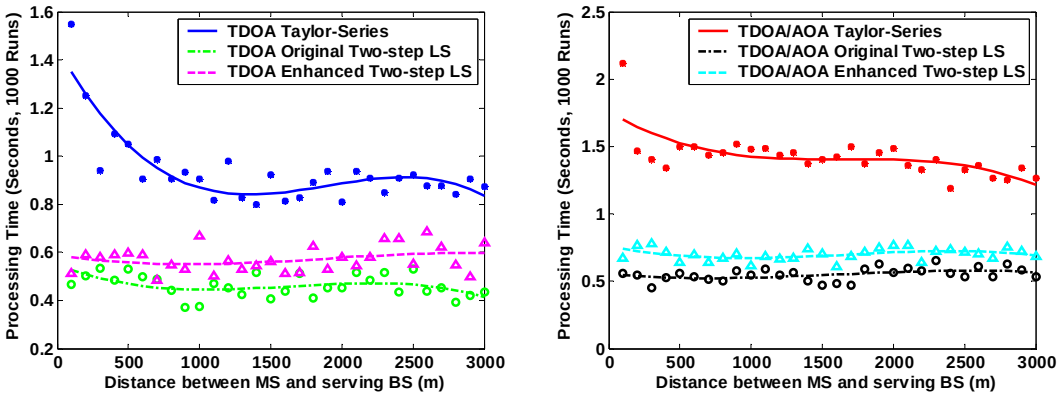

Figure 4.16: Processing Time Comparison between Taylor-Series Method and Two-Step LS Method (Initial Error: 0 metres)

It is evident that Taylor-series method has the heaviest computation burden; the original two-step LS method has the lightest computation burden; the computational burden of the enhanced two-step LS method is only slightly greater than that of the original two-step LS method. This is expected since, as mentioned above, the Taylor-series method is a recursive method and each step needs to conduct linearization and solve the LS problem. The two-step LS method is a non-recursive method and only two LS problems need to be solved. The approximation of the cone and a larger dimension LS problem in the second step of the enhanced two-step LS method results in a slight greater computation burden compared to the original version method.

It is also worth noting that processing time for the TDOA/AOA case is slightly longer than for the TDOA-only case because more measurements are involved and the model dimension is larger. The processing time for the two-step LS method is almost independent of MS-serving BS separation since the computation procedure is nearly constant. The processing time for the Taylor-series method decreases when the MS

moves away from its serving BS. This means that more iterations are required for the solution to converge when the MS is near its serving BS.

4.5 Conclusions

In this chapter, an enhanced two-step LS approach was proposed for hybrid TDOA/AOA wireless location. Compared to the original two-step LS algorithm, the method herein is capable of providing better performance, and is almost as accurate as a Taylor-series estimator. The reason is that unlike the original two-step method, the second step of this enhanced version can make use of all available measurement information. Compared to the Taylor-series solution, the method has the advantage of lightness of computational burden and the absence of convergence issues. Performance of the hybrid TDOA/AOA scheme can be improved compared to a TDOA-only wireless location scheme. However, performance improvement can be obtained only when AOA measurement accuracy is sufficiently high with respect to TDOA measurement accuracy. For example, AOA measurement accuracy needs to be better than 1 degree in standard deviation in order to improve positioning performance when the standard deviation of TDOA measurements is about 35 metres.

CHAPTER 5

A NON-LINE-OF-SIGHT ERROR MITIGATION METHOD FOR TOA MEASUREMENTS

5.1 Introduction

The major error sources in wireless location consist of non-line-of-sight propagation errors and receiver noise. NLOS errors are actually the dominant error compared to receiver noise (Caffery and Stüber, 1998). Actual field testing shows that the average NLOS range error can be as large as 0.589 km in an IS-95 CDMA system (Woo et al, 2000).

NLOS error identification and removal techniques have to be applied to prevent observations from being seriously corrupted and to yield satisfactory positioning accuracies. In Woo et al (2000), NLOS errors are identified by comparing the standard deviations of range measurements with a detection threshold. In Wylie and Holtzman (1996), a time-history based hypothesis test is proposed to identify and then remove NLOS errors. In Borrás et al (1998), a decision framework for NLOS identification is formulated which can process both Gaussian and non-Gaussian NLOS errors. In Chen (1999b), a residual weighting algorithm proposed for a TOA location system is also able

to identify NLOS errors with unknown distribution. Additional efforts are currently being made in this area and a substantial number of NLOS mitigation algorithms (e.g. Ma et al, 2002; Venkatraman and Caffery, 2002; and Venkatraman et al, 2002) have recently been proposed.

In this chapter, the NLOS errors in a TDOA based wireless location system are investigated and an algorithm is proposed for NLOS error identification and mitigation. Simulation results are presented to demonstrate the performance improvement achieved due to the NLOS error mitigation method proposed.

5.2 Error Issue

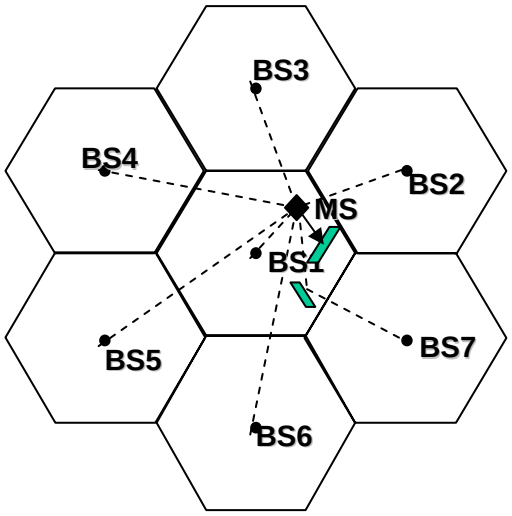

Figure 5.1: NLOS Error

As illustrated by the signal transmission between BS7 and MS in Figure 5.1, an NLOS error results from the blockage of direct signals and the reflection of multipath signals. It is the extra distance that a signal travels from transmitter to receiver and as such always

has a nonnegative value. Normally, an NLOS error can be described as a deterministic error, a Gaussian error, or an exponentially distributed error. However, at a given instant in time, it can be treated as a constant (Cong and Zhuang, 2001).

This section demonstrates the performance degradation of a time-based wireless location scheme due to NLOS errors. The MS location in a time-based wireless location scheme is usually obtained by solving an estimation problem. The observations are a set of range measurements (TOA) or range difference measurements (TDOA), and the parameters to be estimated are the MS coordinates. Taking the TOA method as an example, the LS estimator used for MS location estimation is of the following form,

$$\hat{\mathbf{x}} = \arg\min_{\mathbf{x}} \sum_{i \in S} \left(r_i - \left\| \mathbf{x} - \mathbf{X}_i \right\| \right)^2 \tag{5.1}$$

where $\|\cdot\|$ denotes the norm operation over a vector; $\mathbf{x}$ represents MS position**;** $\hat{\mathbf{x}}$ represents the estimate of MS position; $\mathbf{X}_i$ is the position of the ith BS; $\left\| \mathbf{x} - \mathbf{X}_i \right\|$ is the distance between $\mathbf{x}$ and $\mathbf{X}_i$; S is the set of BSs used; r_i is the range measurement from the MS to the ith BS, $i \in S$; and $\left(r_i - \left\| \mathbf{x} - \mathbf{X}_i \right\| \right)$ is, thus, the range residual.

If no observation errors exist, then $\hat{\mathbf{x}}$ is equal to the true MS position. However, $\hat{\mathbf{x}}$ normally contains estimation errors because raw measurements are, in reality, always observation-error corrupted. If receiver noise and NLOS errors are taken into consideration, the range measurements of an MS with respect to N BSs can be expressed as:

$$r_i = L_i + n_i + NLOS_i \qquad i = 1,...,N \tag{5.2}$$

where r_i is the range observation to the ith BS; L_i is the LOS range $L_i = \|\mathbf{x} - \mathbf{X}_i\|$; n_i is receiver noise; and $NLOS_i$ is the NLOS error. The receiver noise, n_i, is assumed to be a zero mean Gaussian random variable with a standard deviation of about 60 m~100 m for an IS-95 CDMA system. It can be much smaller if better signal receiving techniques are applied.

Expressed in matrix-vector form, the measurements in a TOA wireless location scheme are

$$\mathbf{r} = \mathbf{L} + \mathbf{n} + \mathbf{NLOS} \tag{5.3}$$

where **L** are the true distances between the MS and the BSs; **n** is receiver noise; and **NLOS** are NLOS errors. If the true MS location is used as the initial point in the LS solution, the range measurements can be expressed via a Taylor-series expansion as

$$\mathbf{r} \approx \mathbf{L} + \mathbf{G}\begin{bmatrix}\Delta x \\ \Delta y\end{bmatrix} \tag{5.4}$$

where **G** is the design matrix, and $[\Delta x \quad \Delta y]^T$ is the MS location error. Obviously, the final solution of the problem is

$$\begin{bmatrix}\Delta x \\ \Delta y\end{bmatrix} = \left(\mathbf{G}^{\mathrm{T}}\mathbf{G}\right)^{-1}\mathbf{G}\cdot\mathbf{n} + \left(\mathbf{G}^{\mathrm{T}}\mathbf{G}\right)^{-1}\mathbf{G}\cdot\mathbf{NLOS}. \tag{5.5}$$

Because NLOS errors are much larger than the measurement noise, the positioning errors result mainly from NLOS errors if NLOS errors exist.

5.3 NLOS Error Mitigation Algorithm

Since NLOS errors seriously degrade positioning accuracy, they must be removed from measurements before these measurements are applied in the MS location calculation. In this section, an algorithm is proposed to mitigate NLOS errors. Without losing generality, the TDOA location scheme is taken here as an example to illustrate how the NLOS errors are mitigated.

This algorithm depends on system redundancy and its idea is quite straightforward. As illustrated in Figure 5.2, each TDOA measurement determines a hyperbola between two BSs and two of these hyperbolas determine an intersection that is actually a candidate for the MS location to be computed. Using the hearability improvement techniques discussed in Chapter 3, there are normally more hyperbolas than the minimum number required. Thus, a set of intersections can be produced to form an intersection distribution.

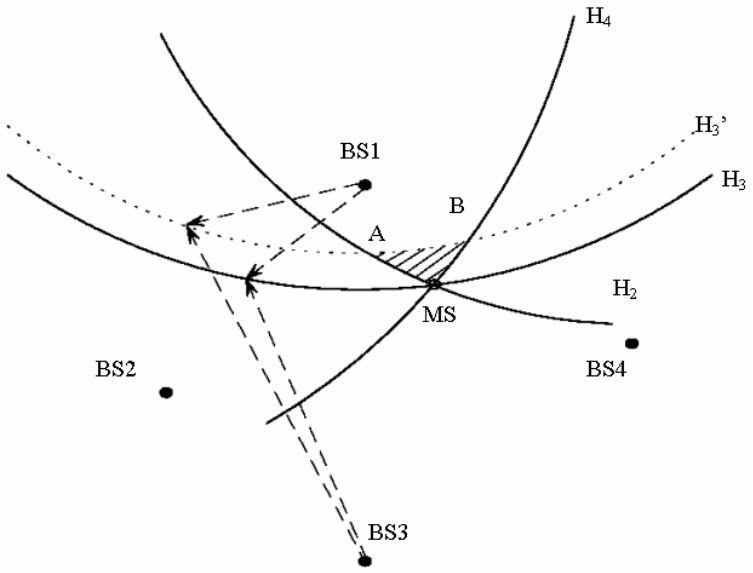

Figure 5.2: Hyperbola Intersection

The intersection distribution has the following properties. The area of uncertainty is small if there are no NLOS errors. In other words, the intersections are concentrated near the true MS location as shown in Figure 5.3(a). The area of uncertainty is large if there are BSs suffering from NLOS errors. Assuming that the LOS signal of a BS is blocked, the TDOA measurements related to this BS will have a bias equal to the NLOS error and the associated hyperbolas will be offset from the true MS location. Consequently, the intersections between these biased hyperbolas and other hyperbolas will also be offset from the true MS location, forming a larger area of uncertainty. As shown in Figure 5.3(b), hyperbola H4 contains an NLOS error, so both this hyperbola and all of its intersections with other hyperbolas are offset from the true MS location.

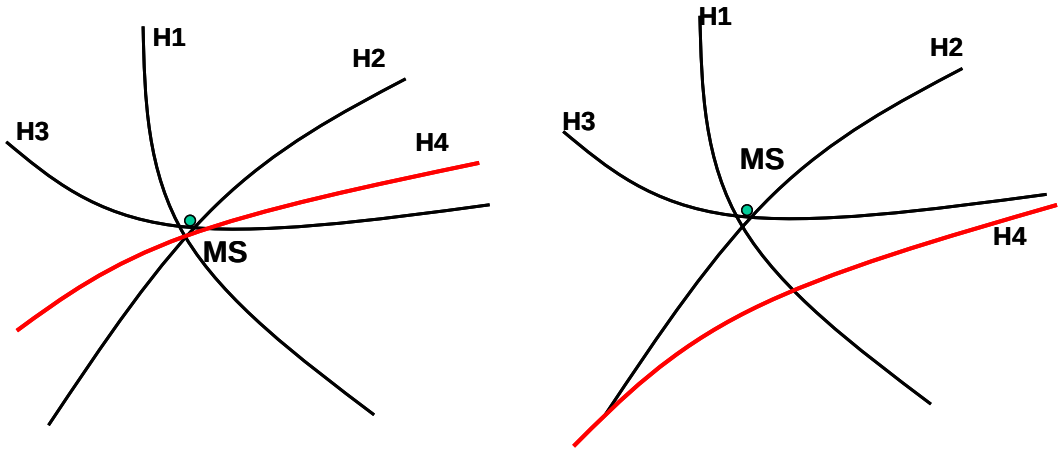

(a) NLOS Error Free Case (b) NLOS Error Corrupted Case

Figure 5.3: Intersections Offset by NLOS Errors

The proposed NLOS error mitigation algorithm is based on the different distributions of NLOS-free intersections (clear intersections) and NLOS-corrupted intersections (biased intersections). A clear intersection is calculated from two NLOS-free TDOA measurements, and a biased intersection is calculated from two TDOA measurements at

least one of which is NLOS error corrupted. If the system redundancy is high enough and only a small number of observations contain NLOS errors, it can be expected that there exists a significant number of clear intersections near the true MS position. Therefore, a higher intersection density should occur near the true MS position. By seeking the maximum point of the intersection distribution, a rough estimate of the MS position can be computed from which NLOS errors can be identified and removed. The procedure to mitigate NLOS errors is summarized in Figure 5.4, and all of these steps are thoroughly discussed in the following sections.

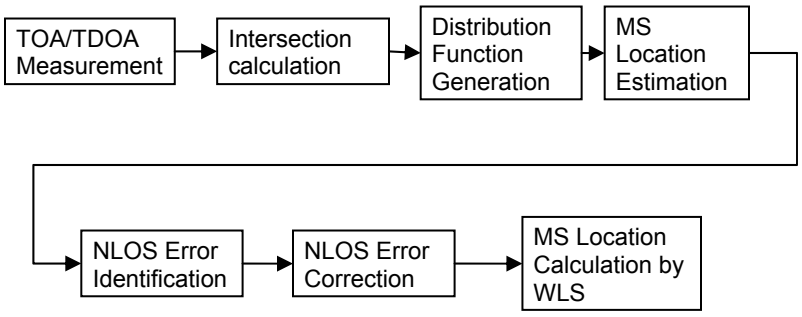

Figure 5.4: Steps in NLOS Mitigation Algorithm

In this chapter, it is assumed that the original measurements are TOA measurements and that TDOA measurements are derived by the combination of these TOA measurements.

5.3.1 Hyperbola Intersection Calculation

The intersection of two hyperbolas is the solution of the following two equations.

$$\begin{cases} \sqrt{(x-x_1)^2+(y-y_1)^2}-\sqrt{(x-x_2)^2+(y-y_2)^2}=TDOA_1 \\ \sqrt{(x-x_3)^2+(y-y_3)^2}-\sqrt{(x-x_4)^2+(y-y_4)^2}=TDOA_2 \end{cases} \tag{5.6}$$

where $\mathbf{X}_1 = (x_1, y_1)^{\mathrm{T}}$, $\mathbf{X}_2 = (x_2, y_2)^{\mathrm{T}}$, $\mathbf{X}_3 = (x_3, y_3)^{\mathrm{T}}$, and $\mathbf{X}_4 = (x_4, y_4)^{\mathrm{T}}$ are the coordinates of four BSs, and $\mathbf{X} = (x, y)^{\mathrm{T}}$ represents the intersections to be solved. It is difficult to obtain a closed-form solution since these equations are non-linear in nature. In this chapter, the following optimization problem is solved to calculate hyperbola intersections:

$$\hat{\mathbf{x}} = \arg\min_{\mathbf{x}} \left\{ \left(\|\mathbf{x} - \mathbf{X}_1\| - \|\mathbf{x} - \mathbf{X}_2\| - TDOA_1 \right)^2 + \left(\|\mathbf{x} - \mathbf{X}_3\| - \|\mathbf{x} - \mathbf{X}_4\| - TDOA_2 \right)^2 \right\} \quad (5.7)$$

since the intersection satisfying the equations (5.6) will also minimize the cost function in equation (5.7). This method is not suitable for real-world implementation because of a high computational burden, but is convenient for performance analysis with MATLAB.

5.3.2 Construction of Distribution Function

The distribution function is key in this NLOS mitigation algorithm. It is used to quantify the intersection distribution density and thereby to arrive at an intermediate MS location estimate. This estimate will be used for succeeding NLOS error identification and mitigation. The Distribution function is defined as

$$DF(x, y) = \sum_{i=1}^{M} \exp\left(- \frac{\left((x - x_i)^2 + (y - y_i)^2 \right)}{\varepsilon^2} \right) \quad (5.8)$$

where M is the total number of intersections; (x_i, y_i) are the coordinates of the intersections computed via the method proposed above; and ε^2 is a value to control the coverage or the contribution of an intersection to the final distribution function. ε needs to be well selected because it corresponds to the solution uncertainty due to receiver

noise. If one is too optimistic and selects a very small value of ε, the uncertainty area of each intersection will be unreasonably small such that the final distribution function has only discrete spikes. In this case, one is unable to determine where the distribution density is high and where it is low. If one is too pessimistic and selects a very large value of ε, the uncertainty area of each intersection will be too large and the final distribution function will be too flat. This will result in the insensitivity of the optimization process to receiver errors and will result in poor location accuracy. As a rule of thumb, ε should be chosen as $1 \sim 2$ times the standard deviation of the receiver noise. Figure 5.5 demonstrates how a distribution function varies with ε. In Figure 5.5(a), ε is selected as 0.1 times the standard deviation of the measurement noise. In this case, the final distribution function has only discrete spikes that prevent estimation of the MS position because of the lack of a dominant peak. In Figure 5.5(b), because ε is chosen to be equal to 10 times the standard deviation of the measurement noise, the final distribution function has only one flat peak that will result in poor estimation accuracy. In Figure 5.5(c), ε is equal to 1.5 times of the standard deviation of the measurement noise; here, the final distribution function has a much better-shaped peak and yields an adequate estimate of the MS position.

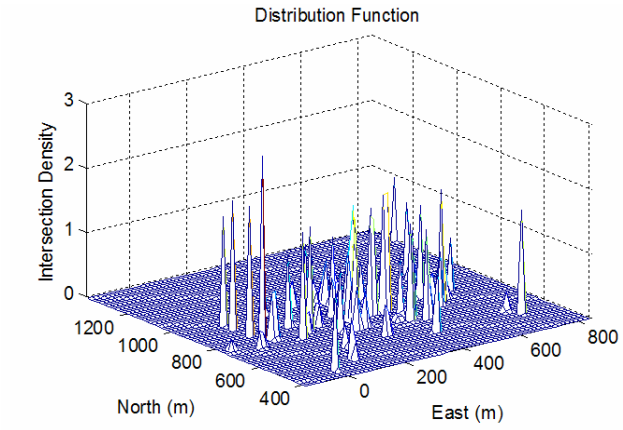

(a) $\varepsilon = 0.1 \cdot \mathrm{STD}_{\mathrm{TDOA}}$

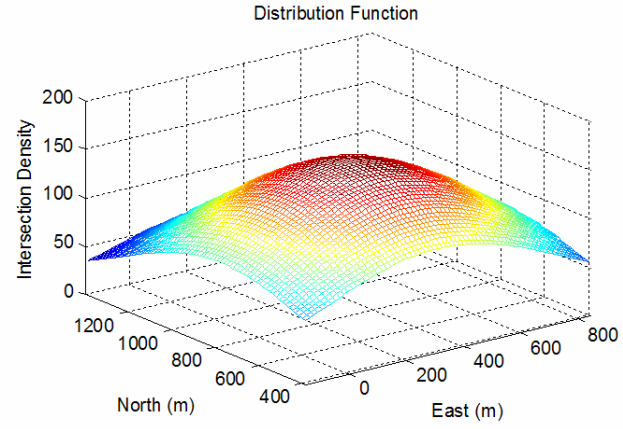

(b) $\varepsilon = 10 \cdot \mathrm{STD}_{\mathrm{TDOA}}$

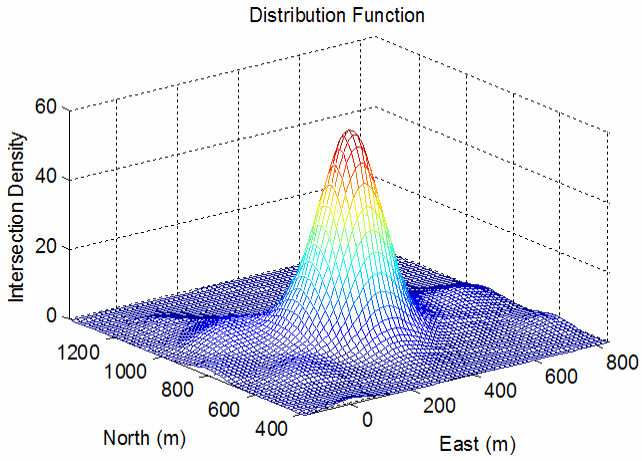

(c) $\varepsilon = 1.5 \cdot \mathrm{STD}_{\mathrm{TDOA}}$

Figure 5.5: Selection of ε for Distribution Function Construction

5.3.3 MS Location Estimation

Two types of solutions can be used as the estimate of the MS position. One is the point that maximizes the distribution function

$$(x,y)=\arg\max_{(x,y)}\left\{\sum_{i=1}^{M}\exp\left(-\frac{\left((x-x_i)^2+(y-y_i)^2\right)}{\varepsilon^2}\right)\right\}. \tag{5.9}$$

The other is the weighted combination of local maximum points. Supposing that there are N local maximum points, $P_i=(x_i,y_i), i=1,\cdots,N$ with the corresponding distribution density values of $q_i=DF(x_i,y_i)$, the MS estimation is

$$(x,y)=\sum_{i=1}^{N}\frac{q_i}{\sum_{j=1}^{N}q_j}P_i. \tag{5.10}$$

The solution of equation (5.9) is used in each of the simulation tests that is described in this chapter.

5.3.4 NLOS Identification

For each BS, a cost function can be formed to identify if the measurement of this BS is NLOS error corrupted. The cost function proposed here has the following form:

$$L(BS_i)=\sum_{k=1\,k\neq i}^{M}\left(TDOA_{i,k}^{m}-TDOA_{i,k}^{0}\right) \tag{5.11}$$

where M is the number of BSs used, $TDOA_{i,k}^{m}$ is the measured distance difference between $\mathrm{MS-BS}_i$ and $\mathrm{MS-BS}_k$, and $TDOA_{i,k}^{0}$ is the true distance difference. By

definition, a measured distance difference can be further expressed as its true value plus NLOS error and receiver noise.

$$\begin{aligned} TDOA_{i,k}^{m} &= TOA_{i}^{m} - TOA_{k}^{m} \\ &= TOA_{i}^{0} + NLOS_{i} + n_{i} - TOA_{k}^{0} - NLOS_{k} - n_{k} \\ &= \left(NLOS_{i} - NLOS_{k}\right) + \left(n_{i} - n_{k}\right) + TDOA_{i,k}^{0} \ . \end{aligned} \tag{5.12}$$

If there is no receiver noise, the cost function reduces to

$$\begin{aligned} L\left(BS_{i}\right) &= \sum_{k=1\ k\neq i}^{M}\left(NLOS_{i} - NLOS_{k}\right) = \left(M-1\right)NLOS_{i} - \sum_{k=1\ k\neq i}^{M} NLOS_{k} \\ &= M \cdot NLOS_{i} - \sum_{k=1}^{M} NLOS_{k} \ . \end{aligned} \tag{5.13}$$

For those BSs which are not NLOS-corrupted, the cost functions simplifies to

$$L\left(BS_{i}\right) = -\sum_{k=1}^{M} NLOS_{k} \ . \tag{5.14}$$

It is negative since all NLOSs are non-negative. For the BS, say BS_{h}, which contains the largest NLOS error, the cost function is

$$L\left(BS_{h}\right) = \sum_{k=1\ k\neq h}^{M}\left(NLOS_{h} - NLOS_{k}\right) = \sum_{k=1}^{M}\left(NLOS_{h} - NLOS_{k}\right). \tag{5.15}$$

It is positive since $NLOS_{h} \geq NLOS_{k}$. For other BSs, the cost functions can be either negative or positive, but lie in the region of

$$-\sum_{k=1}^{M} NLOS_{k} \leq L\left(BS_{i}\right) \leq \sum_{k=1}^{M}\left(NLOS_{h} - NLOS_{k}\right). \tag{5.16}$$

Based on this property, the following can be derived: (1) the number of NLOS-free BSs or the number of NLOS-corrupted BSs. This can be found by identifying how many cost

functions have the same smallest negative value; and (2) the values of NLOS errors. The subtraction of a cost function of an NLOS-corrupted BS (BS_n) and that of an NLOS-free BS (BS_c) is

$$L(BS_n) - L(BS_c) = \sum_{k=1\ k\neq n}^{M} (NLOS_n - NLOS_k) + \sum_{k=1}^{M} NLOS_k = M \cdot NLOS_n \qquad (5.17)$$

thus,

$$NLOS_n = \frac{L(BS_n) - L(BS_c)}{M} \qquad (5.18)$$

Taking receiver noise into consideration, a cost function in this case consists of two parts; one is the NLOS error component, and the other is the measurement noise component, as shown in the following equation

$$\begin{aligned} L(BS_i) &= \sum_{k=1\ k\neq i}^{M} (NLOS_i - NLOS_k) + \sum_{k=1\ k\neq i}^{M} (n_i - n_k) \\ &= \underbrace{(M-1)NLOS_i - \sum_{k=1\ k\neq i}^{M} NLOS_k}_{NLOS \text{ part}} + \underbrace{(M-1)n_i - \sum_{k=1\ k\neq i}^{M} n_k}_{noise \text{ part}} \\ &= \underbrace{M \cdot NLOS_i - \sum_{k=1}^{M} NLOS_k}_{NLOS \text{ part}} + \underbrace{M \cdot n_i - \sum_{k=1}^{M} n_k}_{noise \text{ part}} \end{aligned} \qquad (5.19)$$

Receiver noise has a zero mean Gaussian distribution, $N(0, \sigma^2)$, so that the noise portion - a combination of receiver noise - is also zero mean Gaussian distributed but with a different variance, $N(0, M(M-1)\sigma^2)$. As a result, the cost function in this case is of a Gaussian distribution but with a non-zero mean value,

$$L(BS_i) \sim N\left(M \cdot NLOS_i - \sum_{k=1}^{M} NLOS_k, M(M-1)\sigma^2 \right) \tag{5.20}$$

Specially, the cost function of an NLOS-free BS is of the following distribution

$$L(BS_c) \sim N\left(-\sum_{k=1}^{M} NLOS_k, M(M-1)\sigma^2 \right) \tag{5.21}$$

To identify if a BS is NLOS-corrupted or not, hypothesis tests need to be conducted. To this end, γ_c^i, the difference between the cost function of the BS to be evaluated and that of an NLOS-free BS, is selected

$$\begin{aligned} \gamma_c^i &= \frac{L(BS_i) - L(BS_c)}{M} \\ &= \frac{\left\{ \underbrace{M \cdot NLOS_i - \sum_{k=1}^{M} NLOS_k}_{NLOS \text{ part}} + \underbrace{M \cdot n_i - \sum_{k=1}^{M} n_k}_{noise \text{ part}} \right\} - \left\{ \underbrace{-\sum_{k=1}^{M} NLOS_k}_{NLOS \text{ part}} + \underbrace{M \cdot n_c - \sum_{k=1}^{M} n_k}_{noise \text{ part}} \right\}}{M} \\ &= NLOS_i + (n_i - n_c) \end{aligned} \tag{5.22}$$

γ_c^i is a Gaussian random variable with a mean of $NLOS_i$ and a variance of $2\sigma^2$. Obviously, the hypothesis test is to decide whether or not γ_c^i is a zero mean Gaussian random variable. γ_c^i is zero mean if BS_i is a NLOS-free BS; otherwise, γ_c^i is of a positive mean and BS_i is NLOS-corrupted.

$$\begin{cases} H1: \quad \gamma_c^i \sim \text{N}(0, 2\sigma^2) \quad \text{NLOS - free BS} & (5.23) \\ H2: \quad \gamma_c^i \sim \text{N}(NLOS_i, 2\sigma^2) \quad \text{NLOS - corrupted BS} & (5.24) \end{cases}$$

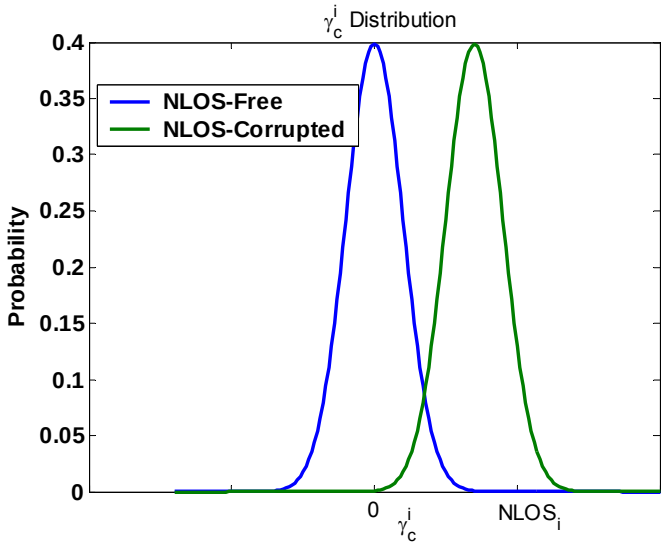

Figure 5.6: The Distribution of γ_c^i for NLOS-Free BS and NLOS-Corrupted BS

The distributions of γ_c^i in the NLOS-free case and in the NLOS-corrupted case are shown in Figure 5.6. Techniques of quality control or reliability analysis can be used to identify which type of distribution γ_c^i is. If $\alpha/2$ is chosen as the false-alarm probability of recognizing a NLOS-free γ_c^i as NLOS-corrupted and β as the miss-detection probability of accepting a NLOS-corrupted γ_c^i as a NLOS-free one, the minimum detectable NLOS error can be calculated from Figure 5.7 and the results are presented in Table 5.1

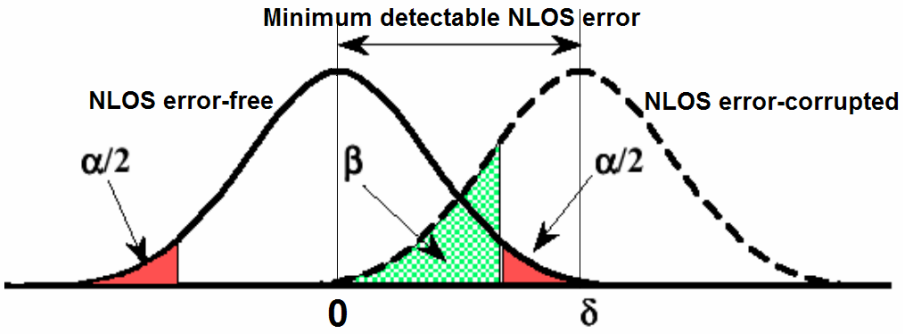

Figure 5.7: Determination of Minimum Detectable NLOS Error

Table 5.1: Minimum Detectable NLOS Error

α	β	Minimum detectable NLOS Error
5.0%	20%	3.96σ
2.5%	20%	4.38σ
5.0%	10%	4.58σ
2.5%	10%	4.98σ
0.1%	20%	5.83σ
0.1%	10%	6.46σ

Supposing that α is 5% and β is 20%, the minimum detectable NLOS error is 3.96σ. If σ is 60 m ~ 80 m for TOA measurements, the minimum NLOS error that can be identified is around 250 m ~ 320 m. This value is sufficiently large that the positioning accuracy cannot be improved to a satisfactory level. Two methods can be used to decrease measurement noise and to increase NLOS error removal capability. One method is using advanced signal reception techniques to decrease measurement noise. Similar techniques to those used in modern GPS receivers can be applied here. A narrow correlator technique, together with coupled PLL-DLL tracking loop techniques, can reduce the receiver noise to less than 1 m (Parkinson and Spilker, 1996). With this small level of receiver noise, most NLOS errors can be identified. The second method to decrease measurement noise is based on the phenomenon that NLOS errors are low frequency components compared to receiver noise, especially in low kinematic situations.

In this case, the cost functions of several consecutive time epochs in which NLOS errors are generally unchanged can be combined together as follows

$$\hat{L}(BS_i) = \frac{1}{N}\sum_{q=1}^{N} L^q(BS_i) = \underbrace{\frac{1}{N}\sum_{q=1}^{N}\left[(M-1)NLOS_i^q - \sum_{k=1\,k\neq i}^{M} NLOS_k^q\right]}_{NLOS\text{ part}} + \underbrace{\frac{1}{N}\sum_{q=1}^{N}\left[(M-1)n_i^q - \sum_{k=1\,k\neq i}^{M} n_k^q\right]}_{noise\text{ part}}$$

$$\approx \underbrace{M\cdot NLOS_i - \sum_{k=1}^{M} NLOS_k}_{NLOS\text{ part}} + \underbrace{\frac{1}{N}\sum_{q=1}^{N}\left[M\cdot n_i^q - \sum_{k=1}^{M} n_k^q\right]}_{noise\text{ part}} \tag{5.25}$$

where N is the number of consecutive cost functions combined together. Obviously, the new cost function is of the following distribution:

$$\hat{L}(BS_i) \sim \mathrm{N}\left(M\cdot NLOS_i - \sum_{k=1}^{M} NLOS_k, \frac{M(M-1)\sigma^2}{N}\right) \tag{5.26}$$

The variance decreases from $M(M-1)\sigma^2$ to $\frac{M(M-1)\sigma^2}{N}$. $\hat{\gamma}_c^i$ changes to

$$\begin{aligned}\hat{\gamma}_c^i &= \frac{\hat{L}(BS_i) - \hat{L}(BS_c)}{M} \\ &= \frac{\left\{\underbrace{M\cdot NLOS_i - \sum_{k=1}^{M} NLOS_k}_{NLOS\text{ part}} + \underbrace{\frac{1}{N}\sum_{q=1}^{N}\left\{M\cdot n_i^q - \sum_{k=1}^{M} n_i^q\right\}}_{noise\text{ part}}\right\} - \left\{\underbrace{-\sum_{k=1}^{M} NLOS_k}_{NLOS\text{ part}} + \underbrace{\frac{1}{N}\sum_{q=1}^{N}\left\{M\cdot n_c^q - \sum_{k=1}^{M} n_c^q\right\}}_{noise\text{ part}}\right\}}{M} \\ &= NLOS_i + \frac{1}{N}\sum_{q=1}^{N}(n_i - n_c)\end{aligned} \tag{5.27}$$

It now has the distribution of $\mathrm{N}\left(NLOS_i, \frac{2\sigma^2}{N}\right)$. When 16 cost functions are combined together, the minimum detectable NLOS decreases to $NLOS_{\min} = \frac{3.96\sigma}{\sqrt{16}} \approx \sigma$ with the same probabilities of $\alpha = 5\%$ and $\beta = 20\%$.

5.3.5 NLOS Error Correction

A higher positioning accuracy can be obtained if only NLOS-free TDOA measurements are used and a better geometry is maintained. However, these two requirements cannot be easily satisfied at the same time due to poor hearability. To get better positioning accuracy, one must estimate and remove NLOS errors from the BSs first and then use the corrected measurements from all available BSs to compute the MS location. This is especially true when the geometric layout of LOS BSs does not favour location estimation, i.e. when DOP_{LOS} is relatively large.

NLOS errors can be explicitly estimated via the following method that requires the true MS location and an NLOS-free BS. Since the true MS location is unknown, it is quite natural to use the intermediate MS location derived from the Distribution Function. The NLOS-free BS can be selected as that BS for which the cost function is the smallest.

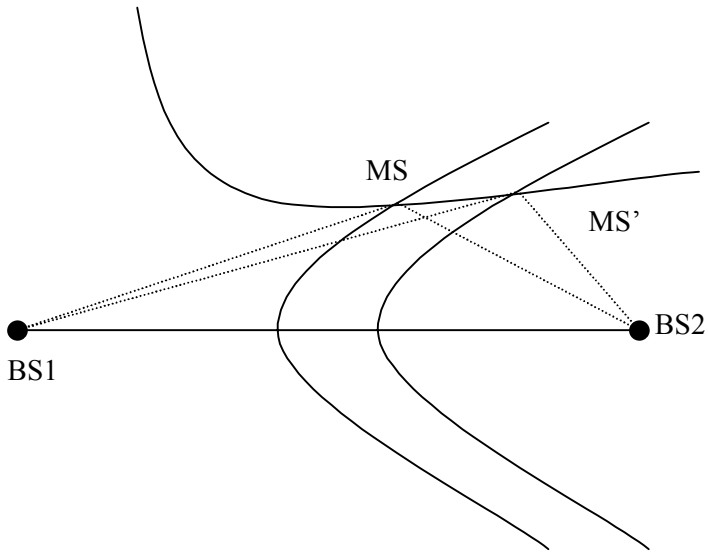

Figure 5.8: NLOS Error Correction

As shown in Figure 5.8, BS1 is assumed to be an NLOS-free BS; BS2 is the BS for which the range measurement contains an NLOS error, MS is the true MS position, and MS' is the NLOS-corrupted MS position estimate due to BS2. On the one hand, one can get a calculated TDOA between BS1 and BS2 with the knowledge of the true MS location,

$$TDOA = TOA_1 - TOA_2 = L_1 - L_2 . \tag{5.28}$$

On the other hand, the direct measurement of this TDOA is

$$TDOA' = TOA_1 - TOA_2^{'} = L_1 - L_2 - NLOS_2 \tag{5.29}$$

if receiver noise is neglected. Thus,

$$NLOS_2 = \left| TDOA - TDOA' \right| . \tag{5.30}$$

The NLOS error is the difference between the true TDOA and the measured TDOA if no receiver noise exists. Of course, with receiver noise, this estimated NLOS error will deviate from its true value. The NLOS error can also be directly estimated from γ_c^i since it is equal to $\gamma_c^i = NLOS_i + \left(n_i - n_c\right)$. Obviously, the smaller the receiver noise, the smaller the minimum detectable NLOS error, and the higher the NLOS estimation accuracy.

5.3.6 NLOS Error Detection Ability

The NLOS error mitigation algorithm proposed here depends on system redundancy since the intermediate MS location necessary for NLOS error identification and removal is computed from clear hyperbola intersections. Given the total number of BSs that can be heard and the number of NLOS-free BSs, the ratio of clear intersections to all

intersections can be determined in advance. Only when the number of clear intersections is larger than one can the clear intersection density be thought to be much larger than that of biased intersections (NLOS-corrupted) since the biased intersections are assumed to be randomly distributed. The number of independent intersections can be calculated via the following equation

$$p = \binom{M}{3} + 3 * \binom{M}{4} \tag{5.31}$$

where p is the total number of intersections and M is the number of BSs that can be heard. The first item is the number of intersections derived from three distinct BSs and the second item is the number of intersections derived from four distinct BSs. Similarly, the number of clear intersections when there are n NLOS errors is

$$q = \binom{M-n}{3} + 3 * \binom{M-n}{4} \tag{5.32}$$

The first item is the number of intersections calculated from 3 distinct NLOS-free BSs and the second item is the number of intersections calculated from 4 distinct NLOS-free BSs.

Table 5.2 is a summary of the ratios of clear intersections to total intersections. Obviously, one cannot mitigate NLOS errors if the number of BSs is less than or equal to four because of the lack of redundancy. With five BSs heard, up to one NLOS error can be identified and removed. With six BSs heard, up to two NLOS errors can be removed.

Table 5.2: Ratios of Clear Intersections to Total Intersections in TDOA Wireless Location

# of NLOS Errors \ # of BSs Heard	4	5	6	7
1	1/7	7/25	25/65	65/140
2	N/A	1/25	7/65	25/140
3	N/A	N/A	1/65	7/140

5.4 Simulation Results

Monte Carlo simulation tests have been done to verify the performance improvement due to the proposed NLOS error identification and removal algorithm. In the simulation, a 7-cell 2D cellular system is used and the MS to be located is in the central hexagonal cell surrounded by six adjacent hexagonal cells of the same size. The results of the following experiments are presented in the following sections:

- Investigation of NLOS error detection capability with respect to the number of BSs used
- Evaluation of the positioning accuracy improvement due to NLOS error mitigation for constant NLOS errors
- Investigation of the NLOS error mitigation capability with respect to receiver noise and the number of consecutive cost functions combined
- Evaluation of the positioning accuracy improvement in real wireless location environments

5.4.1 Successful NLOS Error Detection Probability with Respect to the Number of BS useds

Two types of receiver noise are simulated to evaluate the NLOS error detection capability. The first type of receiver noise in TOA measurements is assumed to have a standard deviation of 70 m. This value comes from the work of Wylie and Holtzman (1996) and is currently thought to be pessimistic. The second type of receiver noise is assumed to have a standard deviation of 25 m. It is obtainable via advanced receiver techniques. The cell radius is 3 km, the MS to be located is at (700m 1200 m), and each Monte Carlo test contains 500 independent runs.

Figure 5.9 shows the successful NLOS error detection probabilities when two NLOS errors exist. A successful NLOS error detection is defined here as a correct identification of NLOS-free BSs and NLOS-corrupted BSs. The horizontal axis shows the number of BSs used and the vertical axis represents the successful detection probability. Six scenarios are studied:

- NLOS errors: 250 m and 450 m; STD of receiver noise: 25 m
- NLOS errors: 350 m and 550 m; STD of receiver noise: 25 m
- NLOS errors: 450 m and 750 m; STD of receiver noise: 25 m
- NLOS errors: 250 m and 450 m; STD of receiver noise: 70 m
- NLOS errors: 350 m and 550 m; STD of receiver noise: 70 m
- NLOS errors: 450 m and 750 m; STD of receiver noise: 70 m

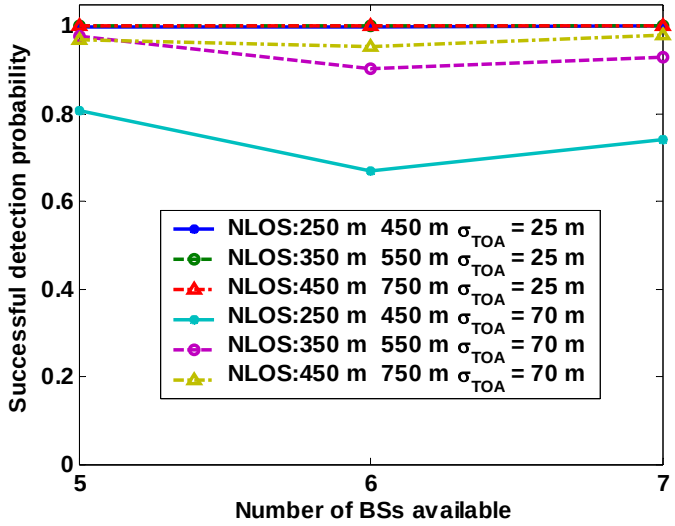

Figure 5.9: Successful NLOS Error Detection Probability with Two NLOS Errors (250 m, 450 m), (350 m, 550 m) , and (450 m, 750 m)

It is obvious that: it is easier to identify NLOS errors when the receiver noise is smaller; the larger the NLOS errors the higher the detection probability; it can not be guaranteed that successful detection probability increases with an increase in the number of BSs used although higher redundancy is preferred. This is because the accuracy of the intermediate MS location may not improve when more BSs are used.

Figure 5.10 shows the successful NLOS error detection probabilities when three NLOS errors exist. The horizontal axis again represents the number of BSs used and the vertical axis represents the successful detection probability. Six scenarios are studied here:

- NLOS errors: 250 m, 350 m and 450 m; STD of receiver noise: 25 m
- NLOS errors: 350 m, 450 m and 550 m; STD of receiver noise: 25 m
- NLOS errors: 450 m, 550 m and 750 m; STD of receiver noise: 25 m
- NLOS errors: 250 m, 350 m and 450 m; STD of receiver noise: 70 m

- NLOS errors: 350 m, 450 m and 550 m; STD of receiver noise: 70 m
- NLOS errors: 450 m, 550 m and 750 m; STD of receiver noise: 70 m

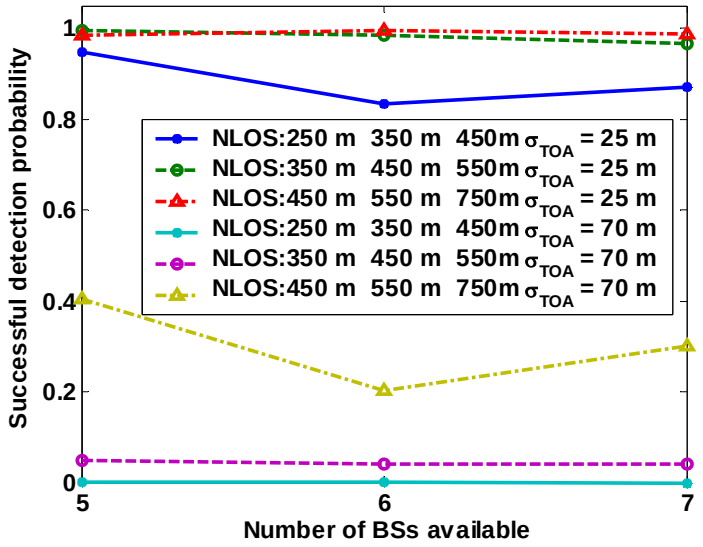

Figure 5.10: Successful NLOS Error Detection Probability with Three NLOS Errors (250 m, 350 m, 450 m), (350 m, 450 m, 550 m) and (450 m, 550 m, 750 m)

Compared to Figure 5.9, it is clear that the successful detection capability degrades significantly. This is because increasing the number of NLOS errors results in less redundancy and thus decreases the NLOS error detection capability. Even in this case, the proposed algorithm can still detect NLOS errors if the receiver noise is small.

5.4.2 MS Location Accuracy

The positioning accuracies of three methods are compared here. The first is the Least-Squares method with NLOS error detection and correction and is denoted as *NLOS-LS*. The second is the Least-Squares method without NLOS error detection and correction and is denoted as *RAW-LS*. The third, denoted as *DF,* is the distribution function method

where the intermediate MS location derived from an intersection distribution function is used as the MS location solution.

Figures 5.11 to 5.13 show the respective performances of these three methods when there is only one NLOS error. It can be seen that the accuracy of *RAW-LS* decreases with an increase in NLOS error, especially when the number of BSs used is small (for example, 4 or 5). *DF* exhibits a similar performance as that of *NLOS-LS* when the number of BSs used is small. Good NLOS error removal can be obtained when receiver errors is small. For example, the RMS value of positioning errors can reduce to 40 metres when the standard deviation of receiver noise is 25 metres while it is about 100 metres when the standard deviation of receiver noise is 70 metres.

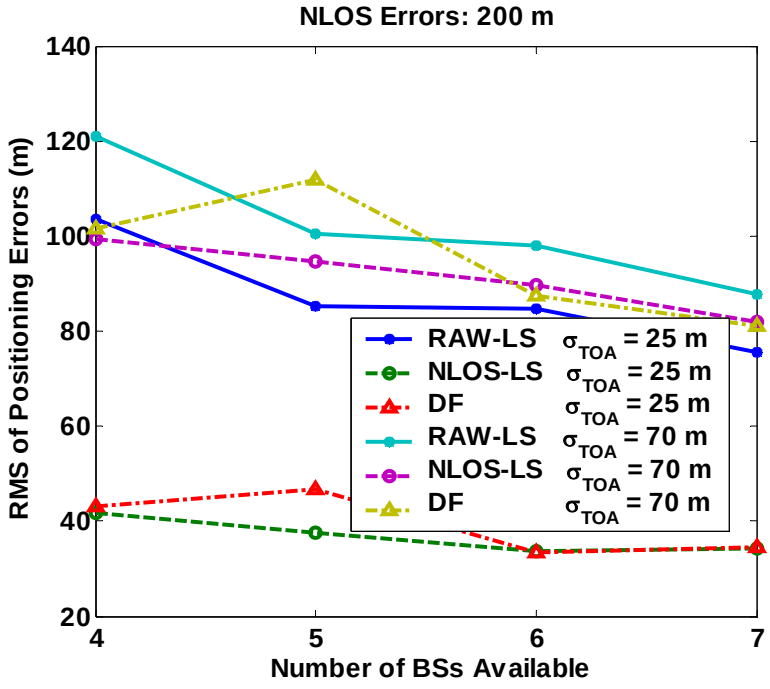

Figure 5.11: MS Position Estimation Accuracy with One NLOS Error of 200 m

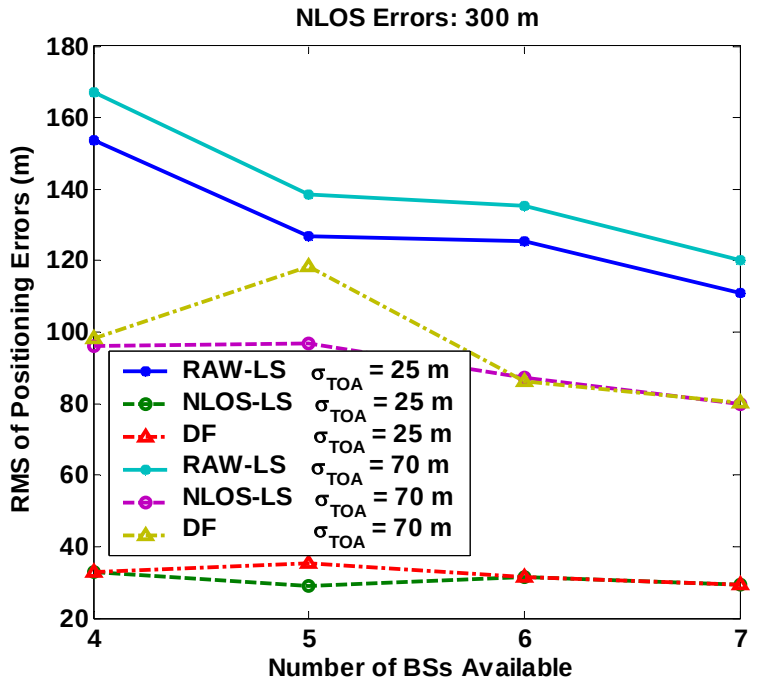

Figure 5.12: MS Position Estimation Accuracy with One NLOS Error of 300 m

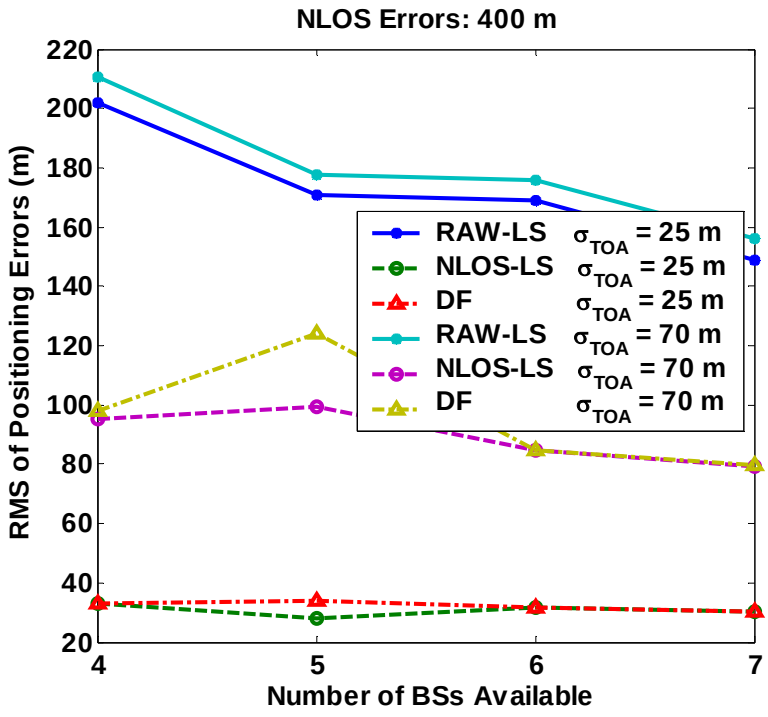

Figure 5.13: MS Position Estimation Accuracy with One NLOS Error of 400 m

Figures 5.14 to 5.19 demonstrate the positioning accuracies of these three methods when there are two or three NLOS errors. The same conclusions can be drawn as those in the single NLOS error case. *RAW-LS* has the worst positioning accuracy since it does not try to remove NLOS errors. The *NLOS-LS* and *DF* methods produce better results especially when the receiver noise is small. However, the positioning accuracy is not as high as in the one NLOS error case shown in Figures 5.11 to 5.13. This is because the NLOS error mitigation algorithm becomes less effective when measurement redundancy decreases. Occasionally, the accuracy can be even worse than the *RAW-LS* method.

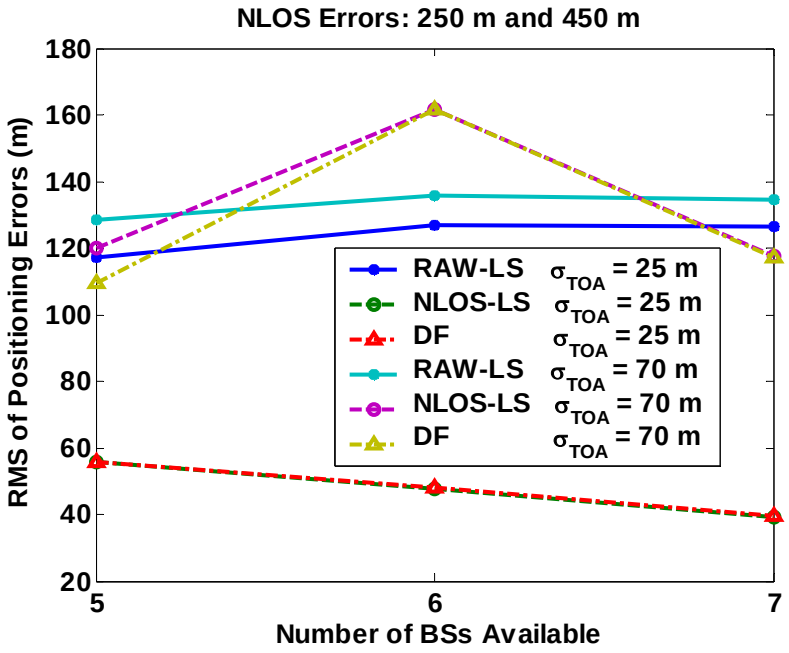

Figure 5.14: Positioning Accuracy with Two NLOS Errors (of 250 m, 450 m)

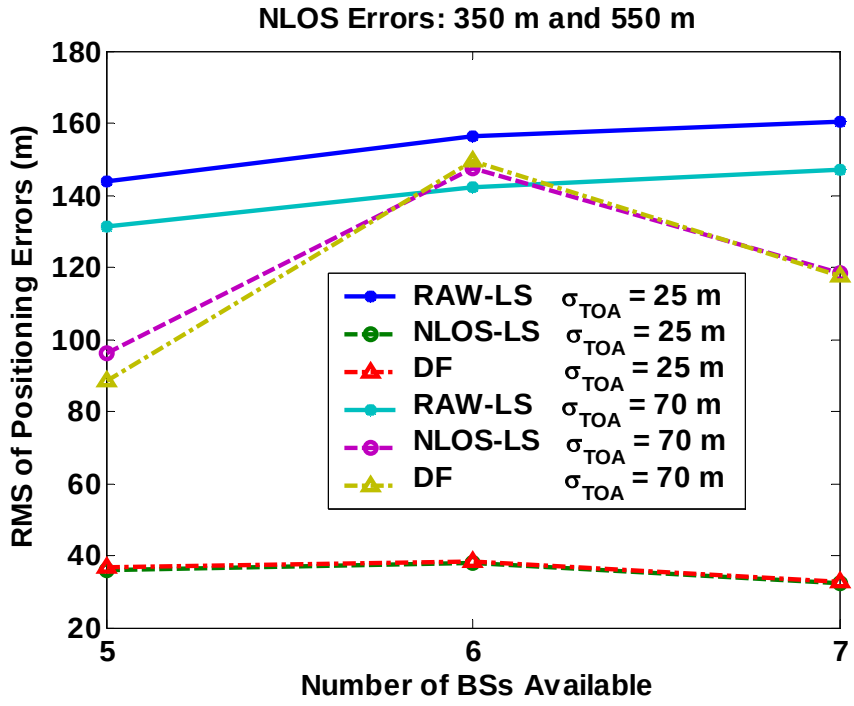

Figure 5.15: Positioning Accuracy with Two NLOS Errors (of 350 m, 550 m)

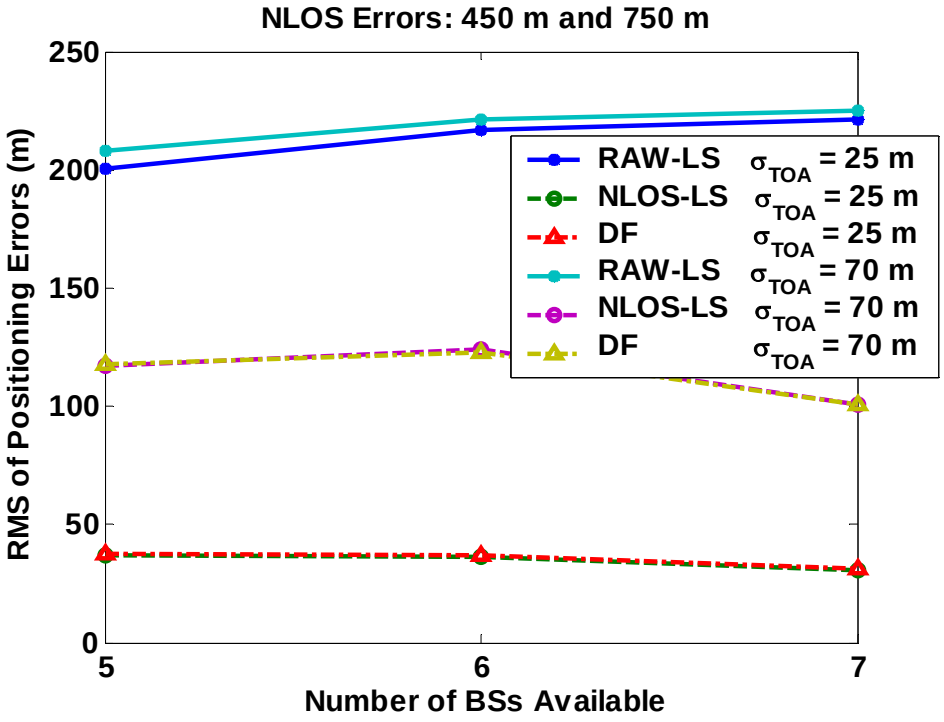

Figure 5.16 Positioning Accuracy with Two NLOS Errors (of 450 m, 750 m)

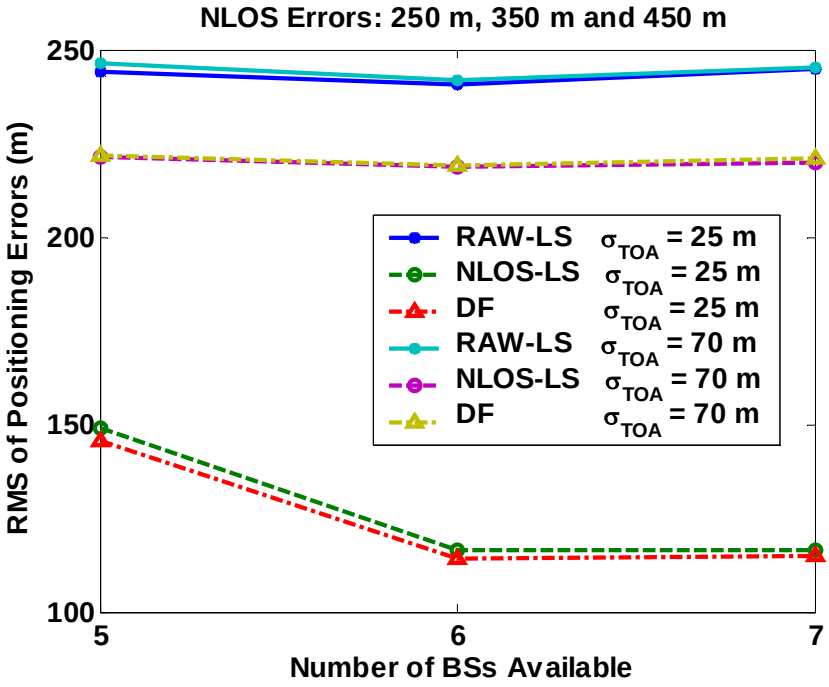

Figure 5.17: Positioning Accuracy with Three NLOS Errors (250 m, 350 m, 450 m)

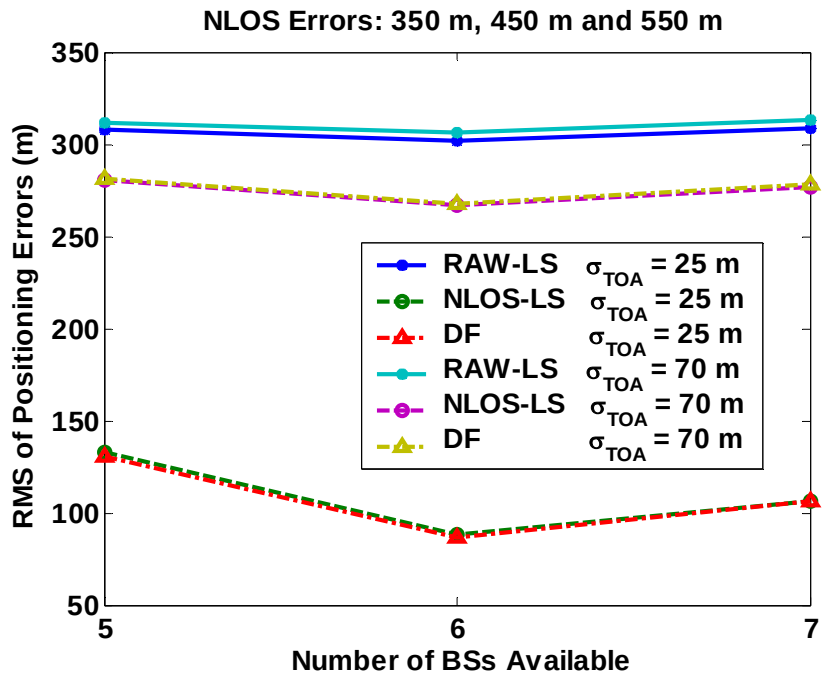

Figure 5.18: Positioning Accuracy with Three NLOS Errors (350 m, 450 m, 550 m)

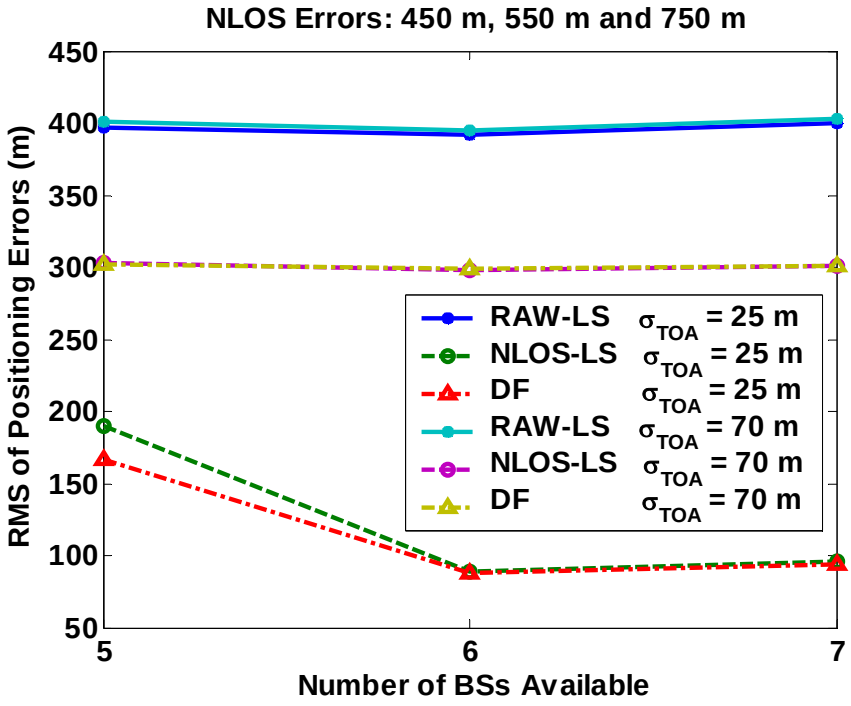

Figure 5.19: Positioning Accuracy with Three NLOS Errors (450 m, 550 m, 700 m)

5.4.3 NLOS Error Mitigation Capability with Respect to Measurement Noise

The experiments in this section aim to demonstrate the importance of minimizing receiver noise for NLOS error mitigation. As mentioned above, two methods can be applied to decrease receiver noise. One method uses advanced signal tracking techniques to physically decrease receiver noise as done in GPS receiver design. In the other method, TOA/TDOA measurements or consecutive cost functions are averaged to decrease the influence of receiver noise on TOA/TDOA measurements. This is based on the phenomenon that NLOS errors are low frequency components in low dynamic situations.

A 7-cell cellular network is used, but with a cell radius of 3 km and the MS to be located is at (800 m, 1380 m). Three BSs (BS3, BS5 and BS7) are assumed to be NLOS error

corrupted, with associated constant NLOS errors of 100 m, 200 m and 500 m, respectively. Receiver noise with three different standard deviations are simulated. The three standard deviations are $\sigma_{\text{TOA}} = 100$ m , $\sigma_{\text{TOA}} = 35$ m , and $\sigma_{\text{TOA}} = 10$ m . With measurement averaging taken into account, six test scenarios are fully discussed. In the measurement averaging, the measurements of 30 epochs are averaged to generate one smoothed data for location estimation.

- *Scenario 1:* $\sigma_{\text{TOA}} = 100$ m without measurement averaging
- *Scenario 2:* $\sigma_{\text{TOA}} = 100$ m with measurement averaging
- *Scenario 3:* $\sigma_{\text{TOA}} = 35$ m without measurement averaging
- *Scenario 4:* $\sigma_{\text{TOA}} = 35$ m with measurement averaging
- *Scenario 5:* $\sigma_{\text{TOA}} = 10$ m without measurement averaging
- *Scenario 6:* $\sigma_{\text{TOA}} = 10$ m with measurement averaging

The actual standard deviation of receiver noise for these scenarios is summarized in the following table.

Table 5.3: Receiver Noise for Six Scenarios

Scenarios	STD of receiver noise
1: σ_{TOA}= 100 m	σ_{TOA}= 100 m
2: σ_{TOA}= 100 m with measurement averaging	σ_{TOA}= 18.3 m
3: σ_{TOA}= 35 m	σ_{TOA}= 35 m
4: σ_{TOA}= 35 m with measurement averaging	σ_{TOA}= 6.4 m
5: σ_{TOA}= 10 m	σ_{TOA}= 10 m
6: σ_{TOA}= 10 m with measurement averaging	σ_{TOA}= 1.8 m

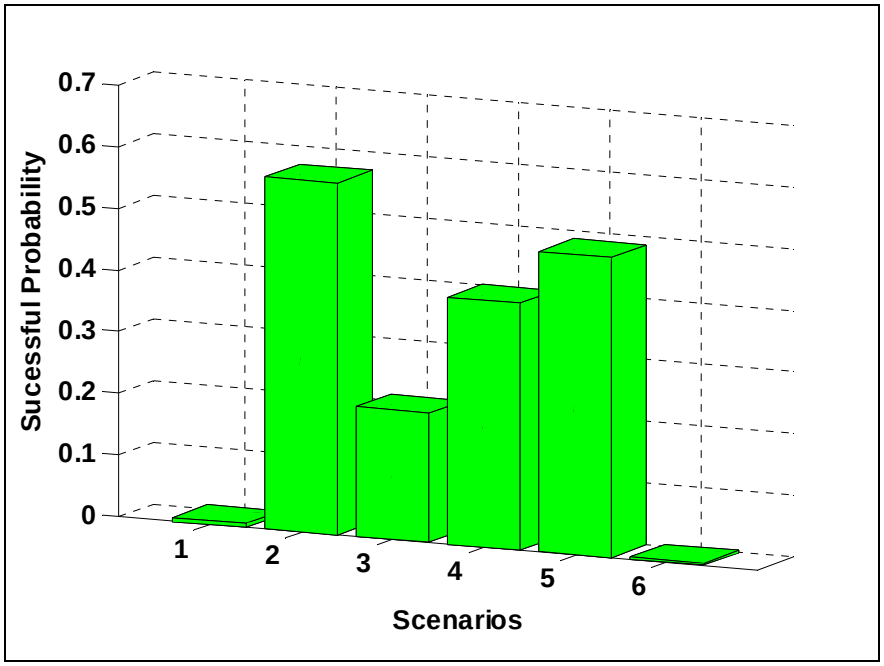

Figure 5.20: Probability of Successful NLOS Error Detection (Both missing detection and false detection not allowed)

Figure 5.20 is the probability of successful NLOS error detection without missing detection and false detection. Missing detection describes the situation where a BS that contains NLOS error is not detected; false detection means that an NLOS-free BS is thought of as NLOS error corrupted by mistake. When receiver noise is large as for scenario 1 (see Table 5.3), the minimum detectable NLOS error is very large, so that missing detection occurs frequently and NLOS detection capability is poor. On the other hand, when receiver noise is very small as for scenario 6, false detection occurs frequently and the NLOS detection capability is also poor.

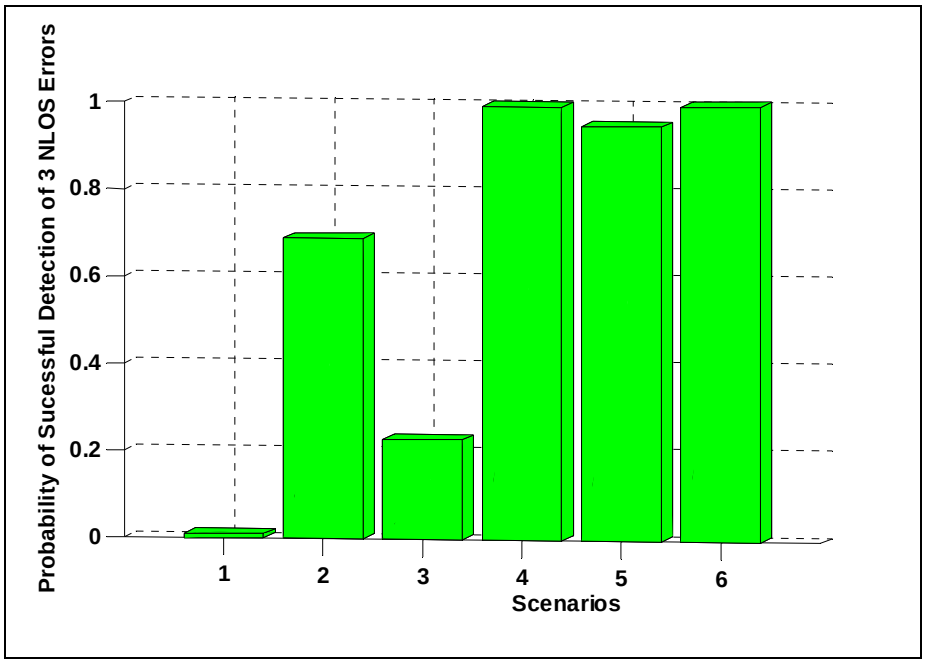

Figure 5.21: Probability of Successful NLOS Error Detection (Missing detection not allowed; False detection allowed)

If false detection is allowed in successful NLOS detection, the probability plot is as represented in Figure 5.21. It can be seen that the smaller the receiver noise, the higher the successful probability. The reason one may consider allowing false detection is that the estimated NLOS error in false detection cases is small and the positioning accuracy will not degrade significantly. To demonstrate this, Figure 5.22 shows the NLOS error estimation for each BS. When the receiver noise is small, only the NLOS error estimates of BS3, BS5 and BS7 are large and roughly equivalent to their true NLOS errors; those of the NLOS -free BSs are relatively small.

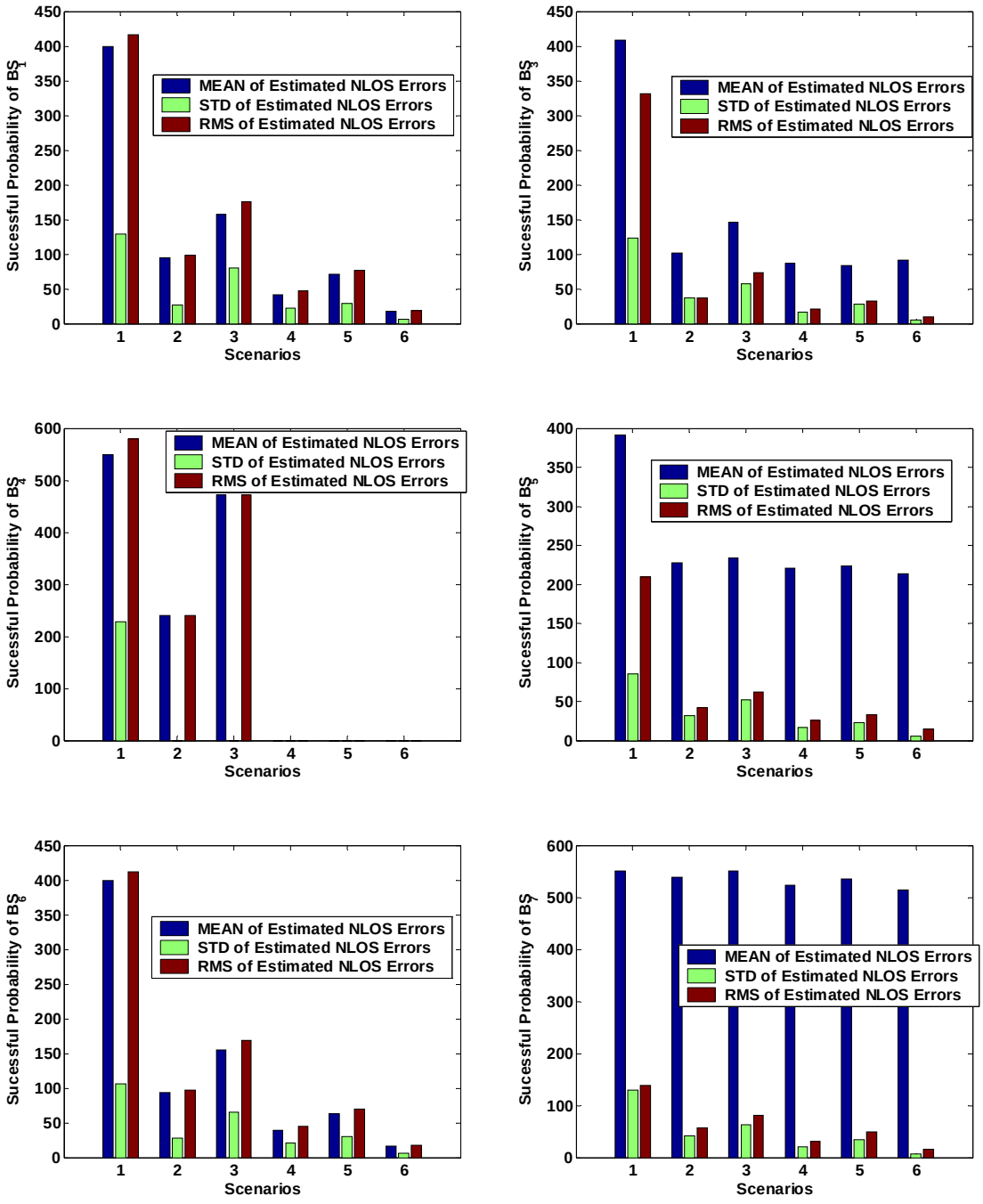

Figure 5.22: Estimated NLOS Errors for Each BS

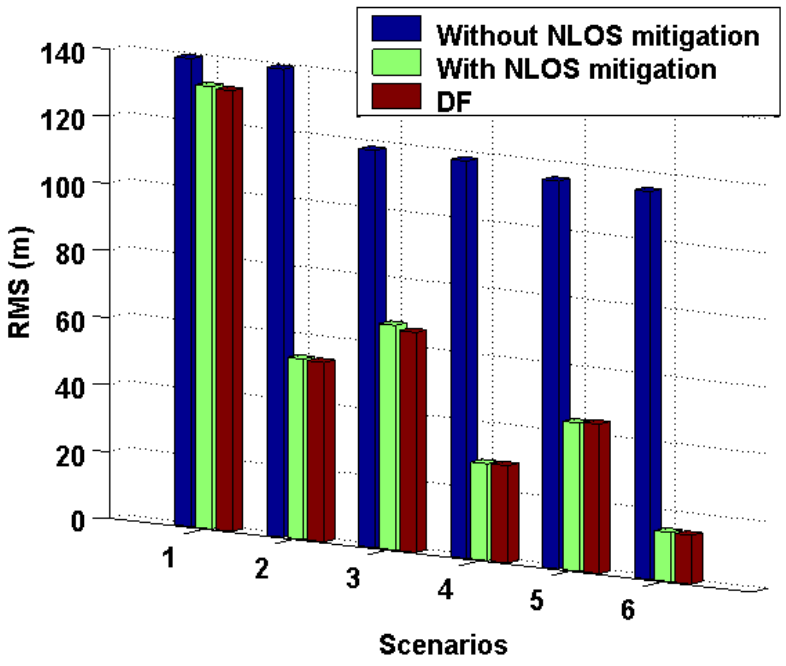

Figure 5.23: Positioning Accuracies of Three Positioning Methods

Figure 5.23 shows the positioning accuracy of these three algorithms in the six different scenarios. Evident is that a normal least squares method without NLOS error mitigation produces poor accuracy, even when receiver noise is very small. A least squares method with NLOS error mitigation and a distribution function-based method yield much better performance because both of them are able to mitigate the influence of NLOS errors. It is worth emphasizing that such performance improvement can be achieved only when the receiver noise is small. Fortunately, receiver noise is theoretically receiver-dependent and can be made quite small by means of sophisticated receiver design techniques.

5.4.4 Positioning Accuracy Improvement in Multipath Propagation Environments

To evaluate the benefits of this NLOS error mitigation method in real world situations, it was applied to a multipath propagation channel where NLOS errors are assumed to be

time-variant and have exponential distribution characteristics in urban areas. The 7-cell system is still used here and the cell size is 3 km in radius. The exponentially distributed NLOS errors are simulated by the inversion method discussed in Section 4.4.4. The location accuracy is evaluated with respect to MS-serving BS separations.

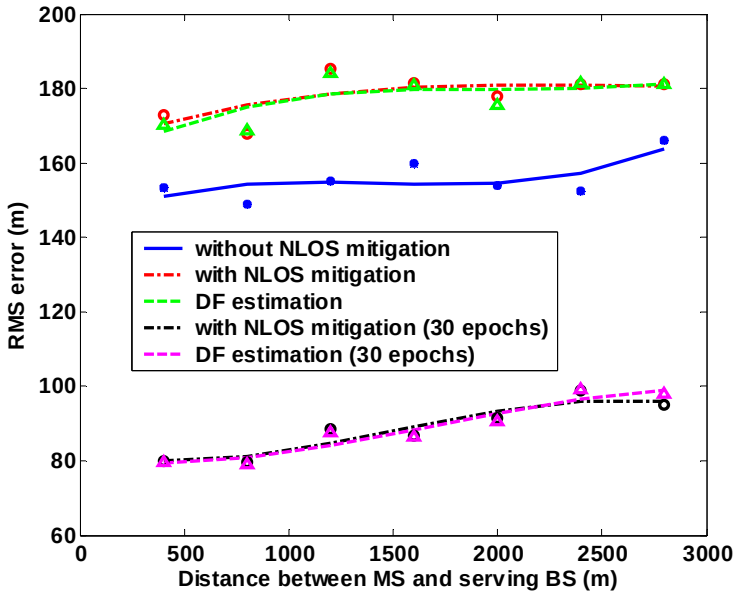

Figure 5.24: Positioning Accuracy with σ_{TOA}=100 m

Figure 5.24 illustrates the location accuracies of the different algorithms when the receiver noise is equal to $\sigma_{\mathrm{TOA}} = 100\,\mathrm{m}$. The horizontal axis represents the MS-serving BS separation and the vertical axis shows RMS values of positioning errors. Note that positioning accuracy may degrade with the use of NLOS error mitigation when the receiver noise is large. This is because large receiver errors make it difficult to correctly estimate NLOS errors and, thus, may introduce residual errors in MS location computation. However, if measurement averaging is applied, the receiver noise can be decreased. In this case, better NLOS mitigation can be achieved and superior location performance is obtained.

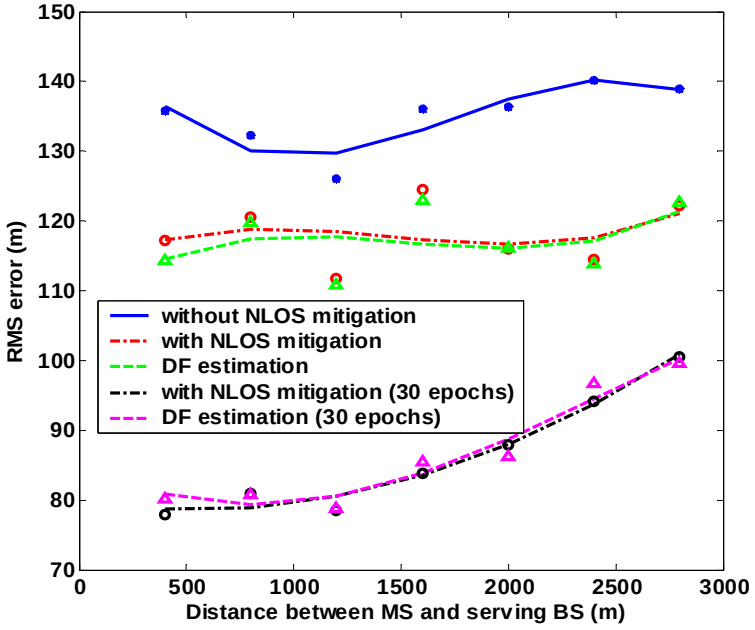

Figure 5.25: Positioning Accuracy with σ_{TOA}=35 m

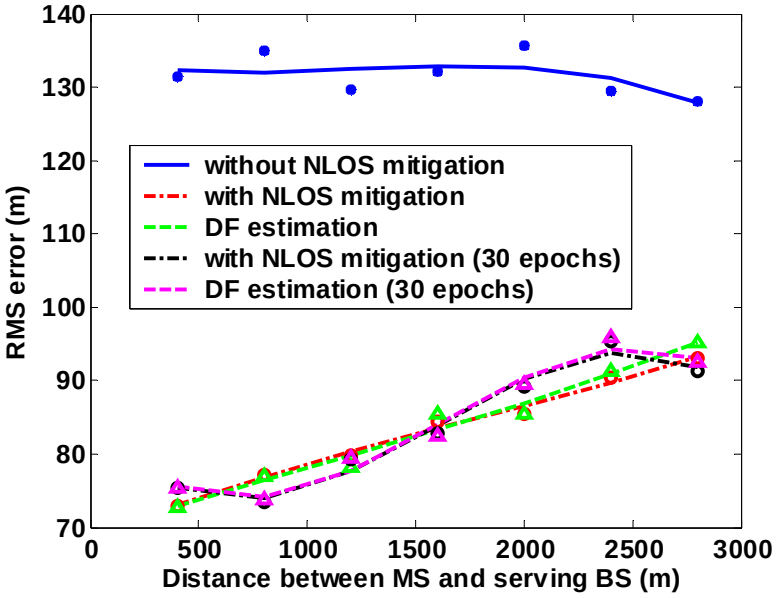

Figure 5.26: Positioning Accuracy with σ_{TOA}=10 m

Figures 5.25 and 5.26 show the location accuracies of the different algorithms when the receiver noise is equal to $\sigma_{\text{TOA}} = 35\,\text{m}$ and $\sigma_{\text{TOA}} = 10\,\text{m}$, respectively. Due to the smaller receiver noise in these two cases, the performance of the NLOS error mitigation method is much better than that of a normal LS method without NLOS mitigation. However, the accuracy is worse than that shown in Figure 5.23 (see scenarios 3 and 5). This is because the NLOS errors in Figure 5.23 are constant and the number of NLOS errors is within the NLOS error detection capability discussed in Section 5.3.6. In a real multipath propagation environment, NLOS errors are time-variant and all of the BSs may have NLOS errors, so the number of NLOS-corrupted BSs is beyond the capability of the proposed method. Even though, the positioning accuracy can still be greatly improved as shown in the above figures.

5.5 Conclusions

The NLOS error corruption problem is a serious issue in wireless location. The proposed *DF* and *NLOS-LS* algorithms provide the capabilities to explicitly reduce NLOS errors in TOA or TDOA measurements. Thus, they can be used to enhance the performance of the commonly used LS algorithm. The proposed NLOS mitigation method is a position-domain method and is suitable for low dynamic users since no spatial diversity is required. Another benefit is that NLOS errors can be thought of as constant over a longer time period. In this case, receiver noise can be decreased by measurement averaging to achieve better performance.

CHAPTER 6

NLOS ERROR MITIGATION FOR AOA MEASUREMENT

6.1 Introduction

The accuracy of AOA observations can significantly impact wireless location performance. For example, the performance of hybrid TDOA/AOA location schemes will not be superior to that of TDOA-only schemes if the standard deviation of the AOA measurements is larger than 5~10 degrees (Ma et al, 2003). Unfortunately, the true AOA of an incoming signal is usually obscured in real world applications because of multipath propagation and receiver noise. Due to reflectors and scatterers around base stations and mobile stations, the signals received by a BS or an MS contain not only the desired LOS signal but also some NLOS replicas. The AOAs of these NLOS signals can be significantly different from that of the LOS signal, which makes it difficult to measure the true AOA. Environmental noise and system thermal noise also result in degraded AOA measurements because they obscure the character of incoming signals.

This chapter focuses on the mitigation of NLOS errors in AOA measurements in a wireless channel characterized by significant multipath effects. The concept is described briefly as follows. The true AOA is the AOA of the LOS signal and the earlier a

multipath replica arrives after the LOS signal, the smaller the AOA NLOS error. It follows, therefore, that more accurate AOA observations can be obtained if one can identify the LOS signal or the earliest multipath replica based on TOA estimation of all multipath signals. To this end, a spatio-temporal 2-D signal processing technique is proposed: (i) to estimate TOAs and AOAs of all incoming signals; and (ii) to select the AOA of the earliest component as the final AOA observation.

The outline of this chapter is as follows. The Geometry Based Single Bounced model (GBSB) is first presented to describe the TOA-AOA distribution of a multipath channel (e.g. Liberti and Rappaport, 1996; Petrus and Reed, 2002). Following this, an array signal processing technique (Van der Veen et al, 1998; Wang et al, 2001) and a 2-D Unitary-ESPRIT technique (Zoltowski et al, 1996) are applied to estimate the vector channel impulse response and the TOAs/AOAs of multipath signals. Finally, simulation results are presented to demonstrate the effectiveness of this algorithm.

6.2 TOA-AOA Distribution in a Multipath Channel

Multipath signals represent the delayed versions of the signals as originally transmitted when electromagnetic waves encounter reflection from large objects, diffraction around small objects, and scattering as it traverses the wireless channel. All of the possible paths within a wireless channel have different properties, so that each multipath signal has its own distinct amplitude, carrier phase shift, time delay, angle of arrival, and Doppler shift characteristics. Furthermore, as multipath channels are time-varying channels, all of the parameters change with time (Nuckols, 1999).

6.2.1 TOA Spread (Delay Spread)

Multipath signals arrive at a receiver at different instants of time, thus giving an arrival time expansion or TOA spread. If an impulse, $\delta(t)$, is transmitted at time instant $t = 0$, the received signal will be $h(t)$

$$h(t) = \sum_{i=1}^{n} a_i \delta(t - T_i) \tag{6.1}$$

where n is the number of multipath replicas; a_i is the "amplitude" of the received impulse due to the ith path; and T_i is the time delay of the ith delayed impulse. The longer the path, the larger the time delay and, normally, the lower the received signal power.

The impulse arrival time, T, is usually characterized by a probability density function, such as a negative exponential distribution (Yacoub, 1993). Accordingly, the mean time delay is the mean of this density function, and the delay spread corresponds to its standard deviation. In practice, the delay spread varies from fractions of microseconds to many microseconds. In urban areas the delays can reach a few microseconds whereas, in suburban areas and in open areas, they are shorter (0.5 μs and less than 0.2 μs, respectively). Figure 6.1 depicts typical impulse arrival profiles for different propagation environments.

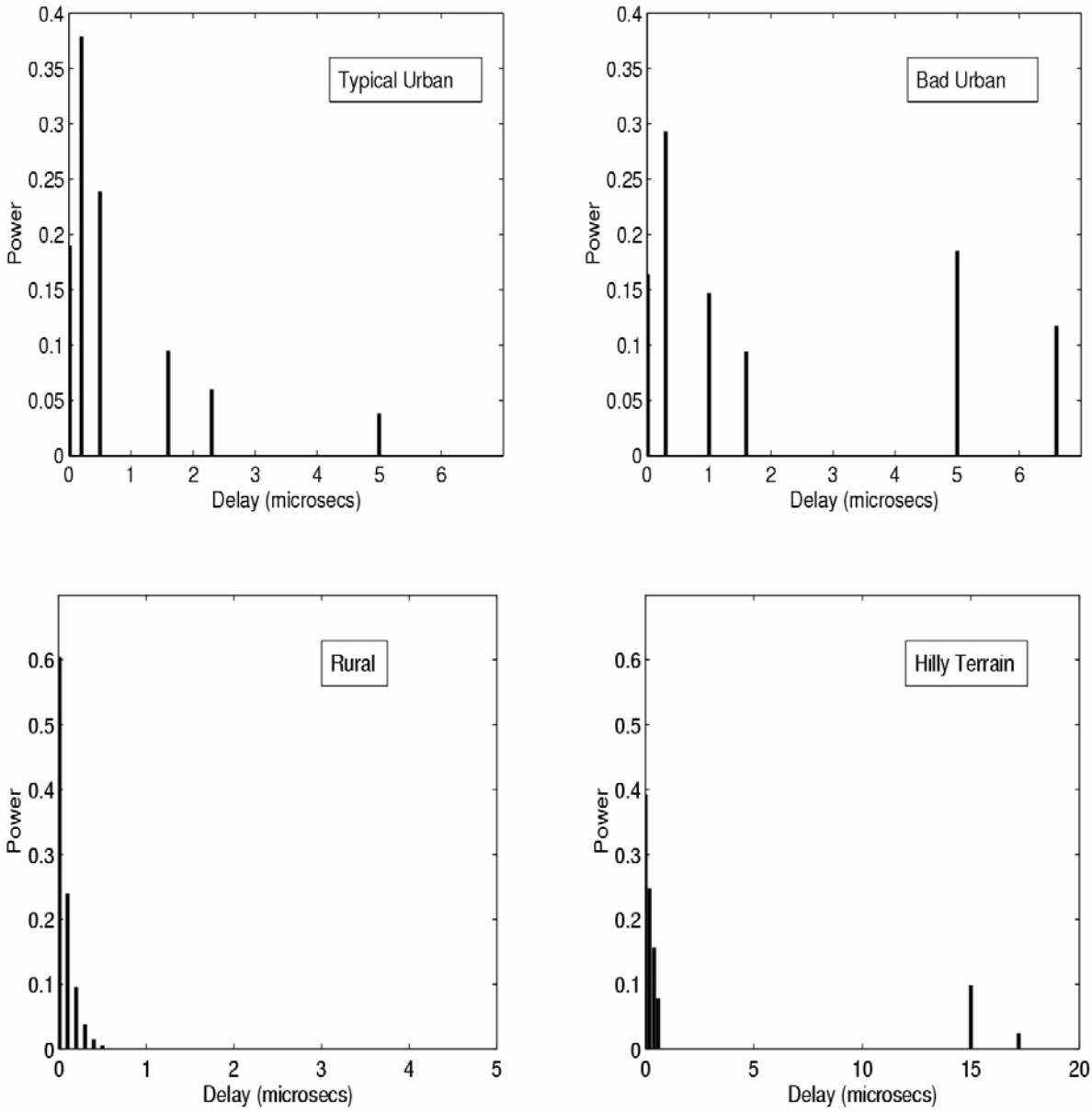

Figure 6.1: Macrocell Power-Delay Profiles (Vanderveen, 1997)

6.2.2 Angle of Arrival (AOA) Spread

Multipath signals arrive at receivers from different directions due to the irregular spatial distribution of scatterers. This results in an expansion of angle of arrival. Paulraj and Papadias (1997) reported a typical angular spread of 360° in indoor scenarios, 20° in

urban scenarios, and 1^{o} in flat rural scenarios. Piechocki et al (1998) presented a general formula for the pdf of AOAs based on the circular scatterer model. The angular distribution is

$$f_{\alpha}(\alpha)=\begin{cases}\dfrac{2d^{2}}{\pi r^{2}}\cos\alpha\sqrt{\cos^{2}\alpha+(r/d)^{2}-1} & -\sin^{-1}(r/d)\le\alpha\le\sin^{-1}(r/d)\\ 0 & \textit{otherwise}\end{cases} \tag{6.2}$$

where d is the MS–BS separation and r is the radius of the circular scatterer area around the MS. The equation is only valid for $d \ge r$. A reasonable estimate for the LOS AOA could be the mean AOA of all multipaths, the AOA of the first arrival, or a composite mean with higher weightings ascribed to the earlier arriving multipaths.

To numerically describe the TOA and AOA distributions of a multipath channel, another simpler channel model, the GBSB model, is presented in the following section. One can see from this model that AOA spread decreases when only earlier signals are considered. This results in better AOA measurements and, consequently, results in superior location accuracy.

6.3 GBSB Model

The GBSB model is a simple and efficient statistical channel model. Based on the following assumptions, it can provide analytical solutions to joint TOA-AOA distributions:

- The signals received at the base station are assumed to be plane waves arriving from the horizon, and hence the AOA calculation includes only the azimuth angle.

- Scatterers are assumed to be uniformly distributed around MSs and BSs.
- Each scatterer is assumed to be an omni directional reradiating element whereby the plane wave, on arrival, is reflected directly to receiver antennas without influence from other scatterers.
- Scatterers are assigned equal scattering coefficients with uniform random phases.

A mobile network has two types of cells, the macrocell and the microcell, depending on the cell radius and the serving BS antenna height. Accordingly, there also exist two types of GBSB models, the GBSB macrocell model and GBSB microcell model, each of which has its own joint TOA-AOA distribution and properties.

6.3.1 GBSB Macrocell Model

For a macrocell, the cell radius is quite large (around 10 km), and the BS antenna is well above surrounding objects. In this case, scatterers are assumed to be only near MSs which are normally quite low, about 1~2 m above ground level. Such a GBSB macrocell model is illustrated in Figures 6.2 and 6.3.

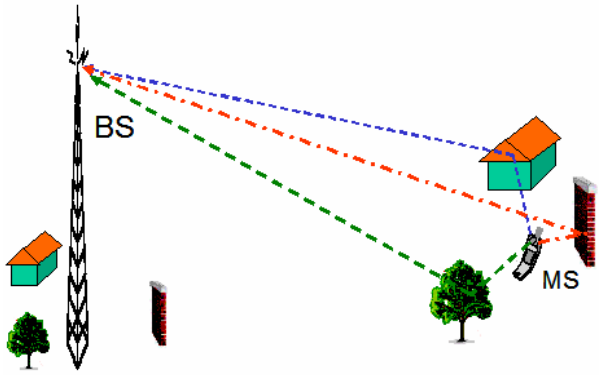

Figure 6.2: GBSB Macrocell Model

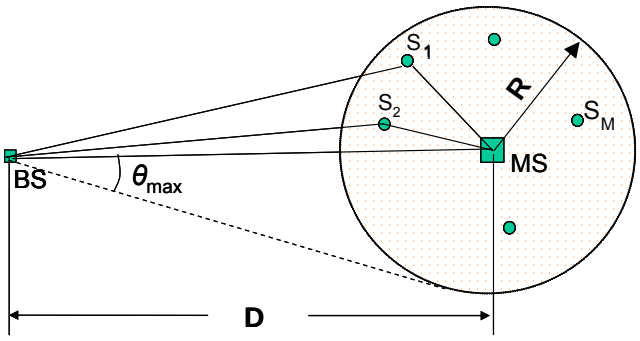

Figure 6.3: Scatterer Region of a GBSB Macrocell Model

The distance between the base station and the mobile station is D. Scatterers, denoted by S, are assumed to be uniformly located around the MS inside a circle of radius R. As a result, the AOAs of multipath components at the base station are restricted to an angular region of $2\theta_{\max}$, where

$$\theta_{\max} = \sin^{-1}\left(\frac{R}{D}\right) \tag{6.3}$$

The joint distribution of TOA and AOA can be obtained by studying scatterer density within the scatterer circle as a function of TOA and AOA. Based on the detailed derivation in Ertel et al (1998), such a joint distribution is of the following form

$$f_{\tau,\theta}(\tau,\theta) = \begin{cases} \dfrac{\left(D^2-\tau^2c^2\right)\left(D^2c+\tau^2c^3-2\tau c^2 D\cos\theta\right)}{4\pi R^2\left(D\cos\theta-\tau c\right)^3} & \dfrac{D^2-2\tau cD\cos\theta+\tau^2c^2}{\tau c-D\cos\theta} < 2R \\ 0 & \textit{otherwise} \end{cases} \tag{6.4}$$

where τ is TOA and θ is AOA measured relative to the LOS BS-MS direction. The respective distributions of τ and θ can be further derived by calculating the marginal probability. Only the AOA distribution (Petrus and Reed, 2002) is provided here

$$f_\theta(\theta)=\begin{cases}\dfrac{2D\cos\theta\sqrt{D^2\cos^2\theta-D^2+R^2}}{\pi R^2}, & -\sin^{-1}\left(\dfrac{R}{D}\right)\le\theta\le\sin^{-1}\left(\dfrac{R}{D}\right)\\ 0, & \textit{otherwise}\end{cases} \quad (6.5)$$

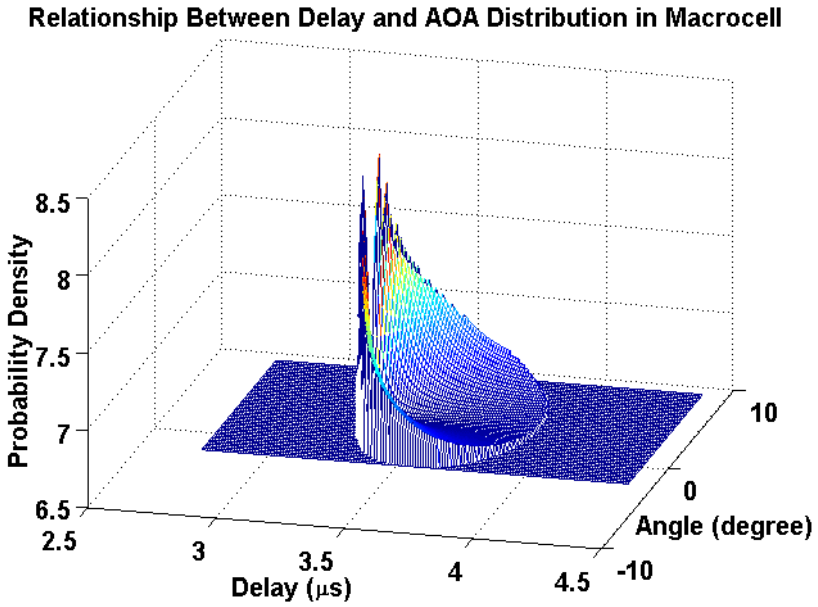

Figure 6.4: Joint TOA/AOA Distribution of GBSB Macrocell Model

Figure 6.4 is an example of the joint TOA-AOA distribution. Evident from this figure is that

- The probability is non-zero only in the region where scatterers occur; and
- The earlier the incoming signals, the narrower the AOA spread.

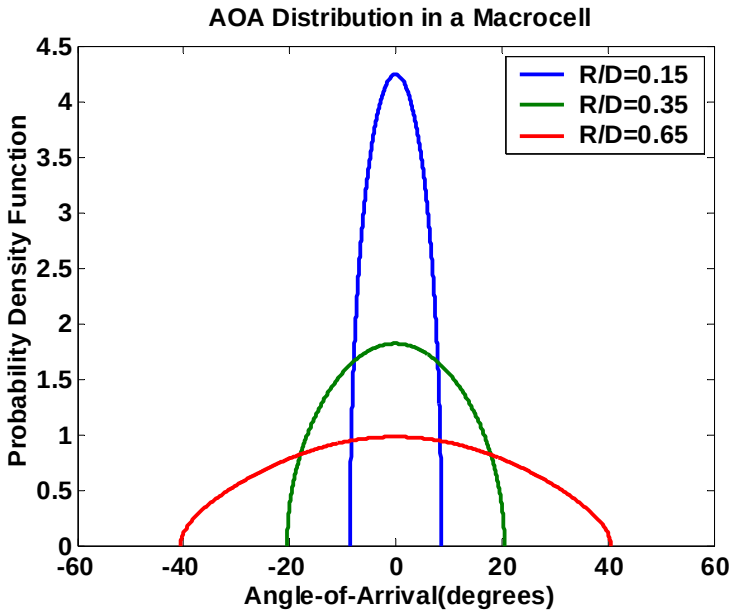

Figure 6.5: AOA Distribution with All multipaths Signals Considered

These conclusions can also be drawn from the marginal distribution of AOA, $f_\theta(\theta)$. Figure 6.5 depicts plots of $f_\theta(\theta)$ for cases of R/D equal to 0.15, 0.35, and 0.65. Suppose that the time difference between the earliest signal and the latest signal is T, which corresponds to the largest TOA NLOS error, $NLOS_{\max}$. If one is able to distinguish the arriving signals with a resolution of $T/16$ and only the earliest $T/16$ incoming signals are used, the plots of the AOA distributions of these earliest signals will change to those shown in Figure 6.6. Compared to the plots in Figure 6.5, one can easily see that the angle spread decreases significantly.

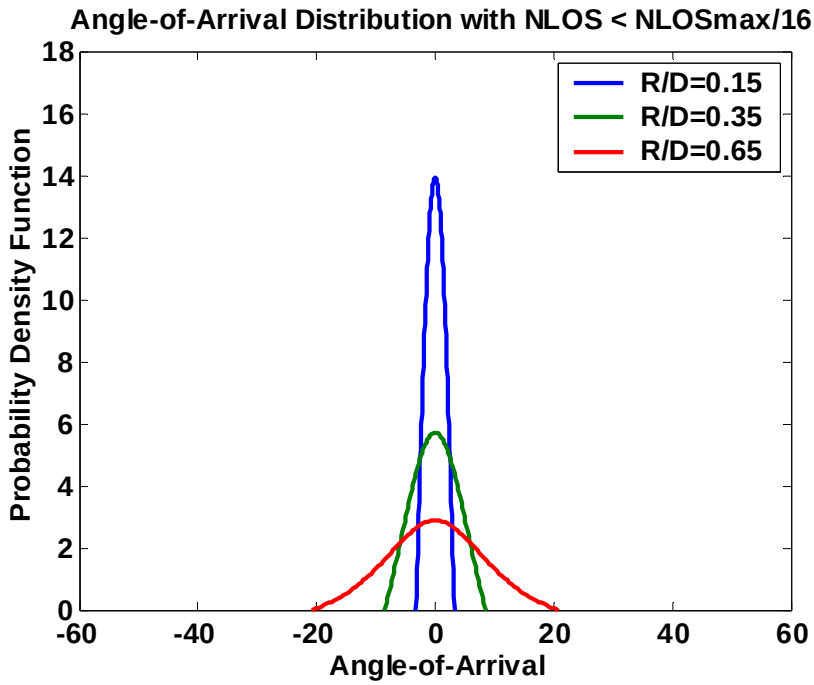

Figure 6.6: AOA Distribution with Only Early Multipath Signals Considered

6.3.2 GBSB Microcell Model

For a microcell, the cell radius is small (about 2~3 km) and the BS antenna is not well above the surrounding objects. In this case, both the BS and MS are surrounded by scatterers. Such a GBSB microcell model is illustrated in Figure 6.7.

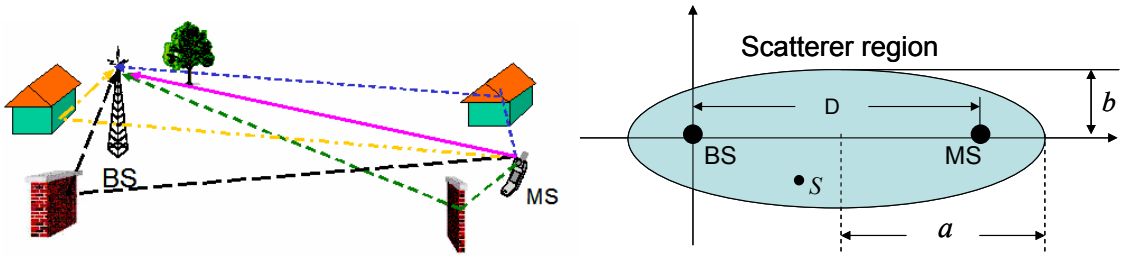

Figure 6.7: GBSB Microcell Model

In this figure, the distance between the base station and the mobile station is D. Scatterers, denoted by S, are assumed to be uniformly located around both the MS and

the BS inside an ellipse. If the maximum time delay of concern is τ_m, the major semi-axis, a, and the minor semi-axis, b, are expressed by

$$a = \frac{c\tau_m}{2} \qquad\qquad b = \frac{\sqrt{c^2\tau_m^2 - D^2}}{2}.$$

Unlike a macrocell, where the AOAs of multipath components are restricted to an angular region of $2\theta_{\max}$ at the base station, AOAs in a microcell can originate from any direction (i.e., from 0^o to 360^o). If the scatterers are assumed to be uniformly distributed in the ellipse, the joint TOA-AOA distribution in the microcell case can also be obtained by studying the scatterer density within the scatterer region as a function of TOA and AOA. The joint TOA-AOA distribution has the following form (Ertel et al, 1998)

$$f_{\tau,\theta}(\tau,\theta) = \begin{cases} \dfrac{\left(D^2 - \tau^2c^2\right)\left(D^2c + \tau^2c^3 - 2\tau c^2 D\cos\theta\right)}{4\pi a_m b_m \left(D\cos\theta - \tau c\right)^3} & \dfrac{D}{c} \le \tau \le \tau_m \\ 0 & \textit{elsewhere} \end{cases} \tag{6.6}$$

where τ is TOA and θ is AOA measured relative to the LOS BS-MS direction. The respective distributions of τ and θ can be further derived by calculating their marginal probability functions. Similarly, only the AOA distribution is provided here (Liberti and Rappaport, 1996).

$$\begin{aligned} f_\theta(\theta) &= \frac{1}{2\pi\beta}\frac{\left(r_m^2 - 1\right)^2}{\left(r_m - \cos\theta\right)^2}, \\ r_m &= \frac{\tau_m}{\tau_0} = \frac{\tau_m}{D/c}, \\ \beta &= r_m\sqrt{r_m^2 - 1} \end{aligned} \tag{6.7}$$

Figure 6.8 is an example of the joint distribution of TOA and AOA for a microcell. The following conclusions can be drawn:

- The probability of AOA is non -zero in all directions; and
- The earlier the arriving signal, the narrower the AOA distribution, and the smaller the AOA spread.

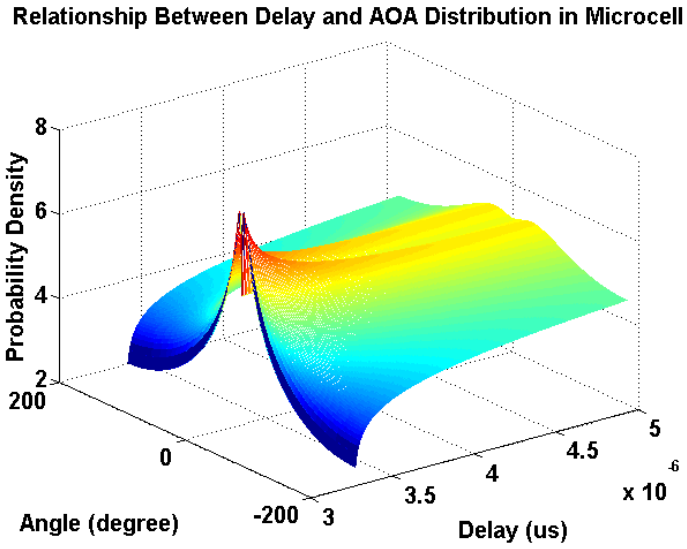

Figure 6.8: Joint TOA/AOA Distribution in a Microcell (GBSB Microcell Model)

These conclusions can also be drawn from analysis of the marginal distribution of AOA, $f_\theta(\theta)$. Figure 6.9 depicts the plots of $f_\theta(\theta)$ in three cases, where the ratio of the maximum NLOS error, $c\Delta\tau$, to the MS-BS distance, D, is equal to 0.01, 0.1, and 0.3. Obviously, $\Delta\tau$ is inversely proportional to the ability to extract the earlier signals. Not surprisingly, the angle spread corresponding to $c\Delta\tau/D = 0.01$ is much smaller than that of $c\Delta\tau/D = 0.3$.

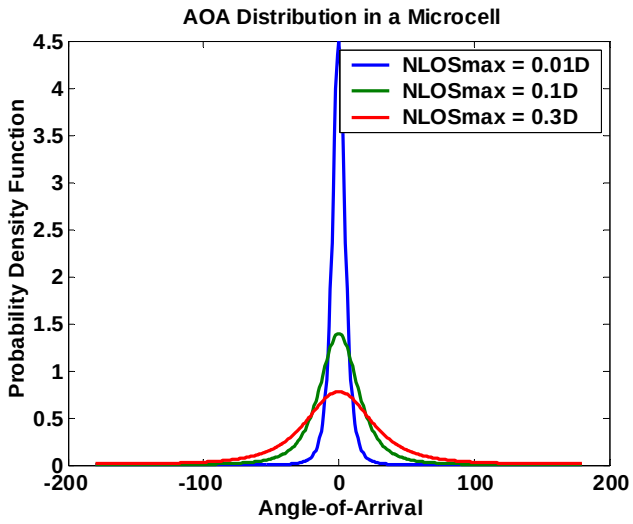

Figure 6.9: Marginal AOA Distribution for GBSB Microcell Model

From the above discussion of the GBSB macrocell and microcell models, it is obvious that the angle spread is smaller when only early arriving signals are considered. This means that AOA measurement accuracy and wireless location performance can be improved if one is able to make use of only early arriving signals. To this end, an algorithm to estimate the vector channel impulse response and to extract early arriving signals is proposed in the following sections.

6.4 Vector Channel Estimation

An antenna array becomes necessary here since AOAs and TOAs of multipath signals need to be estimated in the proposed algorithm. It is also worth pointing out that such an antenna array can only be mounted at BSs because of the large size. Based on this requirement, a system to estimate AOAs and TOAs should have a structure (Van der Veen et al, 1998) as shown in Figure 6.10.

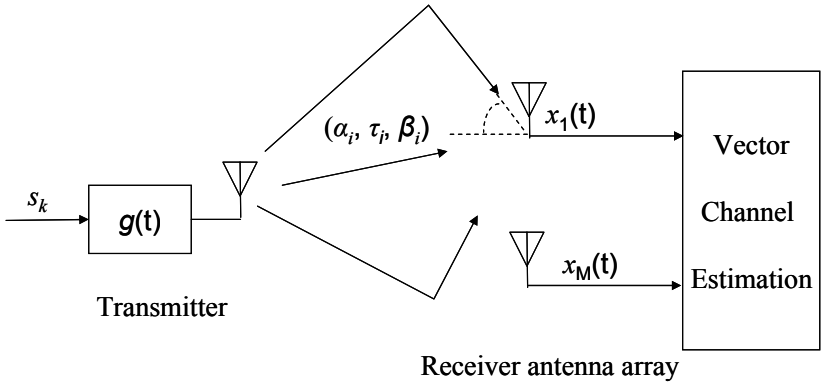

Figure 6.10: Vector Channel Estimation

At an MS transmitter, signal s_k is propagated through a multipath radio channel after waveform shaping where the shaping function is denoted as $g(t)$. At a BS receiver, all sensors of the antenna array receive multipath signals and send them to a channel estimator to estimate TOAs and AOAs. Each multipath replica has its own parameters $(\tau_i, \theta_i, \beta_i)$ which are TOA, AOA, and propagation fading, respectively. Fading is assumed herein to be independent among paths; that is, each path has an individualized signal fading effect. This assumption is reasonable because only physically close paths are correlated and they actually can be treated as one path. In this chapter, such a mobile channel is called a vector channel which is a function of the AOAs and TOAs of multipath signals.

A uniform linear array (ULA) is an adequate modelling device to estimate AOAs if only azimuth angle is of interest. For simplicity's sake, assume that the following two conditions hold. First, that the received signal is a narrow band signal compared to the size of the antenna array, which means that the amplitudes of an incoming signal at all

sensors are the same. Second, the incoming signals are far-field signals, meaning that the signals are plane wave and the incident angles are the same at all sensor locations.

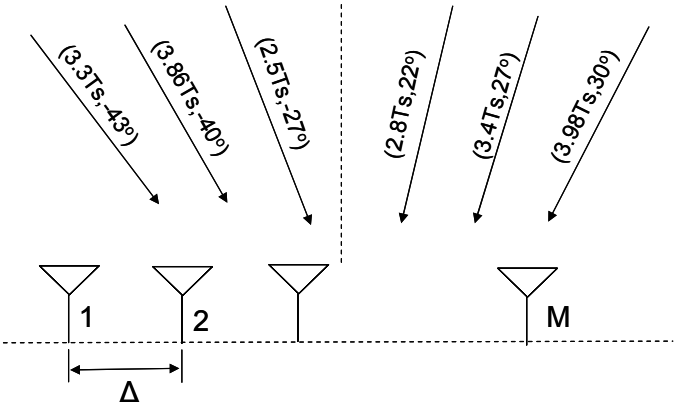

Figure 6.11: Uniform Linear Array

Suppose that a multipath signal due to scatterer i impinges on an M -element ULA in the direction of θ_i, as shown in Figure 6.11. Given the above assumptions, the output of element m is

$$r_m(t) = A\beta_i s(t-\tau_i) e^{-j2\pi f_c \frac{(m-1)\Delta \sin(\theta_i)}{c}} \tag{6.8}$$

where Δ is the distance between two adjacent sensors; A is the amplitude of the original transmitted signal; β_i is the propagation attenuation of this signal (it is uncorrelated with those of other paths); τ_i is TOA; f_c is signal carrier frequency; and c is signal propagation velocity. Stacking the output of array elements into a vector gives

$$\mathbf{r}_i(t) = \begin{bmatrix} e^{-j2\pi f_c \frac{\frac{M-1}{2}\Delta \sin(\theta_i)}{c}} \\ \vdots \\ 1 \\ \vdots \\ e^{j2\pi f_c \frac{\frac{M-1}{2}\Delta \sin(\theta_i)}{c}} \end{bmatrix} A\beta_i s(t-\tau_i) = \mathbf{a}(\theta_i) A\beta_i s(t-\tau_i) \tag{6.9}$$

where $\mathbf{a}(\theta_i)$ denotes the array response, which is normally called the array manifold.

Taking all of the multipath signals into consideration, the final output of the antenna array consists of the superposition of each individual multipath replica since the channel is a linear channel and, thus, the superposition principle holds. Supposing that there are q multipath replicas - each with its own AOA θ_i, TOA τ_i, and path attenuation, β_i - the final output of the antenna array is

$$\mathbf{r}(t) = \sum_{i=1}^{q} \mathbf{a}(\theta_i) A_i \beta_i s(t - \tau_i) \tag{6.10}$$

and the vector channel impulse response is

$$\mathbf{h}_c(t) = \sum_{i=1}^{q} \mathbf{a}(\theta_i) A_i \beta_i \delta(t - \tau_i) \tag{6.11}$$

The above equation is an expression of the vector channel impulse response in a continuous time domain. In real world wireless systems, all signals being processed are sampled as discrete signals, so a discrete channel model is necessary prior to channel estimation.

6.4.1 Discrete Space-Time Channel Model

Discrete channel modelling is closely related to the digital modulation procedure in a cellular network. Digital modulation is the process by which a digital baseband signal is converted into an RF signal for transmission. Normally, the base-band signal is first created by the convolution of digital sequences $\{s_k\}$ with a pulse shaping function $g(t)$

$$s(t) = \sum_{l} s_l g(t - lT) \tag{6.12}$$

where T denotes symbol period. The pulse shaping function, $g(t)$, is band-limited and, thus, is associated with a theoretically infinite length of time. However, it is usually truncated to a finite duration without incurring serious accuracy problems. A commonly used pulse shaping function is the raised cosine pulse function, given by

$$g(t)=\left(\frac{\sin(\pi t)/T}{\pi t/T}\right)\left(\frac{\cos(\alpha\pi t/T)}{1-(2\alpha t/T)^2}\right) \tag{6.13}$$

where α is the roll-off factor. Figure 6.12 shows an example of a raised cosine pulse function (Van der Veen et al, 1998).

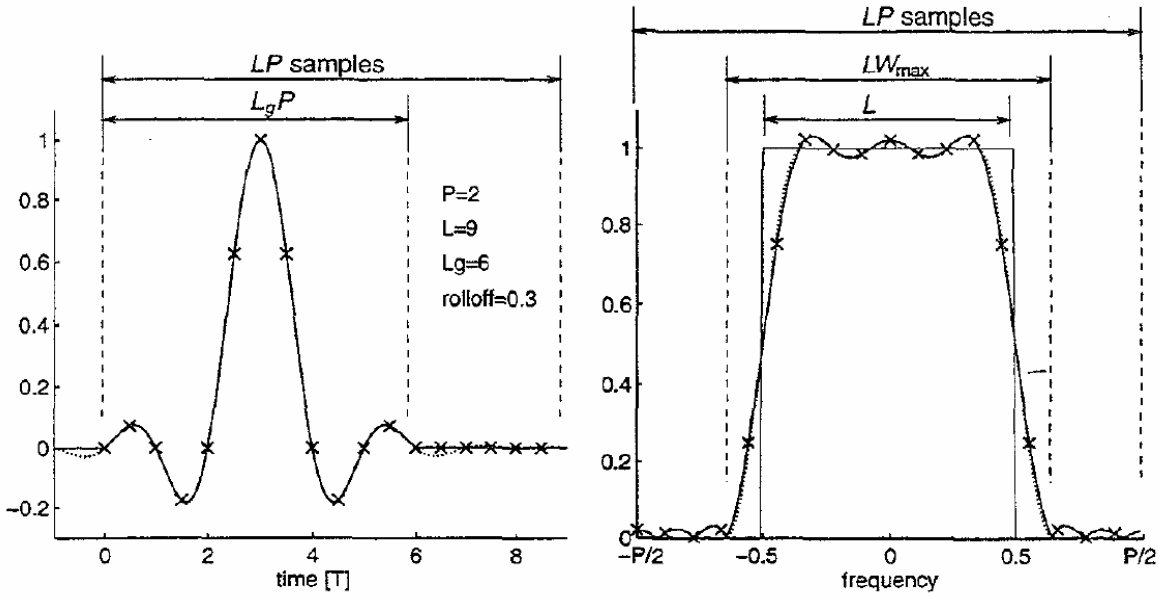

(a) Time Domain (b) Frequency Domain

Figure 6.12: Raised Cosine Pulse Function

Let $\mathbf{x}(t)$ represent the baseband output of a uniform linear array with M elements. Based on equation (6.10), the continuous received signal with measurement noise is

$$\mathbf{x}(t)=\sum_{i=1}^{q}\mathbf{a}(\theta_i)\beta_i s(t-\tau_i)+\mathbf{n}(t) \tag{6.14}$$

Substituting equation (6.12) into this equation,

$$\begin{aligned}\mathbf{x}(t) &= \sum_{i=1}^{q}\mathbf{a}(\theta_i)\beta_i\sum_{l}s_l g(t-lT-\tau_i)+\mathbf{n}(t)\\ &= \sum_{l}s_l\sum_{i=1}^{q}\mathbf{a}(\theta_i)\beta_i g(t-lT-\tau_i)+\mathbf{n}(t)\\ &= \sum_{l}s_l\mathbf{h}(t-lT)+\mathbf{n}(t)\end{aligned} \tag{6.15}$$

it is observed that $\mathbf{x}(t)$, the output of the receiver array, is the convolution of the digital sequence with a new function, $\mathbf{h}(t)$. So, $\mathbf{h}(t)$ is the *discrete vector channel impulse response,* expressed by

$$\mathbf{h}(t)=\sum_{i=1}^{q}\mathbf{a}(\theta_i)\beta_i g(t-\tau_i) \tag{6.16}$$

6.4.2 Discrete Vector Channel Estimation

Channel estimation can be conducted via blind techniques and non-blind techniques. While a blind technique depends only on channel output, employment of a non-blind technique requires knowledge of the waveform of the transmitted signals - that is, a training sequence. In this chapter, a non-blind technique proposed by Van der Veen et al (1998) is used. The derivation of this algorithm is explained as below.

Over-sampling the output of the antenna array during N symbol periods at time, $t=kT, k=0,\frac{1}{P},\cdots,N-\frac{1}{P}$, we then obtain,

$$\mathbf{x}(kT)=\sum_{l}s_l\mathbf{h}((k-l)T)+\mathbf{n}(kT), \qquad k=0,\frac{1}{P},\cdots,N-\frac{1}{P} \tag{6.17}$$

where T is symbol period and P is the over sampling rate, which is the number of samples within one symbol period. As discussed above, the pulse-shaping function, $g(t)$, such as the truncated raised cosine pulse function, is of finite non-zero length. If the non-zero length is symbolized by L, the output can be written as

$$\mathbf{x}(kT) = \sum_{l=\lfloor k-L+1 \rfloor}^{\lfloor k \rfloor} s_l \mathbf{h}((k-l)T) + n(kT), \qquad k = 0, \frac{1}{P}, \cdots, N - \frac{1}{P} \tag{6.18}$$

Both $\mathbf{x}(kT)_{k=0,\frac{1}{P},\cdots,N-\frac{1}{P}}$ and $\mathbf{h}(kT)_{k=0,\frac{1}{P},\cdots,L-\frac{1}{P}}$ can be rearranged into matrix form as follows:

$$\mathbf{X} = \begin{bmatrix} \mathbf{x}(0) & \mathbf{x}(T) & \cdots & \mathbf{x}((N-1)T) \\ \mathbf{x}(T/P) & \mathbf{x}((1+1/P)T) & & \mathbf{x}((N-1+1/P)T) \\ \vdots & & \ddots & \vdots \\ \mathbf{x}((1-1/P)T) & \mathbf{x}((2-1/P)T) & \cdots & \mathbf{x}((N-1/P)T) \end{bmatrix}_{MP \times N} \tag{6.19}$$

$$\mathbf{H} = \begin{bmatrix} \mathbf{h}(0) & \mathbf{h}(T) & \cdots & \mathbf{h}((L-1)T) \\ \mathbf{h}(T/P) & \mathbf{h}((1+1/P)T) & & \mathbf{h}((L-1+1/P)T) \\ \vdots & & \ddots & \vdots \\ \mathbf{h}((1-1/P)T) & \mathbf{h}((2-1/P)T) & \cdots & \mathbf{h}((L-1/P)T) \end{bmatrix}_{MP \times L} \tag{6.20}$$

After some derivation, we can prove that the following equation holds

$$\mathbf{X} = \mathbf{HS} + \mathbf{N} \tag{6.21}$$

where

$$\mathbf{S} = \begin{bmatrix} s_0 & s_1 & \ddots & s_{N-1} \\ s_{-1} & s_0 & s_1 & \ddots \\ \ddots & & & \ddots \\ s_{-L+1} & s_{-L+2} & \ddots & s_{N-L} \end{bmatrix}_{L \times N}$$

and

$$\mathbf{N}=\begin{bmatrix} \mathbf{n}(0) & \mathbf{n}(T) & \cdots & \mathbf{n}((N-1)T) \\ \mathbf{n}(T/P) & \mathbf{n}((1+1/P)T) & & \mathbf{n}((N-1+1/P)T) \\ \vdots & & \ddots & \vdots \\ \mathbf{n}((1-1/P)T) & \mathbf{n}((2-1/P)T) & \cdots & \mathbf{n}((N-1/P)T) \end{bmatrix}_{MP\times N}$$

Equations (6.17) and (6.21) form the theoretical basis of the channel estimation algorithm used here.

In non-blind channel estimation, the transmitted symbols, $\{s_k\}$, called the training sequence, are carefully selected in advance, so that **S** is known and **H** can be computed as

$$\hat{\mathbf{H}}=\mathbf{X}\mathbf{S}^H\left(\mathbf{S}\mathbf{S}^H\right)^{-1}+\tilde{\mathbf{N}} \tag{6.22}$$

$\hat{\mathbf{H}}$ is of the structure shown in equation (6.20), and can be rearranged into an $M\times PL$ matrix,

$$\mathbf{H}'=\left[\mathbf{h}(0)\quad \mathbf{h}\left(\frac{T}{P}\right)\quad \cdots\quad \mathbf{h}\left(\left(L-\frac{1}{P}\right)T\right)\right] \tag{6.23}$$

which is actually of the following form based on the channel model in equation (6.16)

$$\mathbf{H}'=\begin{bmatrix}\mathbf{a}_1 & \cdots & \mathbf{a}_q\end{bmatrix}\begin{bmatrix}\beta_1 & & 0\\ & \ddots & \\ 0 & & \beta_q\end{bmatrix}\begin{bmatrix}\mathbf{g}_1\\ \vdots\\ \mathbf{g}_q\end{bmatrix}=\mathbf{A}\boldsymbol{\beta}\mathbf{G} \tag{6.24}$$

where $\mathbf{a}_i=\mathbf{a}(\theta_i)$ is the array manifold vector for *i*th signal and contains AOA information, θ_i. $\mathbf{g}_i=[g(k-\tau_i)]_{k=0,1/P,\cdots,L-1/P}$ is a delayed version of waveform-shaping function; it is a LP-dimensional row vector and contains TOA information, τ_i.

Matrix $\mathbf{G}$ can be further simplified by introducing the Discrete Fourier Transformation (DFT) to the delayed waveform-shaping functions. Let $\mathbf{\Gamma}$ denote the DFT matrix of size $LP \times LP$,

$$\mathbf{\Gamma} = \begin{bmatrix} 1 & 1 & \cdots & 1 \\ 1 & \phi & \cdots & \phi^{LP-1} \\ \vdots & \vdots & \ddots & \vdots \\ 1 & \phi^{LP-1} & \cdots & \phi^{(LP-1)^2} \end{bmatrix}, \phi = e^{-j\frac{2\pi}{LP}}. \tag{6.25}$$

One can prove that

$$\mathbf{G\Gamma} = \mathbf{F} \cdot \mathrm{diag}(\tilde{\mathbf{g}}) \tag{6.26}$$

where $\mathbf{F}$ is a Vandermonde matrix with a size of $q \times LP$

$$\mathbf{F} = \begin{bmatrix} 1 & \phi_1 & \phi_1^2 & \cdots & \phi_1^{LP-1} \\ \vdots & \vdots & \vdots & & \vdots \\ 1 & \phi_q & \phi_q^2 & \cdots & \phi_q^{LP-1} \end{bmatrix}, \ \phi_i = \phi^{\tau_i P} = e^{-j\frac{2\pi}{L}\tau_i} \tag{6.27}$$

and $\tilde{\mathbf{g}}$ is the DFT of vector $\mathbf{g} = \left[g(0) \quad g\left(1/P\right) \quad \cdots \quad g\left(L - 1/P\right) \right]$. Thus, the vector channel estimate becomes

$$\tilde{\mathbf{H}} = \mathbf{H}' \cdot \mathbf{\Gamma} = \mathbf{A} \cdot \mathbf{\beta} \cdot \mathbf{F} \cdot \mathrm{diag}(\tilde{\mathbf{g}}). \tag{6.28}$$

In order to make the estimation of TOA and AOA easier, it is desirable to remove the item $\mathrm{diag}(\tilde{\mathbf{g}})$ from equation (6.28). This can be done by post-multiplying $\tilde{\mathbf{H}}$ with $\mathrm{diag}^{-1}(\tilde{\mathbf{g}})$. However, because some elements of $\tilde{\mathbf{g}}$ are very small or even zero, they may prevent the inversion operation. To avoid this, only those elements with large absolute values are used. W points inside the main frequency domain lobe that are suitable for inverse operation can be extracted by the following matrix:

$$J_{\tilde{\mathbf{g}}} = \begin{bmatrix} 0 & I_{\lfloor W/2 \rfloor} \\ 0 & 0 \\ I_{\lceil W/2 \rceil} & 0 \end{bmatrix} \tag{6.29}$$

Applying it to $\widetilde{\mathbf{H}}$ gives

$$\begin{aligned} \overline{\mathbf{H}} &= \widetilde{\mathbf{H}} \cdot \mathbf{J}_{\tilde{\mathbf{g}}} \cdot \left\{ \mathrm{diag}\left(\tilde{\mathbf{g}} \cdot \mathbf{J}_{\tilde{\mathbf{g}}} \right)^{-1} \right\} \\ &= \mathbf{A} \cdot \boldsymbol{\beta} \cdot \mathbf{F} \end{aligned} \tag{6.30}$$

where $\mathbf{A}$ is the array manifold matrix with dimensions of $M \times q$; $\mathbf{F}$ is the TOA-related matrix with a size of $q \times W$; and $\boldsymbol{\beta}$ is the multipath signal amplitude-related matrix. They have the following component forms:

$$\mathbf{A} = \begin{bmatrix} 1 & 1 & \cdots & 1 \\ e^{-j2\pi \frac{\Delta \sin\theta_1}{\lambda}} & e^{-j2\pi \frac{\Delta \sin\theta_2}{\lambda}} & \cdots & e^{-j2\pi \frac{\Delta \sin\theta_q}{\lambda}} \\ \vdots & \vdots & & \vdots \\ e^{-j2\pi \frac{(M-1)\Delta \sin\theta_1}{\lambda}} & e^{-j2\pi \frac{(M-1)\Delta \sin\theta_q}{\lambda}} & \cdots & e^{-j2\pi \frac{(M-1)\Delta \sin\theta_q}{\lambda}} \end{bmatrix}$$

$$\boldsymbol{\beta} = \begin{bmatrix} \beta_1 & & & 0 \\ & \beta_2 & & \\ & & \ddots & \\ 0 & & & \beta_q \end{bmatrix}$$

and

$$\begin{aligned} \mathbf{F} &= \begin{bmatrix} \phi_1^{LP-\lceil W/2 \rceil} & \cdots & \phi_1^{LP-1} & 1 & \phi_1 & \cdots & \phi_1^{\lfloor W/2 \rfloor} \\ \vdots & & \vdots & \vdots & \vdots & & \vdots \\ \phi_q^{LP-\lceil W/2 \rceil} & \cdots & \phi_q^{LP-1} & 1 & \phi_q & \cdots & \phi_q^{\lfloor W/2 \rfloor} \end{bmatrix} \\ &= \begin{bmatrix} \phi_1^{LP-\lceil W/2 \rceil} & \cdots & 1 & \cdots & \phi_1^{\lfloor W/2 \rfloor} \\ \vdots & & \vdots & & \vdots \\ \phi_q^{LP-\lceil W/2 \rceil} & \cdots & 1 & \cdots & \phi_q^{\lfloor W/2 \rfloor} \end{bmatrix} \end{aligned}$$

The above derivation of $\overline{\mathbf{H}}$ is the first stage of vector channel estimation. It is actually a deconvolution procedure because the channel impulse response is calculated from the array output. In the second stage, TOAs and AOAs of multipath replicas will be estimated from $\overline{\mathbf{H}}$ and will be used to obtain better AOA measurements.

6.5 TOAs and AOAs Estimation via 2D UESPRIT Super-Resolution Method

Several methods have been proposed to conduct space-time channel estimation, such as: the iterative multidimensional maximum likelihood method (Wax and Leshem, 1997); the JADE algorithm (Van der Veen et al, 1997); and the TST-MUSIC method (Wang et al, 2001). In this chapter, the 2-D Unitary-ESPRIT method (Zoltowski et al, 1996) is used to estimate TOAs and AOAs of multipath signals because it is a closed-form solution and can make use of the centro-Hermitian property of a Uniform Rectangular Array (URA) to decrease the computational burden and improve estimation accuracy.

Studying $\mathbf{A}$ and $\mathbf{F}$ in element form, it can be seen that $\mathbf{A}$ and $\mathbf{F}$, containing AOA and TOA information, are of Vandermonde format. When $\overline{\mathbf{H}}$ is compared with the output of a URA (Yu and Lee, 1997), which is often used for azimuth and elevation direction-finding, we can see that they are of exactly the same format. Hence, $\overline{\mathbf{H}}$ is actually the output of a URA with one dimension in the space domain and the other dimension in the time domain. Given this basis, techniques suitable for a URA can be directly applied here.

The 2-D Unitary ESPRIT method is preferred because it makes use of the centro-symmetric and/or centro-Hermitian property of a URA to improve estimation accuracy and decrease computational burden. A URA is centro-symmetric since its element locations are symmetrical with respect to its centroid. A URA has the dual-direction invariance property; i.e. there exist two identical sub-arrays in the space domain element direction and two identical sub-arrays in the time domain element direction, as shown in Figure 6.13.

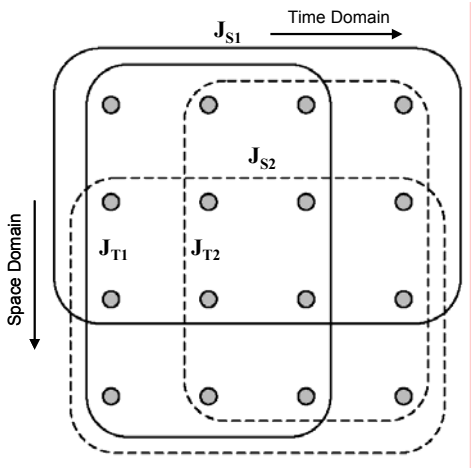

Figure 6.13: Dual Direction Shift Invariance Structure of a URA (Chareyre, 2002)

In summary, the 2-D Unitary-ESPRIT method has the following advantages, making it a high-performance TOA/AOA-finding algorithm:

- Like the original ESPRIT method (Roy and Kailath, 1989), TOAs and AOAs are estimated by exploiting the rotational invariance structure of the signal subspace or the translation invariance structure of the URA.
- Unitary ESPRIT exploits the knowledge that the phase factor for two sub-arrays with a translation invariance property is actually a unitary matrix. The estimation

accuracy can be improved by taking this additional information into consideration.

- The centro-symmetric property is used to transform complex matrices to real matrices while keeping all TOA and AOA information intact. This can decrease the computational burden.
- It is a closed-form solution.
- It has a super-resolution capability.
- It has an automatic pairing ability, which makes this method even more powerful in real world applications.

A detailed derivation of this algorithm can be found in Zoltowski et al (1996).

6.6 Simulation Results

In this section, simulations are used to study algorithm performance in terms of the following:

- The performance of 2-D Unitary-ESPRIT method itself
- TOA/AOA estimation accuracy for a single BS
- Wireless location performance improvement due to mobile channel estimation

6.6.1 Performance of 2-D Unitary-ESPRIT Algorithm

The objective of TOA-AOA estimation is to extract signal information from signal plus noise environments by means of array signal processing techniques. Thus, algorithm

performance will be affected by the structure of the antenna array used, interference and noise. As to the 2-D Unitary-ESPRIT method, its performance is affected by

- The Signal to Interference Ratio (SIR); and
- The number of sensors in the antenna array

In the simulations presented here, six multipath replicas are assumed to be impinging on an antenna array as shown in Figure 6.11. The TOA/AOA pairs are (2.5 T_s , -27º), (2.8 T_s , 22º), (3.3 T_s , -43º), (3.4 T_s , 27º), (3.86 T_s , -40º), and (3.98 T_s , 30º) where T_s is the symbol period. Figures 6.14 to 6.17 show the mean AOA error, the mean TOA error, the RMS of AOA errors, and the RMS of TOA errors which are calculated via,

$$\overline{E}_{AOA} = \frac{1}{q}\sum_{i=1}^{q}\frac{1}{N}\sum_{j=1}^{N}\left|AOA_{ij} - AOA_i^0\right| \tag{6.31}$$

$$\overline{E}_{TOA} = \frac{1}{q}\sum_{i=1}^{q}\frac{1}{N}\sum_{j=1}^{N}\left|TOA_{ij} - TOA_i^0\right| \tag{6.32}$$

$$\overline{RMS_{AOA}} = \frac{1}{q}\sum_{i=1}^{q}\sqrt{\frac{1}{N}\sum_{j=1}^{N}\left(AOA_{ij} - AOA_i^0\right)^2} \tag{6.33}$$

$$\overline{RMS_{TOA}} = \frac{1}{q}\sum_{i=1}^{q}\sqrt{\frac{1}{N}\sum_{j=1}^{N}\left(TOA_{ij} - TOA_i^0\right)^2} \tag{6.34}$$

where q is the number of multipath replicas; N is number of the Monte Carlo runs; TOA_i^0 and AOA_i^0 are the true values of TOA and AOA of the ith multipath replica; and TOA_{ij} and AOA_{ij} are the estimated TOA and AOA of the jth run for the ith multipath replica.

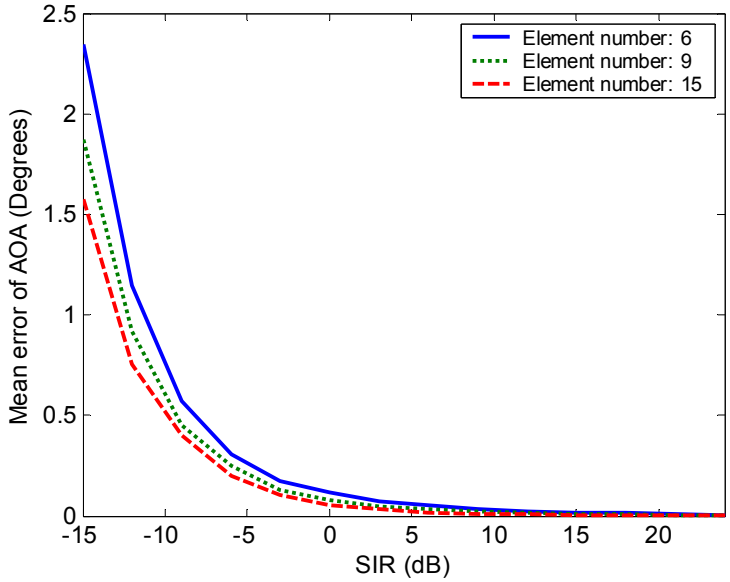

Figure 6.14: Mean AOA Estimation Errors vs. SIR and Sensor Number

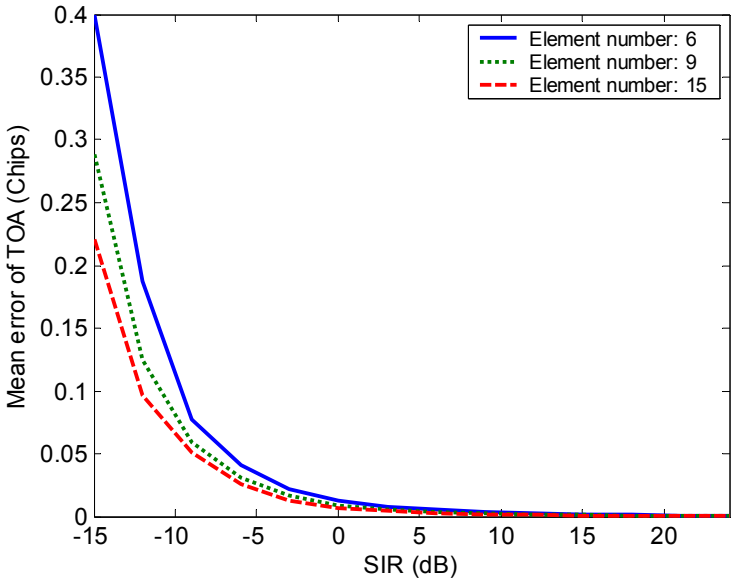

Figure 6.15: Mean TOA Estimation Errors vs. SIR and Sensor Number

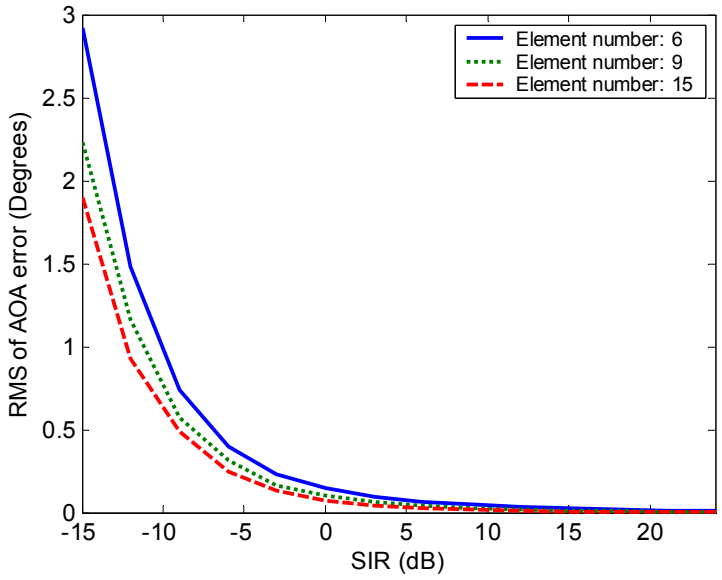

Figure 6.16: RMS of AOA Estimation Errors vs. SIR and Sensor Number

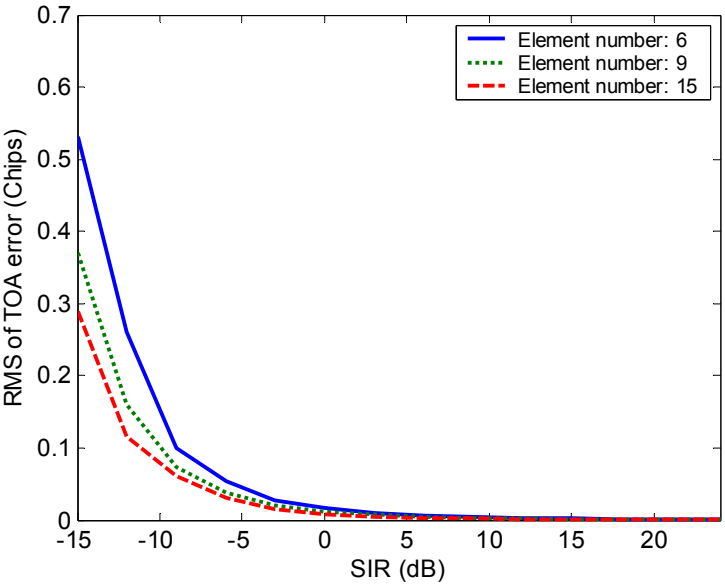

Figure 6.17: RMS of TOA Estimation Errors vs. SIR and Sensor Number

The simulation results demonstrate that both array sensor number and SIR affect the performance quite dramatically. With a larger number of array sensors and a higher SIR, a more accurate TOA/AOA estimation can be obtained. A reasonably acceptable TOA-

AOA estimation - say, $\mathrm{RMS}_{\mathrm{TOA}} < 0.2$ chips and $\mathrm{RMS}_{\mathrm{AOA}} < 0.5$ degree - can be obtained when the SIR is higher than -5dB and the number of sensors is greater than the number of multipath signals.

6.6.2 TOA-AOA Estimation Accuracy for a Single BS

In this part, the TOA-AOA estimation accuracy is evaluated. The tests attempt to show how accurately a BS can measure the TOA-AOA of an MS with variations in the MS-BS distance. The results indicate whether or not a TOA-AOA measurement is suitable for use in an MS location calculation. The following parameters are used to evaluate the performance: the probability of successful TOA-AOA estimation; and the mean and RMS values of TOA and AOA measurement errors. Assumed are that the BS is well above the ground and that the GBSB macrocell model can be used to describe the scatterer distribution. The radius of the scatterer region is 500 m with the MS as the centre of the circular area. A successful TOA-AOA estimation is defined here as the case wherein the calculated scatterer corresponding to the measured TOA-AOA lies in the 500 m scatterer region. The mean value and the RMS value of horizontal location errors are based only on successful TOA measurements and successful AOA measurements. In the simulations, the noise figure of the receivers at the antenna array is assumed to be 5dB, the signal transmission power of the MS to be located is 200mW, and the path loss is assumed to follow the CCIR model or equation (3.16).

Figure 6.18 shows the probability of successful TOA-AOA estimation for a system of which the symbol period is $3.68\ \mu s$. Actually, it is the symbol period of the popular GSM system. For convenience, the discrete results are fitted with curves to clearly show the trend of the performance change with respect to the change of MS-BS distance. One can see that successful estimation probability decreases with the increase of the distance between the BS and MS. This is because the SIR decreases with an increase in MS-BS distance which greatly affects the channel estimation performance.

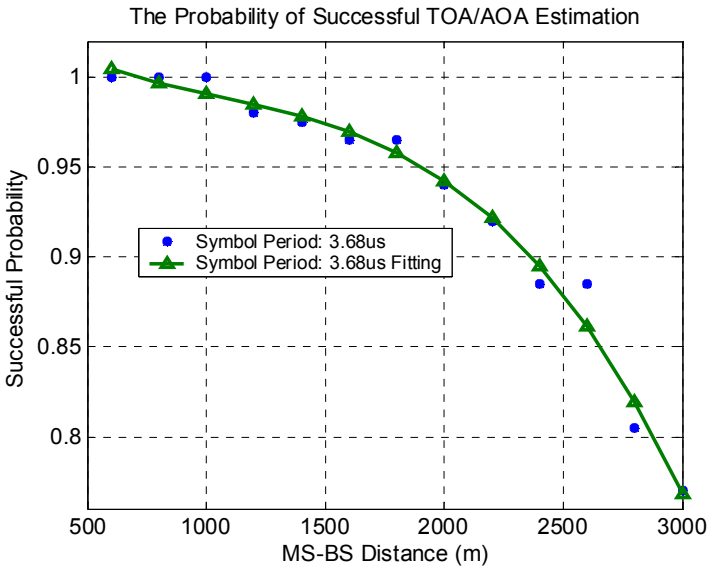

Figure 6.18: The Probability of Successful Estimation

Figures 6.19 to 6.22 demonstrate the change of the mean value and the RMS value of TOA estimation errors and AOA estimation errors. All of these values increase with increasing MS-BS distance, demonstrating that algorithm performance deteriorates with increases in MS-BS distance.

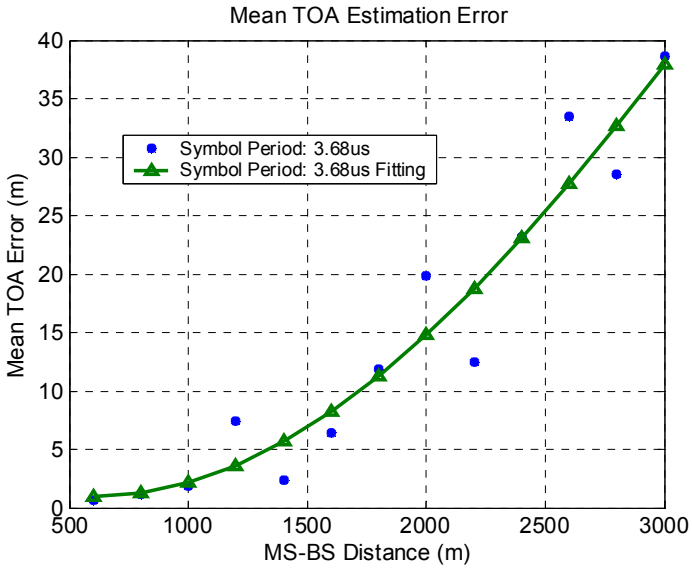

Figure 6.19: The Mean of TOA Estimation Errors

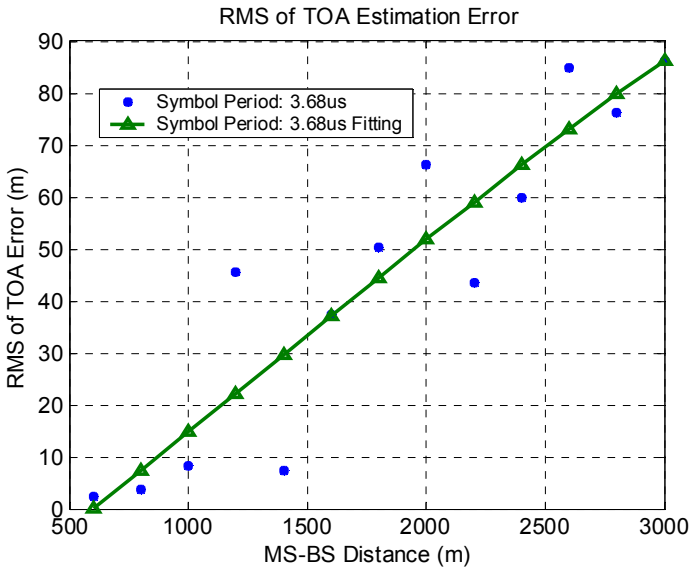

Figure 6.20: The RMS of TOA Estimation Errors

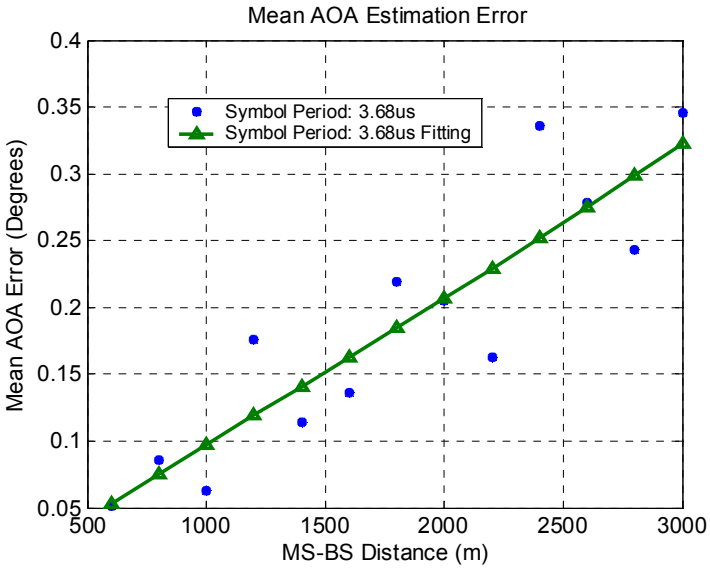

Figure 6.21: Mean of AOA Estimation Errors

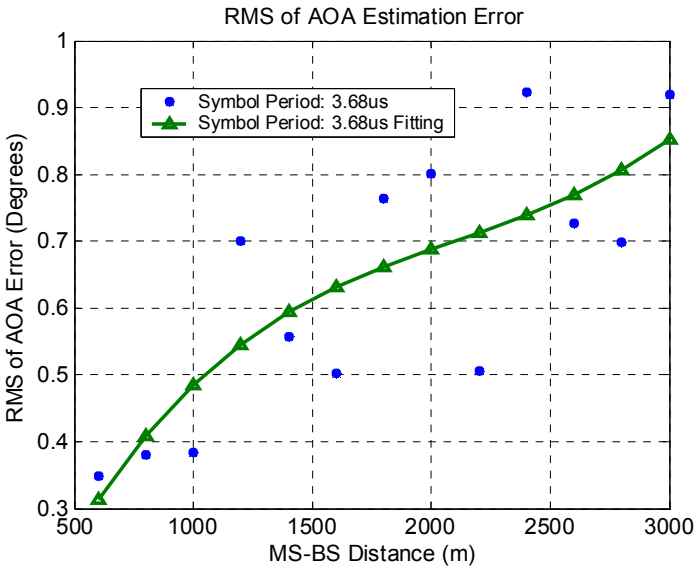

Figure 6.22: RMS of AOA Estimation Errors

6.6.3 Estimation accuracy of MS location

Simulation tests were conducted to verify wireless location performance improvement due to multipath channel estimation. Three methods are compared: (1) the TOA-AOA hybrid solution *without* channel estimation where the TOA and the AOA are selected from all of the multipath replicas based on the received power of each multipath signal; (2) the TOA-AOA hybrid solution *with* channel estimation where the TOA and the AOA of the estimated earliest signal are used in the MS location calculation; and (3) a benchmark method where the TOA and the AOA of the actual earliest signal are used in the MS location calculation. For method (1), the TOA and AOA selected is that of the strongest multipath replica. For method (2), BSs are divided into two categories: BSs with AOA and BSs without AOA. TOAs of the BSs without AOA are those of the strongest multipath replica, while the TOAs and AOAs of the BSs with AOA are the results of channel estimation. For method (3), the TOA and AOA selected is that of the shortest multipath replica. The system used is a 7-cell system with a cell size of 2 km, and the MS is moving from point O, the centre of cell BS1, towards point A as shown in Figure 6.23. The symbol period is $3.68\ \mu s$. The standard deviation of TOA measurement errors due to receiver noise is assumed to be 70 m and the standard deviation of AOA measurement errors due to receiver noise is assumed to be 0.3 degrees.

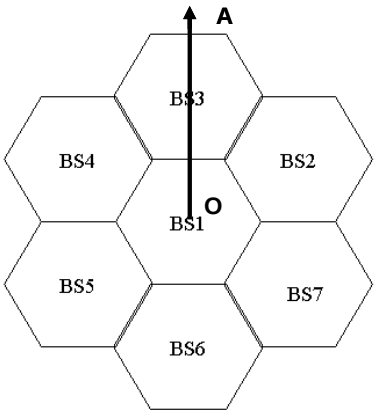

Figure 6.23: The Cellular System Used in Simulation

The simulation results of four scenarios are presented below.

- *Scenario 1: 4 TOAs and 1 AOA without the LOS component*. Four BSs are assumed suitable for TOA measurement, but only one BS is suitable for AOA measurement. For each BS, there are 5 multipath replicas but none of them is the LOS signal. Simulation results are shown in Figure 6.24.
- *Scenario 2: 4 TOAs and 1 AOA with the LOS component*. Four BSs are assumed to be suitable for TOA measurement, but only one BS is suitable for AOA measurement. For each BS there are 5 multipath replicas with one as the LOS signal. Simulation results are shown in Figure 6.25.
- *Scenario 3: 7 TOAs and 3 AOAs without the LOS component*. Very good hearability is assumed to be available. All seven BSs are assumed suitable for TOA measurement and three BSs are suitable for AOA measurement. For each BS there are 5 multipath replicas, but none of them is the LOS signal. Simulation results are shown in Figure 6.26.

- *Scenario 4: 7 TOAs and 3 AOAs with the LOS component*. Very good hearability is assumed to be available. All seven BSs are assumed to be suitable for TOA measurement and three BSs are suitable for AOA measurement. For each BS there are 5 multipath replicas with one functioning as the LOS signal. Simulation results are shown in Figure 6.27.

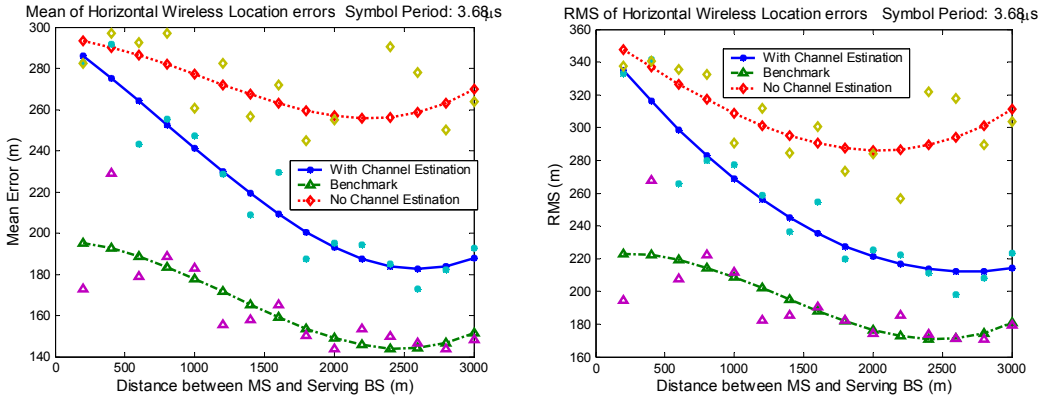

Figure 6.24 Mean and RMS of Location Errors for Scenario 1
(4 TOAs plus 1 AOA without LOS component)

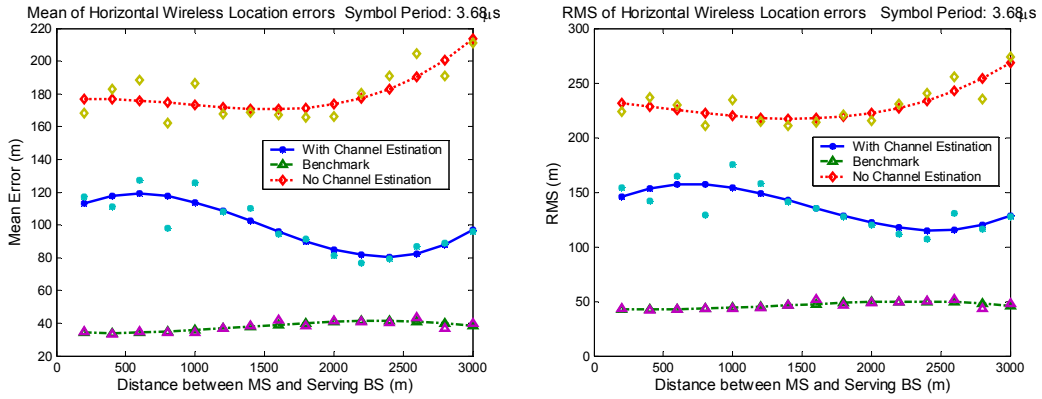

Figure 6.25: Mean and RMS of Location Errors for Scenario 2
(4 TOAs plus 1 AOA with LOS component)

The simulation results of Scenario 1 are shown in Figure 6.24. The location accuracy of the proposed channel estimation-based solution is improved, as compared to no channel estimation, especially in the edge area of a cell where good geometry for location purposes is obtained. The RMS of the horizontal errors changes from about 350 m to 320 m in the area near the serving BS, and from 290 m to 220 m in the edge area (MS-BS distance of 2 km).

Scenario 2 in Figure 6.25 contains LOS propagation. We can see from the figure that both the performance of the channel estimation-based solution and the performance of the theoretical solution increase substantially, as compared to the similar situation but without LOS signals. This is because very accurate TOA-AOA measurements can be obtained since these two methods are able to track LOS signals. Compared to Figure 6.24, the RMS value of the horizontal location errors of the channel estimation-based solution decreases from 330 m to 150 m in the central area of cell BS1, and from 220 m to 120 m in the cell edge area. The RMS value of location errors of the theoretical solution are around 50 m, since the errors result only from receiver thermal noise.

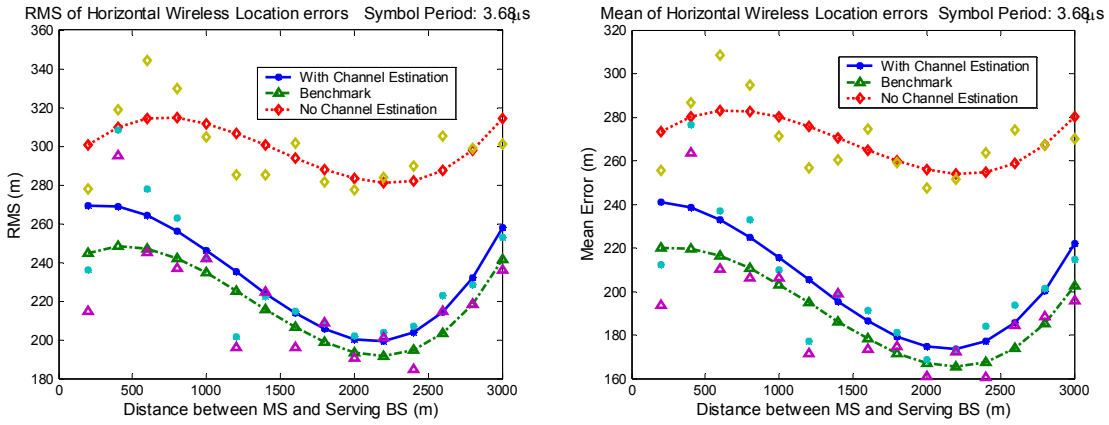

Figure 6.26: Mean and RMS of Location Errors for the Scenario 3
(7 TOAs plus 3 AOAs without LOS component)

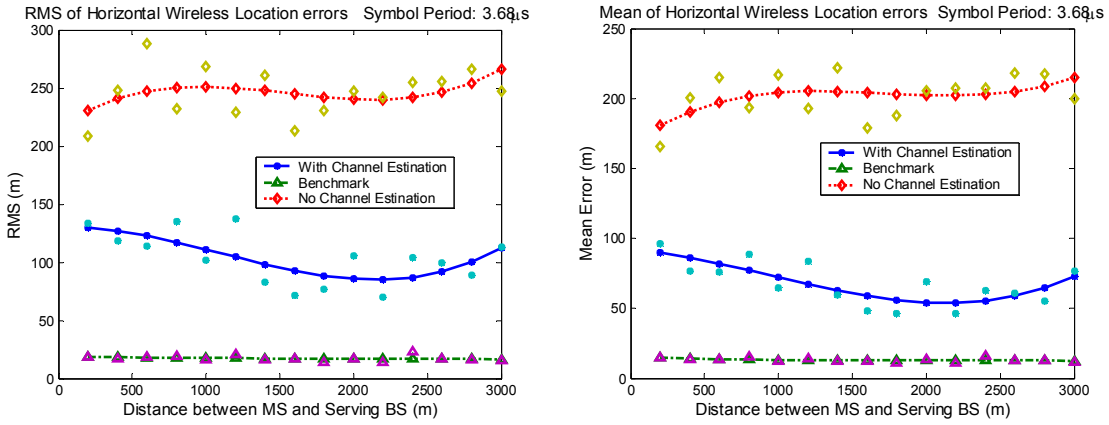

Figure 6.27: Mean and RMS of Location Errors for Scenario 4
(7 TOA plus 3 AOA with LOS component)

The simulation results for Scenario 3 and Scenario 4 are shown in Figures 6.26 and 6.27, where all of the 7 BSs are available for TOA measurement and 3 BSs are available for AOA measurement. The same accuracy change trend is found in these two figures. The accuracy of the method without channel estimation is inferior, whereas the accuracies of the channel estimation-based method and benchmark are better, since they incorporate tracking of early multipath signals.

The accuracy of TOA and AOA measurements and even the final positioning accuracy can also be compared to the so-called Cramer-Rao-Bound (CRB) () to check the effectiveness of the proposed wireless location method. The comparison is meaningful because that the CRB, a function of the number of array elements and signal noise ratio, gives the bound on the covariance matrix an unbiased estimator may reach.

6.7 Conclusions

In this chapter, issues surrounding multipath-afflicted mobile channels are discussed. It was found that a GBSB model describes this issue very well. From the joint distribution of TOA and AOA, it is evident that a better AOA measurement can be obtained if the earliest multipath signal can be extracted and incorporated into the solution.

An elegant multipath channel estimation method, containing two stages, is discussed here. The first stage is vector channel estimation from which the channel impulse response is obtained via an array signal processing technique. The second stage attempts to estimate TOA and AOA information for all multipath replicas. The 2-D Unitary-ESPRIT method is applied for this purpose, as it has a light computational burden and offers super resolution.

Simulation results show that a 2-D Unitary-ESPRIT method produces a good AOA estimation accuracy (<0.5 deg even with SIR<-5 dB) and thus can be used in multipath mobile channel estimation to achieve improved TOA and AOA observation for location

purposes. Compared to normal wireless location methods, the channel estimation-based method provides much better performance especially in areas with good geometry.

CHAPTER 7

INTEGRATION OF GPS AND NETWORK-BASED WIRELESS LOCATION METHODS

7.1 Introduction

GPS is a high-performance satellite-based positioning system. It can provide 5-10 m positioning accuracy (using the L1 C/A code) 24 hours a day under any weather conditions. However, it requires that at least four satellites be seen simultaneously to provide a successful location solution. Due to signal attenuation and blockage, this requirement is difficult to satisfy in a densely constructed area or inside buildings where few if any satellites can be seen. Similarly, cellular signals also suffer from poor hearability problems due to co-channel interference and thermal noise as discussed in Chapter 3. Without using hearability enhancement techniques, a normal MS receiver can hear only 1-3 BSs, which is obviously not sufficient for location purposes.

If working independently, neither of these two systems can provide a satisfactory location service in an area subject to serious attenuation and fading. However, since it is possible to use GPS measurements and cellular network measurements simultaneously, use of an approach that combines both systems may offer a workable solution. In this chapter, three

methods to integrate the GPS and cellular networks are discussed in detail. These methods are: the epoch-by-epoch LS method; the position domain Kalman filter-based MS tracking method; and the measurement domain Kalman filter-based MS tracking method. In the following section, the properties of GPS signals and cellular network signals are first presented, and then the three integration methods are discussed one by one. Performance comparisons among these three methods and some conclusions are given at the end.

7.2 Property Comparison between GPS Signals and Cellular Network Signals

Cellular Network Signals

Mobile channels are far from ideal for wireless location purposes, since cellular systems were originally designed for voice communications, as opposed to MS location. Firstly, a mobile channel is a severe multipath propagation channel; both BSs and MSs are normally very low and there are many objects located nearby. Quite often, the signals received at BSs and MSs do not contain any LOS measurements, especially in a macrocell of which the cell size is quite large. Very large NLOS errors may arise in this case if such cellular signals are used in wireless location. Secondly, hearability is another difficult issue to be solved in cellular network-based wireless location schemes. A cellular system tries to re-use system resources and increase system capacity as much as possible. To this end, several techniques, including power control, have been applied to confine signal propagation within a limited area to decrease cross-interference. Unfortunately, this has the effect of also dramatically decreasing the number of BSs that

can be heard by an MS. As shown in Figure 7.1, an MS can normally receive only one pilot signal when it is near its serving BS and two to three pilot signals when it is at the edge of the serving cell.

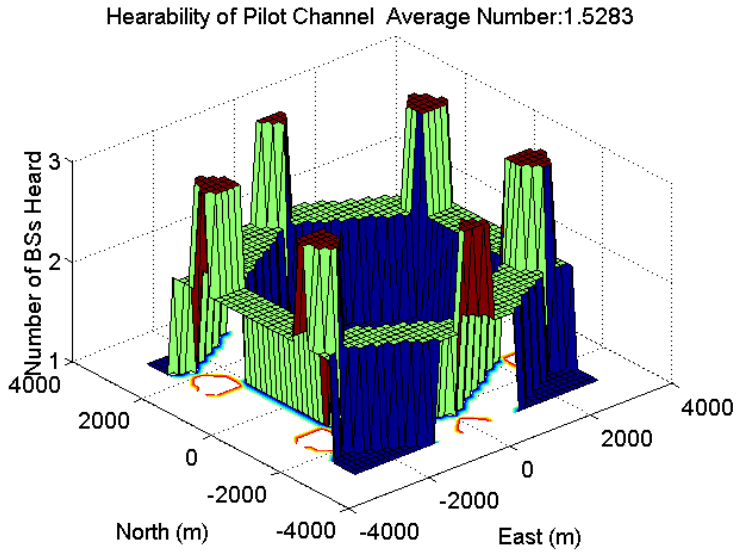

Figure 7.1: Hearability of a Normal Cellular Receiver

GPS Signals

GPS signals are transmitted through satellite communication channels. Compared to cellular network signals, a GPS signal has the following advantages for positioning purposes. Firstly, the C/A and P codes in a GPS signal are well-designed PRN codes. They can be accurately tracked by a GPS receiver with effective DLL and PLL techniques and provide metre-level positioning accuracy. Secondly, the GPS system uses satellite communication channels which are much more reliable than mobile radio channels. It is much easier for an outdoor GPS user to get LOS signals since an outdoor user normally has a clear view of the sky.

However, GPS signals also have some disadvantages. For example, GPS signals are very weak signals. The received power of a LOS GPS signal is about -130 to -125 dBm on the surface of the Earth. It is much weaker than surrounding noise and is also much weaker than cellular signals. Normally, the C/N_0 of an LOS GPS signal is about 40 to 45 dB-Hz. In a serious attenuation/fading environment, the signal power is further decreased. The C/N_0 of an incoming GPS signal inside a room may be at the level of 20 dB-Hz, which is substantially below the tracking threshold of a standard GPS receiver and, thus, cannot be tracked and used for location purposes (MacGougan et al 2002; Lachapelle et al 2003).

Some experiments have been done to demonstrate signal fading distributions in different environments (Ma et al, 2001). Figures 7.2 to 7.4 are histogram plots of fading distributions of GPS signals in open sky areas, urban canyon areas and indoor areas, respectively. The horizontal axis in these figures represents signal fading and the vertical axis represents the probability density. From experimental results, one can see that: in an open sky area, only small signal fading occurs to signals from low elevation satellites due to multipath propagation; quite a few satellites (7 - 12) can be seen in this case. In an urban canyon area, there exist two types of signals: clear signals and seriously faded signals (10 dB to 20 dB). A standard GPS receiver can see from one to three satellites in this type of situation, depending on satellite positions and surrounding object positions. Almost all GPS signals are seriously faded inside a room where a standard GPS receiver can potentially see one or two satellites or none at all.

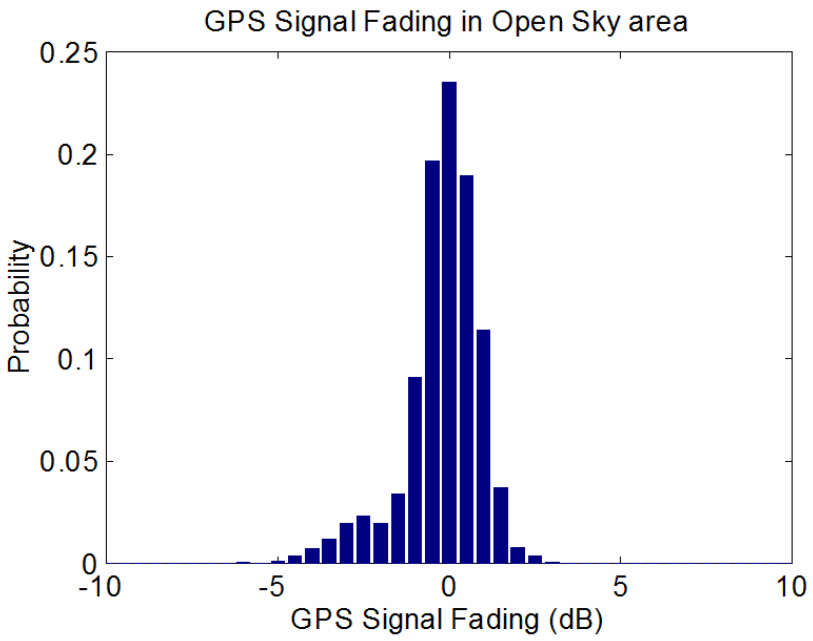

Figure 7.2: GPS Signal Fading Distribution in Open Sky Area

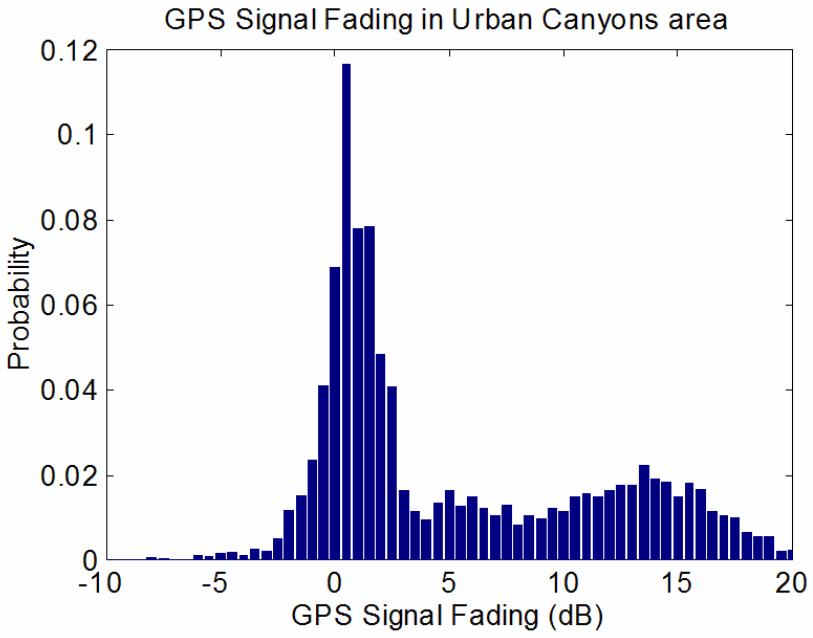

Figure 7.3: GPS Signal Fading Distribution in Urban Canyon Area

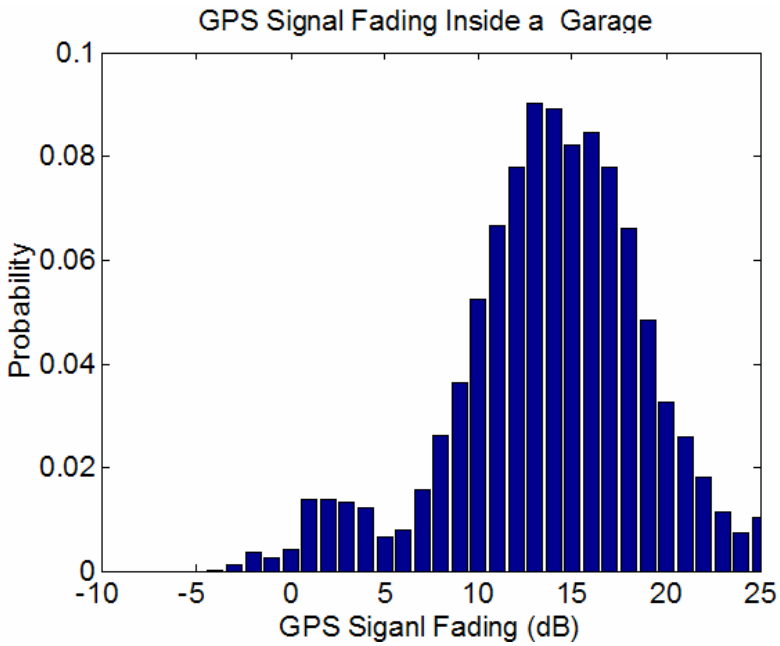

Figure 7.4: GPS Signal Fading Distribution inside a Garage

It is evident from the above discussion that both the cellular and GPS signals suffer from an availability problem and it is quite possible that location performance can be improved if both systems are used in concert. Three methods that can be used to combine GPS and cellular networks to improve positioning accuracy and positioning availability are discussed in the following sections.

7.3 Epoch-by-Epoch Integration of GPS and Cellular Network-Based Methods

As an example, an LS method is used here to combine GPS and network-based TDOA methods together to provide an epoch-by-epoch solution. The measurements of a cellular network are TDOAs, while the measurements used in GPS are pseudoranges. In the WGS84 system, GPS measurements can be expressed by

$$\rho_i = \sqrt{\left(x - x_i^S\right)^2 + \left(y - y_i^S\right)^2 + \left(z - z_i^S\right)^2} + c\Delta T \qquad i = 1 \cdots m \tag{7.1}$$

where ρ_i is the pseudorange of satellite i; $(x,y,z)^T$ is the MS position in the WGS84 system; $(x_i^S, y_i^S, z_i^S)^T$ is the position of satellite i in WGS84; c is the signal propagation speed; ΔT is the receiver clock error; and m is the number of satellites observed. In the WGS84 system, the network-based TDOA measurements are:

$$\Delta\rho_i = \sqrt{(x-x_i^B)^2+(y-y_i^B)^2+(z-z_i^B)^2} - \sqrt{(x-x_0^B)^2+(y-y_0^B)^2+(z-z_0^B)^2} \quad i = 1\cdots n \quad (7.2)$$

where $\Delta\rho_i$ is a TDOA measurement between BS_i and the reference base station BS_0; $(x,y,z)^T$ is the MS position in the WGS84 system; $(x_i^B, y_i^B, z_i^B)^T$ is the position of BS_i in the WGS84 system; and n is the number of TDOA measurements. Perfect time synchronization among BSs is assumed herein.

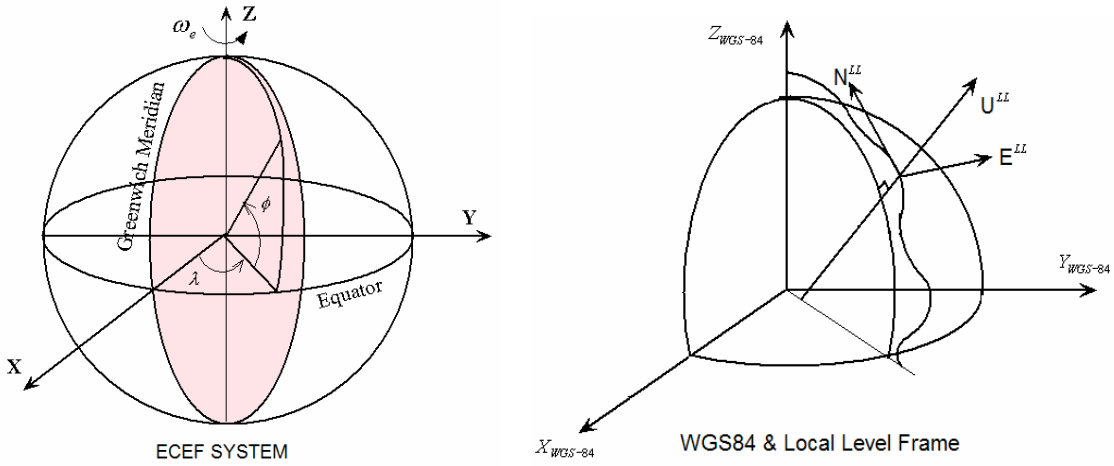

Figure 7.5: ECEF System, WGS84, and Local Level Frame

The above measurement equations are in the WGS84 system, which is an Earth-Centred, Earth Fixed (ECEF) coordinate system. This system is not suitable for wireless location since individual users are more interested in their position in a local system which can be expressed by horizontal and altitude information with respect to a reference point.

Therefore, a local level frame coordinate system, shown in Figure 7.5, is more suitable. The relation between the WGS84 system and the local level frame is as follows.

$$\begin{pmatrix} x \\ y \\ z \end{pmatrix}_{WGS84} = \begin{pmatrix} x_0 \\ y_0 \\ z_0 \end{pmatrix}_{WGS84} + \begin{pmatrix} -\sin\lambda & -\sin\phi\cos\lambda & \cos\phi\cos\lambda \\ \cos\lambda & -\sin\phi\sin\lambda & \cos\phi\sin\lambda \\ 0 & \cos\phi & \sin\phi \end{pmatrix} \begin{pmatrix} E \\ N \\ U \end{pmatrix}_{Local\ Leval\ Frame} \tag{7.3}$$

where $(x_0, y_0, z_0)^T_{WGS84}$ are the coordinates of the origin of the local level frame in the WGS84 system; $(x, y, z)^T_{WGS84}$ are the coordinates of the MS in the WGS84 system; $(E, N, U)^T_{LLF}$ are the coordinates of the MS in the local level frame; and (ϕ, λ) are the latitude and longitude of the origin of the local level frame in the WGS84 system.

After transforming the coordinates of the GPS satellites into the local level frame, GPS pseudorange measurements can be expressed as

$$\rho_i = \sqrt{(E - E_i^S)^2 + (N - N_i^S)^2 + (U - U_i^S)^2} + c\Delta T \qquad i = 1 \cdots m \tag{7.4}$$

where $(E_i^S \quad N_i^S \quad U_i^S)^T$ are the coordinates of satellite *i* in the local level frame. Similarly, TDOA measurements from the cellular network can be expressed as

$$\Delta\rho_i = \sqrt{(E - E_i^B)^2 + (N - N_i^B)^2 + (U - U_i^B)^2} - \sqrt{(E - E_0^B)^2 + (N - N_0^B)^2 + (U - U_0^B)^2} \qquad i = 1 \cdots n \tag{7.5}$$

where $(E_i^B, N_i^B, U_i^B)^T$ are the coordinates of BS *i* in the local level frame. Combining GPS and cellular network measurements, the following equations in component form are formed

$$\begin{bmatrix} \rho_1 \\ \vdots \\ \rho_m \\ \cdots \\ \Delta\rho_1 \\ \vdots \\ \Delta\rho_n \end{bmatrix} = \begin{bmatrix} \sqrt{\left(E-E_1^S\right)^2+\left(N-N_1^S\right)^2+\left(U-U_1^S\right)^2}+c\Delta T \\ \vdots \\ \sqrt{\left(E-E_m^S\right)^2+\left(N-N_m^S\right)^2+\left(U-U_m^S\right)^2}+c\Delta T \\ \cdots\cdots\cdots\

$$\mathbf{C}_l = \begin{bmatrix} \sigma^2_{GPS} & & & & \\ & \ddots & \vdots & \mathbf{0} & \\ & \cdots & \sigma^2_{GPS} & \vdots & \\ & \mathbf{0} & & \sigma^2_{TDOA}\begin{pmatrix} 1 & 0.5 & \cdots & 0.5 \\ 0.5 & 1 & \ddots & 0.5 \\ \vdots & \ddots & \ddots & \vdots \\ 0.5 & \cdots & 0.5 & 1 \end{pmatrix} \end{bmatrix}$$

Letting the DOP matrix be $\mathbf{Q}$,

$$\mathbf{Q} = \begin{bmatrix} q_{EE} & q_{EN} & q_{ET} \\ q_{NE} & q_{NN} & q_{NT} \\ q_{TE} & q_{TN} & q_{TT} \end{bmatrix} = \left(\mathbf{A}^{\mathrm{T}}\mathbf{A}\right)^{-1}$$

EDOP, NDOP, and HDOP can be calculated as

$$EDOP = \sqrt{q_{EE}} \tag{7.11}$$

$$NDOP = \sqrt{q_{NN}} \tag{7.12}$$

$$HDOP = \sqrt{q_{EE} + q_{NN}} \tag{7.13}$$

Simulation Results

Tests have been done to verify the performance improvement realized due to the integration of GPS and cellular networks. The test conducted here is an automobile kinematic test and was done in a suburban area near the University of Calgary. In the test, the GPS receiver used was a NovAtel OEM4 GPS sensor and the cellular network assumed was a 7-cell system with a cell radius of 2 km. The system layout is shown in Figure 7.6 where red triangles represent BSs and the heavy blue plot represents the

automobile trajectory calculated from GPS data. In the following simulations, the GPS data used is real GPS data whereas; the cellular network data used is simulated data. The simulated data was generated by first calculating the true value from the GPS-based benchmark and then corrupting the true value with measurement noise and NLOS errors.

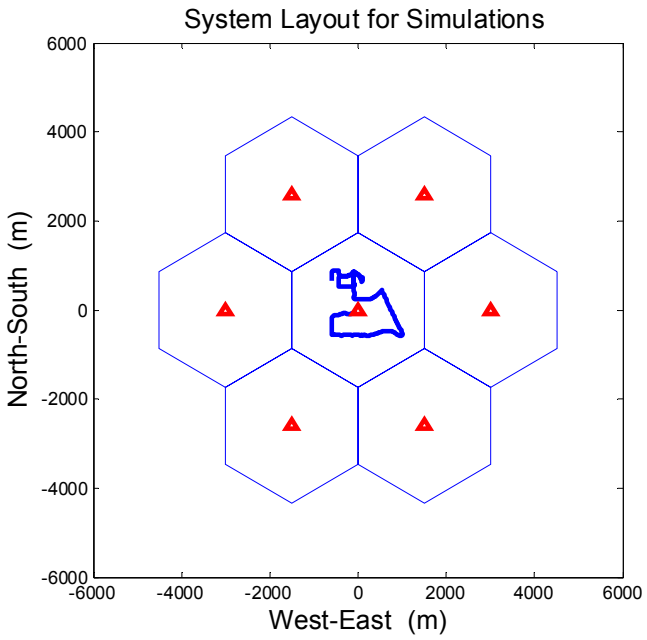

Figure 7.6: System Layout for Simulation

Figures 7.7 to 7.12 show the resultant trajectories and HDOPs for the different scenarios. These scenarios contain cellular network-only wireless location scenarios and cellular network plus GPS wireless location scenarios. The standard deviation of the GPS pseudorange measurements is assumed to be 10 metres, and the standard deviation of the cellular network TDOA measurements is assumed to be 100 metres. The benchmark trajectory and HDOP used in the performance comparisons are shown in Figure 7.7. The HDOP is normally below 2 except where there exists a serious blockage. Figure 7.8 is a cellular network-only case where only two TDOA measurements can be obtained. The

HDOP has a value of about 2, except at the initial stage where the MS is near the serving BS and, thus, results in poor HDOP. Figure 7.9 is another cellular network-only scenario where three TDOA measurements are used. Compared to the result in Figure 7.8, the HDOP at the starting stage decreases significantly. Obviously, this is because another BS is available to provide better geometry. Figures 7.10 to 7.12 depict the results when the TDOAs of a cellular network are combined with pseudoranges of the two highest GPS satellites. It attempts to simulate a densely constructed area where, most likely, only satellites at higher elevations can be seen directly. Figure 7.10 shows that, together with GPS, an MS can be correctly located even if only one TDOA measurement is available although the HDOP in this case is quite high. With a greater number of TDOA measurements available, higher positioning accuracy and lower HDOP can be achieved, as shown in Figures 7.11 and 7.12. Positioning errors in these scenarios are listed in Table 7.1. From the horizontal error columns, one can clearly see that the errors of the combined methods are much smaller than those of cellular network-only methods when the same numbers of TDOA measurements are used. For example, in the case of three TDOAs combined with two GPS satellites, the mean of positioning errors is 34 m and the RMS of the positioning errors is 44 m, which are both 23 m smaller than those of the three TDOAs-only case.

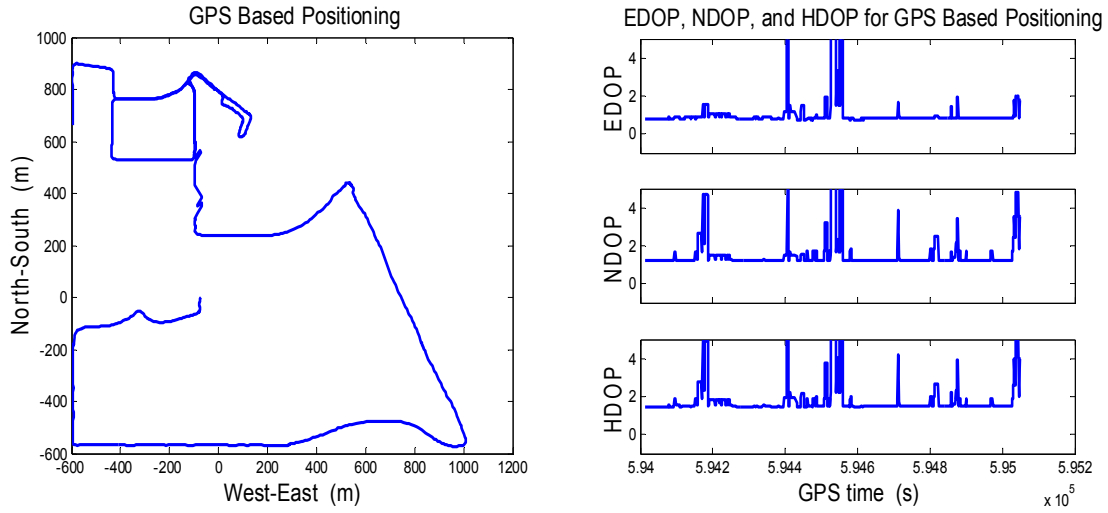

Figure 7.7: Benchmark Trajectory and Observed GPS DOPs for Epoch-by-Epoch Combination

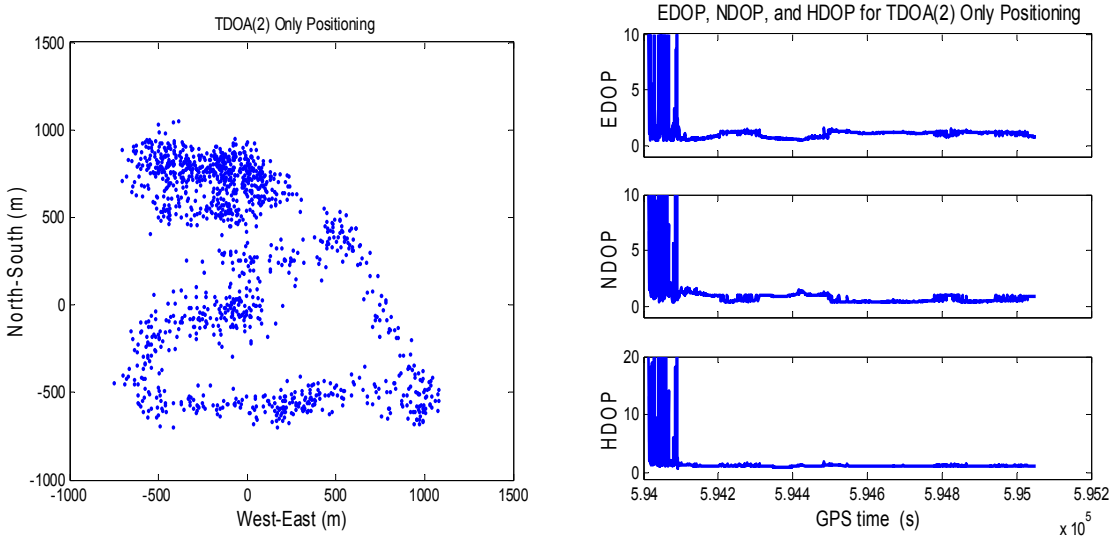

Figure 7.8: Trajectory and DOPs of Two TDOAs-Only Solution

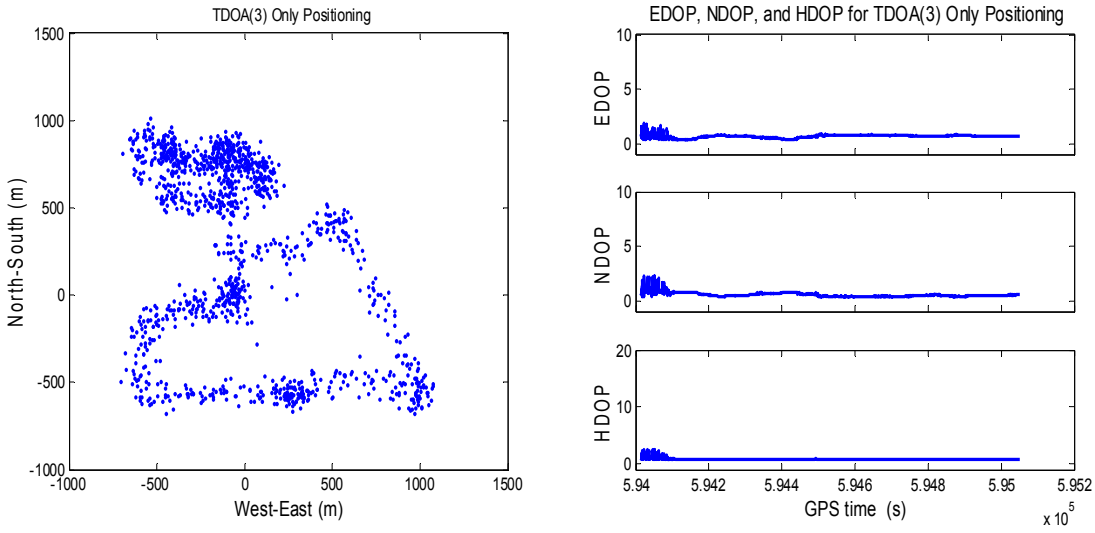

Figure 7.9: Trajectory and DOPs of Three TDOAs-Only Solution

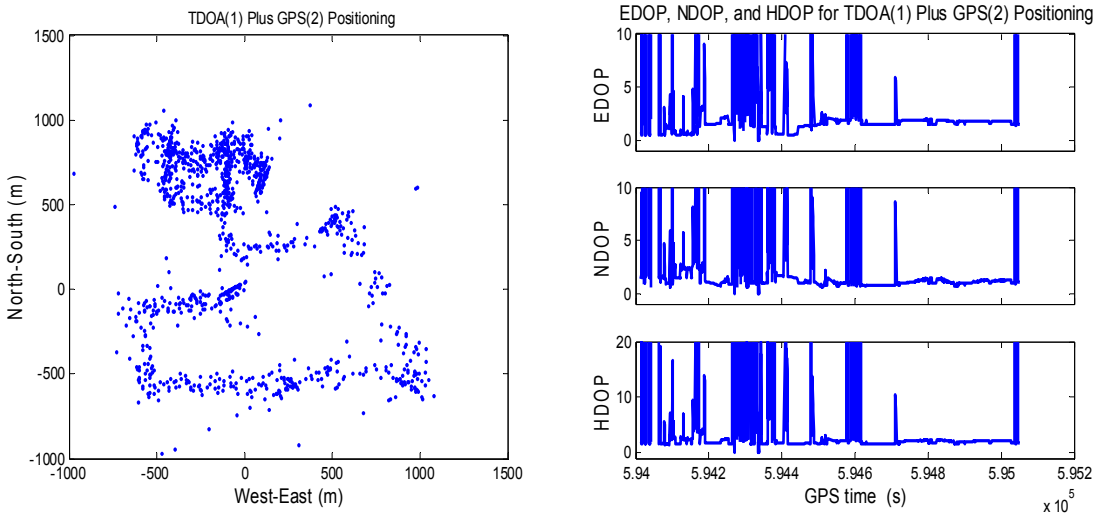

Figure 7.10: Trajectory and DOPs of One TDOA Plus Two GPS Satellites Solution

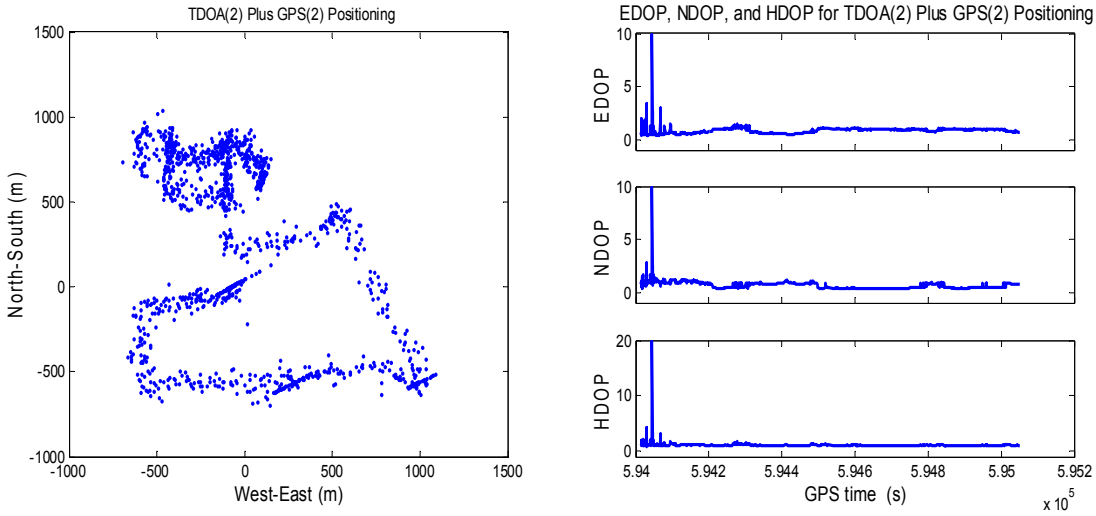

Figure 7.11: Trajectory and DOPs of Two TDOAs Plus Two GPS Satellites Solution

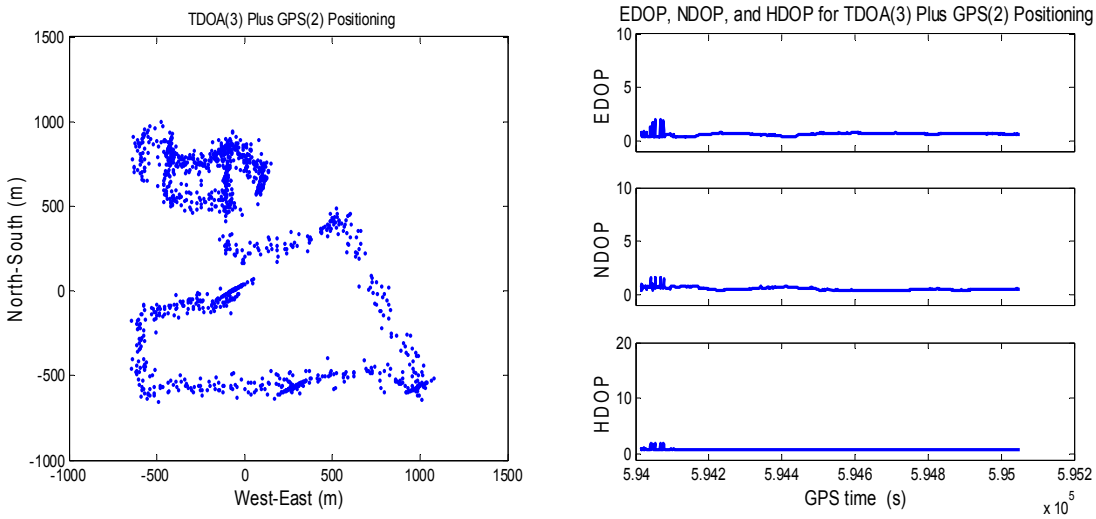

Figure 7.12: Trajectory and DOPs of Three TDOAs Plus Two GPS Satellites Solution

Table 7.1: Positioning Error of Epoch-by-Epoch LS Combination [m]

TDOA Num #	TDOAs Only						TDOAs Plus GPS(2)					
	East		North		Horizontal		East		North		Horizontal	
	Mean	RMS	Mean	RMS	Mean	RMS	Mean	RMS	Mean	RMS	Mean	RMS
1	N/A						1.4	56	-2.2	60	57	80
2	8.6	75	-6.3	58	79	95	0.1	37	-2.3	40	41	54
3	5.7	50	-2.5	45	57	67	0.7	27	-1.2	34	34	44

In the above table, the mean and RMS values of west-eastern, north-southern, and horizontal errors are calculated via the following formulas in the local level frame

$$\text{Mean}_E = \frac{1}{T}\sum_{i=1}^{T}\left(E_i - E_i^0\right), \tag{7.14}$$

$$\text{Mean}_N = \frac{1}{T}\sum_{i=1}^{T}\left(N_i - N_i^0\right), \tag{7.15}$$

$$\text{Mean}_H = \frac{1}{T}\sum_{i=1}^{T}\sqrt{\left(E_i - E_i^0\right)^2 + \left(N_i - N_i^0\right)^2}, \tag{7.16}$$

$$\text{RMS}_E = \sqrt{\frac{1}{T}\sum_{i=1}^{T}\left(E_i - E_i^0\right)^2}, \tag{7.17}$$

$$\text{RMS}_N = \sqrt{\frac{1}{T}\sum_{i=1}^{T}\left(N_i - N_i^0\right)^2}, \tag{7.18}$$

$$\text{RMS}_H = \sqrt{\frac{1}{T}\sum_{i=1}^{T}\left(\left(E_i - E_i^0\right)^2 + \left(N_i - N_i^0\right)^2\right)} \tag{7.19}$$

where T is the total number of position solutions, (E_i, N_i) is the position solution at epoch i, and (E_i^0, N_i^0) is the bench mark MS position at epoch i. These parameters are used in all of the sections of this chapter to evaluate position errors.

7.4 Kinematic Tracking of MSs Based on Kalman Filter Techniques

To improve location accuracy and to track kinematic MSs, Kalman filter-based methods are preferred. Kalman filter-based methods have at least the following advantages compared to epoch-by-epoch LS methods. First, the use of a Kalman filter is suitable for kinematic systems since system transition can be expressed via a dynamic model. Secondly, Kalman filtering makes use of not only current data but also all previous data, so it can obtain higher accuracy. Finally, a Kalman filter can operate based on a dynamic model, even if there are not enough measurements. This means that an MS can predict its position even when signals are totally or partially blocked. Kalman filtering is also an efficient method of integrating two or more different systems. For example, it is often used in GPS/INS integration (Salychev, 1998) and data fusion (Ostmann and Bell, 2001). In this section, a Kalman filtering technique is applied to combine GPS and the cellular network. As examples, two integration architectures, position-domain integration and measurement domain integration, shown in Figure 7.13, are fully discussed in the following section.

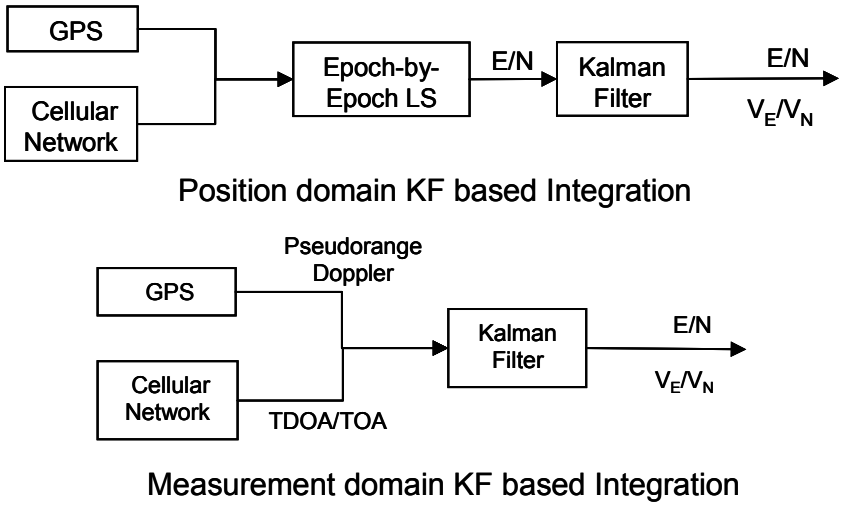

Figure 7.13: Architecture of GPS and Cellular Network Combination

7.4.1 Position Domain Kalman Filtering Technique

The method shown in Figure 7.13(a) is a combination of the epoch-by-epoch LS method and the position domain Kalman filtering technique. The positions calculated by means of the LS method act as only intermediate results. They are further smoothed by a Kalman filter to give better position and velocity estimations. A constant velocity model with random walk velocity disturbances is chosen here to describe the movement of an MS. The states selected are MS position and velocity, $[E, N, V_E, V_N]^T$, so the dynamic equation can be written in the following form:

$$\begin{bmatrix} \dot{E} \\ \dot{N} \\ \dot{V}_E \\ \dot{V}_N \end{bmatrix} = \begin{bmatrix} V_E \\ V_N \\ 0 \\ 0 \end{bmatrix} + \begin{bmatrix} 0 \\ 0 \\ \omega_E \\ \omega_N \end{bmatrix} = \begin{bmatrix} 0 & 0 & 1 & 0 \\ 0 & 0 & 0 & 1 \\ 0 & 0 & 0 & 0 \\ 0 & 0 & 0 & 0 \end{bmatrix} \begin{bmatrix} E \\ N \\ V_E \\ V_N \end{bmatrix} + \begin{bmatrix} 0 \\ 0 \\ \omega_E \\ \omega_N \end{bmatrix} \tag{7.20}$$

or

$$\dot{\mathbf{x}} = \mathbf{F}\mathbf{x} + \mathbf{w} \tag{7.21}$$

The observations are expressed as $[E^{LS}, N^{LS}]$, the output MS positions from an epoch-by-epoch LS estimator. The observation equation is, thus,

$$\begin{bmatrix} E^{LS} \\ N^{LS} \end{bmatrix} = \begin{bmatrix} 1 & 0 & 0 & 0 \\ 0 & 1 & 0 & 0 \end{bmatrix} \begin{bmatrix} E \\ N \\ V_E \\ V_N \end{bmatrix} + \begin{bmatrix} n_E \\ n_N \end{bmatrix} \tag{7.22}$$

or

$$\mathbf{z} = \mathbf{H}\mathbf{x} + \mathbf{v} \tag{7.23}$$

The system noise $\mathbf{w}$ and observation noise $\mathbf{v}$ are both white noise and are uncorrelated with each other. Furthermore, ω_E and ω_N are mutually uncorrelated, as are n_E and n_N.

The above model is a continuous model and needs to be discretized for calculation purposes because the data, in reality, are collected at discrete time instances. The discrete dynamic equation from time t_k to time t_{k+1} is of the following form (Gelb, 1974)

$$\mathbf{x}_{k+1} = \mathbf{\Phi}\mathbf{x}_k + \mathbf{w}_{k+1} \tag{7.24}$$

The transition matrix, $\mathbf{\Phi}$, can be calculated as

$$\mathbf{\Phi}(t_{k+1}, t_k) \approx \mathbf{I} + \mathbf{F}\Delta t = \begin{bmatrix} 1 & 0 & \Delta t & 0 \\ 0 & 1 & 0 & \Delta t \\ 0 & 0 & 1 & 0 \\ 0 & 0 & 0 & 1 \end{bmatrix} \tag{7.25}$$

where $\Delta t = t_{k+1} - t_k$, and the variance-covariance matrix of system noise, $\mathbf{w}_{k+1}$, can be calculated via

$$\begin{aligned} \mathbf{Q} &= \mathrm{E}\left[\mathbf{w}_k \mathbf{w}_k^T\right] \\ &= \mathrm{E}\left\{ \left[\int_{t_k}^{t_{k+1}} \mathbf{\Phi}(t_{k+1}, u) \begin{bmatrix} 0 \\ 0 \\ \omega_E \\ \omega_N \end{bmatrix} du \right] \left[\int_{t_k}^{t_{k+1}} \mathbf{\Phi}(t_{k+1}, v) \begin{bmatrix} 0 \\ 0 \\ \omega_E \\ \omega_N \end{bmatrix} dv \right]^T \right\} \\ &= \begin{bmatrix} \rho_E \Delta t^3/3 & 0 & \rho_E \Delta t^2/2 & 0 \\ 0 & \rho_N \Delta t^3/3 & 0 & \rho_N \Delta t^2/2 \\ \rho_E \Delta t^2/2 & 0 & \rho_E \Delta t & 0 \\ 0 & \rho_N \Delta t^2/2 & 0 & \rho_N \Delta t \end{bmatrix} \end{aligned} \tag{7.26}$$

where ρ_E and ρ_N are spectral densities of velocity disturbances in the west-east direction and in the north-south direction, respectively. In the following simulation, both of these quantities are assumed to be $2\, m/s^2$. The observation matrix is still

$$\mathbf{H} = \begin{bmatrix} 1 & 0 & 0 & 0 \\ 0 & 1 & 0 & 0 \end{bmatrix} \tag{7.27}$$

and the covariance matrix of observation noise is

$$\mathbf{R} = \begin{bmatrix} \sigma_E^2 & 0 \\ 0 & \sigma_N^2 \end{bmatrix} \tag{7.28}$$

σ_E^2 and σ_N^2 can be roughly selected based on the accuracy of the epoch-by-epoch LS method shown in Table 7.2.

Simulation Results

To evaluate algorithm performance, the MS position data obtained via an epoch-by-epoch LS method is further processed by this position domain MS tracking technique. The benchmark trajectory shown in Figure 7.14 is calculated by GPS measurements with high accuracy. The algorithm performance of cellular network-only scenarios is shown in Figure 7.15 where Figure 7.15(a) is the two TDOA measurement case and Figure 7.15(b) depicts the three TDOA measurement case. The blue dots are epoch-by-epoch LS solutions and the red lines are position domain Kalman filter-based MS tracking solutions. The performance of GPS plus cellular network scenarios are shown in Figure 7.16, where Figure 7.16(a) uses only 1 TDOA measurement together with the two highest GPS satellites and Figure 7.16(b) uses two TDOA measurements together with the two highest GPS satellites. Similarly, the blue dots are epoch-by-epoch LS solutions and the red lines are Kalman filter-based MS tracking solutions. The positioning errors compared to the benchmark trajectory are summarized in Table 7.2. Comparing the horizontal error columns in this table to those in Table 7.1, one can see that positioning errors reduce to about half of those obtained with the epoch-by-epoch LS method.

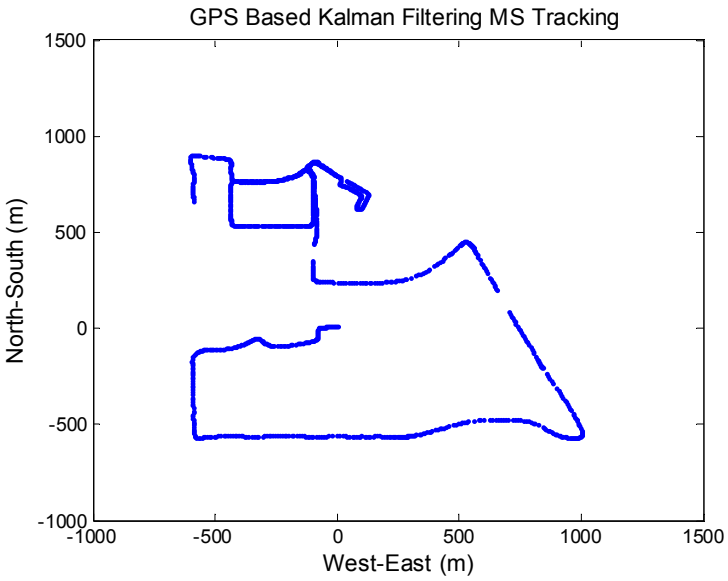

Figure 7.14: Benchmark Trajectory for Position Domain Kalman Filter-Based Combination

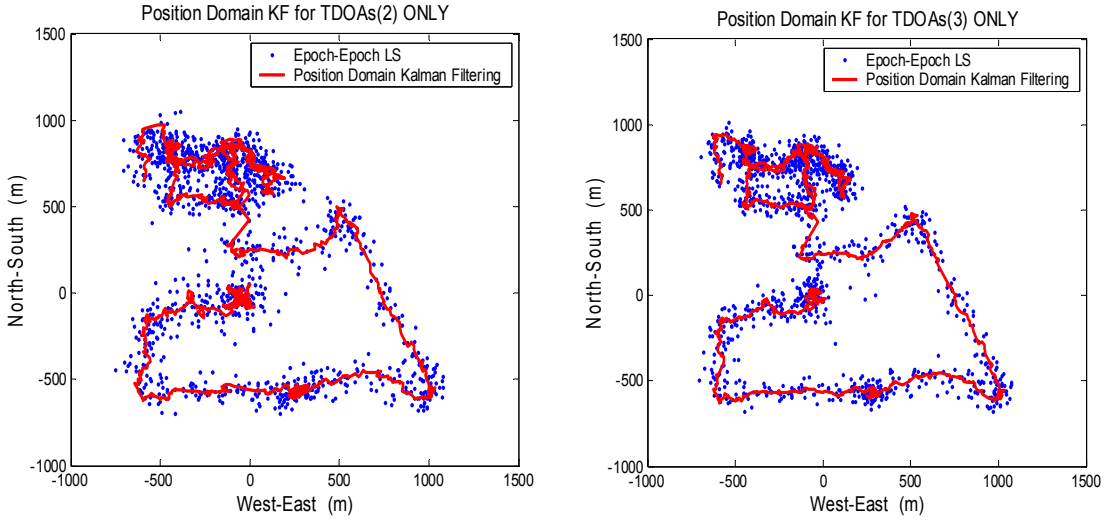

(a) (b)

Figure 7.15: Trajectories of Position Domain KF Based TDOA only Solution

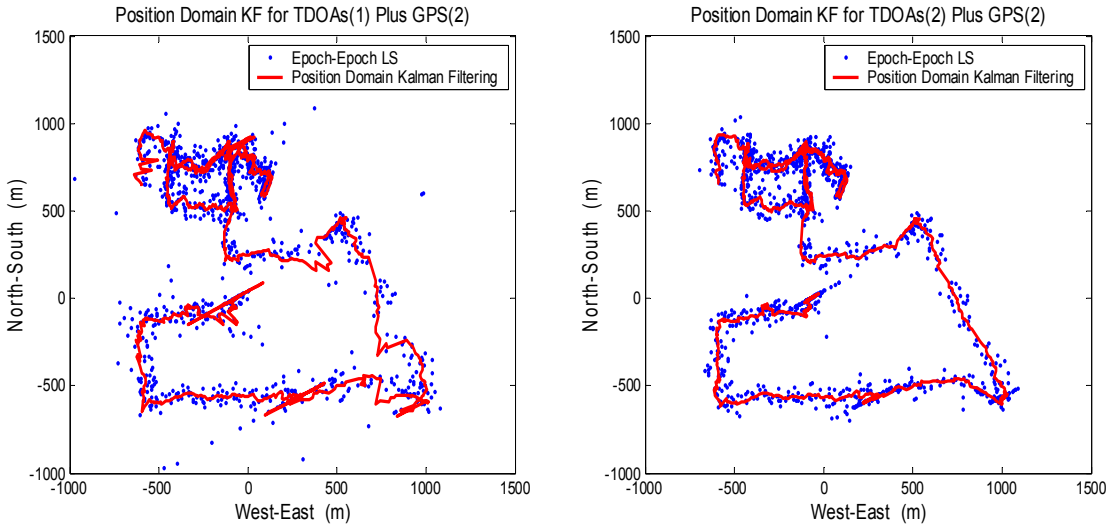

(a) (b)

Figure 7.16: Trajectories of Position Domain KF Based TDOAs and GPS Combination

Table 7.2: Positioning Error of Position Domain KF Based Combination [m]

TDOA Num #	TDOAs Only						TDOAs Plus GPS(2)					
	East		North		Horizontal		East		North		Horizontal	
	Mean	RMS	Mean	RMS	Mean	RMS	Mean	RMS	Mean	RMS	Mean	RMS
1	N/A						2.5	31	-1.6	29	30	42
2	5.4	28	-5.2	25	33	38	-0.8	16	-1.8	17	20	24
3	3.9	18	-1.2	21	24	28	0.5	13	-0.4	16	18	21

7.4.2 Measurement Domain Kalman Filtering Technique

Figure 7.13(b) is a tight integration of GPS and cellular network measurements where MS position and velocity are calculated directly from raw measurements by means of a Kalman filter. It is expected that such methods can produce better performance than that of a position domain MS tracking method. TOA measurements, instead of TDOA

measurements, are used in the following analysis, although they are equivalent from a mathematical point of view.

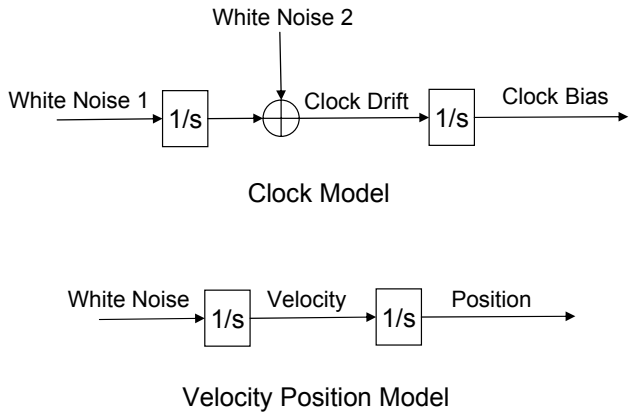

Figure 7.17: System Dynamic Model Used in the Measurement Domain Kalman Filter

If MS height information is assumed to be known via other methods, the states selected to describe the system consist of six elements: Eastern position and velocity, Northern position and velocity, and GPS receiver clock bias and drift. The model for MS position and velocity is assumed to be a constant velocity model with random walk disturbances. The model for clock bias and drift is assumed to be a constant drift model with a random walk disturbance, as shown in Figure 7.17. Therefore, the continuous dynamic equation is

$$\begin{bmatrix} \dot{E} \\ \dot{V}_E \\ \dot{N} \\ \dot{V}_N \\ \dot{b} \\ \dot{f} \end{bmatrix} = \begin{bmatrix} V_E \\ 0 \\ V_N \\ 0 \\ f \\ 0 \end{bmatrix} + \begin{bmatrix} 0 \\ \omega_E \\ 0 \\ \omega_N \\ \omega_b \\ \omega_f \end{bmatrix} = \begin{bmatrix} 0 & 1 & 0 & 0 & 0 & 0 \\ 0 & 0 & 0 & 0 & 0 & 0 \\ 0 & 0 & 0 & 1 & 0 & 0 \\ 0 & 0 & 0 & 0 & 0 & 0 \\ 0 & 0 & 0 & 0 & 0 & 1 \\ 0 & 0 & 0 & 0 & 0 & 0 \end{bmatrix} \begin{bmatrix} E \\ V_E \\ N \\ V_N \\ b \\ f \end{bmatrix} + \begin{bmatrix} 0 \\ \omega_E \\ 0 \\ \omega_N \\ \omega_b \\ \omega_f \end{bmatrix} \tag{7.29}$$

or, in matrix form,

$$\dot{\mathbf{x}} = \mathbf{F}\mathbf{x} + \mathbf{w} \, . \tag{7.30}$$

The observations consist of TOAs ρ_i^B from the cellular network; GPS pseudoranges, ρ_i^S; and GPS Doppler measurements, v_i^S, which are equivalent to pseudorange change rates. TOAs from the cellular network are

$$\rho_i^B = \sqrt{\left(E - E_i^B\right)^2 + \left(N - N_i^B\right)^2 + \left(U - U_i^B\right)^2} + n_i^B . \tag{7.31}$$

Pseudoranges from GPS satellites ρ_i^S are

$$\rho_i^S = \sqrt{\left(E - E_i^S\right)^2 + \left(N - N_i^S\right)^2 + \left(U - U_i^S\right)^2} + b + n_{\rho,i}^S . \tag{7.32}$$

Doppler measurements from GPS satellites, v_i^S, are

$$v_i^S = \frac{\left(V_E - V_{E,i}^S\right)\left(E - E_i^S\right) + \left(V_N - V_{N,i}^S\right)\left(N - N_i^S\right) + \left(V_U - V_{U,i}^S\right)\left(U - U_i^S\right)}{\sqrt{\left(E - E_i^S\right)^2 + \left(N - N_i^S\right)^2 + \left(U - U_i^S\right)^2}} + f + n_{v,i}^S . \tag{7.33}$$

In the above equations, $\begin{bmatrix} E & N & U \end{bmatrix}^T$ represents the MS position; $\begin{bmatrix} E_i^B & N_i^B & U_i^B \end{bmatrix}^T$ is the position of BS_i; $\begin{bmatrix} E_i^S & N_i^S & U_i^S \end{bmatrix}^T$ is the position of GPS satellite i; $\begin{bmatrix} V_E & V_N & V_U \end{bmatrix}^T$ is the velocity of the MS; $\begin{bmatrix} V_{E,i}^S & V_{N,i}^S & V_{U,i}^S \end{bmatrix}^T$ is the velocity of GPS satellite i; b and f are clock bias and drift, respectively; and n_i^B, $n_{\rho,i}^S$, and $n_{v,i}^S$ are measurement noise for TOA measurements, GPS satellite pseudorange measurements, and GPS satellite Doppler measurements, respectively.

Similarly, this continuous system model needs to be transformed to discrete form. The discrete dynamic equation can be written in matrix-vector form as

$$\mathbf{x}_{K+1} = \mathbf{\Phi}\mathbf{x}_k + \mathbf{w}_{k+1} \tag{7.34}$$

where $\mathbf{x} = \begin{bmatrix} E & V_E & N & V_N & b & f \end{bmatrix}^T$; and the transition matrix, $\mathbf{\Phi}$, is

$$\mathbf{\Phi}(t_{k+1}, t_k) \approx \mathbf{I} + \mathbf{F}\Delta t = \begin{bmatrix} 1 & \Delta t & 0 & 0 & 0 & 0 \\ 0 & 1 & 0 & 0 & 0 & 0 \\ 0 & 0 & 1 & \Delta t & 0 & 0 \\ 0 & 0 & 0 & 1 & 0 & 0 \\ 0 & 0 & 0 & 0 & 1 & \Delta t \\ 0 & 0 & 0 & 0 & 0 & 1 \end{bmatrix} \tag{7.35}$$

and $\Delta t = t_{k+1} - t_k$. The covariance matrix of the system noise $\mathbf{w}_{k+1}$ is

$$\begin{aligned} \mathbf{Q} &= \mathrm{E}\left[\mathbf{w}_k \mathbf{w}_k^T\right] \\ &= \mathrm{E}\left\{ \left[\int_{t_k}^{t_{k+1}} \mathbf{\Phi}(t_{k+1}, u) \begin{bmatrix} 0 \\ \omega_E \\ 0 \\ \omega_N \\ \omega_b \\ \omega_f \end{bmatrix} du \right] \left[\int_{t_k}^{t_{k+1}} \mathbf{\Phi}(t_{k+1}, v) \begin{bmatrix} 0 \\ \omega_E \\ 0 \\ \omega_N \\ \omega_b \\ \omega_f \end{bmatrix} dv \right]^T \right\} \\ &= \begin{bmatrix} S_E \Delta T^3/3 & S_E \Delta T^2/2 & 0 & 0 & 0 & 0 \\ S_E \Delta T^2/2 & S_E \Delta T & 0 & 0 & 0 & 0 \\ 0 & 0 & S_N \Delta T^3/3 & S_N \Delta T^2/2 & 0 & 0 \\ 0 & 0 & S_N \Delta T^2/2 & S_N \Delta T & 0 & 0 \\ 0 & 0 & 0 & 0 & S_b \Delta T + S_f \Delta T^3/3 & S_f \Delta T^2/2 \\ 0 & 0 & 0 & 0 & S_f \Delta T^2/2 & S_f \Delta T \end{bmatrix} \end{aligned} \tag{7.36}$$

where S_E, S_N, S_b, and S_f are spectral densities of the corresponding random walk disturbances. S_E and S_N are selected as $2\, m/s^2$ in simulation tests. S_b and S_f are clock type-dependent and can be calculated via the method shown in Brown and Hwang (1996). The measurement matrix, $\mathbf{H}$, can be derived as follows by means of the linearization of the non-linear measurement equations.

$$\mathbf{H} = \begin{bmatrix}
\frac{E_0 - E_1^B}{\rho_{0,1}^S} & 0 & \frac{N_0 - N_1^B}{\rho_{0,1}^S} & 0 & 0 & 0 \\
\vdots & \vdots & \vdots & \vdots & \vdots & \vdots \\
\frac{E_0 - E_m^B}{\rho_{0,m}^S} & 0 & \frac{N_0 - N_m^B}{\rho_{0,m}^S} & 0 & 0 & 0 \\
\cdots & \cdots & \cdots & \cdots & \cdots & \cdots \\
\frac{E_0 - E_1^S}{\rho_{0,1}^S} & 0 & \frac{N_0 - N_1^S}{\rho_{0,1}^S} & 0 & 1 & 0 \\
\vdots & \vdots & \vdots & \vdots & \vdots & \vdots \\
\frac{E_0 - E_n^S}{\rho_{0,n}^S} & 0 & \frac{N_0 - N_n^S}{\rho_{0,n}^S} & 0 & 1 & 0 \\
\cdots & \cdots & \cdots & \cdots & \cdots & \cdots \\
\left(V_E - V_{E,1}^S\right)\left(\frac{\left(N_0 - N_1^S\right)^2 + \left(U_0 - U_1^S\right)^2}{\left(\rho_{0,1}^S\right)^3}\right) & \frac{E_0 - E_1^S}{\rho_{0,1}^S} & \left(V_N - V_{N,1}^S\right)\left(\frac{\left(E_0 - E_1^S\right)^2 + \left(U_0 - U_1^S\right)^2}{\left(\rho_{0,1}^S\right)^3}\right) & \frac{N_0 - N_1^S}{\rho_{0,1}^S} & 0 & 1 \\
\vdots & \vdots & \vdots & \vdots & \vdots & \vdots \\
\left(V_E - V_{E,n}^S\right)\left(\frac{\left(N_0 - N_n^S\right)^2 + \left(U_0 - U_n^S\right)^2}{\left(\rho_{0,n}^S\right)^3}\right) & \frac{E_0 - E_n^S}{\rho_{0,n}^S} & \left(V_N - V_{N,n}^S\right)\left(\frac{\left(E_0 - E_n^S\right)^2 + \left(U_0 - U_n^S\right)^2}{\left(\rho_{0,n}^S\right)^3}\right) & \frac{N_0 - N_n^S}{\rho_{0,n}^S} & 0 & 1
\end{bmatrix} \tag{7.37}$$

where

$$\rho_{0,i}^B = \sqrt{\left(E_0 - E_i^B\right)^2 + \left(N_0 - N_i^B\right)^2 + \left(U_0 - U_i^B\right)^2}$$

and

$$\rho_{0,i}^S = \sqrt{\left(E_0 - E_i^S\right)^2 + \left(N_0 - N_i^S\right)^2 + \left(U_0 - U_i^S\right)^2} \ .$$

The covariance matrix of measurement noise is

$$\mathbf{R} = \begin{bmatrix}
\sigma_{TOA}^2 & & & & & & & & & \\
& \ddots & & & & & & & & \\
& & \sigma_{TOA}^2 & & & & & & & \\
& & & \sigma_{pseudorange}^2 & & & & & & \\
& & & & \ddots & & & & & \\
& & & & & \sigma_{pseudorange}^2 & & & & \\
& & & & & & \sigma_{doppler}^2 & & & \\
& & & & & & & \ddots & & \\
& & & & & & & & \sigma_{doppler}^2
\end{bmatrix}. \tag{7.38}$$

An extended Kalman filter technique can then be applied to the above kinematic system. The performance is discussed via the following simulation tests.

Simulation Results

The same set of raw data is used in the following simulations as that used in the epoch-by-epoch LS method and position domain tracking method. Figure 7.18 gives the estimated trajectories when only TOA measurements from the cellular network are used. In Figure 7.19 are the estimated trajectories when both TOA measurements from the cellular network and pseudoranges are used, along with Doppler measurements from GPS satellites.

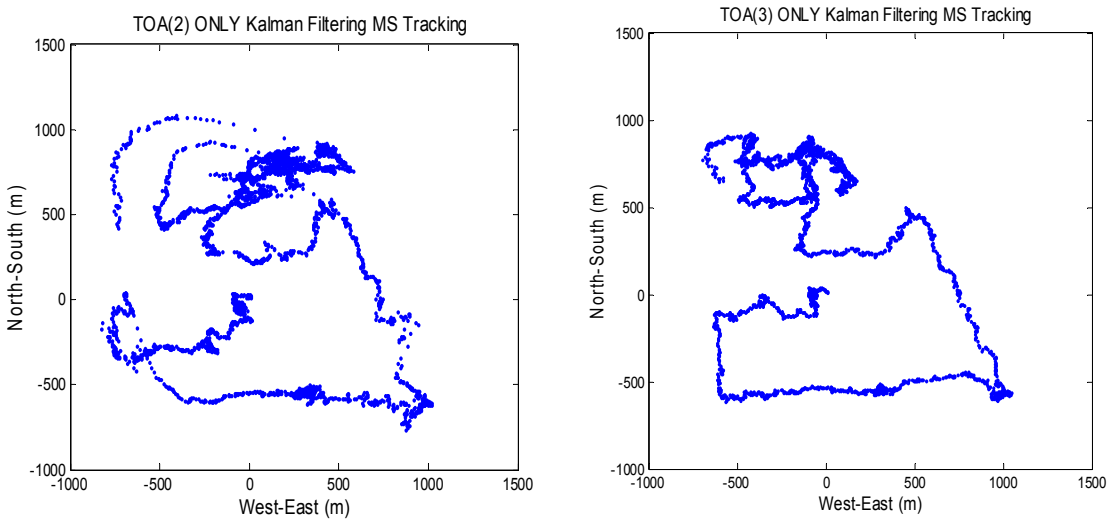

Figure 7.18: Estimated Trajectories by TOA only Measurement Domain Kalman Filter

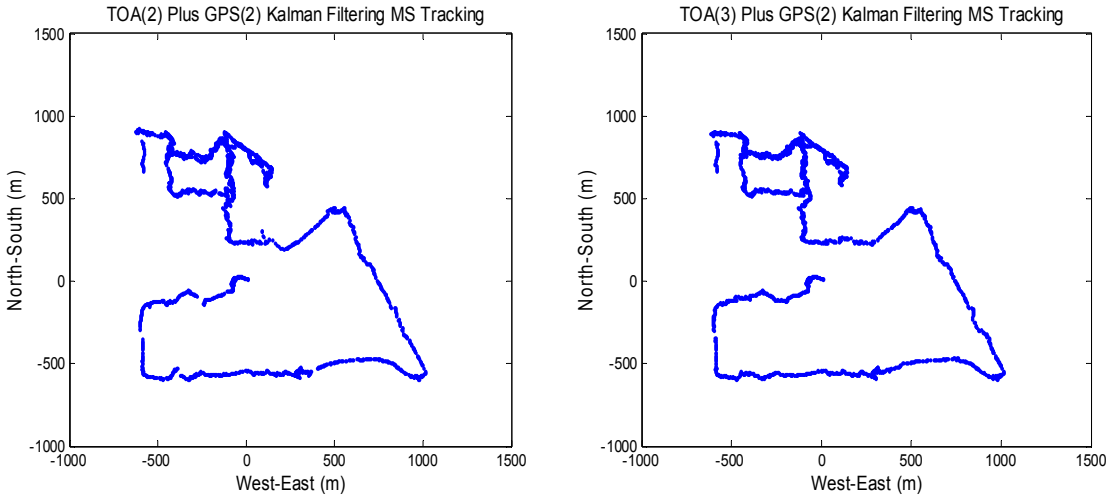

Figure 7.19: Estimated Trajectories by TOA/ GPS Measurement Domain Kalman Filter

Table 7.3 summarizes the positioning errors of this measurement domain MS tracking method in different scenarios. The benchmark is also the trajectory derived from unblocked GPS measurements. To simplify performance comparisons, the horizontal errors in Tables 7.1 to 7.3 are further rearranged in Table 7.4. In this table, the scenarios in each row employ the same number of BSs. Positioning errors of the three integration methods discussed above are listed from left to right. It is obvious that positioning accuracy is improved considerably, in increasing degrees, by all three methods; that is, the third-best performance is obtained by use of the epoch-by-epoch LS method; slightly better performance from the position domain MS tracking method, and the best performance being produced by the measurement domain MS tracking method. For example, when 4 BSs and two GPS satellites are used, the mean of the horizontal errors decreases from 34 m via the epoch-by-epoch LS method; to 18 m via the position domain MS tracking method; and to 12 m via the measurement domain MS tracking method. The

RMS decreases from 44 m, to 21 m, and to 15 m. One can also see the performance improvement due to the combination of GPS with the cellular network. With only 4 BSs available, the mean of positioning errors is 57 m for the epoch-by-epoch LS method; 24 m for position domain MS tracking method; and 22 m for the measurement domain MS tracking method. Understandably, these errors are larger than 34 m, 18 m, and 12 m when these 4 BSs are combined with two GPS satellites.

Table 7.3: Positioning Error of Measurement Domain KF Based Combination [m]

TOA Num #	TOAs Only						TOAs Plus GPS(2)					
	East		North		Horizontal		East		North		Horizontal	
	Mean	RMS	Mean	RMS	Mean	RMS	Mean	RMS	Mean	RMS	Mean	RMS
1	N/A						0.5	15	0.9	20	20	25
2	27	140	-0.1	102	121	175	1.2	12	-0.9	15	15	19
3	0.9	24	3.7	20	27	32	1.1	11	0.3	13	14	17
4	0.1	19	2.7	17	22	25	0.1	9	0.5	11	12	15
5	-0.3	17	2.0	15	21	23	-0.1	9	0.5	10	11	14

Table 7.4: Horizontal Positioning Error Comparison

Scenarios	Positioning Error	Epoch-Epoch LS Method	P-Domain KF Tracking	M-Domain KF Tracking
1 TDOA/ 2 TOA	Mean (m)	N/A	N/A	121
	RMS (m)	N/A	N/A	175
2 TDOA/3 TOA	Mean (m)	79	33	27
	RMS (m)	95	38	32
3 TDOA/4 TOA	**Mean (m)**	**57**	**24**	**22**
	RMS (m)	**67**	**28**	**25**
1 TOA and 2 GPS	Mean (m)	N/A	N/A	20
	RMS (m)	N/A	N/A	25
1 TDOA/ 2 TOA and 2 GPS	Mean (m)	57	30	15
	RMS (m)	80	42	19
2 TDOA/3 TOA and 2 GPS	Mean (m)	41	20	14
	RMS (m)	54	24	17
3 TDOA/4 TOA and 2 GPS	**Mean (m)**	**34**	**18**	**12**
	RMS (m)	**44**	**21**	**15**

7.5 NLOS Error Mitigation in GPS and Cellular Network Integration

TOA/TDOA measurements in the previous simulation tests are assumed to be NLOS error- free. However, NLOS errors always exist in reality and will result in a degraded positioning performance. The values of the positioning errors in Table 7.5 and the trajectories in Figure 7.20 demonstrate the performance difference between the NLOS-free case and the NLOS-corrupted case. In the simulation, receiver noise is assumed to be zero mean Gaussian distributed with a standard deviation of 10 m. NLOS errors are assumed to be of urban exponential distribution as discussed in Chapter 4 and applied to

all TOA measurements. To check the performance degradation due to receiver noise and NLOS errors, six scenarios are simulated. They are:

- *The receiver noise-only case for TOA-only system*
- *The NLOS error-only case for TOA-only system*
- *The receiver noise plus NLOS error case for the TOA-only system*
- *The receiver noise-only case for TOA plus GPS system*
- *The NLOS error-only case for TOA plus GPS system*
- *The receiver noise plus NLOS error case for the TOA plus GPS system*

Seven BSs and the two GPS satellites with the highest elevation angles are used in the GPS and TOA integration scenarios. A measurement domain Kalman filter-based integration scheme is used.

Table 7.5: Performance Degradation Due to NLOS Errors and Receiver Noise

Measurement Errors	TOAs (7) Only						TOAs (7) Plus GPS(2)					
	East		North		Horizontal		East		North		Horizontal	
	Mean (m)	RMS (m)	Mean (m)	RMS (m)	Mean (m)	RMS (m)	Mean (m)	RMS (m)	Mean (m)	RMS (m)	Mean (m)	RMS (m)
NLOS Only	-2.0	41.9	0.7	40.4	50.2	58.2	-1.7	32.0	-0.4	35.2	40.9	47.5
Receiver Noise Only	-0.9	7.4	0.1	4.5	5.7	8.6	-1.1	6.8	-0.1	4.1	5.0	7.9
NLOS and Receiver Noise	-2.4	42.0	0.8	40.4	50.2	58.4	-1.8	32.0	-0.2	35.3	41.0	47.6

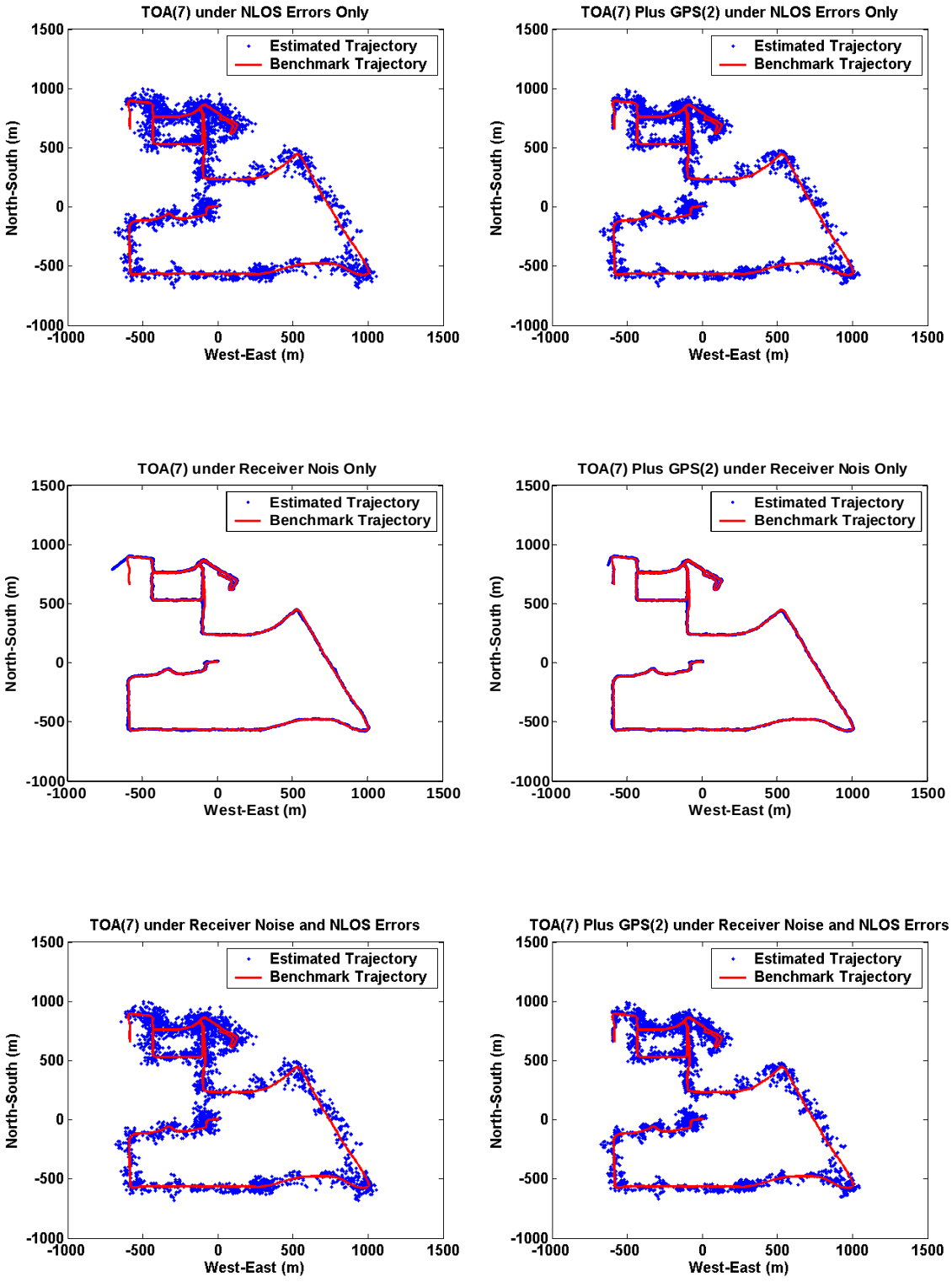

Figure 7.20: Performance Degradation Due to NLOS Errors and Receiver Noise

From the test results, the following conclusions may be drawn:

- Positioning accuracy is quite high (with a RMS of a few metres) in the receiver noise-only case. This is especially true for those receivers that manage to minimize the effects of noise, which can be achieved by utilizing advanced signal tracking techniques.
- Positioning accuracy is low (with a RMS of tens of metres) in the NLOS error-only case.
- Positioning accuracy is low (with a RMS of tens of metres) in the case where both receiver noise and NLOS error exist.
- Position accuracies for the latter two cases are almost the same. This means that performance degradation results mainly from NLOS errors.
- NLOS errors need to be removed first before the affiliated TOA/TDOA measurements can be applied to the MS location calculation.

The NLOS error mitigation method proposed in Chapter 5 is applied in the following to show the performance improvement due to NLOS error mitigation. In a GPS/cellular network integration system, NLOS error mitigation can be realized in two different ways:

- *The intersection distribution function-based solution*. Based on an intersection distribution function calculated from TOA/TDOA measurements, the intermediate MS location is obtained and cost functions for each BS are constructed. Then, hypothesis tests are conducted to identify and remove NLOS errors. The key in this solution is how to get an intermediate estimate of MS location with high

accuracy because an inaccurate MS location estimation can make effective NLOS error mitigation almost impossible.

- *The GPS-assisted solution*. In this solution, the intermediate MS location estimation used in cost function construction comes from a reference trajectory instead of from an intersection distribution function. This is suitable for cases where an accurate MS location estimate can be obtained from other methods, such as GPS when enough satellites are available. With the accurate intermediate MS location estimate, NLOS errors can be more reliably identified and removed, and then more accurate TOA measurements can be used to obtain a better MS location estimate.

Simulation results in Table 7.6 and Figure 7.21 demonstrate the performance improvement resulting from the above two NLOS mitigation methods. In the simulation, receiver noise is assumed to be zero mean Gaussian distributed noise with a standard deviation of 10 metres. NLOS errors are assumed to be of urban exponential distribution as discussed in Chapter 4. Six scenarios are simulated:

- *The no NLOS error mitigation case for TOA-only system*
- *The Distribution function (DF)-based NLOS error mitigation case for TOA-only system*
- *The GPS-assisted NLOS error mitigation case for TOA-only system*
- *The no NLOS error mitigation case for TOA plus GPS system*

- *The Distribution function (DF)-based NLOS error mitigation case for TOA plus GPS system*
- *The GPS-assisted NLOS error mitigation case for TOA plus GPS system*

Similarly, seven BSs and the two GPS satellites with highest elevation angles are used in GPS/TOA integration scenarios and the measurement domain Kalman filter-based integration scheme is used.

Table 7.6: Performance Improvement Due to NLOS Error Mitigation

NLOS Errors Processing	TOAs (7) Only						TOAs (7) Plus GPS(2)					
	East		North		Horizontal		East		North		Horizontal	
	Mean (m)	RMS (m)	Mean (m)	RMS (m)	Mean (m)	RMS (m)	Mean (m)	RMS (m)	Mean (m)	RMS (m)	Mean (m)	RMS (m)
No NLOS Mitigation	-0.9	58.5	17.1	62.9	76.9	85.9	4.8	42.2	-17.2	45.2	54.1	61.8
DF Based NLOS Mitigation	2.1	29.6	0.7	28.4	35.7	41.0	3.8	26.8	-6.6	28.4	34.0	38.9
GPS Assisted NLOS Mitigation	-1.9	9.4	2.7	8.9	10.3	13.0	-1.4	7.9	-1.5	5.5	6.2	9.6

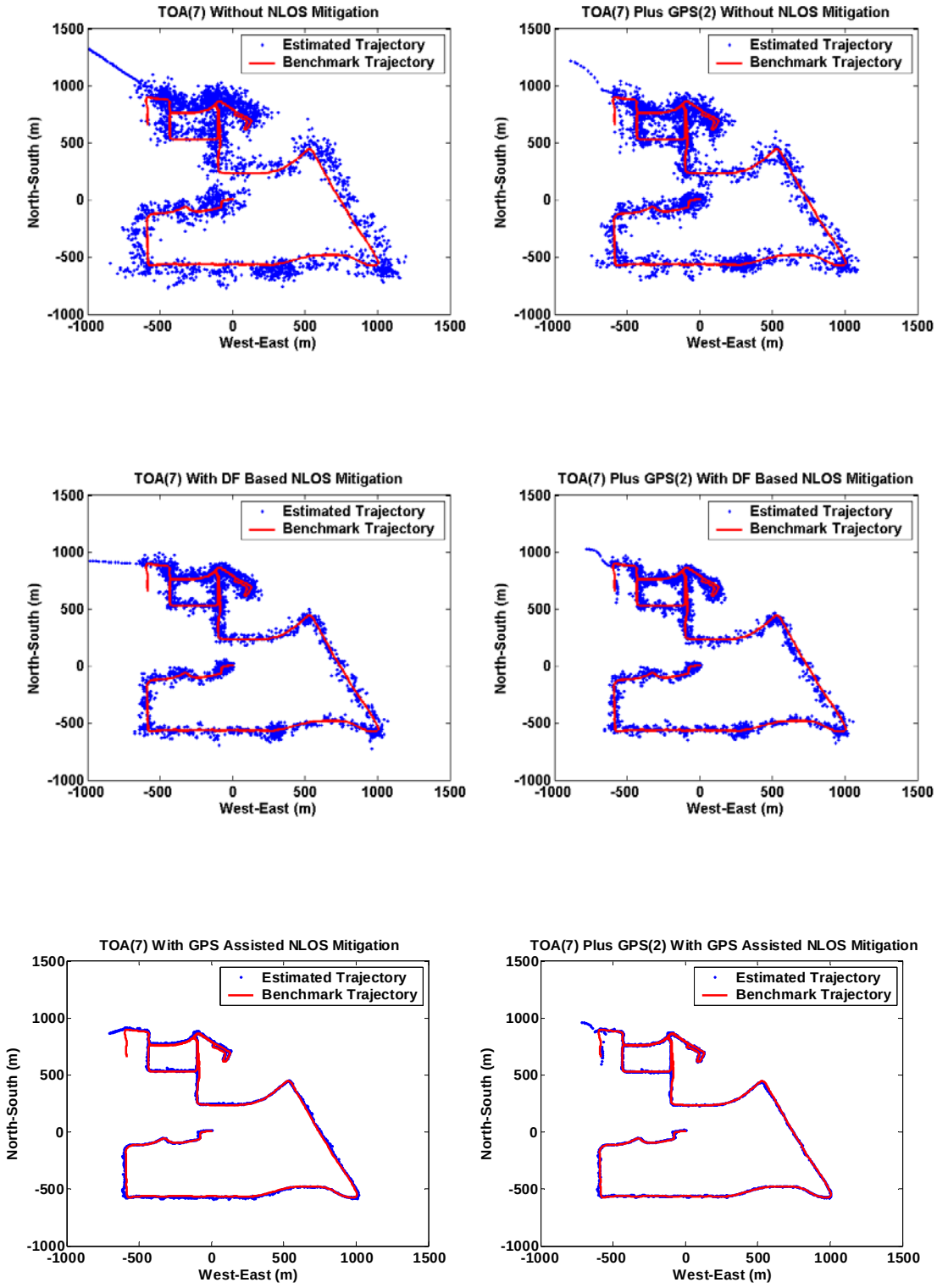

Figure 7.21: Performance Improvement Due to NLOS Error Mitigation

From the simulation results, one can find that

- Positioning accuracy is poor if the NLOS errors are not removed from TOA/TDOA measurements since NLOS errors are the dominant error sources and can reach several hundred metres.
- DF-based NLOS error mitigation can significantly improve positioning accuracy. The horizontal positioning error for both the TOA-only and TOA plus GPS decreases from around 70 metres for the case of no LOS error mitigation, to around 40 metres for the DF-based NLOS error mitigation case.
- The GPS assisted NLOS error mitigation solution produces the best performance. The RMS of the final horizontal location error is in the range of only 7-15 metres.

The reason why the GPS-assisted NLOS error mitigation method is of superior performance is straightforward. In the DF-based NLOS error mitigation solution, the intermediate MS location derives exclusively from TOA measurements. The accuracy is low because large errors exist in TOA measurements. On the contrary, a very accurate MS location estimation can be obtained from GPS when the GPS receiver embedded in a MS to be located can see enough satellites. Taking it as the required intermediate MS location estimation, the proposed NLOS error mitigation algorithm can effectively identify and remove NLOS errors. Therefore, the positioning accuracy is much higher.

If the Kalman filter-based MS tracking method is used, the MS position predicted by the filter can be taken as the intermediate MS location used for NLOS error mitigation. This is especially useful when GPS is not available to provide an accurate MS position due to signal blockage. Thus, the GPS-assisted NLOS error mitigation method actually consists of two states: One is in the period when the GPS system itself can calculate the MS position. In this state, NLOS errors can be mitigated by means of a GPS-derived MS location. The other one is in GPS outage periods. In this state, NLOS errors are mitigated by means of a KF-derived MS location. Of course, such outage periods cannot be too long otherwise the predicted MS location will drift and the NLOS errors cannot be correctly removed.

Table 7.7 and Figure 7.22 show the positioning accuracy when the GPS outage periods are 5 seconds and 10 seconds, respectively. The data rate of the TOA measurements is 5 Hz. Seven BSs and the two GPS satellites with the highest elevation angles are used in the GPS/TOA integration. It is obvious that the GPS-assisted NLOS error mitigation method can still have high positioning accuracy when the outage length is relatively short. However, when the period of outage is long, the MS position predicted by the Kalman filter quickly deviates from its true value and, thus, results in poor NLOS mitigation capability and poor positioning accuracy.

Table 7.7: Performance of GPS Assisted NLOS Error Mitigation

Outage Interval	TOAs (7) Plus GPS(2)					
	East		North		Horizontal	
	Mean (m)	RMS (m)	Mean (m)	RMS (m)	Mean (m)	RMS (m)
5 seconds	-1.5	14.3	-1.1	20.6	18.4	25.1
10 seconds	-0.8	30.1	-1.4	47.0	40.9	55.8

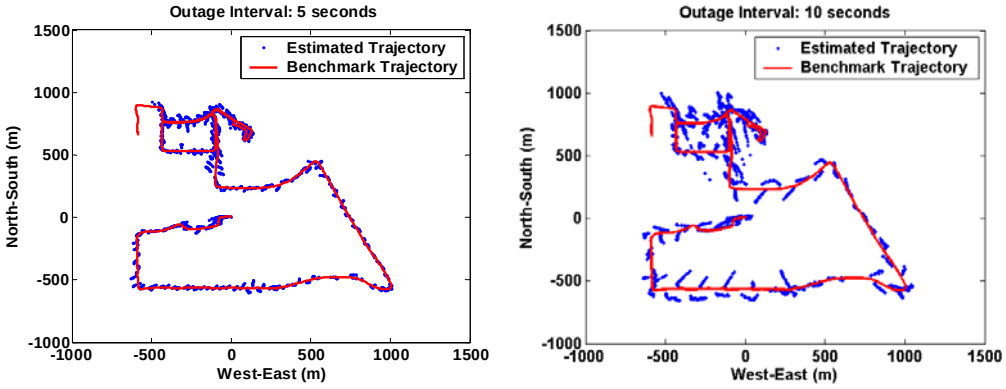

Figure 7.22: Performance of GPS-Assisted NLOS Error Mitigation

7.6 Conclusions

Neither cellular network-only nor GPS-only solutions work in serious fading environments since both systems suffer from signal availability issues. However, the combination of the two may work because more information can be used and better geometry can be obtained. Three schemes are proposed in this chapter to combine a cellular network and GPS.

The epoch-by-epoch LS scheme combines measurements from a cellular network and measurements from GPS via a standard LS formula. Compared to network-only solutions, it can improve both location availability and positioning accuracy since more data elements is involved in the calculation.

Kalman filter-based methods can further improve performance since the movement of the MS is described by a dynamic model and both current information and past information are utilized. While the position domain Kalman filter method processes the output of an epoch-by-epoch LS solution to obtain better MS location estimation, the measurement domain Kalman filter method uses the measurements from the cellular network and GPS system directly. Demonstrated by experimental results, the measurement domain method produces higher positioning accuracy. The RMS value of horizontal location errors can be less than 10 – 20 m, which is within E-911 accuracy requirements.

CHAPTER 8

CONCLUSIONS AND FUTURE WORK

8.1 Conclusions

The primary objective of this thesis was to seek a ground-based wireless location scheme suitable for mobile positioning in cellular phone networks. To this end, several techniques were proposed to handle issues that may occur in a cellular network and which may degrade wireless location performance. These issues include the lack of signal availability or hearability due to co-channel interference, the inefficiency in mobile location calculation, and the large NLOS errors in observations resulting from multipath propagation. With the IS-95 CDMA pilot signal as an example, signal availability/hearability was thoroughly analyzed. The results showed that the hearability is poor for location purposes. To improve signal hearability, two methods, the enhanced signal processing method and the idle period down link (IPDL) method, were introduced. In poor signal hearability environments, another acceptable solution is combining cellular network-based methods with other positioning methods. The integration of GPS and a cellular network was proposed as an example. Location performance that could be obtained with an epoch-by-epoch LS-based integration scheme and a Kalman filter-based integration scheme were discussed.

MS positions are normally obtained by solving non-linear equations. This entails a high computational burden and may suffer from convergence problems. To solve these issues, an enhanced two-step least squares solution was proposed for use with a hybrid TDOA/AOA wireless location algorithm. This method can provide almost the same level of accuracy as that of a normal Taylor-series-based solution while maintaining low computational burden.

NLOS errors within TOA, TDOA, and AOA measurements are very large, compared to errors due to receiver noise. Therefore, NLOS errors should first be removed before applying the measurements to wireless location algorithms. Two NLOS error mitigation methods were proposed and discussed. One is a distribution function-based method. The mitigation of NLOS error depends on system redundancy and a high clear intersection density. The other is a channel estimation-based method in which the mitigation of NLOS error is obtained by making use of only the earliest signal from among all multipath replicas.

Based on mathematical analysis and simulation results in previous chapters, the following detailed conclusions can be drawn for each of the proposed algorithms.

Signal Hearability

The capability of a receiver to receive desired signals is called signal hearability in this thesis. It depends on the Signal to Interference Ratios (SIR) of incoming signals and receiver sensitivity. For a normal cellular network, the hearability is poor from the point

of view of a wireless location application because a network tries to minimize signal power to increase system capacity. Actually, a MS can hear only one BS in most areas of a cell, while the minimum number required for MS location is three.

An enhanced signal processing technique was proposed to improve the hearability, since the receiver sensitivity can be increased by integrating a message-free signal - such as the pilot signal - for a longer time. However, the integration time cannot be extended for too long owing to two constraints. The first is the efficient integration time requirement. If the integration time exceeds this value, the increase of receiver sensitivity becomes insensitive to the increase in integration time. The second constraint is the frequency error between the incoming carrier and the locally generated carrier. If a frequency error exists, the receiver sensitivity begins to degrade after integrating for a certain length of time. In fact, this maximum integration time decreases with the magnitude of the frequency error. Taking these constraints into consideration, the maximum integration time for an IS-95 CDMA pilot signal is 1500 chips with a frequency error less than 160 Hz, or 650 chips with a frequency error less than 400 Hz. Simulation results demonstrated a signal hearability improvement due to such enhanced signal processing techniques.

However, signal hearability is still not good enough for a high sensitivity receiver in the area near the serving BS because of strong Same-cell interference. Two IPDL methods, PR-IPDL and TA-IPDL, were proposed to solve the “near-far” effect. They try to mitigate the interference by stopping signal transmission at the serving BS and other BSs in other

cells. With these methods, a higher SIR of the signals of other BSs can be obtained. The hearability can be increased to a satisfactory level- The number of BSs that can be heard increase from 1 or 2 to more than 10.

Enhanced Two-Step LS Solution to Hybrid TDOA/AOA Wireless Location Schemes

Hybrid TDOA/AOA solutions produce higher accuracy than that of TDOA-only or AOA-only solutions because more information is utilized. However, the equations for the TDOA sub-system are non-linear ones. The normal Taylor-series-based solution entails a higher computational burden due to linearization and may suffer from convergence issues. The original two-step LS method does not make full use of system information, and, thus, results in degraded performance. The enhanced two-step LS method proposed in this thesis solves the nonlinear problem by first identifying that the nonlinear relationship inside the subsystem is, in fact, a cone in a three-dimensional space and then approximating such a cone in a small region with a plane to transform the nonlinear subsystem into a linear one. The linearization of a cone with a plane is quite simple because of the well known shape of cones. Together with all TDOA/AOA measurement equations, a solution with higher accuracy is obtained.

This method provides a closed-form solution. As a result, it imposes as low a computational burden as that of the original two-step LS solution and has no convergence issue, while the accuracy is almost as high as that of a Taylor series-based solution.

Distribution Function-Based NLOS Error Mitigation

NLOS errors are much larger than receiver noise and can easily overwhelm proposed solutions of a wireless location algorithm. Therefore, NLOS errors should be reduced in advance before the measurements are used in location calculation. The distribution function-based NLOS error mitigation method proposed in Chapter 5 can resolve this issue to some degree. It depends on system redundancy. If more BSs are available than the necessary, multiple candidate MS locations can be obtained and form a distribution function. If the number of NLOS errors is not too large, the clear intersections will have a higher density near the true MS location. The maximum point gives us an estimate of the MS location. Based on this intermediate MS location estimate, cost functions can be formed for every BS from which NLOS errors can be identified and reduced. Experiment results demonstrated the effectiveness of the algorithm. The larger the NLOS errors, the easier they can be identified and mitigated. The more BSs used, the higher the ability to identify NLOS errors.

This NLOS mitigation method is a position-domain method and is suitable for low dynamic users since no spatial diversity is required. Another benefit is that NLOS errors can be seen as constant over a longer time period. In this case, receiver noise can be decreased by superposition of the cost function over several epochs to obtain better performance.

Channel Estimation-Based NLOS Error Mitigation

Since NLOS errors result from multipath propagation, we can mitigate NLOS errors by conducting a multipath channel estimation to extract the LOS signal or the earliest multipath component. The GBSB model gives the joint distribution of TOAs and AOAs of multipath channels. One can draw the conclusion from this model that the accuracies of both TOA measurements and AOA measurements can be improved if only early incoming signals are used. To extract the earliest component, an effective multipath channel estimation method is discussed in Chapter 6. This method contains two stages. The first stage obtains the vector channel impulse response by means of an array signal processing technique. The second stage tries to estimate TOAs and AOAs of all multipath replicas via a 2-D Unitary-ESPRIT method that it is of super resolution and light computational burden. The TOA and the AOA corresponding to the multipath replica with the smallest TOA are used as the final observations.

Simulation results show that the 2-D Unitary-ESPRIT method produces good performance and can be used in multipath mobile channel estimation to obtain better TOA and AOA observations for location purposes. Compared to those wireless location methods without NLOS error mitigation, this channel estimation-based method yields better performance, especially in an area with good geometry.

The Integration of GPS and Cellular Networks

In serious fading environments, both GPS and the cellular network wireless location method suffer from poor signal availability issues. In this case, neither of them can work

well independently for location purposes. However, the combination of these two systems may work well because more information is used and better geometry can be obtained. Three schemes to combine cellular network and GPS for wireless location purposes are fully discussed in Chapter 7: the epoch-by-epoch LS scheme; the position domain Kalman filter-based MS tracking scheme; and the measurement domain Kalman filter-based MS tracking scheme.

The epoch-by-epoch LS scheme combines network measurements and GPS measurements and calculates the MS location via the normal LS formula. It can improve both location availability and positioning accuracy compared to a network-only solution since greater volumes of data are involved in the calculation.

Kalman filter-based methods can further improve performance in some cases, since the movement of a MS is described by a dynamic model and both current information and past information are utilized. While a position domain Kalman filter method processes the output of the epoch-by-epoch LS solution to obtain a better MS location estimation, a measurement domain Kalman filter method directly uses TOA measurements from the cellular network and pseudorange and Doppler measurements from the GPS system. Comparing the experiment results, the measurement domain method provides the higher performance. The RMS value of horizontal location errors can be less than 10 - 20 metres.

8.2 Future Work

Besides what has been presented in this thesis, the following items are also recommended as topics for future research and investigation to further improve the accuracy and reliability of location techniques.

Performance Analysis in Terms of Cramer-Rao Bound (CRB)

The accuracy of TOA and AOA measurements and even the final positioning accuracy can also be compared to the so-called Cramer-Rao Bound (CRB) to check the effectiveness of the proposed wireless location method. The comparison is meaningful because that the CRB, a function of signal noise ratio, gives the bound on the covariance matrix for an unbiased estimator. In the future, the relationship between CRB and DOP should also be addressed.

Application of Interactive Multiple Model (IMM) Technique

Position calculation using one motion model, such as the standard Kalman filter, may not be the most suitable algorithm. It is quite often the case that using more than one motion model and adjusting them adaptively within an IMM frame may give better results in terms of location accuracy, track continuity and coverage than normal KF when the user is moving in urban environments (Shalom et al, 1989). A possible study in the future would, therefore, be focused on parallel execution of coupled dynamic filters to make the IMM filter able to follow the very different motions of the vehicular users or pedestrians without losing track and with acceptable accuracy.

Blind Channel Estimation Based NLOS Error Mitigation

In Chapter 6, the channel estimation method presented is non-blind since a training sequence is used to estimate the vector channel impulse response. This method is suitable for a GSM system where the symbol period is $3.68\,\mu s$ which can provide a TOA resolution of about 50 m. However, this method is difficult to apply to a CDMA system because of a large symbol period. For example, the symbol period is 128 chips long for an IS-95 CDMA system. One possible solution is blind channel estimation with super-resolution. Some blind channel estimation algorithms (Doukopoulos and Moustakides, 2003) have been proposed, but their abilities need to be further investigated to determine if they are suitable for wireless location purposes.

Provision of Height Information

A cellular network cannot provide reliable height information because all BSs are not high enough and the VDOP of such a solution would be extremely poor. Two methods may be feasible to provide height information. One is the integration of GPS and cellular networks since GPS satellites are high enough to allow a robust geometry that overcomes the BS height problem. The second method is a barometer-based technique. With a better temperature compensation scheme or with GPS aiding (Collin et al, 2002), a barometer may be able to provide satisfactory height information. Extensive experiments need to be done in the future to evaluate the capability.

Field Tests

Usually, simulation tests tend to be optimistic since they are often based on simplified models and aim to verify algorithms that only solve one specific problem. However, the actual performance depends on a variety of conditions which are simultaneously present. For example, poor hearability, poor geometry, and NLOS errors may each, in and of themselves, result in poor performance. A combination of these, however, can exacerbate the situation. Multipath in particular is difficult to model and its characterization as a function of the specific user environment remains a challenge. Thus actual field tests in different types of environments should be done to verify the claims made in this thesis. One example is the integration of GPS and a cellular network. In Chapter 7, only vehicular tests were considered which is relatively simple because the dynamics of a vehicle are easy to predict. The pedestrian case, for which the dynamics are difficult to predict by Kalman filters, should be investigated.

REFERENCES

Bartlett, D. (2002). Hearability Analysis for OTDOA positioning in 3G UMTS Networks, *CPS white paper CTN-2002-4-V1.0*, http://cursorsystem.com

Baumann, S., F. Collomb, H. P. Dien, G. Fischer, G. Paris, P. Pilloni, and C. R. Casal (2001), Overview of location services-LOCUS-Deliverable 1, http://www.telematica.de/locus/index.html

Borrás, J., P. Hatrack, and N. B. Mandayam (1998). Decision theoretical framework for NLOS identification, in *Proc. IEEE VTC*, vol. 2, pp. 1583–1587, 1998.

Brown, R. G. and P. Y.C. Hwang (1996). *Introduction to Random Signal and Applied Kalman Filter,* 3rd EDITION, Wiley.

Caffery, J., Jr. (2000). *Wireless Location in CDMA Cellular Radio Systems*, Kluwer Academic Publishers.

Caffery, J., Jr. (2002), Wireless communications, Lecture notes for ECES 719, Dept. of ECECS, University of Cincinnati

Caffery, J., Jr. and G. Stüber, (1994). Vehicle Location and Tracking for IVHS in CDMA Microcells, in *Proceedings of IEEE PIMRC'1994*, pp. 1227–1231.

Caffery, J., Jr. and G. Stüber (1998). Overview of Radiolocation in CDMA Cellular Systems, in *IEEE Communications Magazine*, April 1998

Chan, Y. T. and K. C. Ho (1994), A simple and efficient estimator for hyperbolic location, *IEEE Transactions on Signal Processing*, Vol.42(8), pp.1905-1915.

Chansarkar M., Garin L. J. (2000). Acquisition of GPS signals at very low signal to noise ratio. In: Proc Institute of Navigation ION National Technical Meet 2000, 26–28 January 2000, Anaheim, California, pp 731–737.

Chareyre, V. (2002), Double-Direction Estimation for MIMO Channels, Master thesis of the Toyal Institute of Technology, www.s3.kth.se/signal/reports/ exjobb/02/IR-SB-EX-0214.pdf

Chen, P-C, (1999a). Mobile position location estimation in cellular systems. PhD thesis, the state University of New Jersey, New Brunswick, New Jersey, 1999.

Chen, P-C, (1999b). A non-line-of-sight error mitigation algorithm in location estimation, in *Proc. IEEE Wireless Communications Networking Conference*, vol. 1, pp. 316–320.

Collin J., G. Lachapelle, and J. Käppi, (2002). MEMS-IMU for Personal Positioning in a Vehicle –A Gyro-Free Approach, *ION GPS 2002*,Sept., 24-27 Portland, OR, USA

Cong L. and W. Zhuang (2001), Non-line-of-sight error mitigation in TDOA mobile location, i*Proc. IEEE Globecom 2001*, pp.680-684, 2001.

Cong, L. and W. Zhuang (2002), Hybrid TDOA/AOA mobile user location for wideband CDMA cellular systems, *IEEE Transactions on Wireless Communications*, Vol.1, pp.439-447.

Dana, P.H. (2000), Global Positioning System Overview, http://www.colorado.edu/geography/gcraft/notes/gps/gps_f.html

Doukopoulos X. and G.V. Moustakides (2003), Blind channel estimation for downlink CDMA systems, *IEEE International Conference on Communications*, *ICC'2003*, Alaska.

Enge, P.K., F.B. Vivksell, R. B. Goddard, and F. V. Graas (1990), Combining pseudoranges from GPS and Loran-C for air navigation, *Navigation: Journal of the institute of navigation,* Vol.37, No.1, pp.281-298.

Ericsson (1999). Recapitulation of the IPDL positioning method, *TSGR1#4(99)346*

Ertel, R.B., P. Cardieri, K.W. Sowerby, T.S. Rappaport, J.H. Reed (1998), Overview of spatial channel models for antenna array communication systems, *IEEE Personal Communications*, Vol.5 No.1, pp:10-22

FCC (2001). Fact sheet: FCC wireless 911 requirements, *http://www.fcc.gov/911/enhanced/releases/factsheet_requirements_012001.pdf*

Foy, W. H. (1976), Position location solution by Taylor-series estimation, *IEEE Trans. on Aerospace Electronic System*, Vol:12, pp. 187-194.

Friedlander B. (1987), A passive localization algorithm and its accuracy analysis, *IEEE Journal of ocean engineering*, Vol:12, pp.234-244

Gelb, A. (1974), Applied Optimal Estimation, *MIT press*, Cambridge Mass

Greenstein L. J., V. Erceg, Y. S. Yeh, and M. V. Clark (1997), A new path gain/delay spread propagation model for digital cellular channels, *IEEE Transactions on Vehicular Technology*, Vol.46, No.2, pp.477-484.

Haardt, M. and A. N. Nossek (1995). Unitary Esprit: How to Obtain Increased Estimation Accuracy with a Reduced Computational Burden, *IEEE Transactions on Signal Processing*, Vol.43(5), pp.1232-1242.

Kaplan, E.D. (1996), *Understanding GPS: Principles and Applications*, Artech House Publishers.

Klukas, R.W. (1997). A Superresolution Based Cellular Positioning System Using GPS Time Synchronization, PhD Thesis, Department of Geomatics Engineering, the University of Calgary. http://www.geomatics.ucalgary.ca/research/publications/index.php.

Kuruppillai, R., Dontamsetti, Mahi, and F. J. Cosentino (1997). *Wireless PCS – Personal Communications Services*, McGraw-Hill.

Lachapelle, G., M.E. Cannon, R. Klukas, S. Singh, R. Watson, P. Boulton, A. Read and K. Jones (2003). Hardware Simulator Models and Methodologies for Controlled Performance Assessment of High Sensitivity AGPS Receivers. *Proceedings of GNSS 2003, The European navigation Conference* (Graz, Austria, 22-25 April).

Lähteenmäki, J. (2000), MobileLocation Methods, VTT Information Technology, http://www.vtt.fi/tte/rd/location-techniques/mobile_location.pdf

Landa, L., D. Muñoz, and H. Maturio (2000), Performance analysis of power up function in position location, in *Proc. IEEE VTC*, pp. 2418–2423, 2000.

Laitinen H., Ahonen S., Kyriazakos S., Lähteenmäki J., Menolascino R., and Parkkila S. (2001), Cellular Location Technology, *http://www.telecom.ece.ntua.gr/cello/documents/CELLO-WP2-VTT-D03-007-Int.pdf*

Lee, J. S, and L. E. Miller (1998). *CDMA Systems Engineering Handbook*, Artech Houses Publishers.

Lee, W.C.Y. (1997), *Mobile communication engineering*, 2nd edition, McGraw-Hill, ,

Liberti, J. C. and T. S. Rappaport (1996), A geometrically based model for line-of-sight multipath radio channels, *IEEE Vehicular Technology Conference*, Atlanta, GA, pp.844-848,1996.

Ludden, B. and L. Lopes (2000), Cellular based location technologies for UMTS: a comparison between IPDL and TA-IPDL, in *Proc. IEEE VTC*, pp. 1348–1353, 2000.

Ma, C., G. Jee, G. MacGougan, G. Lachapelle, S. Bloebaum, G. Cox, L. Garin and J. Shewfelt (2001) GPS Signal Degradation Modeling. *Proceedings of GPS2001*, pp. 882-893.

Ma, C., R. Klukas, and G. Lachapelle (2002), an efficient non-line-of-sight error mitigation method for wireless location, *Proc. Wireless'2002*, Calgary, Alberta.

Ma, C., R. Klukas, and G. Lachapelle (2003), an enhanced two-step least squared approach for TDOA/AOA wireless location, P*roceedings of IEEE Communication Confere*nce*, 2003,* Anchorage, Alaska.

MacGougan G., G. Lachapelle, R. Klukas, K. Siu, L. Garin, J. Shewfelt, and G. Cox (2002). Performance Anyalysis of a Stand-Alone High-Sensitivity Receiver, *GPS Solutions*, Vol.6, pp.179-195

Motorola (1999), Time aligned IPDL positioning technique, TSGR1#7(99)b79.

Nuckols, J. E. (1999), Implementation of Geometrically Based Single-Bounce Models for Simulation of Angle-of-Arrival of Multipath Delay Components in the Wireless Channel Simulation Tools, SMRCIM and SIRCIM, *Master thesis in Electrical & Computer Engineering, Virginia Polytechnic Institute and State University*, 1999.

Ostmann, T. K. and A. E. Bell (2001). A Data Fusion Architecture for Enhanced Position Estimation in Wireless Networks, *IEEE COMMUNICATIONS LETTERS*, Vol. 5, No. 8, pp.343-345.

Parkinson, B. W. and J. J. Spilker (editor) (1996). Global Positioning System: Theory and Applications. Volume I, *American Institute of Aeronautics and Astronautics. Inc*.

Paton, I., E. Crompton, J. Gardner, and J. Noras (1991). Terminal Self-Location in Mobile Radio Systems, in *Proceedings of.6th Int'l. Conf. Mobile Radio and Personal Communications*, pp. 203–207.

Paulraj, A. and C. Papadias (1997), Space-time processing for wireless communications, IEEE Signal Processing Magzine, pp.49-93, Nov. 1997.

Petrus, P. and J. H. Reed (2002), Geometrical-based statistical macrocell channel model for mobile environments, *IEEE Trans. on Communications*, pp.495-502, 2002.

Piechocki, R. J., G. V. Tsoulos, and J. P. McGeehan (1998), Simple general formula for PDF of angle of arrival in large cell operational environments, Electronics Letters, vol. 34, pp. 1784–1785, Sep 1998.

Porcino, D. (2001). Standardisation of Location Technologies, in *proceedings of Mobile Location Workshop*, http://www.vtt.fi/tte/rd/location-techniques/porcino.pdf

Rappaport, T. S. (1996). Wireless *Communications – Principles and Practice*, PrenticeHall, Inc., Upper Saddle River, NJ.

Reed, J. H. and R. D. James (1997), Position Location: Technology Overview and Business Opportunities, Wireless Opportunities Workshop, Roanoke, VA, October 1997, http://www.mprg.org/Tech_xfer/ppt/USAt_r.shtml

Roy, R. and T. Kailath (1989), ESPRIT-Estimation of signal parameters via rotational invariance techniques, *IEEE Trans. on Acoust., Speech, Signal Processing*, Vol.37, No.7, pp.984-995.

Said, F. (2002), Introduction to the Mobile Radio Channel, http://www.ctr.kcl.ac.uk/lectures/fatin/Mobile/fading(mobile).pdf

Salychev, O. (1998), Inertial Systems in Navigation and Geophysics, *Bauman MSTU Press*, Moscow.

Sengupta, C. (1998), Algorithms and architectures for channel estimation in wireless CDMA communication systems, PhD thesis, Rice University, Houston, Texas.

Shalom Y.B., K.C. Chang, and H.A.P. B1om (1989), Tracking a maneuvering target using input estimation vs. the interacting multiple model algorithm, *IEEE Trans. Aerospace Electronics Systs*, AES-25, pp. 296-300.

Syrjärinne J. (2001), Studies of Modern Techniques for personal positioning, PhD thesis, Tampere University of Technology.

Syrjärinne J. (2002), Satellite-based positioning technologies, Research & technology access NOKIA mobile phones, www.vtt.fi/tte/rd/location-techniques/syrjarinne.pdf

Thomas, N. J. (2001), Techniques for mobile location estimation in UMTS, PhD thesis, the University of Edinburgh, 2001.

Torrieri, D. J. (1984), Statistical theory of passive location systems, *Trans. on Aerospace Electronic System*, Vol:24, pp.320-327.

Vanderveen, M.C. (1997). Estimation of Parametric Channel Models in Wireless Communication Networks, PhD thesis of Stanford University, http://www-sccm.stanford.edu/pub/sccm/theses/Michaela_Vanderveen.ps.gz

Van der Veen, A.-J., M.C. Vanderveen, and A. Paulraj (1997), SI-JADE: an algorithm for joint angle and delay estimation using shift-invariance properties, *First IEEE Signal*

Processing Workshop on Signal Processing Advances in Wireless Communications, pp.: 161-164

Van der Veen, A. J., M. C. Vanderveen, and A. Paulraj (1998), Joint angle and delay estimation (JADE) using shift-invariance properties, *IEEE Trans. on Signal Processing*, vol.46, pp.405-418, Feb., 1998.

Venkatraman, S. and J. Caffery (2002), A Statistical Approach to Non-line-of-Sight BS Identification, IEEE Wireless Personal Multimedia Communications (WPMC) Conference, Honolulu, HI. *http://www.ececs.uc.edu/~jcaffery/nlos_id.pdf*.

Venkatraman S., J. J. Caffery, and H.-R. You (2002), Location Using LOS Range Estimation in NLOS Environments, *IEEE Vehicular Technology Conference (VTC)* Spring, Birmingham, AL, May 2002, pp. 856-860

Viterbi, A. J. (1995), CDMA: principles of spread spectrum communication, Addison-Wesley publishing company, 1995.

Walters, L. O. and P. S. Kritzinger (2000), Cellular Networks: Past, Present, and Future, *http://www.acm.org/crossroads/xrds7-2/cellular.html*

Wang, Y.Y., J. T. Chen, and W. H. Fang (2001), TST-MUSIC for joint DOA-delay estimation, IEEE *Trans. on signal processing*, Vol.49(4), pp.721-729.

Wax, M., A. Leshem (1997), Joint estimation of time delays and directions of arrival of multiple reflections of a known signal, IEEE Transactions on Signal Processing, Vol:45, No.10, pp.: 2477-2484

Woo, S.-S., H-R. You, and J-S. Koh (2000). The NLOS mitigation technique for position location using IS-95 CDMA networks, in *Proceedings of. IEEE VTC'2000 Fall*, vol.4, pp. 2556–2560.

Wylie, M. P. and J. Holtzman (1996). The non-line of sight problem in mobile location estimation, in *Proc. IEEE International Conference on Universal Personal Communications*, vol. 2, pp. 827–831.

Yacoub, M. D. (1993), Foundations of Mobile Radio Engineering, CRC Press, 1993

Yeh, Y. S. and S. C. Schwart (1984), Outage probability in mobile telephony due to multiple log-normal interferences, IEEE Trans. on Communications, Vol.32(4), April 1984

Yu, Shiann-Jeng and Ju-Hong Lee (1997), Design of two-dimensional rectangular array beamformers with partial adaptivity, *IEEE Transactions on Antennas and Propagation*, Vol.45, No.1,pp.:157-167.

Zoltowski, M. D., M. Haardt, and C. P. Mathews (1996), Closed-form 2-D angle estimation with rectangular arrays in element space or beamspace via unitary ESPRIT, *IEEE Trans. on Signal Processing*, vol.44, pp.316-328, Feb., 1996.